

---

All ETDs from UAB

UAB Theses & Dissertations

---

2017

## Investigating Phenotypic Severity Associated With Sister Chromatid Cohesion Defects In Human Disease

Stefanie Marie Percival  
*University of Alabama at Birmingham*

Follow this and additional works at: <https://digitalcommons.library.uab.edu/etd-collection>

---

### Recommended Citation

Percival, Stefanie Marie, "Investigating Phenotypic Severity Associated With Sister Chromatid Cohesion Defects In Human Disease" (2017). *All ETDs from UAB*. 2707.  
<https://digitalcommons.library.uab.edu/etd-collection/2707>

This content has been accepted for inclusion by an authorized administrator of the UAB Digital Commons, and is provided as a free open access item. All inquiries regarding this item or the UAB Digital Commons should be directed to the [UAB Libraries Office of Scholarly Communication](#).

INVESTIGATING PHENOTYPIC SEVERITY ASSOCIATED WITH SISTER  
CHROMATID COHESION DEFECTS IN HUMAN DISEASE

by

STEFANIE M. PERCIVAL

JOHN M. PARANT, COMMITTEE CHAIR  
MARY ANN BJORNSTI  
ALECIA GROSS  
MICHAEL MILLER  
JOHN SHACKA

A DISSERTATION

Submitted to the graduate faculty of The University of Alabama at Birmingham,  
in partial fulfillment of the requirements for the degree of  
Doctor of Philosophy

BIRMINGHAM, ALABAMA

2016

Copyright by  
Stefanie M. Percival  
2016

INVESTIGATING PHENOTYPIC SEVERITY ASSOCIATED WITH SISTER  
CHROMATID COHESION DEFECTS IN HUMAN DISEASE

STEFANIE M. PERCIVAL

GRADUATE BIOMEDICAL SCIENCES

ABSTRACT

Sister chromatid cohesion (SCC) is a process that utilizes a proteinaceous ring, cohesin, for accurate chromosome segregation. An essential process in S phase termed cohesion establishment is necessary to stabilize cohesin rings around sister chromatids. Mutations in establishment of cohesion homolog 2 (*ESCO2*), a protein essential for cohesion establishment, cause a developmental disorder called Roberts Syndrome (RBS). Cytogenetic analysis in patients reveals heterochromatic repulsion (HR), a centromeric puffing, indicative of cohesion defects. The severity of phenotypes varies from preterm lethal to mild phenotypes into adulthood. Animal models investigating SCC are often embryonic lethal, limiting cellular analysis. To overcome these obstacles, we use zebrafish to take advantage of their *ex vivo* fertilization and transparent tissue during embryogenesis. Because mutations in SCC often lead to improper chromosome segregation, we first developed an assay to observe mitosis in a live zebrafish embryo to determine the extent and outcomes of these mitotic defects. Utilizing this assay, we characterize an embryonic lethal *esco2* mutant zebrafish and find that lethality is due to complete cohesion loss, chromosome missegregation, genomic instability, and apoptosis. Surprisingly, a subset of cells overcomes *Esco2* loss, displays mild cohesion defects, and divides normally indicating a possible compensation mechanism exists. *Esco2* heterozygous embryos are viable and exhibit a weakened cohesion phenotype similar to

the HR in RBS. Interestingly, *esco2* heterozygous animals have enhanced tumor onset in a predisposed model system. The variation in disease phenotype and cohesion defects between homozygous and heterozygous embryos suggest a gene dose effect of *Esco2* that impacts the extent of phenotypic severity. To further understand how cohesion establishment impacts cellular and organismal viability, we employ genome editing technology to generate mutants in establishment of cohesion homolog 1 (*Esco1*), Shugoshin-Like 1 (*SgoL1*), and Sororin (Cell division cycle-associated protein 5, *Cdca5*) due to their involvement in cohesion establishment and maintenance. Though all are lethal in cell culture, we observe a phenotypic spectrum in severity at the gross morphology level that strongly correlates to their severity in cohesion defects. This has significant implications in understanding the variable phenotypes associated with RBS, other cohesinopathies, and disorders associated with cohesion defects.

## ACKNOWLEDGEMENTS

Graduate school is often filled with many ups and downs, twists and turns, and it would not have been possible had it not been for several significant people to help me through this journey.

I would first like to thank my mentor, Dr. John Parant, for providing me the opportunity to join his lab to complete my thesis work. I had minimal research experience at the time of joining and he was always active in helping me design experiments or teach me a new technique. His passion for all things science and laid back nature were qualities that I often admired and strived to emulate. The experience I have gained in his lab has truly made me a better scientist.

Secondly, I would like to thank my committee members, Drs. Mary Ann Bjornsti, Alecia Gross, Michael Miller, and John Shacka for being the most responsive and involved committee I could ask for. The expertise you each hold in your fields was invaluable to my success. I would also like to thank the Cell, Molecular and Developmental Biology theme for accepting me into this program. UAB was never on my radar until you all showed me how much of a hidden gem it is. Additionally, I would like to thank the Department of Pharmacology and Toxicology for their support and many opportunities for growth throughout the years.

Next, I would like to thank Dr. Holly Thomas, our lab's research assistant/lab manager/lab mom/Alabama fan/candy supplier. Her patience as I optimized protocols and asked annoyingly dumb questions, still to this day, is unmatched. It has been such a

pleasure working with her and I would not have been able to accomplish nearly half as much without her.

Finally, I would like to thank my family and friends for their unwavering support during the past six years. To my parents, Jim and Cindy, thank you for all of your love, care and always supporting my decisions, even if they mean moving eight hours away to spend six years in an intensive graduate program. To my sister, Jamie, even though I am your older sister, I have always looked up to you as a source of inspiration and happiness. Thank you for always being there. A special thanks to my grandma and grandpa for their love and support. CUBS WIN!!! I next would like to thank my boyfriend, Adam, for going above and beyond with your love and support. Having you by my side the past few years has been indispensable to my success. Lastly, I would like to thank my friends, both new and old, for their friendship, support, laughter, and intellect. You all have been there through thick and thin and have made me a better person through it all.

## TABLE OF CONTENTS

	<i>Page</i>
ABSTRACT.....	iii
ACKNOWLEDGEMENTS.....	v
LIST OF TABLES.....	x
LIST OF FIGURES.....	xi
INTRODUCTION.....	1
Sister Chromatid Cohesion.....	1
Discovery of the Cohesin Ring.....	1
Cohesin Ring Structure.....	4
One Ring Cohesin Models.....	6
Two Ring Cohesin Models.....	7
The Cohesin Ring Loading Complex.....	9
Localization.....	10
Opening of the Ring.....	12
Cohesion Establishment.....	13
Balancing Cohesion Establishment and Anti-Establishment.....	18
Cohesion Removal in Mitosis.....	21
The Prophase Pathway.....	21
Cohesin Ring Cleavage.....	25
Non-canonical SCC Roles: Gene Expression.....	27

Non-canonical SCC Roles: DNA Repair .....	29
Non-canonical SCC Roles: Centriole Disengagement .....	30
Cohesinopathies .....	31
Roberts Syndrome.....	32
Gene Expression and Roberts Syndrome.....	34
Ribosome Biogenesis and Roberts Syndrome .....	35
Scientific Voids in Cohesion Establishment.....	37
Introduction References .....	40
OBSERVING MITOTIC DIVISION AND DYNAMICS IN A LIVE ZEBRAFISH	
EMBRYO .....	54
VARIATIONS IN SISTER CHROMATID COHESION DYSFUNCTION IN <i>ESCO2</i>	
MUTANT ZEBRAFISH REFLECTS THE PHENOTYPIC DIVERSITY OF ROBERTS	
SYNDROME .....	85
EMBRYONIC MITOTIC DEFECTS DUE TO HETEROZYGOUS LOSS OF <i>ESCO2</i>	
ENHANCES TUMORIGENESIS IN VIVO.....	144
EVOLUTION OF GENE MANIPULATION IN ZEBRAFISH .....	
	172
THE EXTENT OF COHESION DYSFUNCTION CONTRIBUTES TO	
COHESINOPATHY PATHOGENESIS AND CORRELATES WITH PHENOTYPIC	
SEVERITY .....	198
THESIS CONCLUSIONS .....	
	242
CONCLUSION REFERENCES.....	
	265

APPENDIX: IACUC APPROVAL FORM .....272

LIST OF TABLES

*Table* *Page*

INTRODUCTION

1 Sister Chromatid Cohesion Gene Homology across Species.....3

## LIST OF FIGURES

*Figure* *Page*

### INTRODUCTION

1	Structure of cohesin ring components.....	3
2	The Single Ring Model.....	7
3	The Handcuff Model.....	8
4	The Oligomeric Model.....	9
5	Cohesin Ring Loading .....	10
6	Cohesion Establishment Requires SMC3 Acetylation by ESCO1/ESCO2.....	16
7	SORORIN Recruitment Blocks Anti-Establishment Activity.....	19
8	Prophase Removal Pathway.....	22
9	Cohesin Ring Cleavage.....	26

### OBSERVING MITOTIC DIVISION AND DYNAMICS IN A LIVE ZEBRAFISH

#### EMBRYO

1	Protocol Drawings Outline .....	70
---	---------------------------------	----

LIST OF FIGURES (Continued)

<i>Figures</i>		<i>Page</i>
2	Time-lapse Imaging Captures Multiple Mitotic Events in a Live Zebrafish Embryo.....	72
3	Individual Cell Analysis Captures Each Phase of Mitosis and Mitotic Duration .....	73
4	Single Cell Live Imaging Captures Multiple Mitotic Defects Associated with Chromosome Missegregation and Division in Mitotic Mutant Zebrafish .....	75

VARIATIONS IN SISTER CHROMATID COHESION DYSFUNCTION IN ESCO2  
MUTANT ZEBRAFISH RELECTS THE PHENOTYPIC DIVERSITY OF  
PHENOTYPES

1	Genetic screen identifies the retroviral insertion embryonic lethal mutant, hi2865 .....	93
2	P53 activation and neural tube apoptosis is an early consequence of loss of <i>esco2</i> .....	98
3	<i>esco2</i> deficiency results in elevated mitotic index and scattered chromosomes .....	101

LIST OF FIGURES (Continued)

<i>Figure</i>		<i>Page</i>
4	In vivo analysis of <i>esco2</i> mutants reveals chromosome scattering and prolonged division time.....	104
5	Depletion of <i>esco2</i> results in genomic instability .....	107
6	Most cells of the <i>esco2</i> <sup>m/m</sup> embryo display complete cohesion loss, however some cells display mild cohesion defects, mild aneuploidy, and almost normal mitotic transition .....	112
7	Model depicting cellular outcomes in <i>esco2</i> mutant zebrafish embryos and hypothesized impact compensation may have on RBS phenotypes .....	115

EMBRYONIC MITOTIC DEFECTS DUE TO HETEROZYGOUS LOSS OF ESCO2  
ENHANCES TUMORIGENESIS IN VIVO

1	Gene dose-dependent reduction in cohesion establishment leads to aneuploidy .....	150
2	Embryonic <i>esco2</i> heterozygosity lead to chromosome instability.....	153
3	<i>esco2</i> haploinsufficiency enhances tumor onset in a p53 heterozygous but not in p53 wild-type or homozygous mutant background .....	155

LIST OF FIGURES (Continued)

<i>Figure</i>		<i>Page</i>
EVOLUTION OF GENE MANIPULATION IN ZEBRAFISH		
1	Gene knock-down using morpholinos .....	176
2	Schematic of zinc finger nuclease.....	183
3	Schematic of a TALEN.....	185
4	Schematic of CRISPR/Cas9 system .....	187
5	HRM established genotype-phenotype correlation within Esco2 mutant embryos from a G0 intercross.....	192
THE EXTENT OF COHESION DYSFUNCTION CONTRIBUTES TO COHESINOPATHY PATHOGENESIS AND CORRELATES WITH PHENOTYPIC SEVERITY		
1	Cohesion establishment mutant generation using CRISPR/Cas9.....	204
2	Cohesion establishment mutants display variable morphology defects .....	206
3	Cohesion establishment mutant validation .....	208
4	Spectrum of cohesion defects in cohesion establishment mutants .....	211
5	In vivo analysis of cohesion establishment mutants reveal variations in division time and genomic instability outcomes.....	216

## LIST OF FIGURES (Continued)

<i>Figure</i>		<i>Page</i>
6	Broad range of apoptotic responses among cohesion establishment mutants ....	220
7	The SCC Gradient Model .....	225

## THESIS CONCLUSIONS

1	The Sister Chromatid Cohesion Gradient Model.....	258
2	Applying the SCC gradient model to HR+ cohesinopathies .....	260
3	Genetic interactions to investigate in future studies .....	263

## INTRODUCTION

### *Sister Chromatid Cohesion*

Sister chromatid cohesion (SCC) is an essential process for chromosome segregation and genome integrity. This process utilizes a proteinaceous ring to encircle sister chromatids to ensure that they are properly paired until the metaphase-anaphase transition in mitosis so that sister chromatids are equally distributed into the two new daughter cells. Within this process is an essential step termed cohesion establishment that ensures the cohesin ring is stable for proper pairing of sister chromatids. This step is performed by establishment factors that are essential for cell and organismal viability. Defects in SCC and cohesion establishment often result in genomic instability and cell death. Interestingly, a subset of developmental disorders called cohesinopathies is due to mutations in this process. In this document we discuss the role SCC plays in cell and organismal viability to further understand cohesinopathies and other disease states affected by cohesinopathies.

### *Discovery of the Cohesin Ring*

Scientists observing the cell cycle hypothesized that a cellular mechanism must be responsible for sister chromatid pairing and potentially necessary for tension sensing functions for biorientation during metaphase (Nicklas & Staehly, 1967; Nicklas et al.,

1995; Sundin & Varshavsky, 1980). Prior to the discovery of the cohesin ring, it was largely believed that DNA entanglements were responsible for sister chromatid pairing and that upon entrance into mitosis, the DNA entanglements would resolve via topoisomerase II (topo II) to yield proper segregation of chromatids. Surprisingly, suppression of topo II either genetically or chemically in yeast cultures allow centromeres to separate and for cells to exit mitosis suggesting an alternative regulatory mechanism (Downes et al., 1991; Funabiki et al., 1993). Some catenation serves as a mechanism of holding sister chromatids together but the more prominent mechanism for chromatid pairing was hypothesized to be proteinaceous in nature (Toyoda & Yanagida, 2006; Vagnarelli & Earnshaw, 2004). This unknown proteinaceous complex theory was further supported by the discovery that the ubiquitin ligase, anaphase promoting complex/cyclosome (APC/C), is required for chromatid separation in mitosis (Irniger et al., 1995).

The ring structure components were eventually discovered through several yeast genetic screens designed to identify mutants that have genes defective in sister chromatid cohesion. In these yeast genetic screens, the main ring components, SMC1, SMC3, Scc1 (RAD21), and Scc3 (STAG1/2), were discovered. Inactivation mutations in these components reveal lethality, improper sister chromatid pairing, and sensitivity to genotoxic stress. Further co-immunoprecipitation (co-IP) experiments established interactions between SMC1 and SMC3; SMC1, SMC3, and RAD21; and STAG1/2 and RAD21 suggesting these proteins work as a complex (Figure 1) (Guacci et al., 1997; Michaelis et al., 1997; Toth et al., 1999). These four components, in addition to other

components in the SCC pathway, have been found to be homologous throughout evolution, from yeast and fly to mouse and human (Table 1).

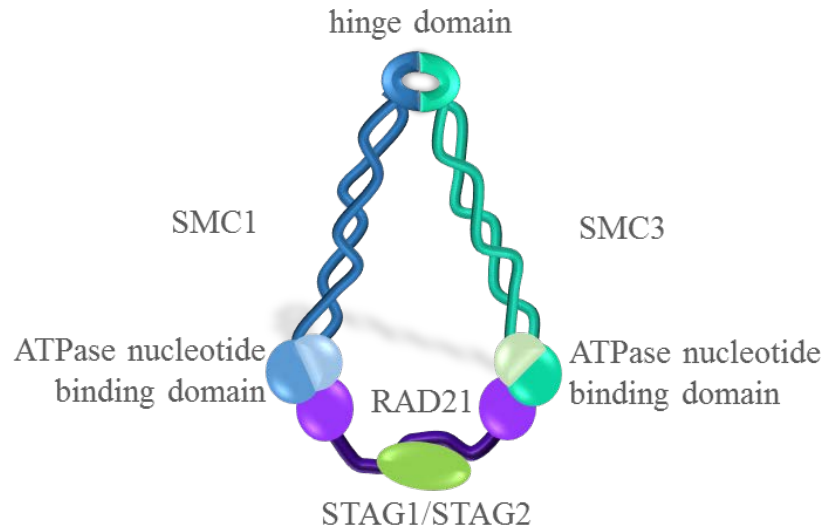


**Figure 1: Structure of cohesin ring components.**

	Saccharomyces cerevisiae	Schizosaccharomyces pombe	Drosophila melanogaster	Xenopus laevis	Danio rerio	Mus musculus	Homo sapien
<b>SMC subunit</b>	Smc1	psm1 <sup>+</sup>	Smc1	Smc1	Smc1a	SMC1a	SMC1a
					Smc1b	SMC1b	SMC1b
	Smc3	psm3 <sup>+</sup>	Smc3	Smc3	Smc3	SMC3	SMC3
<b>Kleisen subunit</b>	Sec1	rad21 <sup>+</sup>	Rad21	Rad21	Rad21a	RAD21	RAD21
					Rad21b		
<b>Kleisen-associated subunit</b>	Sec3	psc3 <sup>+</sup>	SA1	Stag1	Stag1a	STAG1	STAG1
					Stag1b		
			SA2	Stag2	Stag2a	STAG2	STAG2
					Stag2b		
<b>HEAT repeat protein</b>	Pds5	pds5 <sup>+</sup>	pds5	Pds5a	Pds5a	PDS5a	PDS5a
				Pds5b	Pds5b	PDS5b	PDS5b
<b>Releasin</b>	Rad61	wpl1 <sup>+</sup>	Wapl	Wapal	Wapal1a	WAPL	WAPAL
					Wapal1b		
<b>Sororin</b>	-	-	Dalmatian	Sororin	Cdca5	CDCA5	CDCA5
<b>Shugoshin</b>	Sgo1	sgo1 <sup>+</sup>	Mei-S332	Sgo1	SgoL1	SGOL1	SGOL1
					SgoL2	SGOL2	SGOL2
<b>Kollerin/adherin</b>	Sec2	mis4 <sup>+</sup>	Nipped-B	Nipbl	Nipbla	NIPBL	NIPBL
					Nipblb		
<b>Cohesin loading</b>	Sec4	ssl3 <sup>+</sup>		Mau2	Mau2	MAU2	MAU2
<b>Cohesin cleavage</b>	Esp1	cut1 <sup>+</sup>	Separase	Esp1	Esp1	ESPL1	ESPL1
<b>Acetyltransferase</b>	Ctf7/Eco1	eso1 <sup>+</sup>	Deco	Esco1	Esco1	ESCO1	ESCO1
				Esco2	Esco2	ESCO2	ESCO2
<b>Deacetylase</b>	Hos1			Hdac8	Hdac8	HDAC8	HDAC8

**Table 1: Sister chromatid cohesion gene homology across species.**

### *Cohesin Ring Structure*

Though a full crystal structure of cohesin has not been resolved, much is still known about this unique complex. SMC proteins are approximate 50 nanometer (nm) long coiled coil proteins in which the N-terminal region forms  $\frac{1}{2}$  of an adenosine triphosphatase (ATPase) nucleotide binding domain (NBD) that extends out as a coiled coil, forms a globular hinge domain, and then folds back on itself to form the remaining  $\frac{1}{2}$  of the ATPase domain at the C-terminus (Figure 1) (Gandhi et al., 2006; Haering et al., 2002; Melby et al., 1998). The coiled coil domains are highly conserved and structurally important in that addition of five amino acids to the coiled coil domain abolishes cohesin's association with chromatin (Milutinovich et al., 2007). As part of the cohesin ring, the SMC1 and SMC3 hinge domains heterodimerize and display a tight, low  $K_D$  interaction (Anderson et al., 2002; Losada et al., 2002).

Interaction of SMC proteins with  $\alpha$ -kleisen proteins, such as RAD21, is found throughout several biological processes and organisms (Britton et al., 1998; Haering et al., 2004; Moriya et al., 1998). The SMC3 NBD binds the N-terminus of RAD21, while the NBD of SMC1 binds the C-terminus of RAD21 (Figure 1) (Heidinger-Pauli et al., 2010). The RAD21 C-terminus forms a winged helix domain that is essential for SMC1 binding to RAD21 and ATP hydrolysis. Conversely, mutations in the ATPase binding pocket abolish association of RAD21 with SMC1/3 and, subsequently, its association with chromatin (Hu et al., 2011). SMC1-RAD21 binding must occur first in order for the N-terminus of RAD21 to bind to the NBD of SMC3 (Haering et al., 2004). The central portion of RAD21 consists of several  $\alpha$ -helices as a scaffolding site for additional SCC regulator proteins (Hara et al., 2014).

The fourth and final cohesin ring subunit, STAG1/STAG2 acts as one of RAD21's scaffolding proteins. STAG1/STAG2 is a multi-domain protein consisting of a Huntingtin, elongation factor 3, protein phosphatase 2A, and yeast kinase TOR (HEAT) repeat scaffold domains with a largely unknown function (Neuwald & Hirano, 2000). Yeast have just one of these scaffold proteins, Scc3, while vertebrate organisms have two paralogue units, STAG1/STAG2 (Sumara et al., 2000; Toth et al., 1999). Only one STAG unit binds to each cohesin ring and this binding is essential for cohesin function (Figure 1) (Losada et al., 2000). Crystal structure of STAG2 bound to RAD21 has been resolved to show STAG2 binds centrally to RAD21 which is creatively described as looking "like a dragon" (Figure 1) (Hara et al., 2014; Roig et al., 2014). Human cell culture studies suggest STAG2 binding is to strengthen the ring and give more surface area for additional proteins to bind (Hara et al., 2014).

The classical view of the cohesin rings describes these four proteins as creating a ring structure to perform its SCC function by topologically trapping chromatin within the ring. Interaction of SMC1, SMC3, RAD21 and STAG1/STAG2 proteins indeed have been shown to make an asymmetric ring structure (Gligoris et al., 2014). Additionally, several electron microscopy (EM) images of purified cohesin complexes display cohesin as a ring structure (Anderson et al., 2002). The cohesin ring is predicted to be 40 nm in diameter which is large enough to encompass two 10 nm chromatin fibers (Ivanov & Nasmyth, 2005). Using molecular genetics to generate mutant strains, Tobacco Etch Virus nuclear-inclusion- $\alpha$  endopeptidase (TEV) sites were placed throughout yeast Rad21 and Smc3 allowing for experimental control over ring cleavage. Upon cleavage, dissociation of cohesin rings from chromatin is observed (Gruber et al., 2003; Uhlmann

et al., 2000). Using the reverse approach, non-cleavable RAD21 induced after S phase does not dissociate cohesin prematurely (Haering et al., 2004; Ivanov & Nasmyth, 2005; Lengronne et al., 2006; Strom et al., 2007). In 2005, Nasmyth's group was able to show, using circular mini-chromosomes, that cleavage of the cohesin ring prevents the association of cohesin and chromatin (Ivanov & Nasmyth, 2005).

Recent confounding data, based on new EM results, suggests the cohesin ring is more of a rod structure (Surcel et al., 2008). Though this study had been performed to analyze cohesin's function in DNA damage, it still gives precedence towards an alternative cohesin ring binding function, albeit these two structures may not be mutually exclusive. For example, the two different ring conformations could be due to post-translation modifications that alter ring structure to perform different cellular processes (i.e. DNA damage).

### *One Ring Cohesin Models*

As stated above in the previous section, the ability for cohesin rings to be topological in nature lends to the idea that one ring encircles both sister chromatids (Figure 2). Early studies found no co-IP between rings (Haering et al., 2002); however, later studies in Zhang et al 2008 found this to not be the case. Further evidence for the one ring model is demonstrated by the sedimentary velocity of soluble cohesin rings which remains consistent with a monomer sized cohesin complex (Hauf et al., 2005; Losada et al., 2000; Sumara et al., 2000). The latest studies arguing for the single ring model suggest that STAG1/STAG2 have the ability to interact with the SMC hinge domain and fold over chromatin to form a rod structure (Murayama & Uhlmann, 2014).

However, these studies are often performed by overexpressing the cohesin proteins in yeast and maintain levels of cohesin at non-physiologically relevant levels. Clearly, there is still much to learn of how the cohesin ring interacts with chromatin.

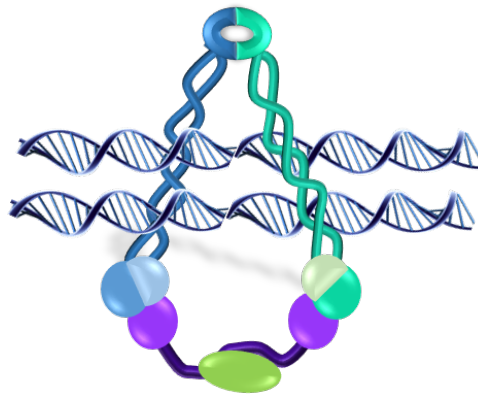


**Figure 2: The Single Ring Model**

#### *Two Ring Cohesin Models*

Researchers have also proposed models using two cohesin rings. The handcuff model describes the STAG1/STAG2 subunit of cohesin interacting with another cohesin ring at the RAD21 subunit (Figure 3) (Hauf et al., 2005; Losada et al., 2000; Sumara et al., 2000; J. Zhang et al., 2008). In Zhang et al. overexpression of the SMC1, SMC3, and RAD21 subunits revealed that all three were able to interact with themselves. The effect is found to be STAG-dependent, providing evidence for the handcuff model. This study, however, uses an overexpression model which does not mimic the natural *in vivo* stoichiometry suggesting that this model may not be present in a cellular context.

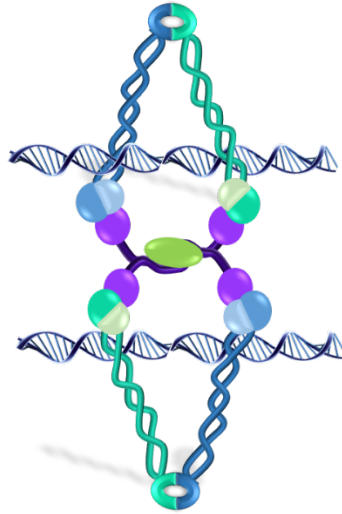


**Figure 3: The Handcuff Model**

The bracelet model is another dual ring model that describes the STAG1/STAG2 molecule as a binding surface and links cohesin rings together like a chain. Nasmyth 2004 and Huang 2005 first discussed the possibility of this model yet substantial data remains to be found. A related model, the oligomeric model, recently found support to describe cohesin rings stacking up on one another in anti-parallel fashion (Figure 4). Yeast genetic screens identify inter-allelic complementation in genes involved in the cohesin ring indicating that protein-protein interactions of cohesin rings are present. Inactivating mutations in both Smc3 and Rad21 alone are lethal but in their dual presence, rescue lethality. Due to the well-known stoichiometry of cohesin ring proteins, this group suggests that direct linking of multiple rings allows for mutations in one ring to compensate for mutations in another and that these mutations alone in one ring would not allow for this rescue (Eng et al., 2015). This group further hypothesizes that oligomeric cohesin is utilized for regulation of gene expression due to the long range capabilities of this form rather than mitosis.

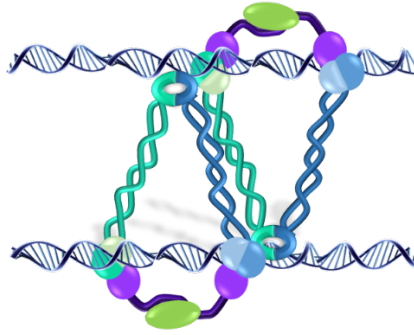


**Figure 4: The Oligomeric Model**

*The Cohesin Ring Loading Complex*

Though most noted for its action at the metaphase-anaphase transition, sister chromatid cohesion is a full cell cycle process that begins in Gap 1 (G1) phase of the cell cycle. At the onset of G1, cohesin rings are loaded onto chromatin via the loading complex, NIPPED-B-LIKE/MAU2 (NIPBL/MAU2) (Figure 5) (Ciosk et al., 2000; Tonkin et al., 2004; Watrin et al., 2006). Note at this point there is not a sister chromatid, just a single chromatid. NIPBL is a small protein with an unstructured N-terminal region and a HEAT repeat-containing C-terminal region that binds MAU2 (Neuwald & Hirano, 2000). MAU2 is a small tetratricopeptide (TRP) repeat protein. In similar fashion as Smc1, Smc3, and Rad 21, the loading complex was also discovered in yeast genetic screens and is conserved throughout evolution (Bernard et al., 2006; Ciosk et al., 2000; Gillespie & Hirano, 2004).

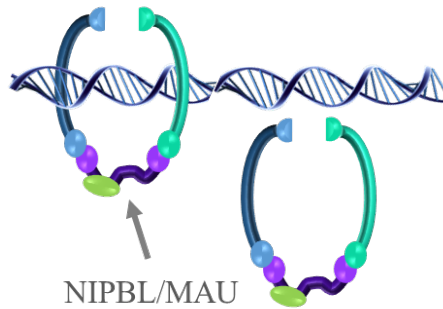


**Figure 5: Cohesin Ring Loading**

To tease out its function in the cell cycle, temperature sensitive yeast NIPBL mutants were inactivated at different points in the cell cycle. Using this assay, the groups were able to determine that the complex is necessary for cohesin binding but not for SCC establishment or maintenance required for chromosome segregation (Bernard et al., 2006; Ciosk et al., 2000). There is controversial data over whether the complex directly binds the cohesin ring. Co-IP studies found that cohesin does not bind the loading complex; however more sensitive studies using mass spectrometry have found that they do in fact bind each other but dynamically dissociate, suggesting a transient interaction (Arumugam et al., 2003; Bernard et al., 2006; Ciosk et al., 2000).

### *Localization*

Whether cohesin is loaded on at critical sites or whether the rings eventually move towards its functional position is crucial in understanding cohesin's role in the cell cycle. Approximately 44% of a cell's cohesin pool is bound to chromatin in G1 phase. In G2, this percentage increases to 60%. Approximately half of that number (30%) is believed to be involved in chromosome segregation while the other half is thought to

regulate gene expression (Gerlich et al., 2006). These experimental percentages were based off fluorescent recovery after photobleaching (FRAP) of EGFP-bound STAG1. They do not include STAG2-bound cohesin which could increase the amount of stably bound cohesin if included in the analysis. In fact, recent data suggests that STAG1-bound cohesin primarily plays a role in gene expression and replication of telomeres while STAG2-bound cohesin functions in chromosome segregation (Remeseiro et al., 2012). Controversial data however suggests there is no preference of STAG molecules that indicate their function (Schmidt et al., 2010; Wendt et al., 2008). In either instance, a large portion of stably bound cohesin was left out of the analysis suggesting a greater than 30% population of total cohesin is responsible for proper chromosome segregation.

The complete mechanism of how cohesin is localized to certain regions is unclear; however, it is known that there are certain regions where cohesin is likely to be associated. Cohesin is highly enriched at 40 kilobase pair (kbp) regions outside of the centromere and MAU2 shows to be critical to this centromeric localization (Hinshaw et al., 2015). Whether cohesin is recruited to the centromere first or actively moved once loaded onto chromatin is still unknown (Weber et al., 2004). Evidence points towards convergent transcription being responsible for cohesin localization due to the non-overlapping nature of cohesin binding sites to NIPBL/MAU2 loading sites (Filipski & Mucha, 2002; Glynn et al., 2004; Lengronne et al., 2004). Recently, ribonucleic acid polymerase II (RNA Pol II) displays a role in the convergent transcription movement of cohesin (Ocampo-Hafalla & Uhlmann, 2011). Additional data showing overlap of the loading complex to Pol II demonstrates in *Drosophila* that convergent transcription is

responsible for cohesin ring localization though this mechanism has yet to be shown in humans (Misulovin et al., 2008).

More specifically, cohesin associated regions (CARs) were defined as approximately 10-15 kbp segments containing highly probable cohesin binding sites in yeast. These regions were often intergenic and AT rich (Glynn et al., 2004; Laloraya et al., 2000; Lengronne et al., 2004). Again, it is hypothesized that cohesin rings move via convergent transcription to these sites. In an elegant study using total internal reflection fluorescence microscopy (TIRF), purified cohesin on linear arrays of DNA confirms the loading complex is necessary for cohesin binding. In addition, this group is able to measure the rate of ring movement along DNA and found that the ring moves close to the theoretical diffusion rate which further supports the ring is topological in nature and moves towards its final site (Stigler et al., 2016). Cohesin is also found localized to CCCTC binding factor (CTCF) domains to aid in gene expression regulation during G1 (Lengronne et al., 2004; Wendt et al., 2008). For more information on the loading complex's role in gene expression, see Non-canonical SCC Roles: Gene Expression.

### *Opening of the Ring*

The ability to detect unbound, assembled cohesin rings suggests that cohesin must be “opened” to embrace DNA (Arumugam et al., 2003; Gruber et al., 2003). Molecular studies are able to determine that fusion of the ring at the NBD of SMC1/3 to RAD21 shows no cohesion defects suggesting the opening gate is not at these access points (Gruber et al., 2006). The access point is in fact, at the hinge domain (interface of SMC1 and SMC3) as demonstrated both *in vitro* and *in vivo* (Figure 5). Mutations that fuse the

hinge domain cause improper chromosome segregation and a decreased residence time on chromatin (Buheitel & Stemmann, 2013; Gruber et al., 2006; Huis in 't Veld et al., 2014; Mishra et al., 2010). NIPBL has also been shown to be necessary for hinge opening in yeast suggesting the loading complex plays a role not only in cohesin ring deposition but in opening as well (Murayama & Uhlmann, 2014).

The structure of the hinge domain advances further understanding of cohesin ring opening. In these studies, researchers discover that the hinge domain of the SMC1 and SMC3 heterodimer creates a channel that requires a positive charge for proper SCC (Kurze et al., 2011). Although not definitive, this study also suggests that the ATPase domain of SMC3, a region opposite of the hinge domain, is required and the energy provided through ATP hydrolysis opens the hinge to allow for cohesin loading. This mechanism has expanded to include a molecule called Wings-apart-like (WAPL) (discussed in the Balance of Cohesion Establishment and Anti-establishment) to have a role in cohesin loading by acting upon the SMC3-RAD21 interface in yeast (Murayama & Uhlmann, 2014, 2015). This new data suggests the true mechanism for cohesin loading or an alternative mechanism, though these mechanisms do not have to be mutually exclusive.

### *Cohesion Establishment*

Although less well-known, the most critical step in sister chromatid cohesion for proper chromosome segregation occurs next in the Synthesis phase (S phase) of the cell cycle. In a yeast genetic screen for chromosome loss, an acetyltransferase called establishment of cohesion homolog 1 (Eco1, ESCO1/ESCO2 in vertebrates) was discovered to be essential for stabilization of the cohesin ring (Hou & Zou, 2005;

Skibbens et al., 1999; Tanaka et al., 2001). This stable pool of cohesin is further analyzed *in vivo* and determined that the residence time of the majority of cohesin is approximately 25 minutes in G1. Interestingly in G2 phase, a secondary population is discovered to be more stable. These populations of stable cohesin amounts to one-third of the total cohesin present (Gerlich et al., 2006). The stabilization process is named cohesion establishment. Subsequently, the ‘cohesin without cohesion’ term is coined to describe the phenomenon that cohesin rings alone do not hold sister chromatids together but must be converted to “cohesion” via ESCO1/ESCO2 for ring stabilization and proper chromosome segregation.

ESCO1 and ESCO2 are Gcn5-related N-acetyltransferases (GNAT) with highly variable N-terminal regions, but highly conserved C-terminal regions which include an acetyltransferase domain and a zinc finger domain (Vega et al., 2010). They lack a critical  $\alpha$ -helix that allows for histone acetyltransferase activity. Between the two proteins in humans, they share 77% similarity within the acetyltransferase domain; however the N-terminal region shares little similarity suggesting they may have different cellular functions (Hou & Zou, 2005).

In yeast and human, the acetyltransferase activity required for cohesion establishment is restricted to S phase. Expression of cohesin components after S phase cannot generate cohesion except in the presence of DNA damage (Haering et al., 2004; Lengronne et al., 2006; Strom & Sjogren, 2005; Unal et al., 2007). For more information on the role of SCC in DNA damage, see Non-canonical Roles of SCC: DNA Repair. In conjunction with the requirement for acetyltransferase activity in S phase, acetylation levels are found to only increase during S-phase which strongly supports that

ESCO1/ESCO2 activity is regulated in S phase (Rolef Ben-Shahar et al., 2008; Unal et al., 2008; J. Zhang et al., 2008). In yeast, to control Eco1 expression levels, cyclin-dependent kinase 1 (CDK1) phosphorylation in S phase targets Eco1 for degradation (Lyons & Morgan, 2011).

The functional targets of the establishment factors were identified through a yeast genetic screen for genetic suppressors of cohesion dysfunction. In this screen, mutations at two Lysine residues of SMC3 (K112 and K113 in yeast, K105 and K106 in vertebrates) were found to suppress cohesion dysfunction in a yeast Eco1 mutant background (Figure 6) (J. Zhang et al., 2008). The function of these residues in vertebrates is less clear. Conditional knockout of ESCO2 in mouse embryonic fibroblasts (MEFs) show diminished, but not eliminated, acetylation suggesting ESCO1 and ESCO2 may have redundant functions (Whelan et al., 2012). Mutating Lysine residue 113 but not Lysine 112 (K112 and K113) in yeast to an arginine is lethal and abolish the functional need for Eco1. The purpose of acetylation is believed to counteract anti-establishment factors that remove cohesin rings from chromatin in the subsequent phases of the cell cycle (to be discussed in Balancing Cohesion Establishment and Anti-Establishment section) (Rolef Ben-Shahar et al., 2008; Rowland et al., 2009; Sutani et al., 2009). Additional Eco1 acetylation residues have been discovered suggesting SMC3 K112 and K113 are not the only targets. Rad21, Scc3, Eco1 autoacetylation, and precocious dissociation of sisters 5 (Pds5) are all targets of Eco1 in yeast. However, these targets fail to produce cohesion defects suggesting their role in chromosome segregation is negligible (Ivanov et al., 2002).

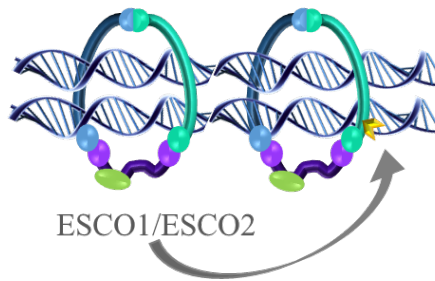


**Figure 6: Cohesion Establishment Requires SMC3 Acetylation by ESCO1/ESCO2**

At the structural level, the key lysine residues in yeast and human are near the adenosine triphosphate (ATP) binding pocket of SMC3. Their close proximity to this region is believed to regulate ATPase activity and play a role in the conversion of ‘cohesin’ to ‘cohesion’ (Gligoris et al., 2014; Murayama & Uhlmann, 2015; J. Zhang et al., 2008). Molecular analysis linking the ATPase domain to cohesion establishment was originally discovered in a yeast genetic screen that identify several mutations in the ATPase active site that stabilize cohesin. Mutations in the hinge ATPase domain do not show this effect suggesting the ATPase domain proximal to the acetylation residues is critical in cohesion establishment (Camdere et al., 2015; Ladurner et al., 2014). These ATPase mutants are critical in determining that ATPase activity is not only required in cohesin loading but also for cohesion establishment and that they coordinate with each other as opposed to being two distinct processes.

The requirement for cohesion establishment to entrap replicated sister chromatids during S phase suggested that replication machinery may be essential in this process. A novel DNA polymerase, Kappa polymerase, was discovered in yeast to be required for SCC providing the first evidence to link replication to SCC (Wang et al., 2000). Additional factors involved in replication, such as proliferating cell nuclear antigen

(PCNA) and chromosome transmission fidelity 4 (CTF4), were found to be important for cohesion establishment as well (Gambus et al., 2006; H. Xu et al., 2007). The C-terminal portion of Eco1 contains a Glutamine, any amino acid, any amino acid, Leucine or Isoleucine (QXXL/I) motif that binds PCNA and is required for viability (Moldovan et al., 2006). Furthermore, replication factor C (RFC) component, enhanced level of genomic instability 1 (Elg1), was found to rescue Eco1 lethality and have a role in coordinating the replication fork and cohesion establishment (Maradeo & Skibbens, 2009; Parnas et al., 2009). Recent data developed more of the mechanism linking sister chromatid cohesion to DNA replication. Classical yeast molecular assays determined that Ctf4, a molecule required for SCC, recruits cell adhesion molecule like 1 (Chl1) (DNA helicase) to the replication fork and initiates a direct cohesin binding to mediate cohesion establishment (Samora et al., 2016).

If DNA replication is linked to cohesion establishment, how is the replication fork and cohesin rings interaction physically accomplished? Initial studies suggested the DNA replisome is able to pass through the cohesin ring opening if assuming a singular cohesin ring model (Gruber et al., 2003). The cohesin ring is predicted to be 40 nm in diameter while chromatin fibers and the replisome are projected to be 10 nm and 20 nm in size, respectively (Ivanov & Nasmyth, 2005). With these measurements, the cohesin ring should be large enough to encircle the replisome and two chromatin fibers. Use of single molecule analysis and engineered obstacles for pass over by cohesin rings were constructed to test the dynamics of cohesin ring passage. Their results suggest that the limit for passage of cohesin over DNA bound proteins is between 10.6 and 19.5 nm. The replisome being approximately 20 nm in size indicates that it is unable to physically pass

through cohesin rings. The authors of this paper suggest the previously described rod model in which the cohesin ring collapses to decrease the diameter of the ring is a viable option based off of their data (Stigler et al., 2016). An alternative mechanism could be that Eco1 activity is required to transiently open up the ring as the replisome passes through (Hu et al., 2011).

#### *Balancing Cohesion Establishment and Anti-Establishment*

Once the cohesin ring has been converted to its more stable cohesion form, maintenance factors are required to sustain the cohesive state to inhibit anti-establishment factors from prematurely removing cohesion. Maintenance factors dynamically act on the newly established cohesion rings from S phase through mitosis. One main player in cohesion maintenance is a protein called Sororin. This protein was discovered in a *Xenopus* screen for additional substrates of the APC/C (Rankin et al., 2005). Yeast does not have a Sororin ortholog, yet in other systems it is essential and shows similar cohesion defects as Eco1 mutants (Rankin et al., 2005; Schmitz et al., 2007). Protein interaction studies show that Sororin is recruited by PDS5 after cohesion establishment occurs and physically binds to RAD21 via its C-terminal domain (Figure 7) (Nishiyama et al., 2010; Schmitz et al., 2007; Wu et al., 2011). It is cell-cycle regulated by specific targeting to the proteasome at the metaphase-anaphase transition (Rankin et al., 2005).

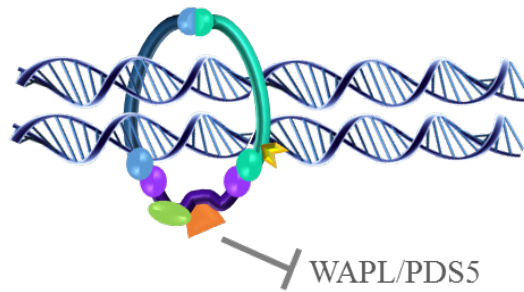


**Figure 7: SORORIN Recruitment Blocks Anti-Establishment Activity**

Sororin's main role in cohesion maintenance is antagonizing the anti-establishment factors, WAPL and PDS5, which are necessary for cohesion removal in prophase (Figure 7) (Ladurner et al., 2016; Nishiyama et al., 2010). WAPL was originally identified in *Drosophila* (Verni et al., 2000). Different effects of WAPL depletion are observed across species. The original *Drosophila* data investigating WAPL mutants show mild cohesion defects at the centromere. In other species, the role of WAPL does not lie in cohesion establishment but removal of cohesion. *S. pombe* mutants behave similar to human cell culture data in that depletion of WAPL displays overly-cohesed chromosomes and poor sister chromatid resolution (Bernard et al., 2008; Gandhi et al., 2006; Kueng et al., 2006; Rowland et al., 2009). Physically, WAPL has been shown to depend on the scaffold proteins RAD21, STAG1, and STAG2 for cohesin binding and subsequent cohesion removal (Gandhi et al., 2006; Kueng et al., 2006). Similarly, PDS5 has been coined as another anti-establishment factor critical in cohesion removal. Protein interaction studies suggest that PDS5 forms a complex with WAPL, RAD21, and STAG1/STAG2 in a cohesin-dependent manner (Chatterjee et al., 2013; Ouyang et al.,

2013; Rowland et al., 2009). Of the four proteins, PDS5 appears to have the weakest association between all protein interactions (Hartman et al., 2000; Panizza et al., 2000).

PDS5 is an interesting protein as it has different roles in yeast, fly and worm compared to more complex vertebrate systems. In budding yeast, fly, and worm, PDS5 is required for viability due to cohesion defects whereas in mouse and human no cohesion defects are observed (Hartman et al., 2000; Tanaka et al., 2001; B. Zhang et al., 2009). This is very similar to the case with WAPL suggesting that the cohesion removal process has evolved different functions over time. Unclear roles could also be due to the fact that frog, fish, mouse, and humans harbor two paralogs of PDS5, PDS5A and PDS5B. PDS5 has recently been characterized as having positive functions in establishing cohesion as well as negative functions by working with WAPL to enact anti-establishment removal which lends to the complex nature of this protein (Losada et al., 2005; Minamino et al., 2015).

One of the more interesting aspects of cohesion is the genetic interactions between cohesion establishment/maintenance proteins and its anti-establishment counterparts. This dynamic relationship begins right after cohesion establishment via the ESCO1/ESCO2 acetylation of SMC3. Sequentially, Sororin binds and physically destabilizes the WAPL-PDS5 interaction with the cohesin ring (Nishiyama et al., 2010; Skibbens, 2009; Terret et al., 2009). Sororin and WAPL interact at the genetic level in that WAPL depletion can rescue Sororin-dependent cohesion defects (Nishiyama et al., 2010). Expanding on this trend, loss of PDS5 or WAPL rescues ESCO2 mutant cohesion defects and lethality across species (Gandhi et al., 2006; Kueng et al., 2006; Nishiyama et al., 2010; Rowland et al., 2009; Tanaka et al., 2001). Looking forward, these genetic

interactions will become important in understanding the role of cohesion in human disease.

### *Cohesion Removal in Mitosis*

Early on, researchers speculated there was a connection between cohesion that regulates chromosome segregation and the spindle assembly checkpoint (SAC) (Irniger et al., 1995; King et al., 1995; Sudakin et al., 1995). The spindle assembly checkpoint and cohesion pathways each work together to ensure proper segregation. In the absence of sister chromatid pairing, the SAC is activated while inversely, activation of the SAC prevents cohesin cleavage. Cohesion creates tension by opposing spindle forces to indicate correct microtubule attachment and create biorientation of chromosomes (Ocampo-Hafalla et al., 2007; Z. Tang et al., 2004; Uhlmann et al., 1999).

### *The Prophase Pathway*

Cohesion removal is a two-step process (Peters et al., 2008; Sumara et al., 2000; Waizenegger et al., 2000). Step one is called the prophase pathway which involves removal of intact cohesion rings around sister chromatid arms. 90% of cohesion is removed during this time in order to quickly associate with chromatin during telophase and G1 (Peters et al., 2008). Removal of cohesion around chromosome arms is what is responsible for generating the classic “X” morphology of chromosomes that is observed in metaphase spreads.

The prophase pathway begins with SORORIN phosphorylation by polo like kinase 1 (PLK1) (Figure 8). This initiates the anti-establishment complex of WAPL and

PDS5 to act on the cohesion rings for removal (Dreier et al., 2011; Nishiyama et al., 2010; N. Zhang et al., 2011). Additional steps for WAPL-PDS5 to interact with the cohesin ring include STAG1/STAG2's C-terminal end phosphorylation by CDK1 and PLK1 (Hauf et al., 2005; Liu et al., 2013; Losada et al., 2002; Schmitz et al., 2007; Sumara et al., 2002). Non-phosphorylatable STAG2 has been shown to decrease cohesion dissociation similar to the observed effects in WAPL depleted cultures (Hauf et al., 2005). As well, depletion of WAPL and PDS5 in *Xenopus* reduces cohesion dissociation during the prophase removal pathway (Shintomi & Hirano, 2009). Conversely, overexpression of WAPL led to enhanced cohesion removal and precocious sister chromatid separation (Peters et al., 2008).

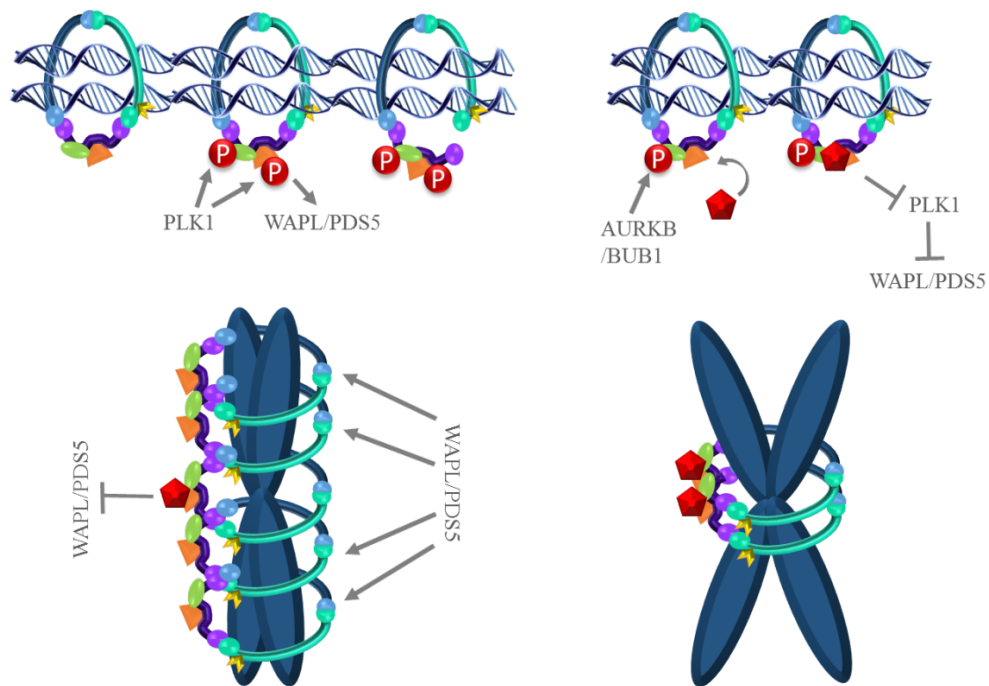


**Figure 8: Prophase Removal Pathway**

At the same time SORORIN and other cohesin proteins are being modified for cohesion removal, a separate pathway is initiated to protect centromeric cohesion during the remainder of mitosis. This step is necessary for proper segregation and use in creating tension for the spindle assembly checkpoint. AURORA KINASE B (AURKB) phosphorylation of STAG1/STAG2 and histone phosphorylation via budding uninhibited by benzimidazoles (BUB1) on H2A-pT120 recruits a protein called SHUGOSHIN (SGO) to the centromere via the chromosome passenger complex (Figure 8)(Kerrebrock et al., 1995; Liu et al., 2015). SGO, meaning “guardian spirit” in Japanese, is a centromere-specific maintenance factor critical for ensuring cohesion remains secure around the centromere until proper microtubule attachment. SGO was discovered in *Drosophila* as Mei-S332 (Sandler, 1974). SGO contains a functional coiled coil domain that binds protein phosphatase 2A (PP2A), a phosphatase that actively reverses AUKB and PLK1 activity to prevent premature cohesion removal at the centromere (Riedel et al., 2006; J. Tang et al., 2006). Aberrant SGO is shown to localize to chromosome arms in the absence of anti-establishment factors, however PP2A does not follow suggesting additional centromeric factors are required to localize PP2A. This potentially proposes an alternative role for SGO at these sites in the absence of anti-establishment factors (Shintomi & Hirano, 2009).

Higher eukaryotes have two SGO paralogs, SHUGOSHIN LIKE 1 and SHUGOSHIN LIKE 2 (SGOL1 and SGOL2). SGOL1 functions during mitosis whereas SGOL2 functions primarily in meiosis (Gomez et al., 2007; Llano et al., 2008; McGuinness et al., 2005; Salic et al., 2004). There has been some evidence to suggest that SGOL2 also plays a role in centromeric cohesion and biorientation of the spindle

giving SGOL2 a dual function in both meiosis and mitosis (Kitajima et al., 2006; Lee et al., 2008; Orth et al., 2011). Interestingly, SGOL1 localization at the centromere is also dependent on ribonucleic acid polymerase II (RNA pol II) activity. Active transcription at the centromere is suggested to aid in localizing SGOL1 deep into centromeric chromatin regions (Hara et al., 2014; Liu et al., 2015). In the presence of SGOL1, SORORIN is not phosphorylated due to PP2A action; therefore WAPL is unable to bind to cohesin (Hara et al., 2014).

Our understanding of the mechanism of cohesion removal during the prophase pathway is still in its infancy; however there are a few insights into how this removal process spares intact cohesin rings. In conjunction with SORORIN removal, phosphorylation of STAG1 and STAG2 is hypothesized to trigger a conformational change of WAPL and PDS5 to contact the cohesin ring. It is this WAPL-PDS5 association that is suggested to influence the ATPase binding pocket to hydrolyze ATP to release intact cohesion. The exit gate for cohesion removal is believed to be at the SMC3-RAD21 interface, a different interface than that of the hinge entry gate (Beckouet et al., 2016; Camdere et al., 2015; Elbatsh et al., 2016; Murayama & Uhlmann, 2015; Peters et al., 2008). Fusion of the SMC3-RAD21 interface prevents cohesion removal in interphase in both yeast and HeLa cell culture in a WAPL-dependent manner (Beckouet et al., 2016; Buheitel & Stemmann, 2013; Chan et al., 2012). Inversely, destabilization of this interface results in precocious sister chromatid separation (Huis in 't Veld et al., 2014). It is still unknown as to how exactly acetylation stabilizes the cohesin ring structurally or why two separate openings are necessary.

### *Cohesin Ring Cleavage*

Step two of the removal process involves proteolytic cleavage of the RAD21 portion of the cohesion rings concentrated at the centromere. This population of cohesion is unable to reassociate with chromatin post-mitosis but plays a vital role in creating tension necessary for biorientation and microtubule attachment at the metaphase-anaphase transition. Cleavage of RAD21 removes centromeric cohesion by actions of the cysteine protease, SEPARASE (Figure 9) (Hauf et al., 2001; Kumada et al., 2006; Nakajima et al., 2007; Uhlmann et al., 1999; Wirth et al., 2006). SEPARASE activation process begins with biorientation of chromosomes in metaphase. Proper microtubule attachment to kinetochores satisfies the spindle assembly checkpoint and initiates a cascade of events beginning with cell division cycle 20 (CDC20) being released from APC/C (Izawa & Pines, 2015). CDC20 dissociation frees SECURIN from SEPARASE and targets SECURIN, along with CYCLIN B, to the APC/C for degradation (Musacchio & Salmon, 2007; Nasmyth, 2005; Uhlmann et al., 2000). At this point, free SEPARASE is permitted to cleave RAD21 (Y. Sun et al., 2009; Waizenegger et al., 2000). SGOL1 is redistributed to the kinetochore for RAD21 cleavage and degraded by the APC/C (Fu et al., 2007; Karamysheva et al., 2009; Liu et al., 2015).

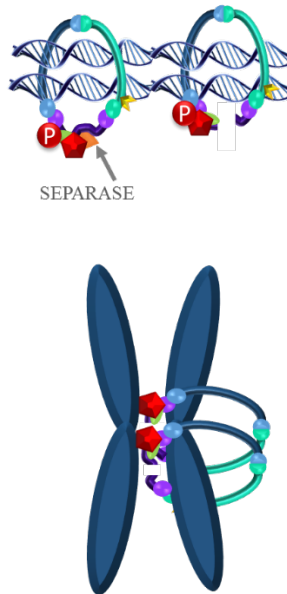


**Figure 9: Cohesin Ring Cleavage**

To complete the cohesion cycle and re-license cohesin rings for cohesion establishment in the next cell cycle, cohesin rings that are removed by the prophase pathway must be deacetylated. This process was initially discovered when studies found that SMC3 acetylation decreases in telophase. Had 1 similar (Hos1) was the first deacetylase discovered to remove SMC3 K112 and K113 acetylation in G1 (Borges et al., 2010; Xiong et al., 2010). Later in 2012, Deardorff et al discovered the vertebrate deacetylase, histone deacetylase 8 (HDAC8) that has deacetylase activity starting in anaphase to ensure naïve cohesin rings are prepared for their cellular functions in the next cell cycle.

The complexity of the cohesion removal process lends to its intricate regulation. The two step removal process evolved from a one-step removal process that was originally characterized in yeast. It is suggested that an additional removal pathway provides another level of control to the process even though, theoretically, SEPARASE

activity on RAD21 is enough to completely disengage sister chromatids (Kueng et al., 2006). It has also been suggested that the prophase pathway could aid in decatenation of sister chromatids and/or readily available re-association of cohesin rings for gene expression regulation (Nasmyth & Haering, 2009).

#### *Non-canonical SCC Roles: Regulation of Gene Expression*

The above description details the canonical or “cohesion” SCC process. Recently, SCC has been discovered to have other cellular functions in gene expression, DNA repair, and centriole disengagement. Arguably the most well documented of the non-canonical SCC roles is gene expression. Studies show that the stability of cohesin rings around chromatids falls into two populations: those that are considered to be the stable rings around sister chromatids involved in cohesion establishment for proper segregation and those that are stable rings around single chromatids creating intra-chromatid cohesion likely to be involved in gene expression (Gerlich et al., 2006).

Chromatin is organized into approximately 2,000 topologically associated domains (TAD). From there, the genome architecture can then be divided into two categories: short range interactions that mediate enhancer-promoter contacts for singular/gene family expression and long-range interactions that structure the chromatin into topological areas for genome organization, i.e. TADs (Tolhuis et al., 2002). In terms of short range interactions, DNA creates loops between enhancers and promoters to either enhance or inhibit gene expression. These short range interactions are often regulated by CTCF. Cohesin-dependent gene expression often requires CTCF for recruitment to gene promoters to aid in DNA looping. CTCF was first characterized as a vertebrate

transcription factor, and shown to insulate genomic regions at their boundaries (Felsenfeld et al., 2000; Hark et al., 2000; Klenova et al., 1993; Lobanenko et al., 1990). It was later discovered that TAD domains are generally defined by CTCF binding (Dixon et al., 2012). Shorter range CTCF domains aid in chromatin loops that regulate enhancer and promoter distance (Lengronne et al., 2004; Merkenschlager & Odom, 2013). More specifically, Doyle et al 2014 suggested that elements within a CTCF boundary are expressed while elements that are outside CTCF boundaries are blocked. An example of CTCF gene expression regulation is their function within homeobox (HOX) domains in embryonic stem cells. Using clustered regularly interspersed palindromic repeats/CRISPR associated protein 9 (CRISPR/Cas9), CTCF binding site deletion in a HOX domain was found to activate previously silenced genes and disrupted the TAD associated with this region (Narendra et al., 2015). The number of CTCF sites necessary for transcriptional regulation is currently not known.

The colocalization of cohesin and CTCF is well documented in the literature (Horsfield et al., 2007; Parelho et al., 2008; Rubio et al., 2008; Stedman et al., 2008; Wendt et al., 2008). Cohesin localizes to a range of 10,000 to 60,000 sites depending on the assay and 60% of these sites are also bound by CTCF (Kagey et al., 2010; Schmidt et al., 2010; Wendt et al., 2008; Zuin et al., 2014). Using chromosome conformation capture carbon copy (5C), researchers found that CTCF and SMC1 co-localize approximately 80% of time in embryonic stem cells (Sanyal et al., 2012). This type of analysis has a relatively short coverage therefore the percentage of colocalization should be understood to be limited and does not apply to the whole genome (de Wit & de Laat, 2012). In terms of the cell cycle, the loading complex shows a role in localization of cohesin to gene

promoters (Kagey et al., 2010). Interestingly, ESCO1 acetylates cohesin at CTCF sites throughout the cell cycle to mediate gene silencing (Minamino et al., 2015; Rahman et al., 2015). This suggests that its paralog, ESCO2, plays the primary role in the canonical SCC process.

What happens to the cohesin-CTCF DNA loops as cells undergo mitosis? There is an observed decrease in cohesin-bound CTCF sites in G2 and M phase although this is controversial due to other data suggesting it is not cell cycle regulated (Stedman et al., 2008; Wendt et al., 2008). Several groups suggest that loop structures are not maintained throughout the cell cycle but must be restructured after each cell division (Naumova et al., 2013; Sanborn et al., 2015). Still, there is no evidence showing intact cohesin rings around DNA but in situ approaches come close to this visualization (Jhunjhunwala et al., 2008). With the emergence of super-resolution microscopy, it is possible that visualization of cohesin rings along DNA is not far off.

#### *Non-canonical SCC Roles: DNA Repair*

SCC's role in DNA repair is less known, however at sites of double stranded DNA breaks, cohesin has been found to localize. It is suggested that cohesin rings aid in homologous recombination by using the ring structure to preserve homologous strand proximity for strand invasion. Eco1 mutants have overall lower repair rates but higher rates of homologous recombination. This suggests that functional cohesion establishment preferentially uses the sister chromatid for repair while defects in cohesion preferentially use homologous repair (Lu et al., 2010). Cohesin localization to sites of DNA damage is dependent on the loading complex NIPBL/MAU2 (Heidinger-Pauli et al., 2008). Cell

cycle checkpoint kinase 1 (CHK1) phosphorylation of RAD21 is the signal to establish cohesion outside of post-S phase. In yeast, the Eco1 target is K84 and K210 of Rad21 (Heidinger-Pauli et al., 2008; Strom et al., 2007; Strom & Sjogren, 2005; Unal et al., 2007). Cohesion establishment also occurs on chromosomes that are not damaged suggesting this could be an unregulated process and/or a mechanism to double check for any undetected breaks (Strom et al., 2007; Unal et al., 2007). Corresponding to its need for stabilization in cohesion establishment, SORORIN is necessary for DNA repair to maintain that stability (Schmitz et al., 2007).

Cohesin also has an independent role to recruit S-phase checkpoint proteins (Kim et al., 2002; Watrin et al., 2006). Ataxia –telangiectasia mutated/ataxia-telangiectasia and rad3-related (ATM/ATR) has been demonstrated to phosphorylate the SMC1 and SMC3 portions of the cohesin ring. In addition, CHK2 activation is shown to be dependent on cohesin in response to DNA damage (Watrin & Peters, 2009). There is still an unclear idea of whether the independent S-phase checkpoint functions work in conjunction with cohesin-dependent DNA repair or if these two pathways are unique and separate.

#### *Non-canonical SCC Roles: Centriole disengagement*

Similar to DNA, centrioles are replicated in S phase before their separation in prometaphase to initiate spindle pole formation (Sluder & Rieder, 1985). The initial discovery of a potential function of cohesin at centrioles was the observation that SEPARASE, the cysteine protease essential for centromeric cohesion cleavage, is necessary in centriole disengagement (Tsou & Stearns, 2006). It is still not clear if

centriole disengagement is a direct or indirect effect of cohesion dysfunction (Kong et al., 2009; Wong & Blobel, 2008).

The belief in a centriole-cohesin relationship was challenged recently by several groups. A study done by the Nasmyth group in *Drosophila* find no detectable differences in centriole disengagement in mitosis using an artificial cohesin cleavage model (Oliveira & Nasmyth, 2013). Interestingly, another group looked at Separase activity in *C.elegans* and noted centriolar defects during the meiotic to mitotic transition but no differences observed beyond that point. These confounding results suggest that cohesin could have a function in a context/tissue-dependent manner but is not essential for global centriole disengagement (Cabral et al., 2013). No establishment factors have been found to act on the cohesin ring involved, however one could imagine that if the cohesin ring is essential, a stabilization process for centriole pairing would not be unreasonable.

### *Cohesinopathies*

Despite their important roles in gene regulation, DNA repair, and cell division, five disorders have been characterized as cohesinopathies, a subset of developmental disorders caused by mutations in the SCC pathway (Remeseiro et al., 2013). These disorders include: 1) Cornelia de Lange syndrome (CdLS) caused by mutations in SMC1a, SMC3, NIPBL, RAD21, and HDAC8). 2) Roberts syndrome (RBS) caused by mutations in ESCO2. 3) Rothmund Thomson syndrome (RTS) caused by mutations in RECQ like protein 4 (RECQL4). 4) Warsaw Breakage syndrome (WBS) caused by mutations in DEAD/H BOX 11 (DDX11). 5) Chronic atrial and intestinal dysrhythmia syndrome (CAIDS) caused by mutations in SGOL1. While CdLS is considered to be a

disorder due to defects in G1 cohesin roles such as gene expression, RBS, RTS, WBS, and CAIDS are thought to be due to defects in cell division. Further dividing this group, CdLS is an autosomal dominant disorder while the remaining disorders are inherited in an autosomal recessive fashion. The focus of this study is in RBS and the unexplained variable phenotypes which will be discussed in the next section.

### *Roberts Syndrome*

Roberts syndrome (RBS) was first documented by John Roberts in 1919 describing a subset of patients with retrognathia, limb defects, hypertelorism, microcephaly, and mental retardation that often led to post-natal lethality. Fifty years later, J. Hermann described a similar disorder called SC phocomelia containing more mild versions of those same phenotypes. A decade later, a centromeric puffing in metaphase spreads, termed heterochromatic repulsion (HR), determined to be unique to RBS and SC phocomelia patients (Tomkins et al., 1979). This clinical finding suggests similar etiologies between the disorders and in 2005, Shule et al proposed combining both disorders under one name. RBS now describes a disorder encompassing patients with the originally described phenotype and those that were previously diagnosed with SC phocomelia.

RBS is a rare, autosomal recessive disorder. The largest study to date includes 49 patients and 39 families with 28 different mutations. Most mutations in ESCO2 result in a truncated protein leading to nonsense mediated decay. A few unique mutations in RBS patients to note are (1) a glutamic acid deletion in exon 9 (E451del) and (2) a missense mutation in the acetyltransferase domain (G581R). Beginning with the latter, a Guanine

to Cytosine (G→C) mutation was found that substitutes a Glycine for an Arginine in the acetyltransferase domain. The drastic change in structure perturbs the active domain of ESCO2. *In vitro* studies show that this mutation has no acetyltransferase activity. The glutamic acid deletion is similar in that it deletes a critical amino acid near the acetyltransferase domain. Interestingly, *in vitro* autoacetylation studies show this mutation has no effect on acetyltransferase activity (Vega et al., 2010). The underlying pathogenesis of this mutation and its role in RBS manifestation remains unclear.

To date, there is no genotype-phenotype correlation that has been established across several parameters including the type of mutation, the length of the mutant protein, and the domain harboring the mutation despite the drastic phenotypic spectrum (Vega et al., 2010). Although several have died in utero, at least nine adult cases of RBS have been documented (Goh et al., 2010). To illustrate this spectrum, a middle aged man entered a clinic for a query diagnosis for Noonan syndrome that required genetic analysis. Upon further inspection, metaphase spread analysis showed HR. Sequencing confirmed a frameshift mutation leading to a premature stop in exon 3 of ESCO2, which confirms an RBS diagnosis. His craniofacial defects were mild and his ability to complete college level courses pointed towards minor mental disabilities. The mechanism behind this drastic spectrum of phenotypes is still unresolved and thus the subject of this research.

Several animal models of ESCO2 loss have been essential to further understand RBS. Initially, a knockout mouse model of RBS was made to study the pathogenesis of loss of ESCO2. This model yielded early embryonic lethal ESCO2 null animals leading investigators to develop a conditional knockout mouse. To determine the neurological impacts of loss of ESCO2, an empty spiracles homeobox 1 (Emx1)-Cre recombinase

mouse is used to knockout ESCO2 in the cortex epithelium. In these studies, an increase in mitotic index and apoptosis is observed leading to severe microcephaly, a common phenotype associated with RBS. At the chromosome level, severe cohesion defects are observed (Whelan et al., 2012). However, tissue-specific consequences of ESCO2 loss outside of cortical progenitors has not been evaluated in a mouse model so it is unknown as to the consequence of ESCO2 loss in other tissues in a mammalian system.

Due to the embryonic lethality, many researchers, including ourselves, have turned to non-mammalian systems to answer questions about SCC's involvement in RBS. Using morpholino knockdown in zebrafish, Julia Horsfield's group determined that early embryonic lethality occurs with *Esco2* knockdown along with flawed fin development, increased apoptosis, and mitotic defects in. Importantly, this group discovered that developmentally regulated genes were not affected by knockdown of *Esco2* suggesting that gene expression changes are not the cause of RBS phenotypes. Further, those genes that are dysregulated in the zebrafish model of CdLS do not overlap with the dysregulated genes in the RBS model which fall under cell cycle regulation (Monnich et al., 2011). One caveat to these studies, however, is that knockdown does not accurately recapitulate RBS patients who typically lack functional ESCO2 activity. In addition, morpholinos are known for off-target effects and thus *Esco2* mutant studies are warranted for further analysis.

### *Gene Expression and Roberts Syndrome*

Despite the aggressive cell cycle defects, many authors attribute variable phenotypes in RBS to gene expression changes. Some of the first evidence was the co-

immunoprecipitation of ESCO2 with Notch 1 intracellular domain (NICD). However, many of these experiments were performed using transfected 293T cells that do not represent the physiological stoichiometry of ESCO2 or NICD. As well, many of these experiments utilized knockdown methodology instead of knockout which may not be physiologically relevant to RBS patients with truncation mutations (Leem et al., 2011). Gerton et al 2016 describes differences in mitochondrial and small nucleolar RNA gene expression (B. Xu et al., 2016). If metabolic defects are present, one would expect to observe gene expression changes in these pathways further suggesting expression changes are a consequence of ribosomal/mitochondrial dysfunction and not a cause (See Ribosome Biogenesis in RBS). This principal is illustrated in an *Esco2* zebrafish morphant study. Monnich et al. 2012 provides evidence that gene expression changes in cell cycle genes are, in fact, unchanged in a zebrafish model of RBS. This study concludes that while cell cycle genes are altered in response to the knockdown of *Esco2* (a consequence of improper mitoses), developmentally regulated genes such as runt related transcription factor 1 (*runx1*) are not altered. Furthermore, there is no overlap between gene expression changes of *Rad21* and *Esco2* knockdown suggesting the mechanisms behind Cornelia de Lange syndrome are drastically different than that of RBS. Strong evidence showing gene expression changes of developmentally regulated pathways in RBS models is yet to be discovered.

### *Ribosome Biogenesis and Roberts Syndrome*

A new, surfacing mechanism behind RBS pathogenesis involves defective ribosome biogenesis. Ribosome biogenesis defects lead to nucleolar defects and are

shown to activate p53 (Fumagalli et al., 2009; Lindstrom et al., 2007; W. Zhang et al., 2009). Ribosomal DNA (rDNA) is affected in RBS leading to dysregulation of protein synthesis and production. These defects, in addition to nucleolar defects, have been observed in yeast and human cell culture (Bose et al., 2012; Gardiner, 2010).

Gerton et al. publishes extensively on the effects of ribosome biogenesis in RBS. RBS cell lines from patients exhibit decreased proliferation, rRNA production, and protein synthesis. Surprisingly, activation of the mechanistic target of rapamycin (mTOR) pathway shows partial rescue of cohesion defects via L-leucine administration in RBS cell lines and ESCO2 zebrafish mutants (B. Xu et al., 2013). mTOR is a prominent pathway involved in ribosome biogenesis (Holzel et al., 2005; Zoncu et al., 2011). L-leucine activates leucyl-transfer ribonucleic acid (tRNA) synthase that activates guanosine triphosphate (GTP) activating proteins that promote the protein synthesis pathway, mTOR (Bonfils et al., 2012; Han et al., 2012). Interestingly, our lab is unable to repeat the partial rescue in our *esco2* mutant calling into question these conclusions.

Interestingly, ribosome biogenesis defects are also observed in SMC1 and SMC3 yeast mutants suggesting this mechanism could apply to overall defects in SCC and not defects specific to ESCO2 alone (Bose et al., 2012). In addition, ribosomal defects have been observed in Warsaw breakage syndrome (X. Sun et al., 2015). Similar to cohesinopathies, there is a subset of developmental disorders caused by mutations in the ribosome biogenesis pathway called ribosomopathies. Unlike cohesinopathies, particularly RBS in which there is a vast pleiotropic effect that accounts for the lethal to viable adult spectrum of phenotypes, ribosomopathies have distinct clinical features that affect discrete cell populations that often lack a phenotypic spectrum (Choismel et al.,

2008; Narla & Ebert, 2010; Sakai & Trainor, 2009). Ribosome biogenesis could be the underlying common pathogenic consequence between all cohesinopathies, not gene expression or cell cycle defects. If true, then what is the mechanism behind the spectrum of phenotypes observed in RBS?

### *Scientific Voids in Cohesion Establishment*

Current research attempts to address the role of sister chromatid cohesion while understanding the implications of its function and role in human development and disease. With that being said, there are considerable questions and details remaining that require proper elucidation. The data presented in this dissertation addresses several of these scientific voids relating to cohesion establishment, RBS and other cohesinopathies utilizing high resolution, in vivo confocal microscopy and CRISPR/Cas9 genome editing.

#### *1. Understanding the pathogenesis of RBS: What is the cause of lethality in the absence of Esco2?*

Embryonic loss of ESCO2 in mouse is embryonic lethal (Whelan et al., 2012). Though cell culture studies are performed to overcome this lethality, in order to address cellular defects associated with Roberts syndrome, an organismal model is necessary. Zebrafish are a great model system to address this concern. Morpholino knockdown of Esco2 in zebrafish is able to address several organismal consequences of Esco2 loss showing fin and cartilage

defects. More importantly it shows that the mitotic defects are associated with cell lethality compared to gene expression alterations (Monnich et al., 2011). This study did not address the variable phenotypes associated with RBS in a genetic mutant and how RBS phenotypic variability may result at the cellular level. **Therefore, we investigate the hypothesis that, with the aid of high resolution *in vivo* imaging of cell divisions, the presence of variable mitotic defects will be detected in *esco2* mutants that lead to variable phenotypes.**

2. *How does gene dosage of *Esco2* affect cohesion at the cellular and organismal level?*

Although *esco2* heterozygous animals are viable, little is known of any gene dose effects of *Esco2* on cohesion function. Gene dose contributions are observed in other SCC genes such as *PDS5A*, *PDS5B*, and *SGOL1* and are linked to increased tumorigenesis or developmental defects (Yamada et al., 2012; B. Zhang et al., 2007). In addition, CdLS is a heterozygous disorder in that it is inherited in an autosomal dominant manner. However, only transient gene dose effects have been observed in an *esco2* morphant study showing that dose-dependent effects are based on the extent of knockdown (Monnich et al., 2011). **Based on preliminary data, we hypothesized that *Esco2* heterozygosity leads to mild cohesion defects that are viable but will result in a mild adult phenotype.**

3. *What is the role of the essential cohesion establishment (Esco1) and maintenance factors (ShugoshinL1 and Sororin) in vivo?*

Cohesion establishment utilizes establishment factors (ESCO1/ESCO2) and maintenance factors (SORORIN/SHUGOSHINL1) to ensure cohesion rings are stabilized until the metaphase-anaphase transition. Many of these genes are embryonic lethal in animal and cell culture models (Ladurner et al., 2016; Minamino et al., 2015; Yamada et al., 2012). In order to understand cohesion establishment in an *in vivo*, vertebrate, multi-cellular organism, we utilize CRISPR/Cas9 genome editing to generate zebrafish mutants in Esco1, ShugoshinL1, and Sororin. **We hypothesize the genes involved in cohesion establishment and maintenance (Esco1, ShugoshinL1, and Sororin) will exhibit severe cohesion defects and embryonic lethality due to their role in the essential process of cohesion establishment.**

## INTRODUCTION REFERENCES

- Anderson, D. E., Losada, A., Erickson, H. P., & Hirano, T. (2002). Condensin and cohesin display different arm conformations with characteristic hinge angles. *J Cell Biol*, *156*(3), 419-424. doi: 10.1083/jcb.200111002
- Arumugam, P., Gruber, S., Tanaka, K., Haering, C. H., Mechtler, K., & Nasmyth, K. (2003). ATP hydrolysis is required for cohesin's association with chromosomes. *Curr Biol*, *13*(22), 1941-1953.
- Beckouet, F., Srinivasan, M., Roig, M. B., Chan, K. L., Scheinost, J. C., Batty, P., . . . Nasmyth, K. (2016). Releasing Activity Disengages Cohesin's Smc3/Sccl Interface in a Process Blocked by Acetylation. *Mol Cell*, *61*(4), 563-574. doi: 10.1016/j.molcel.2016.01.026
- Bernard, P., Drogat, J., Maure, J. F., Dheur, S., Vaur, S., Genier, S., & Javerzat, J. P. (2006). A screen for cohesion mutants uncovers Ssl3, the fission yeast counterpart of the cohesin loading factor Sccl. *Curr Biol*, *16*(9), 875-881. doi: 10.1016/j.cub.2006.03.037
- Bernard, P., Schmidt, C. K., Vaur, S., Dheur, S., Drogat, J., Genier, S., . . . Javerzat, J. P. (2008). Cell-cycle regulation of cohesin stability along fission yeast chromosomes. *EMBO J*, *27*(1), 111-121. doi: 10.1038/sj.emboj.7601955
- Bonfils, G., Jaquenoud, M., Bontron, S., Ostrowicz, C., Ungermann, C., & De Virgilio, C. (2012). Leucyl-tRNA synthetase controls TORC1 via the EGO complex. *Mol Cell*, *46*(1), 105-110. doi: 10.1016/j.molcel.2012.02.009
- Borges, V., Lehane, C., Lopez-Serra, L., Flynn, H., Skehel, M., Rolef Ben-Shahar, T., & Uhlmann, F. (2010). Hos1 deacetylates Smc3 to close the cohesin acetylation cycle. *Mol Cell*, *39*(5), 677-688. doi: 10.1016/j.molcel.2010.08.009
- Bose, T., Lee, K. K., Lu, S., Xu, B., Harris, B., Slaughter, B., . . . Gerton, J. L. (2012). Cohesin proteins promote ribosomal RNA production and protein translation in yeast and human cells. *PLoS Genet*, *8*(6), e1002749. doi: 10.1371/journal.pgen.1002749
- Britton, R. A., Lin, D. C., & Grossman, A. D. (1998). Characterization of a prokaryotic SMC protein involved in chromosome partitioning. *Genes Dev*, *12*(9), 1254-1259.
- Buheitel, J., & Stemmann, O. (2013). Prophase pathway-dependent removal of cohesin from human chromosomes requires opening of the Smc3-Sccl gate. *EMBO J*, *32*(5), 666-676. doi: 10.1038/emboj.2013.7
- Cabral, G., Sans, S. S., Cowan, C. R., & Dammermann, A. (2013). Multiple mechanisms contribute to centriole separation in *C. elegans*. *Curr Biol*, *23*(14), 1380-1387. doi: 10.1016/j.cub.2013.06.043
- Camdere, G., Guacci, V., Stricklin, J., & Koshland, D. (2015). The ATPases of cohesin interface with regulators to modulate cohesin-mediated DNA tethering. *Elife*, *4*. doi: 10.7554/eLife.11315
- Chan, K. L., Roig, M. B., Hu, B., Beckouet, F., Metson, J., & Nasmyth, K. (2012). Cohesin's DNA exit gate is distinct from its entrance gate and is regulated by acetylation. *Cell*, *150*(5), 961-974. doi: 10.1016/j.cell.2012.07.028

- Chatterjee, A., Zakian, S., Hu, X. W., & Singleton, M. R. (2013). Structural insights into the regulation of cohesion establishment by Wpl1. *EMBO J*, *32*(5), 677-687. doi: 10.1038/emboj.2013.16
- Choemmel, V., Fribourg, S., Aguisa-Toure, A. H., Pinaud, N., Legrand, P., Gazda, H. T., & Gleizes, P. E. (2008). Mutation of ribosomal protein RPS24 in Diamond-Blackfan anemia results in a ribosome biogenesis disorder. *Hum Mol Genet*, *17*(9), 1253-1263. doi: 10.1093/hmg/ddn015
- Ciosk, R., Shirayama, M., Shevchenko, A., Tanaka, T., Toth, A., Shevchenko, A., & Nasmyth, K. (2000). Cohesin's binding to chromosomes depends on a separate complex consisting of Scc2 and Scc4 proteins. *Mol Cell*, *5*(2), 243-254.
- de Wit, E., & de Laat, W. (2012). A decade of 3C technologies: insights into nuclear organization. *Genes Dev*, *26*(1), 11-24. doi: 10.1101/gad.179804.111
- Dixon, M. J., Gray, A., Schenning, M., Agacan, M., Tempel, W., Tong, Y., . . . Batty, I. H. (2012). IQGAP proteins reveal an atypical phosphoinositide (aPI) binding domain with a pseudo C2 domain fold. *J Biol Chem*, *287*(27), 22483-22496. doi: 10.1074/jbc.M112.352773
- Downes, C. S., Mullinger, A. M., & Johnson, R. T. (1991). Inhibitors of DNA topoisomerase II prevent chromatid separation in mammalian cells but do not prevent exit from mitosis. *Proc Natl Acad Sci U S A*, *88*(20), 8895-8899.
- Dreier, M. R., Bekier, M. E., 2nd, & Taylor, W. R. (2011). Regulation of sororin by Cdk1-mediated phosphorylation. *J Cell Sci*, *124*(Pt 17), 2976-2987. doi: 10.1242/jcs.085431
- Elbatsh, A. M., Haarhuis, J. H., Petela, N., Chapard, C., Fish, A., Celie, P. H., . . . Rowland, B. D. (2016). Cohesin Releases DNA through Asymmetric ATPase-Driven Ring Opening. *Mol Cell*, *61*(4), 575-588. doi: 10.1016/j.molcel.2016.01.025
- Eng, T., Guacci, V., & Koshland, D. (2015). Interallelic complementation provides functional evidence for cohesin-cohesin interactions on DNA. *Mol Biol Cell*, *26*(23), 4224-4235. doi: 10.1091/mbc.E15-06-0331
- Felsenfeld, G., Clark, D., & Studitsky, V. (2000). Transcription through nucleosomes. *Biophys Chem*, *86*(2-3), 231-237.
- Filipski, J., & Mucha, M. (2002). Structure, function and DNA composition of *Saccharomyces cerevisiae* chromatin loops. *Gene*, *300*(1-2), 63-68.
- Fu, G., Ding, X., Yuan, K., Aikhionbare, F., Yao, J., Cai, X., . . . Yao, X. (2007). Phosphorylation of human Sgo1 by NEK2A is essential for chromosome congression in mitosis. *Cell Res*, *17*(7), 608-618. doi: 10.1038/cr.2007.55
- Fumagalli, S., Di Cara, A., Neb-Gulati, A., Natt, F., Schwemberger, S., Hall, J., . . . Thomas, G. (2009). Absence of nucleolar disruption after impairment of 40S ribosome biogenesis reveals an rpL11-translation-dependent mechanism of p53 induction. *Nat Cell Biol*, *11*(4), 501-508. doi: 10.1038/ncb1858
- Funabiki, H., Hagan, I., Uzawa, S., & Yanagida, M. (1993). Cell cycle-dependent specific positioning and clustering of centromeres and telomeres in fission yeast. *J Cell Biol*, *121*(5), 961-976.
- Gambus, A., Jones, R. C., Sanchez-Diaz, A., Kanemaki, M., van Deursen, F., Edmondson, R. D., & Labib, K. (2006). GINS maintains association of Cdc45

- with MCM in replisome progression complexes at eukaryotic DNA replication forks. *Nat Cell Biol*, 8(4), 358-366. doi: 10.1038/ncb1382
- Gandhi, R., Gillespie, P. J., & Hirano, T. (2006). Human Wapl is a cohesin-binding protein that promotes sister-chromatid resolution in mitotic prophase. *Curr Biol*, 16(24), 2406-2417. doi: 10.1016/j.cub.2006.10.061
- Gardiner, K. J. (2010). Molecular basis of pharmacotherapies for cognition in Down syndrome. *Trends Pharmacol Sci*, 31(2), 66-73. doi: 10.1016/j.tips.2009.10.010
- Gerlich, D., Koch, B., Dupeux, F., Peters, J. M., & Ellenberg, J. (2006). Live-cell imaging reveals a stable cohesin-chromatin interaction after but not before DNA replication. *Curr Biol*, 16(15), 1571-1578. doi: 10.1016/j.cub.2006.06.068
- Gillespie, P. J., & Hirano, T. (2004). Scc2 couples replication licensing to sister chromatid cohesion in *Xenopus* egg extracts. *Curr Biol*, 14(17), 1598-1603. doi: 10.1016/j.cub.2004.07.053
- Gligoris, T. G., Scheinost, J. C., Burmann, F., Petela, N., Chan, K. L., Uluocak, P., . . . Lowe, J. (2014). Closing the cohesin ring: structure and function of its Smc3-kleisin interface. *Science*, 346(6212), 963-967. doi: 10.1126/science.1256917
- Glynn, E. F., Megee, P. C., Yu, H. G., Mistrot, C., Unal, E., Koshland, D. E., . . . Gerton, J. L. (2004). Genome-wide mapping of the cohesin complex in the yeast *Saccharomyces cerevisiae*. *PLoS Biol*, 2(9), E259. doi: 10.1371/journal.pbio.0020259
- Goh, E. S., Li, C., Horsburgh, S., Kasai, Y., Kolomietz, E., & Morel, C. F. (2010). The Roberts syndrome/SC phocomelia spectrum--a case report of an adult with review of the literature. *Am J Med Genet A*, 152A(2), 472-478. doi: 10.1002/ajmg.a.33261
- Gomez, R., Valdeolillos, A., Parra, M. T., Viera, A., Carreiro, C., Roncal, F., . . . Suja, J. A. (2007). Mammalian SGO2 appears at the inner centromere domain and redistributes depending on tension across centromeres during meiosis II and mitosis. *EMBO Rep*, 8(2), 173-180. doi: 10.1038/sj.embor.7400877
- Gruber, S., Arumugam, P., Katou, Y., Kuglitsch, D., Helmhart, W., Shirahige, K., & Nasmyth, K. (2006). Evidence that loading of cohesin onto chromosomes involves opening of its SMC hinge. *Cell*, 127(3), 523-537. doi: 10.1016/j.cell.2006.08.048
- Gruber, S., Haering, C. H., & Nasmyth, K. (2003). Chromosomal cohesin forms a ring. *Cell*, 112(6), 765-777.
- Guacci, V., Koshland, D., & Strunnikov, A. (1997). A direct link between sister chromatid cohesion and chromosome condensation revealed through the analysis of MCD1 in *S. cerevisiae*. *Cell*, 91(1), 47-57.
- Haering, C. H., Lowe, J., Hochwagen, A., & Nasmyth, K. (2002). Molecular architecture of SMC proteins and the yeast cohesin complex. *Mol Cell*, 9(4), 773-788.
- Haering, C. H., Schoffnegger, D., Nishino, T., Helmhart, W., Nasmyth, K., & Lowe, J. (2004). Structure and stability of cohesin's Smc1-kleisin interaction. *Mol Cell*, 15(6), 951-964. doi: 10.1016/j.molcel.2004.08.030
- Han, J. M., Jeong, S. J., Park, M. C., Kim, G., Kwon, N. H., Kim, H. K., . . . Kim, S. (2012). Leucyl-tRNA synthetase is an intracellular leucine sensor for the mTORC1-signaling pathway. *Cell*, 149(2), 410-424. doi: 10.1016/j.cell.2012.02.044

- Hara, K., Zheng, G., Qu, Q., Liu, H., Ouyang, Z., Chen, Z., . . . Yu, H. (2014). Structure of cohesin subcomplex pinpoints direct shugoshin-Wapl antagonism in centromeric cohesion. *Nat Struct Mol Biol*, *21*(10), 864-870. doi: 10.1038/nsmb.2880
- Hark, A. T., Schoenherr, C. J., Katz, D. J., Ingram, R. S., Levorse, J. M., & Tilghman, S. M. (2000). CTCF mediates methylation-sensitive enhancer-blocking activity at the H19/Igf2 locus. *Nature*, *405*(6785), 486-489. doi: 10.1038/35013106
- Hartman, T., Stead, K., Koshland, D., & Guacci, V. (2000). Pds5p is an essential chromosomal protein required for both sister chromatid cohesion and condensation in *Saccharomyces cerevisiae*. *J Cell Biol*, *151*(3), 613-626.
- Hauf, S., Roitinger, E., Koch, B., Dittrich, C. M., Mechtler, K., & Peters, J. M. (2005). Dissociation of cohesin from chromosome arms and loss of arm cohesion during early mitosis depends on phosphorylation of SA2. *PLoS Biol*, *3*(3), e69. doi: 10.1371/journal.pbio.0030069
- Hauf, S., Waizenegger, I. C., & Peters, J. M. (2001). Cohesin cleavage by separase required for anaphase and cytokinesis in human cells. *Science*, *293*(5533), 1320-1323. doi: 10.1126/science.1061376
- Heidinger-Pauli, J. M., Onn, I., & Koshland, D. (2010). Genetic evidence that the acetylation of the Smc3p subunit of cohesin modulates its ATP-bound state to promote cohesion establishment in *Saccharomyces cerevisiae*. *Genetics*, *185*(4), 1249-1256. doi: 10.1534/genetics.110.116871
- Heidinger-Pauli, J. M., Unal, E., Guacci, V., & Koshland, D. (2008). The kleisin subunit of cohesin dictates damage-induced cohesion. *Mol Cell*, *31*(1), 47-56. doi: 10.1016/j.molcel.2008.06.005
- Hinshaw, S. M., Makrantonis, V., Kerr, A., Marston, A. L., & Harrison, S. C. (2015). Structural evidence for Scc4-dependent localization of cohesin loading. *Elife*, *4*, e06057. doi: 10.7554/eLife.06057
- Holzel, M., Rohrmoser, M., Schlee, M., Grimm, T., Harasim, T., Malamoussi, A., . . . Eick, D. (2005). Mammalian WDR12 is a novel member of the Pes1-Bop1 complex and is required for ribosome biogenesis and cell proliferation. *J Cell Biol*, *170*(3), 367-378. doi: 10.1083/jcb.200501141
- Horsfield, J. A., Anagnostou, S. H., Hu, J. K., Cho, K. H., Geisler, R., Lieschke, G., . . . Crosier, P. S. (2007). Cohesin-dependent regulation of Runx genes. *Development*, *134*(14), 2639-2649. doi: 10.1242/dev.002485
- Hou, F., & Zou, H. (2005). Two human orthologues of Eco1/Ctf7 acetyltransferases are both required for proper sister-chromatid cohesion. *Mol Biol Cell*, *16*(8), 3908-3918. doi: 10.1091/mbc.E04-12-1063
- Hu, B., Itoh, T., Mishra, A., Katoh, Y., Chan, K. L., Upcher, W., . . . Nasmyth, K. (2011). ATP hydrolysis is required for relocating cohesin from sites occupied by its Scc2/4 loading complex. *Curr Biol*, *21*(1), 12-24. doi: 10.1016/j.cub.2010.12.004
- Huis in 't Veld, P. J., Herzog, F., Ladurner, R., Davidson, I. F., Piric, S., Kreidl, E., . . . Peters, J. M. (2014). Characterization of a DNA exit gate in the human cohesin ring. *Science*, *346*(6212), 968-972. doi: 10.1126/science.1256904
- Irniger, S., Piatti, S., Michaelis, C., & Nasmyth, K. (1995). Genes involved in sister chromatid separation are needed for B-type cyclin proteolysis in budding yeast. *Cell*, *81*(2), 269-278.

- Ivanov, D., & Nasmyth, K. (2005). A topological interaction between cohesin rings and a circular minichromosome. *Cell*, *122*(6), 849-860. doi: 10.1016/j.cell.2005.07.018
- Ivanov, D., Schleiffer, A., Eisenhaber, F., Mechtler, K., Haering, C. H., & Nasmyth, K. (2002). Eco1 is a novel acetyltransferase that can acetylate proteins involved in cohesion. *Curr Biol*, *12*(4), 323-328.
- Izawa, D., & Pines, J. (2015). The mitotic checkpoint complex binds a second CDC20 to inhibit active APC/C. *Nature*, *517*(7536), 631-634. doi: 10.1038/nature13911
- Jhunjunwala, S., van Zelm, M. C., Peak, M. M., Cutchin, S., Riblet, R., van Dongen, J. J., . . . Murre, C. (2008). The 3D structure of the immunoglobulin heavy-chain locus: implications for long-range genomic interactions. *Cell*, *133*(2), 265-279. doi: 10.1016/j.cell.2008.03.024
- Kagey, M. H., Newman, J. J., Bilodeau, S., Zhan, Y., Orlando, D. A., van Berkum, N. L., . . . Young, R. A. (2010). Mediator and cohesin connect gene expression and chromatin architecture. *Nature*, *467*(7314), 430-435. doi: 10.1038/nature09380
- Karamysheva, Z., Diaz-Martinez, L. A., Crow, S. E., Li, B., & Yu, H. (2009). Multiple anaphase-promoting complex/cyclosome degrons mediate the degradation of human Sgo1. *J Biol Chem*, *284*(3), 1772-1780. doi: 10.1074/jbc.M807083200
- Kerrebrock, A. W., Moore, D. P., Wu, J. S., & Orr-Weaver, T. L. (1995). Mei-S332, a *Drosophila* protein required for sister-chromatid cohesion, can localize to meiotic centromere regions. *Cell*, *83*(2), 247-256.
- Kim, S. T., Xu, B., & Kastan, M. B. (2002). Involvement of the cohesin protein, Smc1, in Atm-dependent and independent responses to DNA damage. *Genes Dev*, *16*(5), 560-570. doi: 10.1101/gad.970602
- King, R. W., Peters, J. M., Tugendreich, S., Rolfe, M., Hieter, P., & Kirschner, M. W. (1995). A 20S complex containing CDC27 and CDC16 catalyzes the mitosis-specific conjugation of ubiquitin to cyclin B. *Cell*, *81*(2), 279-288.
- Kitajima, T. S., Sakuno, T., Ishiguro, K., & Watanabe, Y. (2006). [Roles and molecular mechanisms of chromosome cohesion at centromeres]. *Tanpakushitsu Kakusan Koso*, *51*(13), 1809-1816.
- Klenova, E. M., Nicolas, R. H., Paterson, H. F., Carne, A. F., Heath, C. M., Goodwin, G. H., . . . Lobanenkova, V. V. (1993). CTCF, a conserved nuclear factor required for optimal transcriptional activity of the chicken c-myc gene, is an 11-Zn-finger protein differentially expressed in multiple forms. *Mol Cell Biol*, *13*(12), 7612-7624.
- Kong, X., Ball, A. R., Jr., Sonoda, E., Feng, J., Takeda, S., Fukagawa, T., . . . Yokomori, K. (2009). Cohesin associates with spindle poles in a mitosis-specific manner and functions in spindle assembly in vertebrate cells. *Mol Biol Cell*, *20*(5), 1289-1301. doi: 10.1091/mbc.E08-04-0419
- Kueng, S., Hegemann, B., Peters, B. H., Lipp, J. J., Schleiffer, A., Mechtler, K., & Peters, J. M. (2006). Wapl controls the dynamic association of cohesin with chromatin. *Cell*, *127*(5), 955-967. doi: 10.1016/j.cell.2006.09.040
- Kumada, K., Yao, R., Kawaguchi, T., Karasawa, M., Hoshikawa, Y., Ichikawa, K., . . . Noda, T. (2006). The selective continued linkage of centromeres from mitosis to interphase in the absence of mammalian separase. *J Cell Biol*, *172*(6), 835-846. doi: 10.1083/jcb.200511126

- Ladurner, R., Bhaskara, V., Huis in 't Veld, P. J., Davidson, I. F., Kreidl, E., Petzold, G., & Peters, J. M. (2014). Cohesin's ATPase activity couples cohesin loading onto DNA with Smc3 acetylation. *Curr Biol*, *24*(19), 2228-2237. doi: 10.1016/j.cub.2014.08.011
- Ladurner, R., Kreidl, E., Ivanov, M. P., Ekker, H., Idarraga-Amado, M. H., Busslinger, G. A., . . . Peters, J. M. (2016). Sororin actively maintains sister chromatid cohesion. *EMBO J*, *35*(6), 635-653. doi: 10.15252/embj.201592532
- Laloraya, S., Guacci, V., & Koshland, D. (2000). Chromosomal addresses of the cohesin component Mcd1p. *J Cell Biol*, *151*(5), 1047-1056.
- Lee, J., Kitajima, T. S., Tanno, Y., Yoshida, K., Morita, T., Miyano, T., . . . Watanabe, Y. (2008). Unified mode of centromeric protection by shugoshin in mammalian oocytes and somatic cells. *Nat Cell Biol*, *10*(1), 42-52. doi: 10.1038/ncb1667
- Leem, Y. E., Choi, H. K., Jung, S. Y., Kim, B. J., Lee, K. Y., Yoon, K., . . . Kim, S. T. (2011). Esco2 promotes neuronal differentiation by repressing Notch signaling. *Cell Signal*, *23*(11), 1876-1884. doi: 10.1016/j.cellsig.2011.07.006
- Lengronne, A., Katou, Y., Mori, S., Yokobayashi, S., Kelly, G. P., Itoh, T., . . . Uhlmann, F. (2004). Cohesin relocation from sites of chromosomal loading to places of convergent transcription. *Nature*, *430*(6999), 573-578. doi: 10.1038/nature02742
- Lengronne, A., McIntyre, J., Katou, Y., Kanoh, Y., Hopfner, K. P., Shirahige, K., & Uhlmann, F. (2006). Establishment of sister chromatid cohesion at the S. cerevisiae replication fork. *Mol Cell*, *23*(6), 787-799. doi: 10.1016/j.molcel.2006.08.018
- Lindstrom, M. S., Jin, A., Deisenroth, C., White Wolf, G., & Zhang, Y. (2007). Cancer-associated mutations in the MDM2 zinc finger domain disrupt ribosomal protein interaction and attenuate MDM2-induced p53 degradation. *Mol Cell Biol*, *27*(3), 1056-1068. doi: 10.1128/MCB.01307-06
- Liu, H., Qu, Q., Warrington, R., Rice, A., Cheng, N., & Yu, H. (2015). Mitotic Transcription Installs Sgo1 at Centromeres to Coordinate Chromosome Segregation. *Mol Cell*, *59*(3), 426-436. doi: 10.1016/j.molcel.2015.06.018
- Liu, H., Rankin, S., & Yu, H. (2013). Phosphorylation-enabled binding of SGO1-PP2A to cohesin protects sororin and centromeric cohesion during mitosis. *Nat Cell Biol*, *15*(1), 40-49. doi: 10.1038/ncb2637
- Llano, E., Gomez, R., Gutierrez-Caballero, C., Herran, Y., Sanchez-Martin, M., Vazquez-Quinones, L., . . . Pendas, A. M. (2008). Shugoshin-2 is essential for the completion of meiosis but not for mitotic cell division in mice. *Genes Dev*, *22*(17), 2400-2413. doi: 10.1101/gad.475308
- Lobanenkov, V. V., Nicolas, R. H., Adler, V. V., Paterson, H., Klenova, E. M., Polotskaja, A. V., & Goodwin, G. H. (1990). A novel sequence-specific DNA binding protein which interacts with three regularly spaced direct repeats of the CCCTC-motif in the 5'-flanking sequence of the chicken c-myc gene. *Oncogene*, *5*(12), 1743-1753.
- Losada, A., Hirano, M., & Hirano, T. (2002). Cohesin release is required for sister chromatid resolution, but not for condensin-mediated compaction, at the onset of mitosis. *Genes Dev*, *16*(23), 3004-3016. doi: 10.1101/gad.249202

- Losada, A., Yokochi, T., & Hirano, T. (2005). Functional contribution of Pds5 to cohesin-mediated cohesion in human cells and *Xenopus* egg extracts. *J Cell Sci*, *118*(Pt 10), 2133-2141. doi: 10.1242/jcs.02355
- Losada, A., Yokochi, T., Kobayashi, R., & Hirano, T. (2000). Identification and characterization of SA/Scs3p subunits in the *Xenopus* and human cohesin complexes. *J Cell Biol*, *150*(3), 405-416.
- Lu, S., Goering, M., Gard, S., Xiong, B., McNairn, A. J., Jaspersen, S. L., & Gerton, J. L. (2010). Eco1 is important for DNA damage repair in *S. cerevisiae*. *Cell Cycle*, *9*(16), 3315-3327. doi: 10.4161/cc.9.16.12673
- Lyons, N. A., & Morgan, D. O. (2011). Cdk1-dependent destruction of Eco1 prevents cohesion establishment after S phase. *Mol Cell*, *42*(3), 378-389. doi: 10.1016/j.molcel.2011.03.023
- Maradeo, M. E., & Skibbens, R. V. (2009). The Elg1-RFC clamp-loading complex performs a role in sister chromatid cohesion. *PLoS One*, *4*(3), e4707. doi: 10.1371/journal.pone.0004707
- McGuinness, B. E., Hirota, T., Kudo, N. R., Peters, J. M., & Nasmyth, K. (2005). Shugoshin prevents dissociation of cohesin from centromeres during mitosis in vertebrate cells. *PLoS Biol*, *3*(3), e86. doi: 10.1371/journal.pbio.0030086
- Melby, T. E., Ciampaglio, C. N., Briscoe, G., & Erickson, H. P. (1998). The symmetrical structure of structural maintenance of chromosomes (SMC) and MukB proteins: long, antiparallel coiled coils, folded at a flexible hinge. *J Cell Biol*, *142*(6), 1595-1604.
- Merkenschlager, M., & Odom, D. T. (2013). CTCF and cohesin: linking gene regulatory elements with their targets. *Cell*, *152*(6), 1285-1297. doi: 10.1016/j.cell.2013.02.029
- Michaelis, C., Ciosk, R., & Nasmyth, K. (1997). Cohesins: chromosomal proteins that prevent premature separation of sister chromatids. *Cell*, *91*(1), 35-45.
- Milutinovich, M., Unal, E., Ward, C., Skibbens, R. V., & Koshland, D. (2007). A multi-step pathway for the establishment of sister chromatid cohesion. *PLoS Genet*, *3*(1), e12. doi: 10.1371/journal.pgen.0030012
- Minamino, M., Ishibashi, M., Nakato, R., Akiyama, K., Tanaka, H., Kato, Y., . . . Shirahige, K. (2015). Esco1 Acetylates Cohesin via a Mechanism Different from That of Esco2. *Curr Biol*, *25*(13), 1694-1706. doi: 10.1016/j.cub.2015.05.017
- Mishra, A., Hu, B., Kurze, A., Beckouet, F., Farcas, A. M., Dixon, S. E., . . . Nasmyth, K. (2010). Both interaction surfaces within cohesin's hinge domain are essential for its stable chromosomal association. *Curr Biol*, *20*(4), 279-289. doi: 10.1016/j.cub.2009.12.059
- Misulovin, Z., Schwartz, Y. B., Li, X. Y., Kahn, T. G., Gause, M., MacArthur, S., . . . Dorsett, D. (2008). Association of cohesin and Nipped-B with transcriptionally active regions of the *Drosophila melanogaster* genome. *Chromosoma*, *117*(1), 89-102. doi: 10.1007/s00412-007-0129-1
- Moldovan, G. L., Pfander, B., & Jentsch, S. (2006). PCNA controls establishment of sister chromatid cohesion during S phase. *Mol Cell*, *23*(5), 723-732. doi: 10.1016/j.molcel.2006.07.007
- Monnich, M., Kuriger, Z., Print, C. G., & Horsfield, J. A. (2011). A zebrafish model of Roberts syndrome reveals that Esco2 depletion interferes with development by

- disrupting the cell cycle. *PLoS One*, 6(5), e20051. doi: 10.1371/journal.pone.0020051
- Moriya, S., Tsujikawa, E., Hassan, A. K., Asai, K., Kodama, T., & Ogasawara, N. (1998). A *Bacillus subtilis* gene-encoding protein homologous to eukaryotic SMC motor protein is necessary for chromosome partition. *Mol Microbiol*, 29(1), 179-187.
- Murayama, Y., & Uhlmann, F. (2014). Biochemical reconstitution of topological DNA binding by the cohesin ring. *Nature*, 505(7483), 367-371. doi: 10.1038/nature12867
- Murayama, Y., & Uhlmann, F. (2015). DNA Entry into and Exit out of the Cohesin Ring by an Interlocking Gate Mechanism. *Cell*, 163(7), 1628-1640. doi: 10.1016/j.cell.2015.11.030
- Musacchio, A., & Salmon, E. D. (2007). The spindle-assembly checkpoint in space and time. *Nat Rev Mol Cell Biol*, 8(5), 379-393. doi: 10.1038/nrm2163
- Nakajima, M., Kumada, K., Hatakeyama, K., Noda, T., Peters, J. M., & Hirota, T. (2007). The complete removal of cohesin from chromosome arms depends on separase. *J Cell Sci*, 120(Pt 23), 4188-4196. doi: 10.1242/jcs.011528
- Narendra, V., Rocha, P. P., An, D., Raviram, R., Skok, J. A., Mazzoni, E. O., & Reinberg, D. (2015). CTCF establishes discrete functional chromatin domains at the Hox clusters during differentiation. *Science*, 347(6225), 1017-1021. doi: 10.1126/science.1262088
- Narla, A., & Ebert, B. L. (2010). Ribosomopathies: human disorders of ribosome dysfunction. *Blood*, 115(16), 3196-3205. doi: 10.1182/blood-2009-10-178129
- Nasmyth, K. (2005). How might cohesin hold sister chromatids together? *Philos Trans R Soc Lond B Biol Sci*, 360(1455), 483-496. doi: 10.1098/rstb.2004.1604
- Nasmyth, K., & Haering, C. H. (2009). Cohesin: its roles and mechanisms. *Annu Rev Genet*, 43, 525-558. doi: 10.1146/annurev-genet-102108-134233
- Naumova, N., Imakaev, M., Fudenberg, G., Zhan, Y., Lajoie, B. R., Mirny, L. A., & Dekker, J. (2013). Organization of the mitotic chromosome. *Science*, 342(6161), 948-953. doi: 10.1126/science.1236083
- Neuwald, A. F., & Hirano, T. (2000). HEAT repeats associated with condensins, cohesins, and other complexes involved in chromosome-related functions. *Genome Res*, 10(10), 1445-1452.
- Nicklas, R. B., & Staehly, C. A. (1967). Chromosome micromanipulation. I. The mechanics of chromosome attachment to the spindle. *Chromosoma*, 21(1), 1-16.
- Nicklas, R. B., Ward, S. C., & Gorbsky, G. J. (1995). Kinetochore chemistry is sensitive to tension and may link mitotic forces to a cell cycle checkpoint. *J Cell Biol*, 130(4), 929-939.
- Nishiyama, T., Ladurner, R., Schmitz, J., Kreidl, E., Schleiffer, A., Bhaskara, V., . . . Peters, J. M. (2010). Sororin mediates sister chromatid cohesion by antagonizing Wapl. *Cell*, 143(5), 737-749. doi: 10.1016/j.cell.2010.10.031
- Ocampo-Hafalla, M. T., Katou, Y., Shirahige, K., & Uhlmann, F. (2007). Displacement and re-accumulation of centromeric cohesin during transient pre-anaphase centromere splitting. *Chromosoma*, 116(6), 531-544. doi: 10.1007/s00412-007-0118-4

- Ocampo-Hafalla, M. T., & Uhlmann, F. (2011). Cohesin loading and sliding. *J Cell Sci*, *124*(Pt 5), 685-691. doi: 10.1242/jcs.073866
- Oliveira, R. A., & Nasmyth, K. (2013). Cohesin cleavage is insufficient for centriole disengagement in *Drosophila*. *Curr Biol*, *23*(14), R601-603. doi: 10.1016/j.cub.2013.04.003
- Orth, M., Mayer, B., Rehm, K., Rothweiler, U., Heidmann, D., Holak, T. A., & Stemmann, O. (2011). Shugoshin is a Mad1/Cdc20-like interactor of Mad2. *EMBO J*, *30*(14), 2868-2880. doi: 10.1038/emboj.2011.187
- Ouyang, Z., Zheng, G., Song, J., Borek, D. M., Otwinowski, Z., Brautigam, C. A., . . . Yu, H. (2013). Structure of the human cohesin inhibitor Wapl. *Proc Natl Acad Sci U S A*, *110*(28), 11355-11360. doi: 10.1073/pnas.1304594110
- Panizza, S., Tanaka, T., Hochwagen, A., Eisenhaber, F., & Nasmyth, K. (2000). Pds5 cooperates with cohesin in maintaining sister chromatid cohesion. *Curr Biol*, *10*(24), 1557-1564.
- Parelho, V., Hadjur, S., Spivakov, M., Leleu, M., Sauer, S., Gregson, H. C., . . . Merkenschlager, M. (2008). Cohesins functionally associate with CTCF on mammalian chromosome arms. *Cell*, *132*(3), 422-433. doi: 10.1016/j.cell.2008.01.011
- Parnas, O., Zipin-Roitman, A., Mazor, Y., Liefshitz, B., Ben-Aroya, S., & Kupiec, M. (2009). The ELG1 clamp loader plays a role in sister chromatid cohesion. *PLoS One*, *4*(5), e5497. doi: 10.1371/journal.pone.0005497
- Peters, J. M., Tedeschi, A., & Schmitz, J. (2008). The cohesin complex and its roles in chromosome biology. *Genes Dev*, *22*(22), 3089-3114. doi: 10.1101/gad.1724308
- Rahman, S., Jones, M. J., & Jallepalli, P. V. (2015). Cohesin recruits the Esco1 acetyltransferase genome wide to repress transcription and promote cohesion in somatic cells. *Proc Natl Acad Sci U S A*, *112*(36), 11270-11275. doi: 10.1073/pnas.1505323112
- Rankin, S., Ayad, N. G., & Kirschner, M. W. (2005). Sororin, a substrate of the anaphase-promoting complex, is required for sister chromatid cohesion in vertebrates. *Mol Cell*, *18*(2), 185-200. doi: 10.1016/j.molcel.2005.03.017
- Remeseiro, S., Cuadrado, A., Carretero, M., Martinez, P., Drosopoulos, W. C., Canamero, M., . . . Losada, A. (2012). Cohesin-SA1 deficiency drives aneuploidy and tumorigenesis in mice due to impaired replication of telomeres. *EMBO J*, *31*(9), 2076-2089. doi: 10.1038/emboj.2012.11
- Remeseiro, S., Cuadrado, A., & Losada, A. (2013). Cohesin in development and disease. *Development*, *140*(18), 3715-3718. doi: 10.1242/dev.090605
- Riedel, C. G., Katis, V. L., Katou, Y., Mori, S., Itoh, T., Helmhart, W., . . . Nasmyth, K. (2006). Protein phosphatase 2A protects centromeric sister chromatid cohesion during meiosis I. *Nature*, *441*(7089), 53-61. doi: 10.1038/nature04664
- Roig, M. B., Lowe, J., Chan, K. L., Beckouet, F., Metson, J., & Nasmyth, K. (2014). Structure and function of cohesin's Scc3/SA regulatory subunit. *FEBS Lett*, *588*(20), 3692-3702. doi: 10.1016/j.febslet.2014.08.015
- Rolf Ben-Shahar, T., Heeger, S., Lehane, C., East, P., Flynn, H., Skehel, M., & Uhlmann, F. (2008). Eco1-dependent cohesin acetylation during establishment of sister chromatid cohesion. *Science*, *321*(5888), 563-566. doi: 10.1126/science.1157774

- Rowland, B. D., Roig, M. B., Nishino, T., Kurze, A., Uluocak, P., Mishra, A., . . . Nasmyth, K. (2009). Building sister chromatid cohesion: smc3 acetylation counteracts an antiestablishment activity. *Mol Cell*, *33*(6), 763-774. doi: 10.1016/j.molcel.2009.02.028
- Rubio, E. D., Reiss, D. J., Welch, P. L., Distèche, C. M., Filippova, G. N., Baliga, N. S., . . . Krumm, A. (2008). CTCF physically links cohesin to chromatin. *Proc Natl Acad Sci U S A*, *105*(24), 8309-8314. doi: 10.1073/pnas.0801273105
- Sakai, D., & Trainor, P. A. (2009). Treacher Collins syndrome: unmasking the role of Tcof1/treacle. *Int J Biochem Cell Biol*, *41*(6), 1229-1232. doi: 10.1016/j.biocel.2008.10.026
- Salic, A., Waters, J. C., & Mitchison, T. J. (2004). Vertebrate shugoshin links sister centromere cohesion and kinetochore microtubule stability in mitosis. *Cell*, *118*(5), 567-578. doi: 10.1016/j.cell.2004.08.016
- Samora, C. P., Saksouk, J., Goswami, P., Wade, B. O., Singleton, M. R., Bates, P. A., . . . Uhlmann, F. (2016). Ctf4 Links DNA Replication with Sister Chromatid Cohesion Establishment by Recruiting the Chl1 Helicase to the Replisome. *Mol Cell*, *63*(3), 371-384. doi: 10.1016/j.molcel.2016.05.036
- Sanborn, A. L., Rao, S. S., Huang, S. C., Durand, N. C., Huntley, M. H., Jewett, A. I., . . . Aiden, E. L. (2015). Chromatin extrusion explains key features of loop and domain formation in wild-type and engineered genomes. *Proc Natl Acad Sci U S A*, *112*(47), E6456-6465. doi: 10.1073/pnas.1518552112
- Sandler, L. (1974). Some observations on the study of the genetic control of meiosis in *Drosophila melanogaster*. *Genetics*, *78*(1), 289-297.
- Sanyal, A., Lajoie, B. R., Jain, G., & Dekker, J. (2012). The long-range interaction landscape of gene promoters. *Nature*, *489*(7414), 109-113. doi: 10.1038/nature11279
- Schmidt, D., Schwalie, P. C., Ross-Innes, C. S., Hurtado, A., Brown, G. D., Carroll, J. S., . . . Odom, D. T. (2010). A CTCF-independent role for cohesin in tissue-specific transcription. *Genome Res*, *20*(5), 578-588. doi: 10.1101/gr.100479.109
- Schmitz, J., Watrin, E., Lenart, P., Mechtler, K., & Peters, J. M. (2007). Sororin is required for stable binding of cohesin to chromatin and for sister chromatid cohesion in interphase. *Curr Biol*, *17*(7), 630-636. doi: 10.1016/j.cub.2007.02.029
- Shintomi, K., & Hirano, T. (2009). Releasing cohesin from chromosome arms in early mitosis: opposing actions of Wapl-Pds5 and Sgo1. *Genes Dev*, *23*(18), 2224-2236. doi: 10.1101/gad.1844309
- Skibbens, R. V. (2009). Establishment of sister chromatid cohesion. *Curr Biol*, *19*(24), R1126-1132. doi: 10.1016/j.cub.2009.10.067
- Skibbens, R. V., Corson, L. B., Koshland, D., & Hieter, P. (1999). Ctf7p is essential for sister chromatid cohesion and links mitotic chromosome structure to the DNA replication machinery. *Genes Dev*, *13*(3), 307-319.
- Sluder, G., & Rieder, C. L. (1985). Centriole number and the reproductive capacity of spindle poles. *J Cell Biol*, *100*(3), 887-896.
- Stedman, W., Kang, H., Lin, S., Kissil, J. L., Bartolomei, M. S., & Lieberman, P. M. (2008). Cohesins localize with CTCF at the KSHV latency control region and at cellular c-myc and H19/Igf2 insulators. *EMBO J*, *27*(4), 654-666. doi: 10.1038/emboj.2008.1

- Stigler, J., Camdere, G. O., Koshland, D. E., & Greene, E. C. (2016). Single-Molecule Imaging Reveals a Collapsed Conformational State for DNA-Bound Cohesin. *Cell Rep*, *15*(5), 988-998. doi: 10.1016/j.celrep.2016.04.003
- Strom, L., Karlsson, C., Lindroos, H. B., Wedahl, S., Katou, Y., Shirahige, K., & Sjogren, C. (2007). Postreplicative formation of cohesion is required for repair and induced by a single DNA break. *Science*, *317*(5835), 242-245. doi: 10.1126/science.1140649
- Strom, L., & Sjogren, C. (2005). DNA damage-induced cohesion. *Cell Cycle*, *4*(4), 536-539. doi: 10.4161/cc.4.4.1613
- Sudakin, V., Ganoth, D., Dahan, A., Heller, H., Hershko, J., Luca, F. C., . . . Hershko, A. (1995). The cyclosome, a large complex containing cyclin-selective ubiquitin ligase activity, targets cyclins for destruction at the end of mitosis. *Mol Biol Cell*, *6*(2), 185-197.
- Sumara, I., Vorlaufer, E., Gieffers, C., Peters, B. H., & Peters, J. M. (2000). Characterization of vertebrate cohesin complexes and their regulation in prophase. *J Cell Biol*, *151*(4), 749-762.
- Sumara, I., Vorlaufer, E., Stukenberg, P. T., Kelm, O., Redemann, N., Nigg, E. A., & Peters, J. M. (2002). The dissociation of cohesin from chromosomes in prophase is regulated by Polo-like kinase. *Mol Cell*, *9*(3), 515-525.
- Sun, X., Chen, H., Deng, Z., Hu, B., Luo, H., Zeng, X., . . . Ma, L. (2015). The Warsaw breakage syndrome-related protein DDX11 is required for ribosomal RNA synthesis and embryonic development. *Hum Mol Genet*, *24*(17), 4901-4915. doi: 10.1093/hmg/ddv213
- Sun, Y., Kucej, M., Fan, H. Y., Yu, H., Sun, Q. Y., & Zou, H. (2009). Separase is recruited to mitotic chromosomes to dissolve sister chromatid cohesion in a DNA-dependent manner. *Cell*, *137*(1), 123-132. doi: 10.1016/j.cell.2009.01.040
- Sundin, O., & Varshavsky, A. (1980). Terminal stages of SV40 DNA replication proceed via multiply intertwined catenated dimers. *Cell*, *21*(1), 103-114.
- Surcel, A., Koshland, D., Ma, H., & Simpson, R. T. (2008). Cohesin interaction with centromeric minichromosomes shows a multi-complex rod-shaped structure. *PLoS One*, *3*(6), e2453. doi: 10.1371/journal.pone.0002453
- Sutani, T., Kawaguchi, T., Kanno, R., Itoh, T., & Shirahige, K. (2009). Budding yeast Wpl1(Rad61)-Pds5 complex counteracts sister chromatid cohesion-establishing reaction. *Curr Biol*, *19*(6), 492-497. doi: 10.1016/j.cub.2009.01.062
- Tanaka, K., Hao, Z., Kai, M., & Okayama, H. (2001). Establishment and maintenance of sister chromatid cohesion in fission yeast by a unique mechanism. *EMBO J*, *20*(20), 5779-5790. doi: 10.1093/emboj/20.20.5779
- Tang, J., Erikson, R. L., & Liu, X. (2006). Ectopic expression of Plk1 leads to activation of the spindle checkpoint. *Cell Cycle*, *5*(21), 2484-2488. doi: 10.4161/cc.5.21.3411
- Tang, Z., Sun, Y., Harley, S. E., Zou, H., & Yu, H. (2004). Human Bub1 protects centromeric sister-chromatid cohesion through Shugoshin during mitosis. *Proc Natl Acad Sci U S A*, *101*(52), 18012-18017. doi: 10.1073/pnas.0408600102
- Terret, M. E., Sherwood, R., Rahman, S., Qin, J., & Jallepalli, P. V. (2009). Cohesin acetylation speeds the replication fork. *Nature*, *462*(7270), 231-234. doi: 10.1038/nature08550

- Tolhuis, B., Palstra, R. J., Splinter, E., Grosveld, F., & de Laat, W. (2002). Looping and interaction between hypersensitive sites in the active beta-globin locus. *Mol Cell*, *10*(6), 1453-1465.
- Tomkins, D., Hunter, A., & Roberts, M. (1979). Cytogenetic findings in Roberts-SC phocomelia syndrome(s). *Am J Med Genet*, *4*(1), 17-26. doi: 10.1002/ajmg.1320040104
- Tonkin, E. T., Wang, T. J., Lisgo, S., Bamshad, M. J., & Strachan, T. (2004). NIPBL, encoding a homolog of fungal Scc2-type sister chromatid cohesion proteins and fly Nipped-B, is mutated in Cornelia de Lange syndrome. *Nat Genet*, *36*(6), 636-641. doi: 10.1038/ng1363
- Toth, A., Ciosk, R., Uhlmann, F., Galova, M., Schleiffer, A., & Nasmyth, K. (1999). Yeast cohesin complex requires a conserved protein, Eco1p(Ctf7), to establish cohesion between sister chromatids during DNA replication. *Genes Dev*, *13*(3), 320-333.
- Toyoda, Y., & Yanagida, M. (2006). Coordinated requirements of human topo II and cohesin for metaphase centromere alignment under Mad2-dependent spindle checkpoint surveillance. *Mol Biol Cell*, *17*(5), 2287-2302. doi: 10.1091/mbc.E05-11-1089
- Tsou, M. F., & Stearns, T. (2006). Mechanism limiting centrosome duplication to once per cell cycle. *Nature*, *442*(7105), 947-951. doi: 10.1038/nature04985
- Uhlmann, F., Lottspeich, F., & Nasmyth, K. (1999). Sister-chromatid separation at anaphase onset is promoted by cleavage of the cohesin subunit Scc1. *Nature*, *400*(6739), 37-42. doi: 10.1038/21831
- Uhlmann, F., Wernic, D., Poupart, M. A., Koonin, E. V., & Nasmyth, K. (2000). Cleavage of cohesin by the CD clan protease separin triggers anaphase in yeast. *Cell*, *103*(3), 375-386.
- Unal, E., Heidinger-Pauli, J. M., Kim, W., Guacci, V., Onn, I., Gygi, S. P., & Koshland, D. E. (2008). A molecular determinant for the establishment of sister chromatid cohesion. *Science*, *321*(5888), 566-569. doi: 10.1126/science.1157880
- Unal, E., Heidinger-Pauli, J. M., & Koshland, D. (2007). DNA double-strand breaks trigger genome-wide sister-chromatid cohesion through Eco1 (Ctf7). *Science*, *317*(5835), 245-248. doi: 10.1126/science.1140637
- Vagnarelli, P., & Earnshaw, W. C. (2004). Chromosomal passengers: the four-dimensional regulation of mitotic events. *Chromosoma*, *113*(5), 211-222. doi: 10.1007/s00412-004-0307-3
- Vega, H., Trainer, A. H., Gordillo, M., Crosier, M., Kayserili, H., Skovby, F., . . . Jabs, E. W. (2010). Phenotypic variability in 49 cases of ESCO2 mutations, including novel missense and codon deletion in the acetyltransferase domain, correlates with ESCO2 expression and establishes the clinical criteria for Roberts syndrome. *J Med Genet*, *47*(1), 30-37. doi: 10.1136/jmg.2009.068395
- Verni, F., Gandhi, R., Goldberg, M. L., & Gatti, M. (2000). Genetic and molecular analysis of wings apart-like (wapl), a gene controlling heterochromatin organization in *Drosophila melanogaster*. *Genetics*, *154*(4), 1693-1710.
- Waizenegger, I. C., Hauf, S., Meinke, A., & Peters, J. M. (2000). Two distinct pathways remove mammalian cohesin from chromosome arms in prophase and from centromeres in anaphase. *Cell*, *103*(3), 399-410.

- Wang, Z., Castano, I. B., De Las Penas, A., Adams, C., & Christman, M. F. (2000). Pol kappa: A DNA polymerase required for sister chromatid cohesion. *Science*, 289(5480), 774-779.
- Watrin, E., & Peters, J. M. (2009). The cohesin complex is required for the DNA damage-induced G2/M checkpoint in mammalian cells. *EMBO J*, 28(17), 2625-2635. doi: 10.1038/emboj.2009.202
- Watrin, E., Schleiffer, A., Tanaka, K., Eisenhaber, F., Nasmyth, K., & Peters, J. M. (2006). Human Scc4 is required for cohesin binding to chromatin, sister-chromatid cohesion, and mitotic progression. *Curr Biol*, 16(9), 863-874. doi: 10.1016/j.cub.2006.03.049
- Weber, S. A., Gerton, J. L., Polancic, J. E., DeRisi, J. L., Koshland, D., & Megee, P. C. (2004). The kinetochore is an enhancer of pericentric cohesin binding. *PLoS Biol*, 2(9), E260. doi: 10.1371/journal.pbio.0020260
- Wendt, K. S., Yoshida, K., Itoh, T., Bando, M., Koch, B., Schirghuber, E., . . . Peters, J. M. (2008). Cohesin mediates transcriptional insulation by CCCTC-binding factor. *Nature*, 451(7180), 796-801. doi: 10.1038/nature06634
- Whelan, G., Kreidl, E., Wutz, G., Egner, A., Peters, J. M., & Eichele, G. (2012). Cohesin acetyltransferase Esco2 is a cell viability factor and is required for cohesion in pericentric heterochromatin. *EMBO J*, 31(1), 71-82. doi: 10.1038/emboj.2011.381
- Wirth, K. G., Wutz, G., Kudo, N. R., Desdouets, C., Zetterberg, A., Taghybeeglu, S., . . . Nasmyth, K. (2006). Separase: a universal trigger for sister chromatid disjunction but not chromosome cycle progression. *J Cell Biol*, 172(6), 847-860. doi: 10.1083/jcb.200506119
- Wong, R. W., & Blobel, G. (2008). Cohesin subunit SMC1 associates with mitotic microtubules at the spindle pole. *Proc Natl Acad Sci U S A*, 105(40), 15441-15445. doi: 10.1073/pnas.0807660105
- Wu, F. M., Nguyen, J. V., & Rankin, S. (2011). A conserved motif at the C terminus of sororin is required for sister chromatid cohesion. *J Biol Chem*, 286(5), 3579-3586. doi: 10.1074/jbc.M110.196758
- Xiong, B., Lu, S., & Gerton, J. L. (2010). Hos1 is a lysine deacetylase for the Smc3 subunit of cohesin. *Curr Biol*, 20(18), 1660-1665. doi: 10.1016/j.cub.2010.08.019
- Xu, B., Gogol, M., Gaudenz, K., & Gerton, J. L. (2016). Improved transcription and translation with L-leucine stimulation of mTORC1 in Roberts syndrome. *BMC Genomics*, 17, 25. doi: 10.1186/s12864-015-2354-y
- Xu, B., Lee, K. K., Zhang, L., & Gerton, J. L. (2013). Stimulation of mTORC1 with L-leucine rescues defects associated with Roberts syndrome. *PLoS Genet*, 9(10), e1003857. doi: 10.1371/journal.pgen.1003857
- Xu, H., Boone, C., & Brown, G. W. (2007). Genetic dissection of parallel sister-chromatid cohesion pathways. *Genetics*, 176(3), 1417-1429. doi: 10.1534/genetics.107.072876
- Yamada, H. Y., Yao, Y., Wang, X., Zhang, Y., Huang, Y., Dai, W., & Rao, C. V. (2012). Haploinsufficiency of SGO1 results in deregulated centrosome dynamics, enhanced chromosomal instability and colon tumorigenesis. *Cell Cycle*, 11(3), 479-488. doi: 10.4161/cc.11.3.18994
- Zhang, B., Chang, J., Fu, M., Huang, J., Kashyap, R., Salavaggione, E., . . . Milbrandt, J. (2009). Dosage effects of cohesin regulatory factor PDS5 on mammalian

- development: implications for cohesinopathies. *PLoS One*, 4(5), e5232. doi: 10.1371/journal.pone.0005232
- Zhang, B., Jain, S., Song, H., Fu, M., Heuckeroth, R. O., Erlich, J. M., . . . Milbrandt, J. (2007). Mice lacking sister chromatid cohesion protein PDS5B exhibit developmental abnormalities reminiscent of Cornelia de Lange syndrome. *Development*, 134(17), 3191-3201. doi: 10.1242/dev.005884
- Zhang, J., Shi, X., Li, Y., Kim, B. J., Jia, J., Huang, Z., . . . Qin, J. (2008). Acetylation of Smc3 by Eco1 is required for S phase sister chromatid cohesion in both human and yeast. *Mol Cell*, 31(1), 143-151. doi: 10.1016/j.molcel.2008.06.006
- Zhang, N., Panigrahi, A. K., Mao, Q., & Pati, D. (2011). Interaction of Sororin protein with polo-like kinase 1 mediates resolution of chromosomal arm cohesion. *J Biol Chem*, 286(48), 41826-41837. doi: 10.1074/jbc.M111.305888
- Zhang, W., Dunkle, J. A., & Cate, J. H. (2009). Structures of the ribosome in intermediate states of ratcheting. *Science*, 325(5943), 1014-1017. doi: 10.1126/science.1175275
- Zoncu, R., Efeyan, A., & Sabatini, D. M. (2011). mTOR: from growth signal integration to cancer, diabetes and ageing. *Nat Rev Mol Cell Biol*, 12(1), 21-35. doi: 10.1038/nrm3025
- Zuin, J., Dixon, J. R., van der Reijden, M. I., Ye, Z., Kolovos, P., Brouwer, R. W., . . . Wendt, K. S. (2014). Cohesin and CTCF differentially affect chromatin architecture and gene expression in human cells. *Proc Natl Acad Sci U S A*, 111(3), 996-1001. doi: 10.1073/pnas.1317788111

OBSERVING MITOTIC DIVISION AND DYNAMICS IN A LIVE ZEBRAFISH  
EMBRYO

by

STEFANIE PERCIVAL AND JOHN PARANT

*Journal of Visualized Experiments*

2016

Format adapted for dissertation

## ABSTRACT

Mitosis is critical for organismal growth and differentiation. The process is highly dynamic and requires ordered events to accomplish proper chromatin condensation, microtubule-kinetochore attachment, chromosome segregation, and cytokinesis in a small time frame. Errors in the delicate process can result in human disease, including birth defects and cancer. Traditional approaches investigating human mitotic disease states often rely on cell culture systems, which lack the natural physiology and developmental/tissue-specific context advantageous when studying human disease. This protocol overcomes many obstacles by providing a way to visualize, with high resolution, chromosome dynamics in a vertebrate system, the zebrafish. This protocol will detail an approach that can be used to obtain dynamic images of dividing cells, which include: *in vitro* transcription, zebrafish breeding/collecting, embryo embedding, and time-lapse imaging. Optimization and modifications of this protocol are also explored. Using H2A.F/Z-EGFP (labels chromatin) and mCherry-CAAX (labels cell membrane) mRNA-injected embryos, mitosis in AB wild-type, *auroraB<sup>hi1045</sup>*, and *esco2<sup>hi2865</sup>* mutant zebrafish is visualized. High resolution live imaging in zebrafish allows one to observe multiple mitoses to statistically quantify mitotic defects and timing of mitotic progression. In addition, observation of qualitative aspects that define improper mitotic processes (*i.e.* congression defects, missegregation of chromosomes, *etc.*) and improper chromosomal outcomes (*i.e.* aneuploidy, polyploidy, micronuclei, *etc.*) are observed. This assay can be applied to the observation of tissue differentiation/ development and is amenable to the use of

mutant zebrafish and pharmacological agents. Visualization of how defects in mitosis lead to cancer and developmental disorders will greatly enhance understanding of the pathogenesis of disease.

The video component of this article can be found at

<http://www.jove.com/video/54218/>

## INTRODUCTION

Mitosis is a critical cellular process essential for growth, differentiation, and regeneration in a living organism. Upon accurate preparation and replication of DNA in interphase, the cell is primed to divide. The first phase of mitosis, prophase, is initiated by activation of cyclin B/Cdk1. Prophase is characterized by condensation of chromatin material into chromosomes. Nuclear envelope breakdown occurs at the transition between prophase and prometaphase. In prometaphase, centrosomes, the nucleating center for spindle formation, begin to migrate to opposite poles while extending microtubules in search of kinetochore attachment. Upon attachment, conversions to end-on microtubule attachment and tension forces orient the chromosomes forming a metaphase plate<sup>1</sup>. If all chromosomes are attached correctly, the spindle assembly checkpoint is satisfied, cohesin rings holding the sister chromatids together are cleaved, and microtubules shorten to pull sister chromatids to opposite poles during anaphase<sup>2,3</sup>. The final phase, telophase, involves elongation of the cell and reformation of the nuclear envelope around the two new nuclei. Cytokinesis completes the division process by separating the cytoplasm of the two new daughter cells<sup>4-6</sup>. Alteration of key mitotic pathways (*i.e.* spindle assembly checkpoint, centrosome duplication, sister chromatid cohesion, *etc.*) can result in metaphase arrest, missegregation of chromosomes, and genomic instability<sup>7-10</sup>. Ultimately, defects in pathways controlling mitosis can cause developmental disorders and cancer, necessitating visualization of mitosis and its defects in a live, vertebrate, multi-cellular organism<sup>10-16</sup>.

Zebrafish embryos serve as a great model organism for live imaging due to the transparent tissue, ease of microinjection, and fast development. Using zebrafish, the overall goal of this manuscript is to describe a method of live 5D (dimensions X, Y, Z, time, and wavelength) imaging of mitosis<sup>17</sup> (**Figure 1C**). The use of mutant zebrafish defective in different mitotic pathways demonstrate the consequence of such defects. For this protocol, Aurora B and Esco2 mutants were chosen to illustrate these defects. Aurora B is a kinase that is part of the chromosome passenger complex (CPC) involved in spindle formation and microtubule attachment. It is also required for cleavage furrow formation in cytokinesis<sup>18,19</sup>. In zebrafish, Aurora B deficiency leads to defects in furrow induction, cytokinesis, and chromosome segregation<sup>20</sup>. Esco2, on the other hand, is an acetyltransferase that is essential for sister chromatid cohesion<sup>21,22</sup>. It acetylates cohesin on the SMC3 portion of the ring thus stabilizing cohesin to ensure proper chromosome segregation at the metaphase-anaphase transition<sup>23</sup>. Loss of Esco2 in zebrafish leads to chromosome missegregation, premature sister chromatid separation, genomic instability, and p53-dependent and independent apoptosis<sup>24,25</sup>. Due to the availability, *auroraB*<sup>hi1045</sup>, and *esco2*<sup>hi2865</sup> mutant zebrafish (hereafter referred to as *aurB*<sup>m/m</sup> and *esco2*<sup>m/m</sup>, respectively) will be used to illustrate this technique<sup>25-27</sup>.

Coupling confocal microscopy with fluorescent-tagged cell machinery has enabled researchers to visualize chromatin and cell membrane dynamics during mitosis<sup>25,28,29</sup>. Fluorescent-tagged histones have historically been used to visualize chromatin. Histones are nuclear proteins composed of four different pairs (H2A, H2B, H3, and H4) that are responsible for the nucleosome structure that composes chromosomes<sup>30</sup>. While H2B is arguably the most used histone for fluorescent proteins in mouse and cell culture, use of Histone 2A, Family Z (H2A.F/Z) has proved well for use in zebrafish<sup>31,32</sup>. Concanavalin A and casein kinase 1-gamma for example, localize to the cell membrane and have previously been shown effective in visualizing the cell membrane in sea urchins and drosophila<sup>33,34</sup>. Other studies have shown that the CAAX fluorescent- tagged protein labels the cell membrane and was successful in zebrafish<sup>31</sup>. CAAX is a motif that is recognized by post-translational modifying enzymes such as farnesyltransferases and geranylgeranyltransferases. Modifications by these enzymes cause proteins to become membrane- associated, thus labeling the cell membrane<sup>35</sup>.

Due to the prior use in zebrafish, this protocol chose to use H2A.F/Z and CAAX to label chromatin and the cell membrane. Application of this method will allow the researcher to monitor mitosis at the individual cell level to observe individual chromosome dynamics, as well as simultaneously monitor multiple cell divisions that may impact tissue differentiation and development. This article will focus on imaging the dynamics of chromosome segregation during mitosis at the individual cell level. Within this manuscript,

the ability to observe several mitotic divisions, calculate division time, and decipher the mitotic phenotypes will be illustrated and discussed. By using these parameters, physiologically relevant data can be collected and applied to several disease states affected by mitotic defects.

## **PROTOCOL**

### *1. In vitro Transcription*

1. Linearize pCS2-H2A.F/Z-EGFP and/or pCS2-mCherry-CAAX vectors by NotI restriction enzyme digest<sup>31</sup>. Using an RNA *in vitro* transcription kit, generate 5' capped mRNA products from each template, according to manufacturer's protocol.
2. Purify the capped mRNA using a purification kit. Follow manufacturer's instructions. Elute with RNase-free H<sub>2</sub>O.
3. Determine the concentration of RNA by absorbance at 260 nm using a spectrophotometer. (OD<sub>260</sub> x dilution x 40 µg/ml).
4. Dilute the RNA to 100 ng/µl for each H2A.F/Z-EGFP and mCherry-CAAX with RNase-free H<sub>2</sub>O. If the RNA concentration is too low, the fluorescence will be diminished or absent. Brighter samples will diminish the concerns over phototoxicity and photobleaching. On the other hand, too much RNA can be toxic and/or cause off target effects. Note: Store the remaining purified mRNA in -80 °C freezer.

## 2. Zebrafish Breeding, Embryo Collection, and mRNA Injection<sup>36-38</sup>

1. Assemble breeding tanks with a barrier to separate the tank into two regions and fill each breeding tank with aquaculture system water used in the zebrafish facility.
2. In order to prevent untimely breeding, place two male fish on one side of the barrier and two female fish on the other side the night before breeding.
3. The next day, thaw the previously prepared mRNA mixture on ice.

Replace the water in breeding tanks with fresh aquaculture system water and remove the barriers. Immediately after the barriers are pulled, warm an injection mold to 28.5 °C and set up the equipment for microinjection.

Note: For information on injection molds, please refer to Gerlach<sup>36</sup>.

4. Collect eggs every 10 - 15 min using a tea strainer and rinse the eggs into a clean 100 x 15 mm petri dish with E3 Blue (5 mM NaCl, 0.17 mM KCl, 0.33 mM CaCl<sub>2</sub>, 0.33 mM MgSO<sub>4</sub>, 10<sup>-5</sup>% Methylene blue). E3 Blue is used to prevent fungal growth and ensure proper development of larval fish. For more information on mating and embryo collection, refer to Gerlach<sup>36</sup> and Porazinski<sup>37</sup>.
5. Embed one-cell staged embryos in a warmed injection mold and inject the RNA into the yolk in the desired amount of embryos (**Figure 1A**). Account for natural embryonic death and unfertilized embryos by performing embryonic injections on 15% more embryos than needed for the experiment. For additional details on microinjection of zebrafish embryos, please refer to Gerlach<sup>36</sup> and

Porazinkski<sup>37</sup>.

NOTE: For first time use of mRNA, perform a dose-curve analysis to determine the optimal dose for fluorescence and viability (defined as no gross developmental defects up to 5 dpf) prior to performing 5D imaging. 150 - 200 ng/μl injected into embryos is often the optimal concentration, therefore it is a good starting point for the final concentration.

6. Carefully extract the injected embryos from the mold using a modified 9" glass Pasteur pipette. To modify the pipette, melt the end using a Bunsen burner until it forms a ball.
7. Place injected embryos in a 100 x 15 mm petri dish in E3 Blue and house in a 28.5 °C incubator.
8. Six hr post-injection, remove any dead or unfertilized embryos from the plates and add clean E3 Blue. House the embryos at 28.5 °C.

### *3. Preparation and Embedding of Live Zebrafish Embryos for Imaging (Figure 1B)*

1. Two hr before imaging, screen the injected embryos for GFP using a fluorescent dissecting microscope. Place bright green GFP-expressing embryos in a new 100 x 15 mm petri dish with E3 Blue.
2. Boil a stock solution of 1% low melt agarose by adding 1 g of low melt agarose to 100 ml of E3 Blue. After using the agarose, cover the flask with aluminum foil. The stock solution remains useful for up to one month.
3. Aliquot 3 ml of the melted agar into a 17 x 100 mm culture tube. Keep the agarose warm by placing the culture tube in a 42 °C water bath until ready

for use. Prepare a 15 mM Tricaine solution in deionized water to anesthetize the zebrafish embryos<sup>36</sup>.

NOTE: If imaging at earlier time points is desired, the concentration of agar can be decreased as low as 0.3%<sup>39</sup>.

4. Bring the 15 mM Tricaine, screened embryos, low melt agarose, E3 Blue, and a 35 mm glass coverslip bottom culture dish to a dissection light microscope. Carefully remove the embryo's chorion with #5 tweezers. Do this for three embryos.
5. Place the dechorionated embryos in a separate container to be anesthetized. The lid of the coverslip bottom dish is often used for this purpose. Using a transfer pipette, add three drops (approximately 150  $\mu$ l) of 15 mM Tricaine to the dish of 5 ml E3 blue (if using the lid of the coverslip bottom dish) or until embryos have been sufficiently anesthetized. In addition, add 3-4 drops (approximately 150 - 200  $\mu$ l) of 15 mM Tricaine solution to the 1% melted agarose tube.
6. Using a p200 pipette with 1 cm of the pipette tip cut off; transfer the anesthetized embryos to the coverslip-bottomed dish. Remove any excess E3 Blue:Tricaine solution.
7. Slowly add 5 - 10  $\mu$ l of low-melt agarose:Tricaine solution over the embryos, keeping each drop separate to ensure the embryos do not accidentally drift close to one another.

Warning: If the agarose is too warm, it will damage the embryo. A good temperature to maintain the agar at is 42 °C.

8. Using a 21G 1 ½ needle, gently orient the embryo in the agarose to the desired position. When using an inverted microscope for time-lapse imaging, orient the region of interest (ROI) as close to the coverslip as possible.

Note: For general purposes, the tail region offers ease of orientation and clarity due to the relatively thin tissue (**Figure 1A**). Other tissues, such as the epithelial layer surrounding the yolk and fin folds, can be used<sup>28,29</sup>. These tissues offer great clarity, however these regions are only a few cell layers thick. For the purpose of this protocol, it is beneficial to image the tail region to acquire as many cell divisions as possible.

9. Allow a few min for partial solidification of the agar. Use the needle to break apart a small piece of agar to test its solidification. When a piece of agar can be pulled away from the drop, proceed to the next step.
10. Cover the entire coverslip with low melt agar forming a dome over the embedded embryos. Allow the agar to solidify before moving the dish for confocal imaging (**Figure 1A**).
11. During the agar solidification process (takes approximately 10 min), prepare 3 ml of E3 Blue solution with five drops of (approximately 250 µl) 15 mM Tricaine to be placed over the embedded embryos during imaging.

#### 4. 5D Confocal Imaging of Live Zebrafish Embryos<sup>40,41</sup>

NOTE: See Ariga<sup>40</sup> and O'Brien<sup>41</sup> for details on how to perform 5D imaging using other confocal systems. For Z-interval, Z-stack, Z-depth, time interval, and 5D definitions see **Figure 1C**.

1. Open the imaging software and set the microscope to 60X NA 1.4 objective lens. Apply immersion oil to the objective lens and place the culture dish in the slide holder on the microscope stage. Using the axis controller, center the embryo of interest above the objective lens and bring the objective lens upward to meet the culture dish.
2. Click on the eye piece icon and switch to the GFP filter on the microscope. Focus on the ROI. Focusing on the tissue closest to the coverslip will offer the best imaging results.
3. Remove the interlock. Select the GFP and mCherry channels (pre-set wavelengths in software) and set the line averaging option to normal.
4. Use "View/Acquisition Controls/A1 Scan Area" command to open the A1 Scan Area tool.
5. Begin scanning. Using the axis-controller, position the embryo so that the scan area is filled with as much of the zebrafish as possible. The laser power does not need to be optimal at this point. Lower the laser power to avoid unnecessary photobleaching.
6. Use the "View/Acquisition Controls/ND acquisition" command to open the ND acquisition control panel.
7. Begin scanning to set the Z-stack parameters. Set the Z-stack upper limit to

where the cells are not in focus and lower limit to where cells are no longer visible. Allow for a 3  $\mu\text{m}$  space above the sample for growth and cell movement, which may expand into the imaging field. The Z- stack for the figures shown in this protocol covered a Z-depth of 40  $\mu\text{m}$  in the embryo tail.

8. Set the Z-interval step size to 2  $\mu\text{m}$ . On average, a cell is 10  $\mu\text{m}$  in diameter; therefore 2  $\mu\text{m}$  will produce five intervals of imaging data to be analyzed for each cell.

NOTE: The depth of the image that can be acquired depends on the Z interval. Z resolution is sacrificed to gain overall depth in the Z dimension in order to image as many cells undergoing mitosis as possible (large Z-depth). The inverse is true, in that, by decreasing the step size, Z resolution is gained, while Z depth is sacrificed (small Z-depth).

9. Adjust the image laser power, HV, and offset levels. For the experiments demonstrated in this protocol, use the following laser power, HV, and offset levels set at the corresponding levels, respectively, for the GFP channel; 2 - 5, 120 - 140, and -9 to -11. For the mCherry channel, use the following laser power, HV, and offset levels, respectively; 3 - 6, 120 - 140, and -3 to -8. Once the parameters are set, shut off the scan to prevent unnecessary laser exposure that may cause phototoxicity and photobleaching of the sample.
10. Select the 2x line averaging icon. "No averaging" produces a grainy image while "4x line averaging" drastically increases the scan time. Use of 2x line averaging provides the best image quality and fastest scan time.
11. Select the appropriate time interval and time duration necessary for the

experiment. For wild-type divisions, two minute time intervals for 2 hr is best for determining mitotic duration (used in **Figures 1, 2, 3A, and 3B**). Divisions that activate the spindle assembly checkpoint for longer than 30 min are more suitable for five minute intervals for four hr in order to preserve fluorescence as demonstrated in **Figure 3C**.

12. Check the "save to file" box and name the file to automatically save the file as it is being acquired. Double check all parameters are set correctly and hit "start run".
13. After acquisition is complete, to view the file in a three dimensional format, click on the volume threshold icon.

## **REPRESENTATIVE RESULTS**

**Figure 2** demonstrates the ability to observe many cell divisions using a wide field view of an AB wild-type zebrafish tail. Over seven mitotic cells are imaged in a 14 min time frame (**Movie 1**). Within the two hr time-course, over 40 mitotic events were captured. On average, 50 dividing cells were observed in the AB and 30 dividing cells in *aur<sup>B<sup>m/m</sup></sup>* embryos (**Figure 2B**). To account for the number of cells imaged, the ratio of mitotic cells to number of cells imaged was calculated (**Figure 2C**). This data suggest that there is not a lower number of cells going through mitosis in the *aur<sup>B<sup>m/m</sup></sup>* embryos (**Figure 2B**) but fewer numbers of cells being imaged. The ability to acquire a statistically significant number of events such as this will aid in statistical power.

**Figure 3** expands on this technique to include quantifying mitotic duration. Once a time-lapse session is acquired, an individual cell can be analyzed for time

spent in mitosis with adequate resolution by using the zoom tool (**Figure 3A, B**). Mitotic duration is calculated manually by counting how many time intervals take up one cell division. The number of time intervals is then multiplied by the interval of time between each Z-stack. For example, in **Figure 3C**, the division took up 12 time intervals and the interval of time between each Z-stack was 2 min. Therefore, the division time for this cell was 24 min. The average AB wild-type division time is 25 min and 58 min for *aurB<sup>m/m</sup>* (**Figure 3B**). A prolonged division time as seen in the *aurB<sup>m/m</sup>* suggests that the spindle assembly checkpoint has not been satisfied due to erroneous kinetochore attachments<sup>1,2</sup>. Taking a closer look at the zoomed in wild-type embryos, each mitotic phase can be distinguished (**Figure 3C, Movie 2**). In addition, mitotic defects can be observed in the *aurB<sup>m/m</sup>* embryo which include mitotic arrest and failed cytokinesis resulting in a binucleated cell and subsequent formation of a micronucleus (**Figure 3D, Movie 3**). This zoomed in analysis showing mitotic defects supports the increased division time acquired in **Figure 3B**.

Various other diverse mitotic defects and cell fates that may be encountered are explored in **Figure 4**; demonstrated in the *esco2<sup>+/m</sup>* and *esco2<sup>m/m</sup>* embryos. In an *esco2<sup>+/m</sup>* embryo, erroneous chromosome movements are captured and can be defined as congression defects. Congression defects occur when improper microtubule attachments are made. These defects will cause failure of the chromosomes to migrate toward the metaphase plate. Paired sister chromatids, particularly identifiable at min 20 and 46, that have not congressed toward the metaphase plate can be first observed at min 14. Anaphase onset separates the sister chromatids aligned at the metaphase plate as well as the paired sister chromatids to

the right, observed at minute 50. Additionally, possible micronucleus formation is observed as these separated sister chromatids remain isolated outside the nucleus (T= 50, **Figure 4A, Movie 4**). In **Figure 4B**, a multi-polar division is visualized (**Movie 5**). Multi-polar divisions often occur due to centrosome amplification, but may occur through other means<sup>42</sup>. In **Figure 4C**, an *esco2<sup>m/m</sup>* cell initially demonstrates premature sister chromatid separation and spindle rotation<sup>9,43,44</sup>. Another cell fate demonstrated in this panel is an anaphase bridge in which merotelic attachments are unresolved<sup>45,46</sup>. The anaphase bridge can be first seen at minute 62. The chromatin appears to prematurely decondense while the cell is undergoing cytokinesis. As cytokinesis occurs, the cleavage furrow impinges on the decondensed chromosomes and, as abscission occurs, pulls the chromatin material to form an anaphase bridge (**Figure 4C, Movie 6**). Though not shown here, in order to quantify the cellular fates, record all the mitotic divisions in each frame and the type of cell fate they exhibit. Divide the number of cells in each fate by the total number of divisions recorded and multiply by 100 to calculate the cell fate percentage.

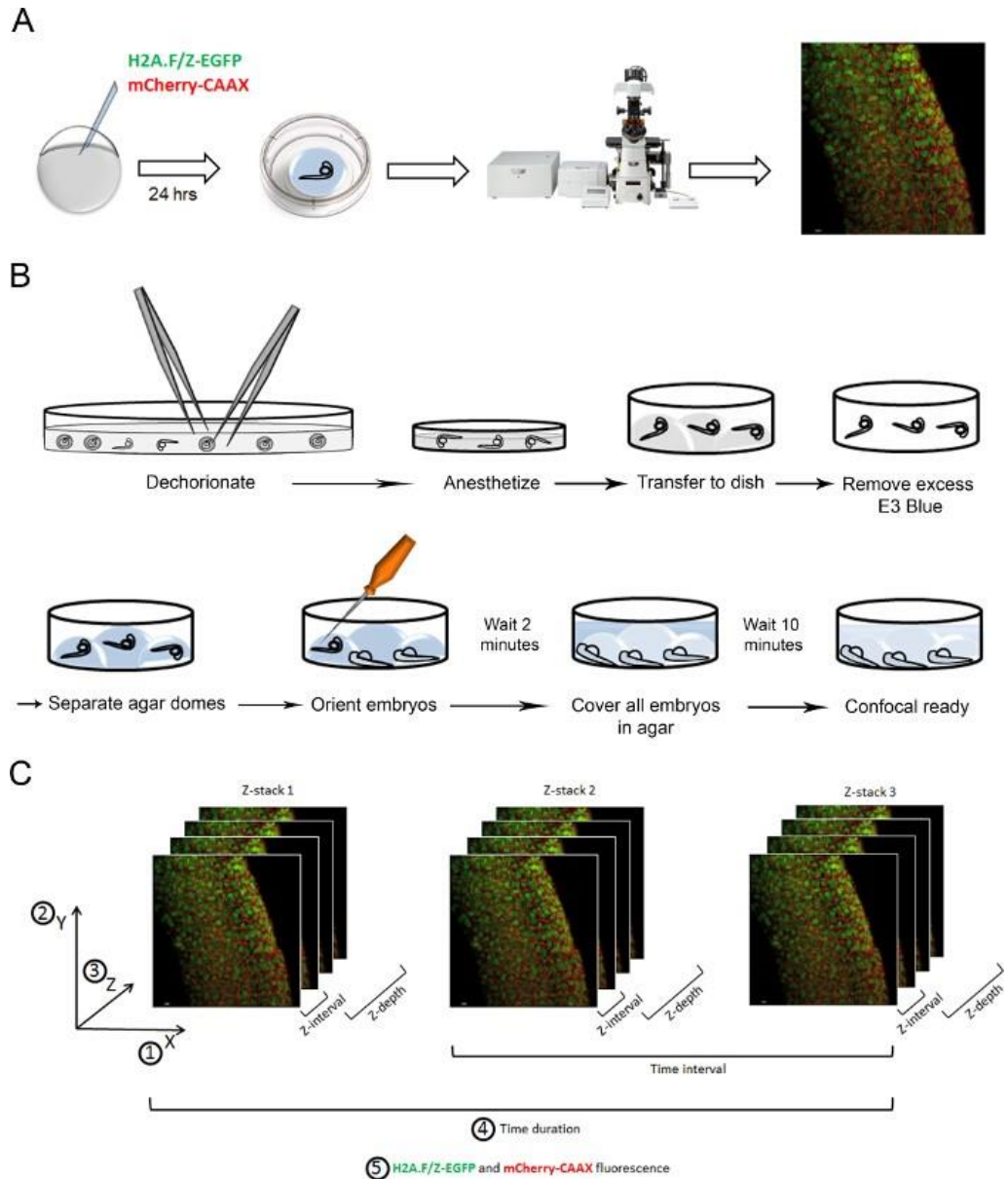


**Figure 1: Protocol Drawings Outline.** (A) Schematic drawing of the imaging technique progression beginning at H2A.F/Z-GFP and CAAX- mCherry mRNA injections, then onto embedding of embryos and procession to confocal microscopy. (B) Schematic drawing of the embryo embedding process. The injected embryos must be dechorionated and anesthetized. Embryos are then transferred to the coverslip-bottom dish and excess E3 Blue is removed. Low melt agar is used to create separate

domes covering each embryo. Orient the embryos so the tail is closest to the coverslip. Wait two min before adding agar covering the whole coverslip. Wait until the agar is solidified before moving to image. (C) Schematic drawing to define the terms Z-interval, Z-stack, Z-depth, time interval, time duration and 5D that are used in the protocol and discussion. Z-interval is defined as the distance between each image as the microscope moves deeper into the sample to create a Z-stack. Z-stack is all of the images taken through a sample at the defined Z-interval. The distance traveled in a Z-stack defines the Z-depth. Time interval is the amount of time between one Z-stack and the next Z-stack to create a time-lapse image. Time duration is the total amount of time used to image. 5D is defined as the dimensions X, Y, Z, time, and fluorescent emission.

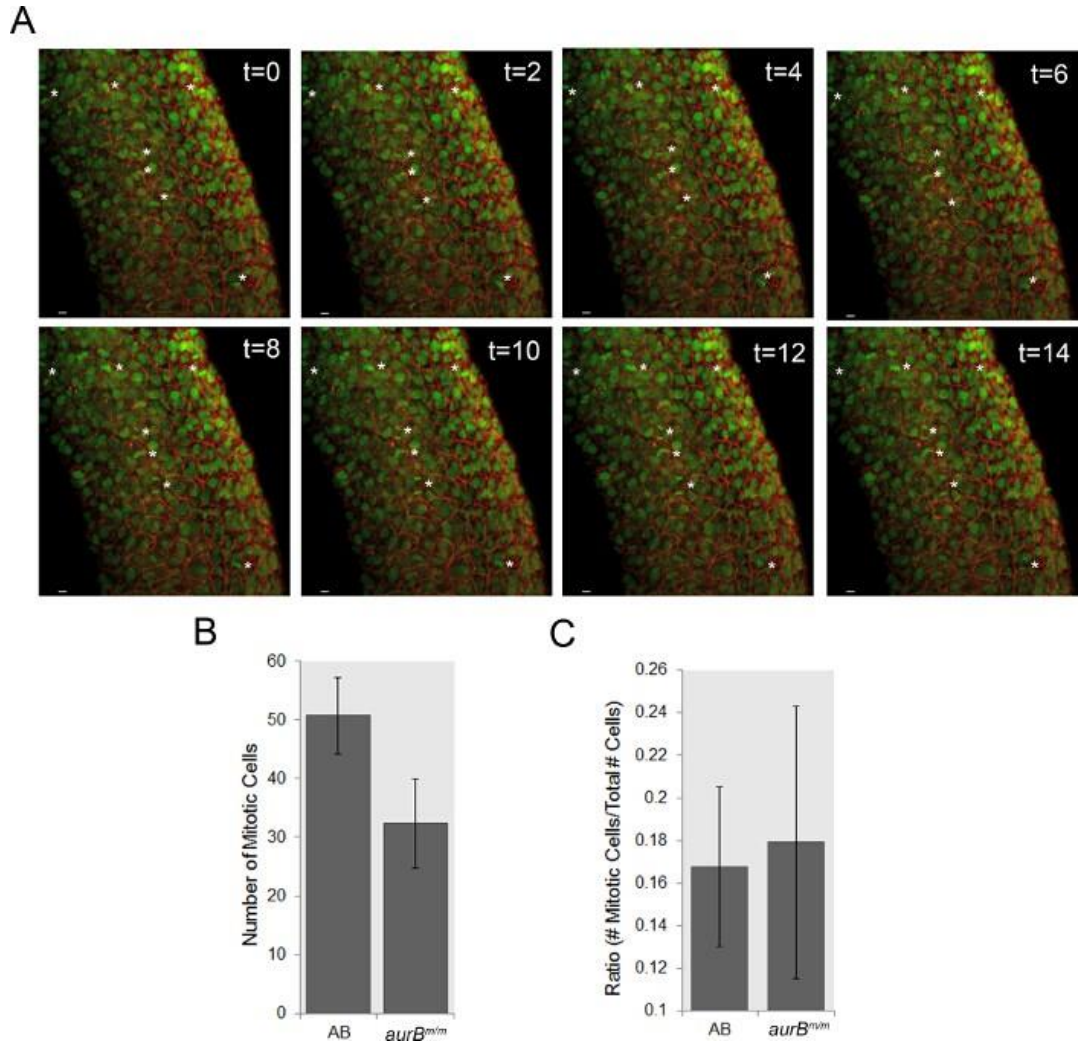


**Figure 2. Time-Lapse Imaging Captures Multiple Mitotic Events in a Live**

**Zebrafish Embryo. (A)** Time-lapse stills from a zoomed out experiment in an AB

wild-type, 24 hpf zebrafish showing multiple mitotic events. Asterisks point

towards seven cells in mitosis. t=time elapsed in min. Scale bar = 5  $\mu$ m. **(B)** The

number of mitotic cells observed in AB and *aurB<sup>m/m</sup>* zebrafish tails at 24 hpf.

Mean  $\pm$  st. dev., n = 3 embryos/ genotype. **(C)** The ratio of mitotic cells per total

number of cells in AB and *aurB<sup>m/m</sup>* zebrafish tails at 24 hpf. Mean  $\pm$  st. dev., n = 3

embryos/ genotype.

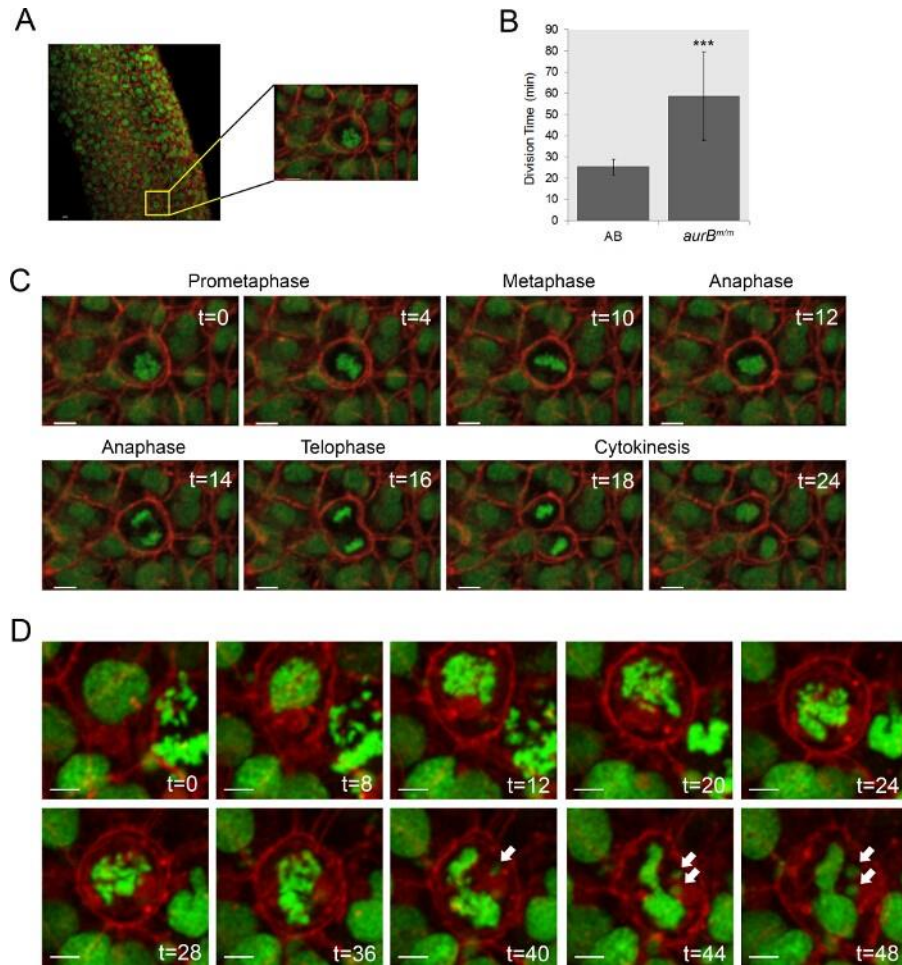


**Figure 3. Individual Cell Analysis Captures Each Mitotic Phase and Mitotic Duration.** (A) A cell selected from the wide field view of AB wild-type, 24 hpf zebrafish embryo shown in **Figure 2A**. (B) Division time is observed for AB and *aurB<sup>m/m</sup>* cells and calculated from inferring nuclear envelope breakdown (NEB) at the first observation of condensed chromatin in a cell to formation of two new daughter cells. n = 3 embryos/genotype, n = 66 divisions for AB, n = 29 divisions for *aurB<sup>m/m</sup>*, \*\*\*p-value < 0.001. (C) AB wild-type cell is cropped to visualize the phase progression through mitosis. t = min. Scale bar = 5  $\mu$ m. (D) *aurB<sup>m/m</sup>* cell is cropped

to visualize mitotic progression through mitosis which includes mitotic arrest resulting in cytokinesis failure and micronuclei formation. Arrows point towards the micronuclei. t = time elapsed in min. Scale bar = 5  $\mu\text{m}$ .

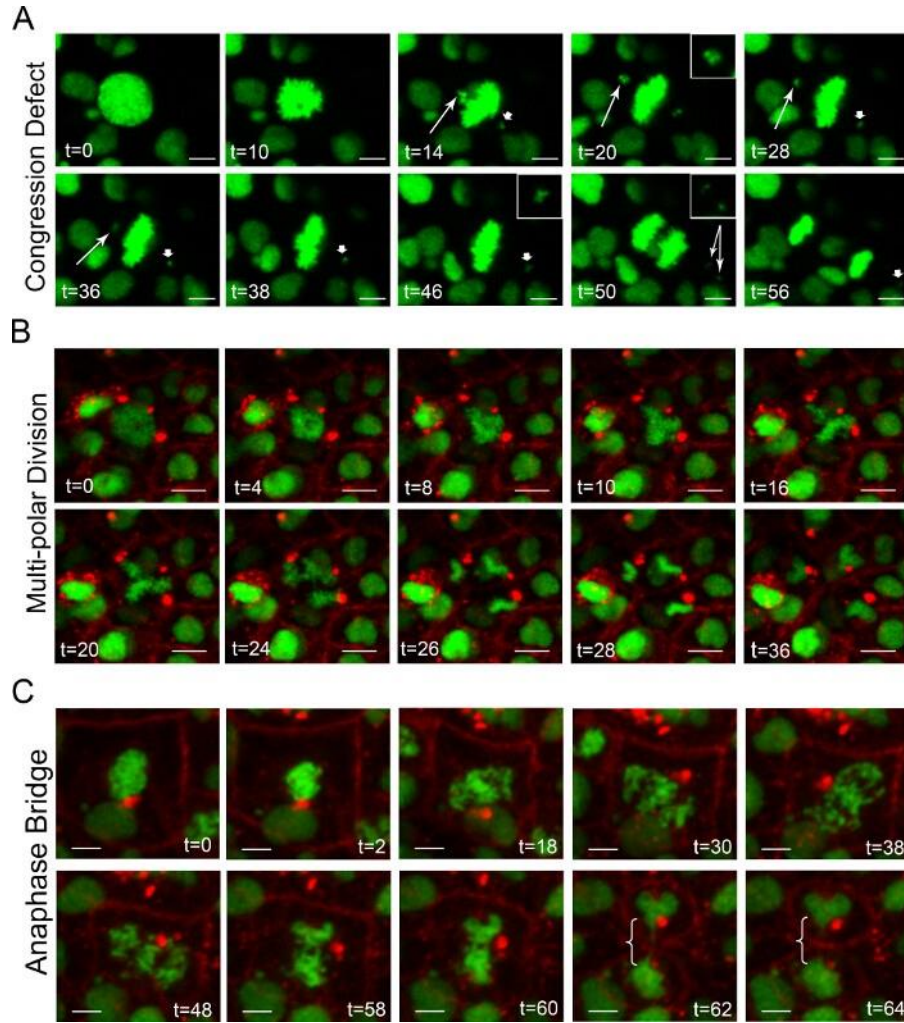


**Figure 4. Single Cell Live Imaging Captures Multiple Mitotic Defects Associated with Chromosome Segregation and Division in Mitotic Mutant Zebrafish. (A)**

A cropped image of a cell undergoing congression defects in an *esco2*<sup>+/*m*</sup> embryo. The thin arrow monitors the left chromosome that is pulled back into the metaphase plate. The thick arrow monitors the right chromosome that is not pulled back into the metaphase plate and inferred to form a micronucleus. The double arrow shows the separation of the right chromosome that did not congress at anaphase onset. Insets show zoomed in views of the chromosomes that failed to congress. Insets were

cropped and brightness enhanced for better visualization. CAAX fluorescence was removed to visualize the chromosomes more easily. Scale bar = 5  $\mu\text{m}$ . **(B)** A cropped image of a cell undergoing mitotic arrest that results in a multi-polar division in an *esco2<sup>+/m</sup>* embryo. Scale bar = 5  $\mu\text{m}$ . **(C)** A cropped image of a cell undergoing cohesion fatigue resulting in anaphase bridge formation seen by the thread-like pulling between the two nuclei noted by the brackets. Scale bar = 5  $\mu\text{m}$ . t=time elapsed in min.

## DISCUSSION

Use of this method allows one to infer nuclear envelope breakdown, formation of a metaphase plate by microtubule-kinetochore attachments, and segregation of sister chromatids to form two new cells *in vivo* and in a time-dependent manner. The ability to observe mitosis in zebrafish is advantageous over fixed samples and cell culture systems because the cells are being imaged in the natural physiology, the tissue is transparent which allows for fluorescent proteins to be used, they develop relatively fast, and time-lapse imaging can be acquired. Use of adult zebrafish for this protocol is restricted due to the limited Z-depth that can be acquired due to the thicker tissue that is not the skin or eyes. While transgenic animals expressing H2A.F/Z-EGFP and mCherry-CAAX could be used for the same purpose, the versatility and ease of the mRNA injections into different mutant zebrafish is advantageous over genetic crosses. In situations where mitotic analysis is required in three days post fertilization (dpf) or later embryos, transgenic animals would be necessary due to the half-life of RNA in this rapidly developing organism.

Other fluorescent proteins for visualizing mitosis are amenable to this protocol. For example, H2B-GFP mRNA is an alternative to H2A.F/Z-EGFP for chromatin, and provides similar labeling. Other fluorescent-tagged proteins that can be used in this technique include POM121, centrin, Eb1, Hec1, and EMTB which would allow for live in-embryo imaging of the nuclear envelope, centrioles, plus-end microtubules, kinetochore, and microtubules, respectively<sup>32,47-51</sup>.

This protocol has several key imaging steps that must be executed to achieve quality results: 1) Make sure to optimize the mRNA quality and concentration to yield the brightest fluorescence and no toxicity as possible. The more fluorescence will lead to less laser exposure and therefore, less photobleaching and phototoxicity. 2) The embryo must be fully anesthetized and secure in the agar. Minor movements will alter results and could ruin the experiment. 3) The agar concentration must be appropriate for the stage of embryo desired to be imaged. At 24 hpf and further, 1% low-melt agarose is suitable. If imaging at 12 hpf or earlier, a 0.3% agarose solution should be used<sup>39</sup>. 4) The ROI in the embryo should be as close to the coverslip as possible. This step does not limit one to imaging the tail. The eyes, skin, dorsal region, yolk, and fin fold are examples of other areas that can use this protocol.

Time is the defining factor that separates this protocol from imaging fixed embryos or tissues. When setting up the Z-stack, Z-interval, time-lapse interval, and time-lapse duration, it is important to keep in mind the context of the experiment (**Figure 1C**). A wild-type cell division usually lasts approximately 25 min at 24 hpf. In this instance, a 2  $\mu\text{m}$  Z-interval covering 40  $\mu\text{m}$  of tissue in a Z-stack, with a two minute time interval for two hr has proven effective. Further, in embryos with

defective mitosis, cells in a mitotic arrest will most likely be present, drastically increasing cell division times. To acquire multiple full divisions, the time duration should be increased, *i.e.* from two hr to four hr. A longer acquisition time will expose the sample to more laser power and increase the risk of photobleaching and phototoxicity. In this case, the time interval between each Z-stack should be increased. Dynamic chromosome movements will be sacrificed by increasing the time interval between Z-stacks, but time duration is gained. This is necessary when imaging cell divisions that may last over two hr.

Though it was not directly discussed, this protocol can be optimized to obtain a higher resolution image in the Z-plane to more accurately visualize individual chromosome movements. For example, in **Figure 4A** two missegregated chromosomes are observed. The chromosome to the right (noted by the thick arrow) is initially bright and in focus but dims in the last few frames. With a 2  $\mu\text{m}$  Z-interval, the uncongressed chromosome falls in between the Z-interval. Capturing minute movements and singular chromosome events can be accomplished by increasing the resolution in the Z plane. To do this, zoom in on an individual cell using the A1 Scan Area tool. When setting up the Z-stack parameters, use a smaller Z-interval distance. A recommended range is 0.5 - 1  $\mu\text{m}$ . In addition, decreasing the time interval between each Z stack will create smoother transitions between each time frame, *i.e.* from two min to 30 sec - 1 min. One caveat to this type of imaging is the limited Z-depth that can be attained. Due to the smaller Z-interval and time interval, more tissue will be exposed to the lasers in a smaller time frame. To overcome this, smaller time

duration can be used; however this is also dependent on how long the researcher would like to capture divisions.

An analogy that may help with these modifications is to think of a Z-stack as an accordion. The distance between each pleat of the bellows is the Z-interval and the Z-depth is represented by the length of the accordion. In an instance where one would not want to accrue any more laser exposure to the sample, as the accordion stretches (increases Z-depth), the distance between the pleats of the bellows (Z-interval) must increase as well. The inverse is true in that as the accordion contracts, the Z-depth decreases. The pleats of the bellows contract as well, corresponding to a decrease in Z-interval. This analogy can be applied to fixed and live samples. The complexity is increased in this protocol when time is added to the equation. There is a finite amount of time that the accordionist can extend or contract the accordion. This represents the time interval. In order to cover more distance (Z-depth) the time interval must increase. As well, in order to hear more music, one must listen for a longer amount of time (time duration) In terms of this protocol, in order to witness more cell divisions, the time duration must increase. A compounding factor to keep in mind is that the more music that is played, the more tired the accordionist. This is analogous to the final dimension, fluorescence. The more laser exposure the sample is given, the more photobleaching and phototoxicity (tiredness) becomes an issue.

In summary, this protocol details a method to visualize mitosis in a live zebrafish embryo applicable to different analyses; 1) division number 2) division time 3) division fate and 4) high resolution chromatin dynamics. Multiple possibilities for visualizing mitotic components ranging from microtubule-

kinetochore attachments to centriole dynamics can be applied. Combining the capability of imaging mitosis *in vivo* with the recent advances in genome editing in zebrafish will make it easy to generate mutants in various aspects of mitosis to model human disease in a vertebrate organism<sup>25,26,52-56</sup>.

## **DISCLOSURES**

The authors have nothing to disclose.

## **ACKNOWLEDGEMENTS**

We thank Kristen Kwan for the pCS2-H2A.F/Z-EGFP and pCS2-mCherry-CAAX vectors. We thank Chris Rodesch for tutoring us in live imaging in zebrafish. We thank Shawn Williams, Erik Malarkey and Brad Yoder for assistance in confocal imaging at UAB and the High Resolution Imaging Facility at UAB. The High Resolution Imaging Facility is supported by the UAB Comprehensive Cancer Center Support Grant (P30CA013148) and the Rheumatic Disease Core Center (P30AR048311). J.M.P. is supported by the National Institute of Neurological Disease and Stroke (NIH R21 NS092105), and pilot grants from American Cancer Society (ACS IRG-60-001-53-IRG) and the UAB Comprehensive Cancer Center (P30CA013148). S.M.P. is supported by the Cell and Molecular Biology T32 Training Grant (5T32GM008111-28).

## REFERENCES

1. Musacchio, A., Hardwick, K. G. The spindle checkpoint: structural insights into dynamic signalling. *Nat Rev Mol Cell Biol.* **3** (10), 731-741 (2002).
2. Li, X., Nicklas, R. B. Mitotic forces control a cell-cycle checkpoint. *Nature.* **373** (6515), 630-632 (1995).
3. Rieder, C. L., Cole, R. W., Khodjakov, A., Sluder, G. The checkpoint delaying anaphase in response to chromosome monoorientation is mediated by an inhibitory signal produced by unattached kinetochores. *J Cell Biol.* **130** (4), 941-948 (1995).
4. Hayles, J., Nurse, P. A review of mitosis in the fission yeast *Schizosaccharomyces pombe*. *Exp Cell Res.* **184** (2), 273-286 (1989).
5. Pederson, T. Historical review: an energy reservoir for mitosis, and its productive wake. *Trends Biochem Sci.* **28** (3), 125-129 (2003).
6. Sobel, S. G. Mini review: mitosis and the spindle pole body in *Saccharomyces cerevisiae*. *J Exp Zool.* **277** (2), 120-138 (1997).
7. Thompson, S. L., Compton, D. A. Chromosome missegregation in human cells arises through specific types of kinetochore-microtubule attachment errors. *Proc Natl Acad Sci U S A.* **108** (44), 17974-17978 (2011).
8. Duijf, P. H., Benezra, R. The cancer biology of whole-chromosome instability. *Oncogene.* **32** (40), 4727-4736 (2013).
9. Lara-Gonzalez, P., Taylor, S. S. Cohesion fatigue explains why pharmacological inhibition of the APC/C induces a spindle checkpoint- dependent mitotic arrest. *PLoS One.* **7** (11), e49041 (2012).
10. Araujo, A., Baum, B., Bentley, P. The role of chromosome missegregation in cancer development: a theoretical approach using agent-based modelling. *PLoS One.* **8** (8), e72206 (2013).
11. Deardorff, M. A. *et al.* HDAC8 mutations in Cornelia de Lange syndrome affect the cohesin acetylation cycle. *Nature.* **489** (7415), 313-317 (2012).
12. Chetaille, P. *et al.* Mutations in SGOL1 cause a novel cohesinopathy affecting heart and gut rhythm. *Nat Genet.* **46** (11), 1245-1249 (2014).
13. Kaiser, F. J. *et al.* Loss-of-function HDAC8 mutations cause a phenotypic spectrum of Cornelia de Lange syndrome-like features, ocular hypertelorism, large fontanelle and X-linked inheritance. *Hum Mol Genet.* **23** (11), 2888-2900 (2014).
14. Snape, K. *et al.* Mutations in CEP57 cause mosaic variegated aneuploidy syndrome. *Nat Genet.* **43** (6), 527-529 (2011).
15. Suijkerbuijk, S. J. *et al.* Molecular causes for BUBR1 dysfunction in the human cancer predisposition syndrome mosaic variegated aneuploidy. *Cancer Res.* **70** (12), 4891-4900 (2010).
16. Vega, H. *et al.* Roberts syndrome is caused by mutations in ESCO2, a human homolog of yeast ECO1 that is essential for the establishment of sister chromatid cohesion. *Nat Genet.* **37** (5), 468-470 (2005).
17. Andrews, P. D., Harper, I. S., Swedlow, J. R. To 5D and beyond: quantitative fluorescence microscopy in the postgenomic era. *Traffic.* **3** (1), 29-36 (2002).

18. Nigg, E. A. Mitotic kinases as regulators of cell division and its checkpoints. *Nat Rev Mol Cell Biol.* **2** (1), 21-32 (2001).
19. Carlton, J. G., Caballe, A., Agromayor, M., Kloc, M., Martin-Serrano, J. ESCRT-III governs the Aurora B-mediated abscission checkpoint through CHMP4C. *Science.* **336** (6078), 220-225 (2012).
20. Yabe, T. *et al.* The maternal-effect gene cellular island encodes aurora B kinase and is essential for furrow formation in the early zebrafish embryo. *PLoS Genet.* **5** (6), e1000518 (2009).
21. Hou, F., Zou, H. Two human orthologues of Eco1/Ctf7 acetyltransferases are both required for proper sister-chromatid cohesion. *Mol Biol Cell.* **16** (8), 3908-3918 (2005).
22. Ivanov, D. *et al.* Eco1 is a novel acetyltransferase that can acetylate proteins involved in cohesion. *Curr Biol.* **12** (4), 323-328 (2002).
23. Beckouet, F. *et al.* An Smc3 acetylation cycle is essential for establishment of sister chromatid cohesion. *Mol Cell.* **39** (5), 689-699 (2010).
24. Monnich, M., Kuriger, Z., Print, C. G., Horsfield, J. A. A zebrafish model of Roberts syndrome reveals that Esco2 depletion interferes with development by disrupting the cell cycle. *PLoS One.* **6** (5), e20051 (2011).
25. Percival, S. M. *et al.* Variations in dysfunction of sister chromatid cohesion in esco2 mutant zebrafish reflect the phenotypic diversity of Roberts syndrome. *Dis Model Mech.* **8** (8), 941-955 (2015).
26. Amsterdam, A., Hopkins, N. Retroviral-mediated insertional mutagenesis in zebrafish. *Methods Cell Biol.* **77** 3-20 (2004).
27. Amsterdam, A. *et al.* Identification of 315 genes essential for early zebrafish development. *Proc Natl Acad Sci U S A.* **101** (35), 12792-12797 (2004).
28. Jeon, H. Y., Lee, H. Depletion of Aurora-A in zebrafish causes growth retardation due to mitotic delay and p53-dependent cell death. *FEBS J.* **280** (6), 1518-1530 (2013).
29. Jeong, K., Jeong, J. Y., Lee, H. O., Choi, E., Lee, H. Inhibition of Plk1 induces mitotic infidelity and embryonic growth defects in developing zebrafish embryos. *Dev Biol.* **345** (1), 34-48 (2010).
30. Bonenfant, D., Coulot, M., Towbin, H., Schindler, P., van Oostrum, J. Characterization of histone H2A and H2B variants and their post-translational modifications by mass spectrometry. *Mol Cell Proteomics.* **5** (3), 541-552 (2006).
31. Kwan, K. M. *et al.* A complex choreography of cell movements shapes the vertebrate eye. *Development.* **139** (2), 359-372 (2012).
32. Pilaz, L. J., Silver, D. L. Live imaging of mitosis in the developing mouse embryonic cortex. *J Vis Exp.* (88) (2014).
33. Davidson, G. *et al.* Casein kinase 1 gamma couples Wnt receptor activation to cytoplasmic signal transduction. *Nature.* **438** (7069), 867-872 (2005).
34. Smith, R. M. *et al.* Exocytotic insertion of calcium channels constrains compensatory endocytosis to sites of exocytosis. *J Cell Biol.* **148** (4), 755-767 (2000).

35. Reid, T. S., Terry, K. L., Casey, P. J., Beese, L. S. Crystallographic analysis of CaaX prenyltransferases complexed with substrates defines rules of protein substrate selectivity. *J Mol Biol.* **343** (2), 417-433 (2004).
36. Gerlach, G. F., Morales, E. E., Wingert, R. A. Microbead Implantation in the Zebrafish Embryo. *J Vis Exp.* (101), e52943 (2015).
37. Porazinski, S. R., Wang, H., Furutani-Seiki, M. Microinjection of medaka embryos for use as a model genetic organism. *J Vis Exp.* (46) (2010).
38. Rosen, J. N., Sweeney, M. F., Mably, J. D. Microinjection of zebrafish embryos to analyze gene function. *J Vis Exp.* (25) (2009).
39. Sugiyama, M. *et al.* Illuminating cell-cycle progression in the developing zebrafish embryo. *Proc Natl Acad Sci U S A.* **106** (49), 20812-20817 (2009).
40. Ariga, J., Walker, S. L., Mumm, J. S. Multicolor time-lapse imaging of transgenic zebrafish: visualizing retinal stem cells activated by targeted neuronal cell ablation. *J Vis Exp.* (43) (2010).
41. O'Brien, G. S. *et al.* Two-photon axotomy and time-lapse confocal imaging in live zebrafish embryos. *J Vis Exp.* (24) (2009).
42. Maiato, H., Logarinho, E. Mitotic spindle multipolarity without centrosome amplification. *Nat Cell Biol.* **16** (5), 386-394 (2014).
43. Gorbsky, G. J. Cohesion fatigue. *Curr Biol.* **23** (22), R986-988 (2013).
44. Daum, J. R. *et al.* Cohesion fatigue induces chromatid separation in cells delayed at metaphase. *Curr Biol.* **21** (12), 1018-1024 (2011).
45. Germann, S. M. *et al.* TopBP1/Dpb11 binds DNA anaphase bridges to prevent genome instability. *J Cell Biol.* **204** (1), 45-59 (2014).
46. Chan, K. L., North, P. S., Hickson, I. D. BLM is required for faithful chromosome segregation and its localization defines a class of ultrafine anaphase bridges. *EMBO J.* **26** (14), 3397-3409 (2007).
47. Wuhr, M., Obholzer, N. D., Megason, S. G., Detrich, H. W., 3rd, Mitchison, T. J. Live imaging of the cytoskeleton in early cleavage-stage zebrafish embryos. *Methods Cell Biol.* **101** 1-18 (2011).
48. Rogers, S. L., Rogers, G. C., Sharp, D. J., Vale, R. D. Drosophila EB1 is important for proper assembly, dynamics, and positioning of the mitotic spindle. *J Cell Biol.* **158** (5), 873-884 (2002).
49. Gascoigne, K. E., Cheeseman, I. M. CDK-dependent phosphorylation and nuclear exclusion coordinately control kinetochore assembly state. *J Cell Biol.* **201** (1), 23-32 (2013).
50. Scott, E. S., O'Hare, P. Fate of the inner nuclear membrane protein lamin B receptor and nuclear lamins in herpes simplex virus type 1 infection. *J Virol.* **75** (18), 8818-8830 (2001).
51. Shankaran, S. S., Mackay, D. R., Ullman, K. S. A time-lapse imaging assay to study nuclear envelope breakdown. *Methods Mol Biol.* **931** 111-122 (2013).
52. Jao, L. E., Wente, S. R., Chen, W. Efficient multiplex biallelic zebrafish genome editing using a CRISPR nuclease system. *Proc Natl Acad Sci U S A.* **110** (34), 13904-13909 (2013).
53. Irion, U., Krauss, J., Nusslein-Volhard, C. Precise and efficient genome editing in

- zebrafish using the CRISPR/Cas9 system. *Development*. **141** (24), 4827-4830 (2014).
54. Hwang, W. Y. *et al.* Efficient genome editing in zebrafish using a CRISPR-Cas system. *Nat Biotechnol*. **31** (3), 227-229 (2013).
55. Hruscha, A. *et al.* Efficient CRISPR/Cas9 genome editing with low off-target effects in zebrafish. *Development*. **140** (24), 4982-4987 (2013).
56. Thomas, H. R., Percival, S. M., Yoder, B. K., Parant, J. M. High-throughput genome editing and phenotyping facilitated by high resolution melting curve analysis. *PLoS One*. **9** (12), e114632 (2014).

VARIATIONS IN SISTER CHROMATID COHESION DYSFUNCTION IN *ESCO2*  
MUTANT ZEBRAFISH REFLECTS THE PHENOTYPIC DIVERSITY OF ROBERTS  
SYNDROME

by

STEFANIE M. PERCIVAL, HOLLY R. THOMAS, ADAM AMSTERDAM, ANDREW  
J. CARROLL, JACQUELINE A. LEES, H. JOSEPH YOST, AND JOHN M. PARANT

*Disease Models and Mechanisms*

2015

Format adapted for dissertation

## ABSTRACT

Mutations in ESCO2, one of two Establishment of Cohesion factors necessary for proper Sister Chromatid Cohesion (SCC), cause a spectrum of developmental defects in the autosomal recessive disorder Roberts Syndrome (RBS), warranting in vivo analysis of the consequence of cohesion dysfunction. Through a genetic screen in zebrafish targeting embryonic lethal mutants with increased genomic instability, we have identified an *esco2* mutant zebrafish. Utilizing the natural transparency of zebrafish embryos, we have developed a novel technique to observe chromosome dynamics within a single cell during mitosis in a live vertebrate embryo. Within *esco2* mutant embryos, we observed premature chromatid separation, a unique chromosome scattering, prolonged mitotic delay, and genomic instability in the form of anaphase bridges and micronuclei formation. Cytogenetic studies indicated complete chromatid separation and high levels of aneuploidy within mutant embryos. Amongst aneuploid spreads, we observed predominantly decreases in chromosome number, suggesting either cells with micronuclei or micronuclei themselves are eliminated. We also demonstrated that the genomic instability leads to p53-dependent neural tube apoptosis. Surprisingly, while many cells require EscO2 to establish cohesion, 10-20% of cells have only weakened cohesion in the absence of EscO2, suggesting that compensatory cohesion mechanisms exist in these cells that undergo a normal mitotic division. These studies provide a unique in vivo vertebrate view of the mitotic defects and consequences of cohesion establishment loss, and they provide a compensation-based model to explain the RBS phenotypes.

## INTRODUCTION

Sister Chromatid Cohesion (SCC) is a dynamic, cell cycle-dependent process essential for proper segregation of chromosomes. A protein complex forms a cohesin ring comprised of SMC1a, SMC3, RAD21, and STAG1/2 that is associated, or “loaded”, onto DNA during the G1 phase of the cell cycle by the NIPBL and Mau-2 proteins (Losada, 2008; Nasmyth and Haering, 2009; Ocampo-Hafalla and Uhlmann, 2011). Upon entry into S-phase, as the sister chromatids are being synthesized, ESCO1 & 2 proteins establish cohesion by securing the cohesin ring around sister chromatids (Skibbens et al., 1999; Hartman et al., 2000; Homer et al., 2005; Skibbens, 2009; Terret et al., 2009). During mitosis, cohesion is removed in two steps: 1) During the transition from prophase to prometaphase, cohesion between chromatid arms is removed through the anti-establishment pathway involving WAPAL, while the centromeric cohesion is protected by establishment/maintenance factors including SGO1/2 and Sororin (Salic et al., 2004; Rankin et al., 2005; Gandhi et al., 2006; Kueng et al., 2006; Sutani et al., 2009); and 2) Upon proper bipolar attachment of all chromosomes, the cell will undergo metaphase-to-anaphase transition in which the enzyme separase cleaves the remaining centromeric cohesin rings, allowing sister chromatid segregation to opposing spindle poles (Waizenegger et al., 2000; Sonoda et al., 2001; Losada, 2008). Improper attachments or lack of kinetochore tension results in maintenance of the spindle assembly checkpoint preventing the metaphase-to-anaphase transition (Li and Nicklas, 1995; Nicklas et al., 1995). Beyond the mitotic function of SCC, studies have expanded its function to a wide assortment of cellular functions including DNA repair (Sjogren and Nasmyth, 2001; Kim et al., 2002; Schar et al., 2004; Strom and Sjogren, 2005; Gause et al., 2008; Gondor and

Ohlsson, 2008; Heidinger-Pauli et al., 2009; Covo et al., 2010; Lu et al., 2010; Dorsett and Strom, 2012), gene regulation (Horsfield et al., 2007; Pauli et al., 2010; Dorsett and Strom, 2012; Horsfield et al., 2012), ribogenesis (Xu et al., 2013), and centrosome duplication (Schockel et al., 2011; Yamada et al., 2012).

Traditionally, SCC is studied in the context of individual cells. However, the recent discovery that components of SCC are responsible for human developmental disorders and tumorigenesis has illuminated the requirement for *in vivo* analysis (Duijf and Benezra, 2013); (Liu and Krantz, 2008). Roberts Syndrome (RBS) patients harboring recessive mutations exclusively in ESCO2 have a range in severity of disease from prenatal lethal to viable beyond 30 years of age, as well as a variety of specific developmental phenotypes, including microcephaly, craniofacial defects, mental retardation, limb deformities, and growth retardation (Schule et al., 2005; Vega et al., 2010). In addition to these hallmark phenotypes, some RBS patients also display cardiac defects and corneal opacity, as well as other less prominent phenotypes (Vega et al., 2010). Interestingly, among the few individuals that live beyond 30, some developed tumors at an early age, suggesting a cancer predisposition (Wenger et al., 1988; Ogilvy et al., 1993; Schule et al., 2005). Metaphase spreads from RBS patients display centromeric separation and low levels of aneuploidy, suggesting the defects are associated with SCC and missegregation of chromosomes (German, 1979; Tomkins et al., 1979). How such an essential gene could have developmental phenotypes is unclear. There are two vertebrate paralogs (ESCO1 and ESCO2) of the yeast ECO1 required for establishing SCC (Skibbens et al., 1999; Toth et al., 1999). Both ESCO1 and ESCO2 contain acetyltransferase domains and have the ability to acetylate SMC3, locking it in the cohesion

position. While they appear to have overlapping activities, the Zou lab demonstrated that they have non-redundant functions since both must be depleted to have complete SCC loss in HeLa cells (Hou and Zou, 2005). Potentially, the tissue-specific phenotypes (ex. limb, craniofacial, neural...) found in RBS patients (exclusively due to ESCO2 mutations) are associated with differential requirements for ESCO1 or ESCO2 in different tissues. In addition to RBS, there are other developmental syndromes due to mutations in SCC components: 1) Cornelia de Lange (CdLS), caused by mutations in NIPBL, SMC1, SMC3, HDAC8, and RAD21 (Krantz et al., 2004; Tonkin et al., 2004; Musio et al., 2006; Deardorff et al., 2007; Liu and Krantz, 2008); 2) Warsaw Breakage Syndrome (WABS), caused by mutations in DDX11 (van der Lelij et al., 2010; Capochichi et al., 2013); and 3) Chronic Atrial and Intestinal Dysrhythmia (CAID), caused by mutations in SGOL1 (Chetaille et al., 2014). Importantly, with the exception of CdLS, these syndromes all display premature chromatid separation in metaphase spreads suggesting this is pathogenic in the diseases.

In the wake of identifying the causal gene for RBS, a few animal models provided key initial studies for the role of ESCO2 in RBS. The mouse knockout of *Esco2* is 8 cell-stage lethal, which unfortunately limits in vivo multicellular analysis (Whelan et al., 2012). Utilizing a conditional allele, *Esco2* null mouse embryonic fibroblasts were generated, and cell culture analysis revealed partial chromatid separation and genomic instability. A zebrafish morphant (morpholino-derived partial knockdown) study focusing largely on RBS phenotypes indicated that zebrafish can recapitulate many of the morphological RBS-like phenotypes (Monnich et al., 2011). Importantly, they observed that different RBS phenotypes occurred at varying levels of morpholino knock-down,

suggesting that the degree of SCC loss correlates with the severity of RBS phenotypes. Notably, they describe that the mitotic and apoptotic phenotypes associated with induction of stress genes, but not cohesin-dependent gene expression changes, drive the RBS phenotypes. While these studies focus on key RBS phenotypes, little knowledge is known about the in vivo, cellular events that result from *Esco2* loss.

In this study, we characterize the dynamic, in vivo, cellular consequences that present in an *esco2* mutant zebrafish. We find that in addition to prolonged mitotic arrest, there are chromosome segregation defects, micronuclei formation, and genomic instability. In addition, we demonstrate a cohesion compensatory mechanism in a portion of cells of an *esco2* mutant embryo; supporting the idea that different cells, and potentially tissues, have different sensitivities (or redundancies) to *Esco2* loss.

## **RESULTS**

### ***esco2* retroviral insertion mutant identified through unique p53 genetic screen**

During tumorigenesis, p53 is activated following cellular stress resulting in sequestration or termination of the stressed cell (Junttila and Evan, 2009; Meek, 2009). Through our previous studies, we observed that either following loss of *mdm2*, the negative regulator of p53, or following Ionizing Radiation (IR) treatment, zebrafish embryos displayed a darkening of the head region referred to as head necrosis at 24 hpf (hours post fertilization), which is derived from an increase in apoptosis in the neural tube (Berghmans et al., 2005; Sidi et al., 2008; Parant et al., 2010; Toruno et al., 2014). To better understand 1) which cellular stresses activate p53, 2) what birth defects result from p53 activation, and 3) the mechanisms of p53 activation following the cellular

stress, we devised a genetic screen to identify p53-dependent embryonic lethal zebrafish mutants. More specifically, this screen was designed to identify embryonic lethal mutants with head necrosis that can be fully or partially rescued by loss of p53. We utilized the Hopkins retroviral insertion-derived embryonic lethal mutant collection as a source of embryonic lethal mutants (Fig. 1A) (Amsterdam et al., 2004). From this collection, we selected 90 embryonic lethal mutants with the head necrosis phenotype. To determine if the head necrosis is p53-dependent, we injected half of the clutch from 60 heterozygous intercrossed mutant families with a p53 knockdown-morpholino. Injected and uninjected embryos were monitored for head necrosis and other morphological phenotypes between 20 and 48 hpf. From this primary screen, we identified 10 mutants that displayed partial rescue following p53 morpholino injection (hi821a, hi1045, hi1477, hi2404, hi 2877b, hi2865, hi 2975, hi3635, hi3662, hi3820a). None of the 10 mutants displayed complete rescue following p53 morpholino injections, suggesting either that additional non-p53-dependent defects are present or the morpholino knockdown was not complete or was no longer effective at inhibiting p53 activity over time.

One of the mutants identified was the hi2865 line, with a retroviral insertion in intron 1 of the ENDARG00000014685 gene (Fig. 1B, Supp. Fig. S1A). To determine if homozygosity for this insertion correlated with the mutant phenotype observed, we performed High Resolution Melt curve analysis (HRMA), in addition to multiplex allele-specific PCR (Supp. Fig. S1B, C respectively). The results confirmed that 100% (n=11 of 11) of mutant embryos were homozygous for the insertion, and that none (n=32 of 32) of the normal siblings were homozygous for the insertion. ENDARG00000014685 has homology to the Establishment of Cohesion homolog 2 gene (ESCO2), and displays

strong synteny with the mouse and human genomic region surrounding ESCO2 (Supp. Fig. S1D).

Previous work has shown that the majority of intron 1 retroviral insertions knockdown the endogenous gene transcript by greater than 80% (Wang et al., 2007). We performed qRT-PCR on pooled wild-type and mutant embryos (henceforth *esco2*<sup>hi2865/hi2865</sup> will be referred to as *esco2*<sup>m/m</sup>) at 18 hpf, 30 hpf, and 48 hpf. By 18 hpf, we observe ~7% of normal transcript and by 48 hpf ~2% of transcript (Supp. Fig. S2), indicating: 1) the retroviral insertion diminished the *esco2* transcript by >95%, and 2) by 18 hpf majority of maternal transcript is absent. To further validate that these morphological phenotypes are due to disruption of *esco2*, we have recently generated an *esco2* exon 3 frameshift mutations (*esco2*<sup>+13</sup>), using the CRISPR genome editing system (Hwang et al., 2013; Jao et al., 2013; Thomas et al., 2014). Homozygous *esco2*<sup>+13/+13</sup> embryos have the same gross morphological phenotypes (Supp. Fig. S3A, B) and decrease in *esco2* mRNA expression (Supp. Fig. S2) as *esco2*<sup>m/m</sup> embryos. Note the reduced mRNA expression in the *esco2*<sup>+13/+13</sup> embryos is most likely due to nonsense mediated decay due to the premature stop in the +13 transcript.

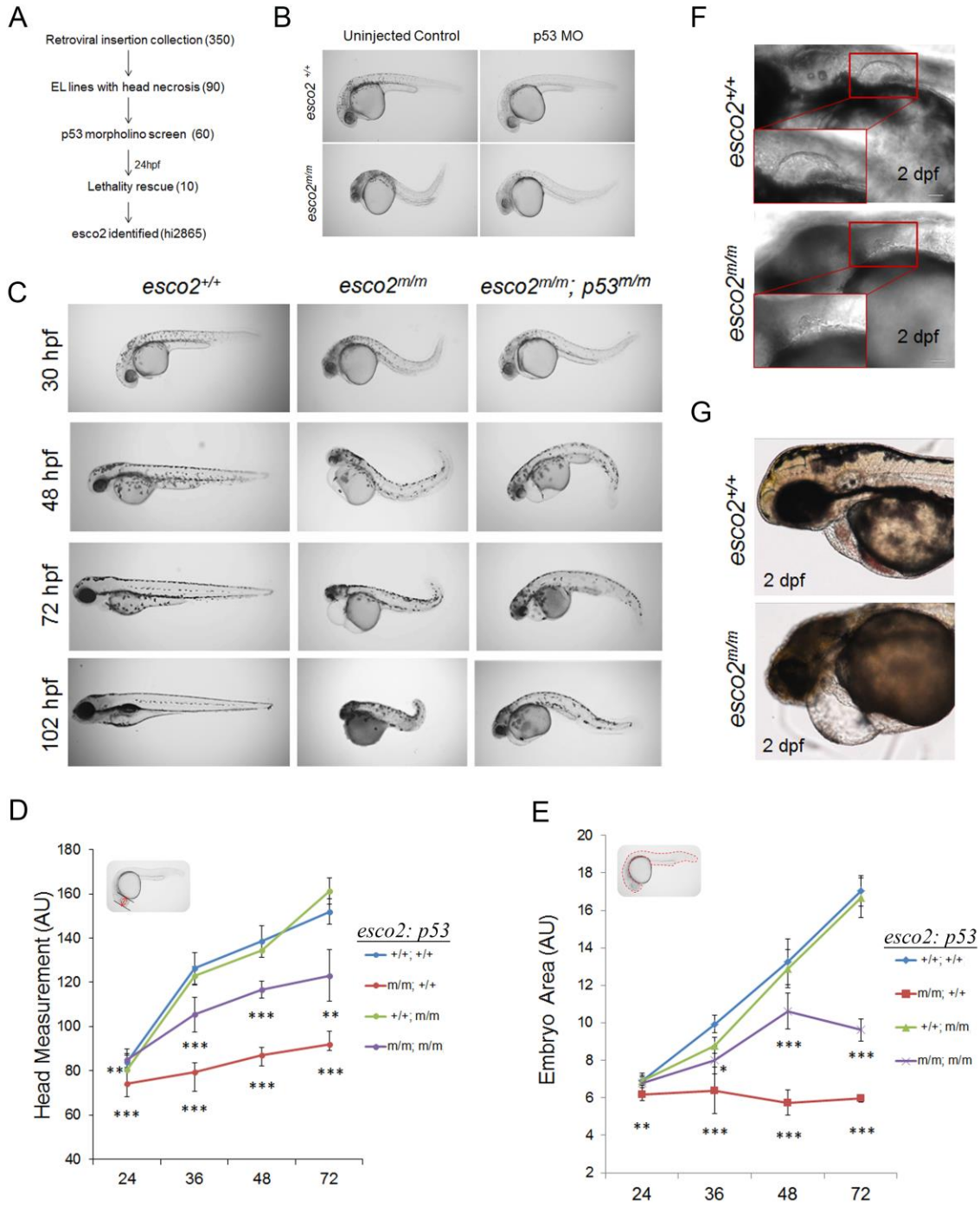


**Figure 1: Genetic screen identifies the retroviral insertion embryonic lethal mutant, hi2865.** (A) Design of the screen used to identify insertion mutants exhibiting microcephaly and head necrosis, amongst 350 embryonic lethal (EL) mutants, that are rescued by morpholino (MO) knockdown of p53 (numbers in parenthesis indicate number of mutants at each stage) at 24 hpf. (B) Bright field images of 24 hpf hi2865 sibling and homozygous mutant (henceforth  $esco2^{hi2865/hi2865}$  will be referred to as  $esco2^{m/m}$ ) embryos injected or uninjected with p53 MO. (C)  $esco2^{+/+}$ ,  $esco2^{m/m}$  and  $esco2^{m/m}; p53^{m/m}$  (henceforth  $p53^{dzy7/dzy7}$  will be referred to as  $p53^{m/m}$ ) gross morphological phenotypes between 30 hpf and 102 hpf (4 dpf). (D) Head measurements and (E) embryo area of  $esco2^{+/+}$ ,  $esco2^{m/m}$ ,  $esco2^{+/+}; p53^{-/-}$ , and  $esco2^{m/m}; p53^{-/-}$  were measured using ImageJ in arbitrary units (n=5/genotype, mean  $\pm$  st. dev., \*p-value<0.05, \*\*p-value<0.01, \*\*\*p-value<0.001; significance below red line are derived from comparing  $esco2^{m/m}$  vs  $esco2^{+/+}$ ; significance below purple line are from comparing  $esco2^{m/m}; p53^{m/m}$  vs  $esco2^{m/m}$ ). Insets in each graph depict the measurement parameters highlighted in red. (F) and (G) DIC images depict fin and heart defects, respectively in  $esco2^{m/m}$ . Insets detail normal fin and remnant fin bud. Scale bar = 50 $\mu$ m.

## ***esco2* deficiency has many severe RBS-like phenotypes**

We wanted to determine if our *esco2* mutant animal modeled the human RBS patient phenotypes. While there are strong variations in the RBS phenotypes, the prenatal lethal RBS patients consistently have microcephaly, growth retardation, craniofacial defects, and limb deformities (Schule et al., 2005). Gross morphology at 30 hpf of the *esco2*<sup>m/m</sup> (Amsterdam et al., 2004) zebrafish shows head necrosis and growth retardation (Fig. 1C). At 48 hpf, the head size is reduced dramatically compared to the wild-type. Importantly, head and gross embryo size measurements suggest a lack of growth compared to wild-type (Fig. 1D & E), reminiscent of human microcephaly and growth retardation. Further, in wild-type embryos at 48 hpf, the early embryonic pectoral fin (analogous to the forelimb in mammals) has formed; however, the fin was absent in the majority (7 out of 10), and only a small nub in the other mutant embryos (Fig. 1F), indicating defects in limb formation. Unfortunately, by 4 days post fertilization (dpf) all *esco2*<sup>m/m</sup> embryos (n=20) are almost completely degraded (Fig. 1C), obscuring the ability to address craniofacial abnormalities since craniofacial bone/cartilage does not begin to appear until 5dpf. While not a hallmark of RBS, heart defects are prevalent in 25-75% of patients (Vega et al., 2010). We observed that while the majority of *esco2* mutant embryos appear to undergo proper morphogenesis (formation of an atrium and ventricle) and have 1:1 A/V contractions, they do not undergo proper heart looping and often have variable heartbeat rates and lack of blood flow (Fig. 1G, Supp. Video 1, 2). While the phenotype of RBS patients is quite pleiotropic (presumed to be due to genetic diversity), the zebrafish phenotypes are very consistent and most likely reflect nearly isogenic backgrounds of our zebrafish.

### **P53 activation and neural tube apoptosis is an early consequence of loss of Esco2.**

Initially, we identified this mutant by the ability of a p53 morpholino to partially rescue the gross morphological phenotypes. To biochemically confirm p53 activation, we probed protein extracts from AB controls, *esco2* mutant and *esco2* sibling embryos for p53. We observed that p53 stabilization was strong in *esco2<sup>m/m</sup>* embryos (179 fold at 30 hpf) but not in WT controls (Fig. 2A). To determine if genetic loss of p53 could rescue our *esco2<sup>m/m</sup>* phenotypes, we generated *esco2<sup>hi2865/hi2865</sup>; p53<sup>dzy7/dzy7</sup>* mutant embryos (henceforth referred to as *esco2<sup>m/m</sup>; p53<sup>m/m</sup>*), where the *dzy7* allele has an I166T mutation in the DNA binding domain of p53 rendering it transcriptionally inactive (Parant et al., 2010). In contrast to the prominent head necrosis phenotype observed in *esco2<sup>m/m</sup>* alone, *esco2<sup>m/m</sup>; p53<sup>m/m</sup>* show severely diminished head necrosis (Fig. 1C), while the p53 mutant protein is being stabilized (Fig. 2A). As observed by gross morphology, our quantitative measurements of microcephaly and growth retardation indicate a partial rescue of these phenotypes (Fig. 1D, E).

One of the major outcomes of p53 activation is apoptosis. Therefore, to further understand the *esco2* mutant phenotype, we stained *esco2<sup>+/+</sup>* and *esco2<sup>m/m</sup>* embryos for apoptosis at 18, 24, 30, 48, and 72 hpf using the live apoptotic dye, acridine orange. Interestingly, we observed that at 18, 24 and 30 hpf *esco2<sup>m/m</sup>* embryos had increased levels of apoptosis with a higher proportion of apoptosis predominantly in the neural tube at 24 and 30 hpf (Fig. 2B, C). Interestingly, this increase in neural tube apoptosis is consistent with our previously described increase in neural tube apoptosis following IR treatment (Fig. 2C). By 48 hpf and later, apoptosis was no longer observed in the mutant embryos, suggesting the sensitivity to stress-inducing apoptosis or the stress no longer

present in these cells; or all the cells sensitive to the stress have died. At 18 hpf in the p53 mutant background, we observed an absence of apoptosis in *esco2<sup>m/m</sup>; p53<sup>m/m</sup>* embryos; however, by 30 hpf we observed a similar level of apoptosis within the *esco2<sup>m/m</sup>; p53<sup>m/m</sup>* embryos as the *esco2<sup>m/m</sup>* embryos (Fig. 2C). This suggests that the initial consequence of *Esco2* loss results in p53-induced apoptosis. However a subsequent stress-induced apoptosis occurs in the absence of p53. This is also reminiscent of irradiation experiments in the p53 mutant embryo, where this initial apoptosis following IR treatment is abrogated in a p53 mutant background but a secondary apoptosis occurs later (Parant et al., 2010). Our interpretation is that while p53 loss abrogates the response, the damage or stress is still present and detrimental to the cell.

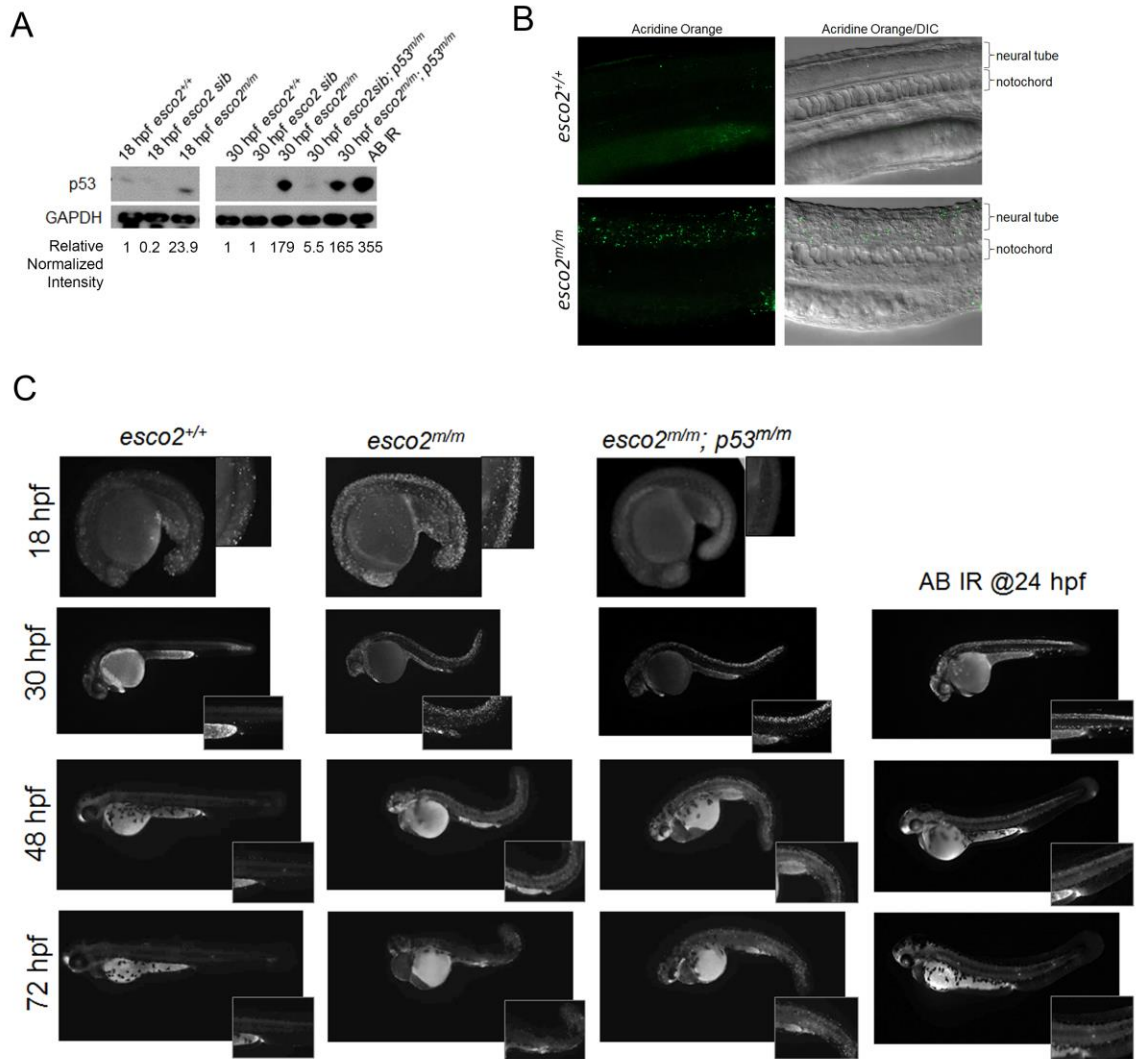


**Figure 2: P53 activation and neural tube apoptosis is an early consequence of loss of *esco2*.**

(A) Western blot for p53 protein levels in protein extracts from AB (*esco2*<sup>+/+</sup>), *esco2* sib (*esco2*<sup>+/+</sup> and *esco2*<sup>m/m</sup>), *esco2* mutant (*esco2*<sup>m/m</sup>), *esco2*sib; *p53*<sup>m/m</sup>, *esco2*<sup>m/m</sup>; *p53*<sup>m/m</sup> embryos at 18 and 30 hpf. Irradiated (IR) embryos at 100 Gy were used as a positive control. Relative intensities were determined using ImageJ; each sample was normalized to GAPDH intensity, and then relative expression was calculated against *esco2*<sup>+/+</sup>

(relative normalized intensity =1). **(B)** Fluorescent and DIC/fluorescent merge images of *esco2*<sup>+/+</sup> and *esco2*<sup>m/m</sup> 24 hpf embryos stained with acridine orange. **(C)** Acridine orange time course staining spatially displaying apoptotic cells in *esco2*<sup>+/+</sup>, *esco2*<sup>m/m</sup> and *esco2*<sup>m/m</sup>; *p53*<sup>m/m</sup>. AB embryos irradiated at 24 hpf were used as a positive control for DNA damage induced neural tube apoptosis. Insets depict higher magnification to visualize neural tube apoptosis.

### **Esco2 deficiency results in embryonic lethality associated with chromosome scattering and increased mitotic index.**

SCC is required for proper mitotic progression. Toward determining the cellular consequences that lead to this embryonic lethality, we performed western blot as well as immunohistochemistry on wild-type (WT) and mutant embryos with an anti-phosphorylated histone-H3 (pH3; a marker of cells in M phase of the cell cycle) antibody. A significant increase in the number of pH3-positive cells (2.3 fold; Fig. 3A, B) and total pH3 protein (8.3 fold; Fig. 3C) was observed in *esco2*<sup>m/m</sup> compared to WT embryos suggesting mutant embryos undergo mitotic arrest.

To determine at which phase of mitosis pH3-positive cells were accumulating, we generated mitotic phase profiles of AB, *esco2*<sup>+/+</sup>, and *esco2*<sup>m/m</sup> embryos. These were immunolabeled with pH3 and observed under confocal imaging. Four independent fields were imaged through the entire embryo to capture all cells in mitosis in a given field (Fig. 3D). Based on pH3 morphology, the phase of mitosis was determined for each pH3-positive cell and quantified for each genotype (Fig. 3E, F). While all genotypes displayed the 5 distinctive mitotic phases (prophase, prometaphase, metaphase, anaphase and

telophase), the *esco2<sup>m/m</sup>* embryos also displayed a unique scattered chromosome morphology (Fig. 3E, F). While AB and *esco2<sup>+/+</sup>* profiles were comparable, the *esco2<sup>m/m</sup>* embryos had a significant increase in the number of scattered chromosome-containing cells (Fig. 3F). Within mutants, 60% of pH3-positive cells had the scattered morphology which accounts for the increase in the total number of pH3- positive cells (Fig. 3B). These data suggest that the scattered phenotype results in a mitotic arrest leading to the early lethality in the *esco2<sup>m/m</sup>*. Further, we did not observe a difference in the presence of scattered phenotype or the mitotic profile in a p53 mutant background (Supp. Fig. S4), suggesting that while p53 responds to this defect and loss of p53 temporarily abrogates the apoptotic response, it does not influence or rescue the actual mitotic defects in the *esco2* mutant embryos.

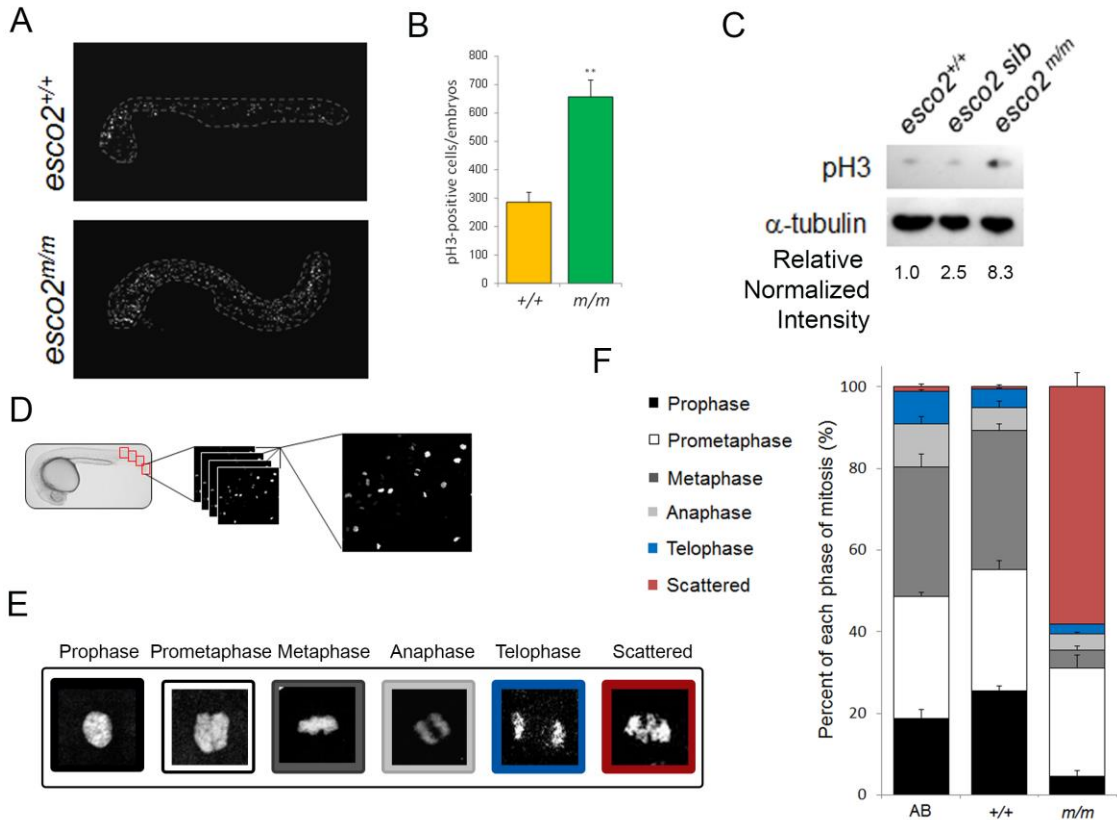


**Figure 3: *esco2* deficiency results in elevated mitotic index and scattered chromosomes.**

(A) Maximum intensity projections of whole embryo confocal z-stack images of pH3-stained fixed WT and mutant embryos. Embryo proper outlined in white dotted line. Yolk has been removed for imaging. (B) Quantification of the number of pH3-positive cells per embryo in (A) (n=3/genotype, mean  $\pm$  st. dev., \*\*p-value<0.01). (C) Western blot analysis for pH3 protein levels from *esco2*<sup>+/+</sup> (AB), *esco2* sibling (<sup>+/+</sup> and <sup>m/+</sup>), and *esco2* mutant (<sup>m/m</sup>) embryo protein lysates. Relative intensity calculated using ImageJ; each sample was normalized to  $\alpha$ -tubulin intensity, and then relative expression was calculated against *esco2*<sup>+/+</sup> (relative normalized intensity =1). (D) Diagram of mitotic profiling.

Four independent fields of a pH3-labeled embryo are imaged, compiled using maximum intensity projection, and scored for each phase of mitosis based on chromosome morphology. (E) Colored panels depict the associated pH3 morphology to its phase in mitosis. (F) Graph depicting the percentage of cells in each phase of mitosis between AB (the WT parental strain) controls, *esco2*<sup>+/+</sup> and *esco2*<sup>m/m</sup> embryos (4 fields/embryo, n=>70 morphologies per embryo, 3 embryos/genotype, , mean ± st. dev.); the p-value of scattered between *esco2*<sup>+/+</sup> and *esco2*<sup>m/m</sup> is 0.0062.

### **Dynamic, in-embryo analysis of chromosome segregation reveals detailed consequences of *Esco2* loss.**

The static analysis of mitosis thus far indicates that many cells in the *esco2*<sup>m/m</sup> embryos undergo a mitotic arrest with a scattered chromosome phenotype and suggests that this extended mitotic arrest leads to cell death during mitosis. To obtain a more dynamic analysis under physiological conditions, we have developed a novel technique to monitor chromosome segregation at the single-cell level within a live zebrafish embryo. One-cell staged embryos are injected with mRNA encoding H2afva-GFP (labels chromatin) and CaaX-mCherry (labels plasma membrane). At 24hpf, embryos are placed in a coverslip-bottom dish and imaged using time-lapse confocal microscopy (Fig. 4A).

With this approach, we demonstrate that AB and *esco2*<sup>+/+</sup> embryos undergo normal progression through mitosis (Fig. 4B) with an average division time—from nuclear envelope breakdown (NEB) to nuclear envelope reformation (NER) in the two daughter cells—of 21 minutes (Fig. 4C, Supp. Video 3). However, cells from *esco2*<sup>m/m</sup> embryos undergo a rapid progression to the scattered chromosome phenotype following

NEB (Fig. 4D; Supp. Video 4) and never form a proper metaphase plate. Upon chromosome scattering, the entire chromatin material proceeds to rotate within the cell for a prolonged period of time (Fig. 4D). To our surprise, the cells with scattered chromosomes do eventually divide with an average division time of 80 minutes (Fig. 4C). The longest complete mitosis from NEB to NER observed for a cell with scattered morphology was 2 hours; however, a number of scattered cells persisted beyond the 4-hour time-lapse recordings. This analysis suggests that loss of Esco2 results in chromosome scattering following NEB, which induces a prolonged mitotic delay most likely due to failure to satisfy the spindle assembly checkpoint.

From the *in vivo* imaging of embryos, we did not observe the formation of apoptotic bodies during mitosis; however, we have observed apoptosis occurring within interphase cells (Supp. Video 5). This suggests the apoptotic event occurs after mitotic exit, potentially in G1 where p53 has been strongly associated with an apoptotic response (Yonish-Rouach et al., 1993).

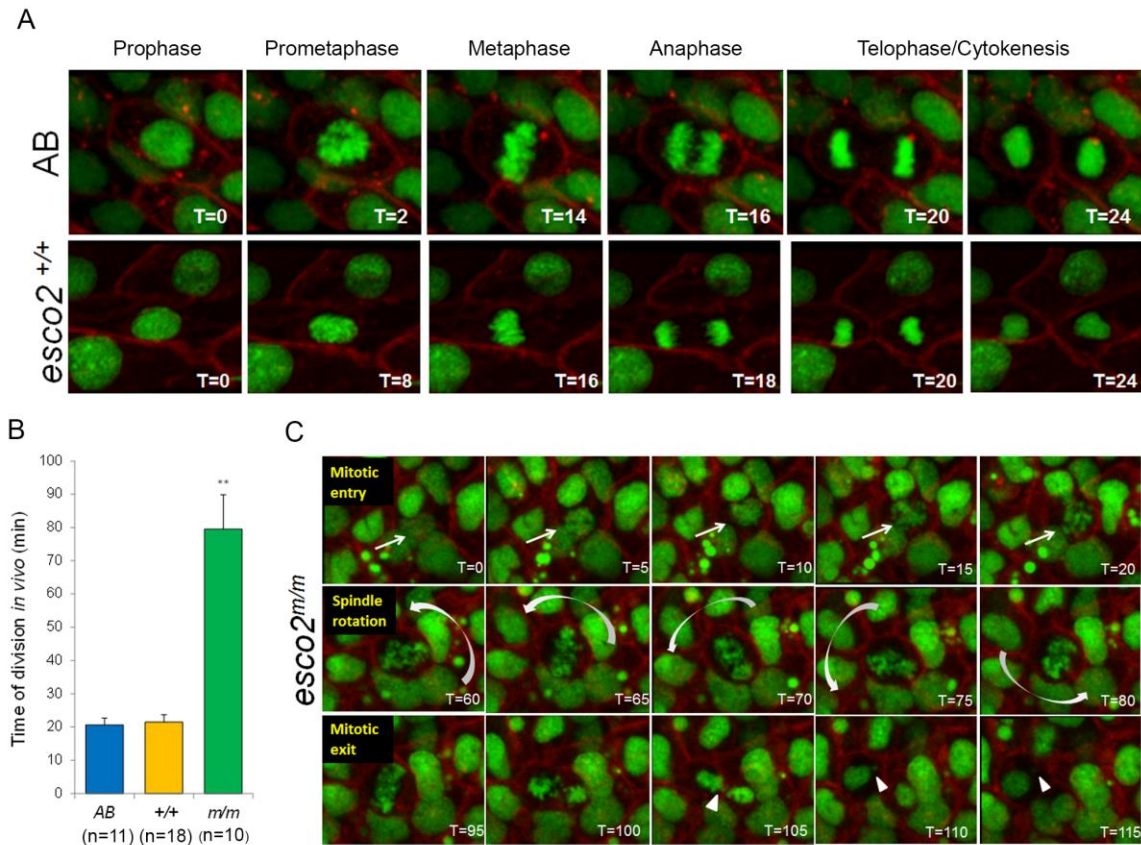


**Figure 4: In vivo analysis of *esco2* mutants reveals chromosome scattering and prolonged division time.** (A) Schematic of in-embryo confocal imaging. Embryos are injected at 1-cell stage, embedded in low melt agarose at 24 hpf in coverslip-bottom dish, and visualized with confocal imaging focusing on the thinner tail region. (B) Stills extracted from time-lapse imaging videos of wild-type embryos emphasizing phases of mitosis beginning at prophase and ending at formation of two daughter cells. Time stamps in minutes. (C) Division time of AB, *esco2*<sup>+/+</sup>, and *esco2*<sup>m/m</sup> calculated from nuclear envelope breakdown (NEB) to division into 2 daughter cells in minutes (mean ± st. dev., \*\*p-value<0.01 derived from comparing m/m to either AB or +/+). (D) Time-lapse imaging stills extracted from videos depict *esco2* mutant's mitotic entry, spindle

rotation and scattering, and mitotic exit resulting in micronuclei formation (arrow head). Arrows point towards the cell of interest. Curved arrows orient to the direction of spinning. Time stamps in minutes.

### **Loss of Esco2 results in genomic instability**

We observed through in-embryo, time-lapse imaging that, upon division, multiple in vivo segregation defects occur. While amongst wild-type embryos (3 embryos, 11 divisions monitored) no erroneous divisions were observed, among 43 mutant divisions monitored from 4 different embryos on average: 37% (+/-9% SD) of the divisions per embryo had lagging chromosomes (66% (n=10/15) involved one sister chromatid; 13% (n=2/15) involved 2 sister chromatids; 7% (n=1/15) involved 3 sister chromatids; 13% (n=2/15) involved 4+ sister chromatids ) that developed into micronuclei (Fig. 5A, B; Supp. Video 6; 85% (n=11/13) of cell divisions result in forming just 1 MN and 15% (n=2/13) of cell divisions result in 2 MN being formed); 29% (+/-7% SD) of divisions per embryo had chromosomes decondense prior to cytokinesis resulting in an anaphase bridges during cytokinesis (Fig. 5A, B; Supp. Video 7); and 13% (+/-13% SD) of divisions per embryo had the chromosomes decondense without cytokinesis (Fig. 5A, B; Supp. Video 8) reminiscent of endoreduplication. We observed a significant increase in phosphorylated-H2AX ( $\gamma$ -H2AX) in mutants compared to AB or WT sibling controls (Fig. 5C), suggesting that chromosome-segregation abnormalities induce a DNA damage response. Interestingly, we observed 8 of the 43 (21%) divisions in *esco2<sup>m/m</sup>* embryos underwent what appears to be a normal “without error” mitotic divisions (Fig. 5A, B, Supp. Video 9).

To further address the consequence of these imprecise divisions, we analyzed our metaphase spreads from AB control and homozygous mutant embryos for the number of chromatids present. Zebrafish have 25 chromosomes and therefore 100 sister chromatids per metaphase cell. Most striking was that the majority (92%) of spreads from *esco2<sup>m/m</sup>* embryos did not have 100 chromatids (Fig. 5D). In fact, there was a bias toward loss of chromatids (73% loss vs. 19% gained), suggesting that either the cells with micronuclei or the chromosome(s) contained in the micronuclei are eliminated. The reduction in the number of micronuclei in interphase cells (Fig. 5E), and our observation of a micronuclei-containing cell undergoing apoptosis (Supp. Video 5), further support the elimination of cells containing micronuclei. The chromosome numbers in *esco2<sup>m/m</sup>* ranged from loss of 25 chromatids to gain of 10 chromatids (Fig. 5D). Since the majority of missegregation results in 1 missegregated chromosome per division, this suggests that the large range of chromatid numbers was the consequence of multiple defective divisions. These data suggest that it is not the aneuploidy (the change in chromosome number), but the micronuclei formation that is deleterious to a cell.

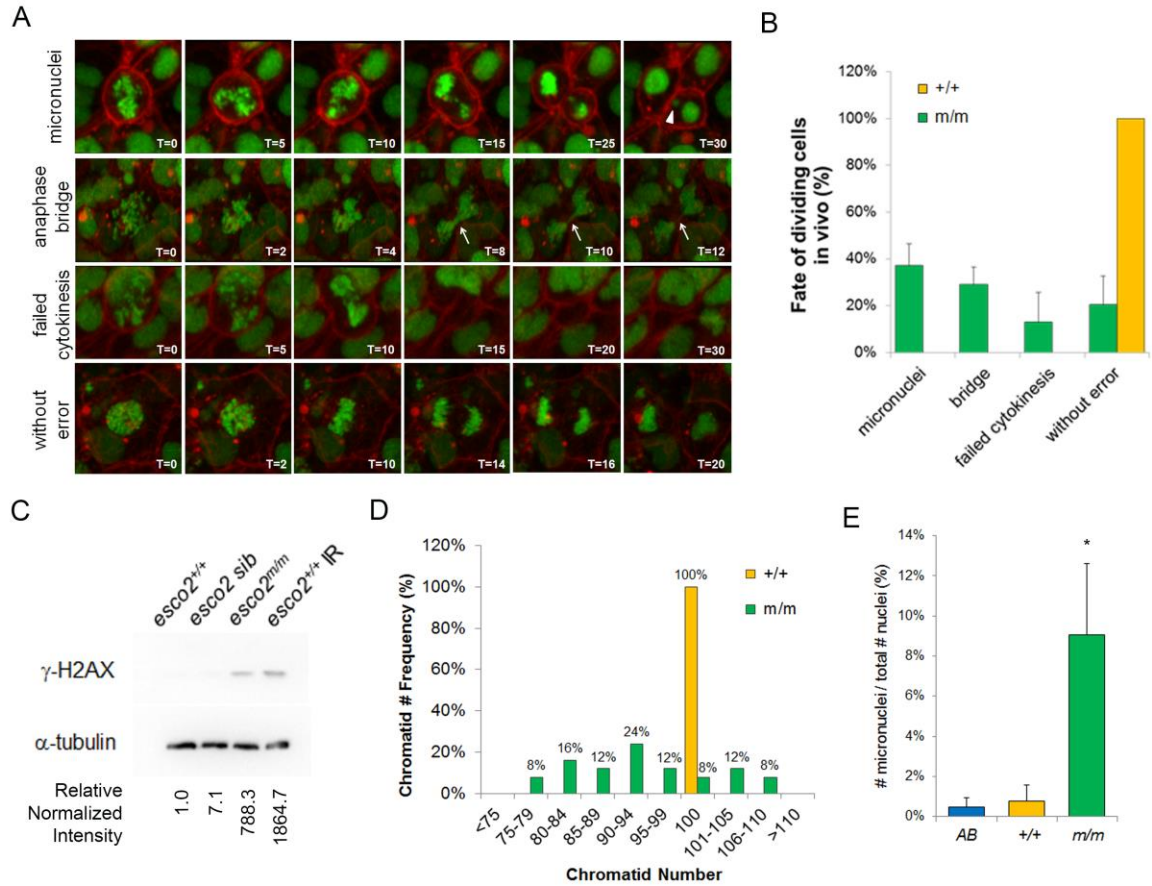


**Figure 5: Depletion of *esco2* results in genomic instability.** (A) Stills taken from time-lapse imaging videos demonstrating the variety of genomic instability observed in 24hpf *esco2* mutant embryos. Micronuclei, anaphase bridges, and failed cytokinesis observed as well as “without error” divisions were observed. Arrow head points towards micronuclei. Arrow points to an anaphase bridge. Time stamps in minutes. (B) Average frequency of above division fates in wild-type (11 divisions taken from 3 embryos) and *esco2* mutant embryos (43 divisions from 4 embryos) based on time-lapse imaging. Error bars show mean +/- st. dev. between embryos. All wild-type cells underwent a normal division therefore there is no standard deviation or error bar to report. (C) Western blot of  $\gamma$ -H2AX in protein lysates from 24hpf *esco2*<sup>+/+</sup> (AB), *esco2* sib. (<sup>+/+</sup> & <sup>+/m</sup>), and *esco2*<sup>m/m</sup>

embryos. IR embryos at 100 Gy at 24hpf and collected at 30hpf serve as a positive control. Relative intensity was calculated using ImageJ; each sample was normalized to  $\alpha$ -tubulin intensity, and then relative expression was calculated against *esco2*<sup>+/+</sup> (relative normalized intensity =1). **(D)** Quantification on of the number of chromatids within metaphase spreads (n=>20 spreads per genotype) from pooled (10-12 embryos) *esco2*<sup>+/+</sup> (AB controls) and *esco2*<sup>m/m</sup> embryos. **(E)** Frequency of micronuclei observed in interphase cells of the tail region of embryos injected with H2afva-eGFP; CAAX-mCherry mRNA. Percent based on total number of micronuclei observed over the number of nuclei observed in interphase cells. (n=3 embryos/genotype, > 75 cells per field, mean  $\pm$  st. dev., \*p-value<0.05).

**Esco2 is required for cohesion establishment; however, compensatory cohesion mechanisms within some cells restore timely divisions and proper chromosome segregation in *esco2* mutant embryos.** Both *esco1* and *esco2* (two homologs of yeast *eco1*) are responsible for establishing cohesion; thus we wanted to determine if loss of *esco2* alone would have an effect on cohesion between sister chromatids. Therefore, we generated metaphase spreads and observed three categories of metaphase spreads in WT and mutant embryos: 1) “paired”, SCC within the arms and the centromere; 2) “paired but separated” phenotype (PBS) in which the centromeres are separated but the sister chromatids still neighbor each other; and 3) “separated”, where sister chromatids are not cohered in the arms or centromere and appear as single chromatids (Fig. 6A). Though 100% of *esco2*<sup>+/+</sup> controls have the classic paired cohesion morphology, 85% of the *esco2*<sup>m/m</sup> spreads yielded a separated morphology, suggesting complete loss of cohesion

in the absence of *Esco2* and that the scattered phenotype is largely due to lack of cohesion between chromatids.

Interestingly, while the majority of *esco2* mutant spreads have complete chromatid separation, 15% of spreads yielded a “paired but separated” (PBS) morphology. These data propose that there is only reduced cohesion within these cells and that alternative cohesion mechanisms exist to compensate for the loss of *Esco2* in these cells. Alternatively, while the analysis of maternal *esco2* mRNA suggests that maternal transcripts are absent by 18 hpf (Supp. Fig. S2), and published data indicate that the *Esco2* protein is degraded during metaphase (therefore degrading maternal protein in early divisions) (Hou and Zou, 2005), there is the potential that at 24 hpf these 15% of cells with the PBS phenotype have a remnant of maternal *esco2*. Therefore, to determine if this phenotype persists beyond normal maternal contributions, we have analyzed the amount of PBS spreads at 24, 48, and 72 hpf. While the number of separated spreads decreases over time, presumably due to cell death or cellular arrest, the number of PBS cells increased (Fig. 6B).

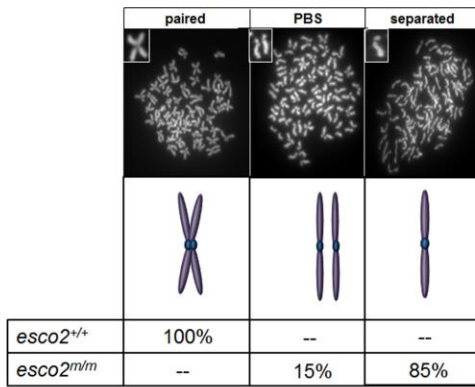
To determine if the PBS cells maintain a different ploidy, we analyzed chromatid number from separated and PBS spreads from *esco2* mutant embryos. The majority of spreads (92%) with “separated” chromatids had improper ploidy (Fig. 6C). Remarkably, the sister chromatids that are partially separated in PBS spreads still achieve proper ploidy in 47% of “paired but separated” (PBS) mitotic spreads, while 53% show only mild aneuploidy (Fig. 6C; ranging from +/- 4 chromatids). This would suggest the spreads with proper ploidy in Fig. 5D are mostly the “paired but separated” cells. The high percentage of normal ploidy spreads (47%) suggests that multiple precise divisions

must have occurred in these “paired but separated” cells. Therefore, mild separation does not seem to impinge greatly on microtubule attachment and segregation of sister chromatids at the metaphase-anaphase transition. These observations suggest there are two pools of mutant cells: 1) cells with complete cohesion loss, separated chromatids, and high aneuploidy biasing toward loss of chromatids; and 2) weakened cohesion, paired but separated chromatids, and none to mild aneuploidy with equivalent gains and losses.

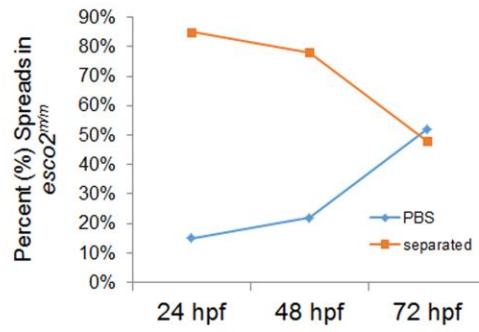
The presence of proper ploidy subsequently led us to hypothesize that the “without errors” divisions present in ~20% of *esco2* mutant cells (Fig. 5B), represents those cells that displayed the “paired but separated” phenotype in chromosome spreads. To determine if there were differences in the division timing of these two populations of cells, we measured the timing from NEB to NER in 56 mitotic divisions in *esco2* mutant embryos using our in-embryo, time-lapse technique (Fig. 2A), with a 2-minute interval between stacks over 2 hours. The majority (73%) of divisions either: 1) underwent NEB but not NER, 2) were in the midst of dividing at the start of time-lapse, or 3) were in mitosis for the entire 2-hour time-lapse. Because these were not complete divisions, accurate division times could not be determined and therefore were not included in this analysis. Complete divisions were segregated based on two categories: 1) those that display “genomic instability” or 2) those that display division “without error”. Consistent with our previous observation on cell fates (20% in Fig. 5A, B), 14% (8 of 56) of the total amount of mitotic cells were “without error”. Importantly, 50% (4 of 8) of “without error” cells underwent a comparable division time to wild-type cells ( $t=26.5$  or  $25.1$  min. respectively), while the other 50% of “without error” had an average division time ( $t=47$

min.), twice the division time of *esco2* wild-type cells (Fig. 6D). We suggest that these divisions, though they undergo no evidence of genomic instability through live imaging, are delayed in satisfying the SAC. While biased because it does not include the scattered genomic instability-prone divisions that last the entire video time (15 of 56 divisions), the average division time for “genomic instability” divisions was 92.8 min., much longer than the “without error” divisions. Overall, these data suggest that in an *esco2* mutant, a weakened cohesion phenotype exists in a subset of cells and that these cells divide with normal mitotic progression and ploidy.

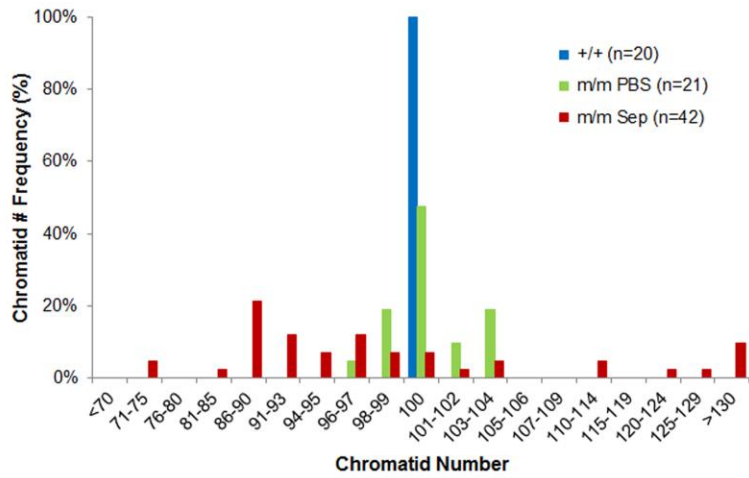
A



B



C



D

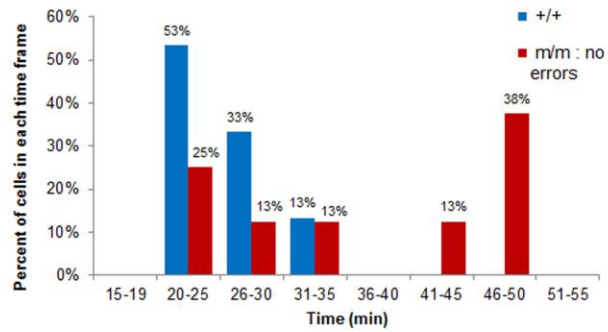


**Figure 6: Most cells of the *esco2*<sup>m/m</sup> embryo display complete cohesion loss, however some cell display mild cohesion defects, mild aneuploidy and almost normal mitotic transition.**

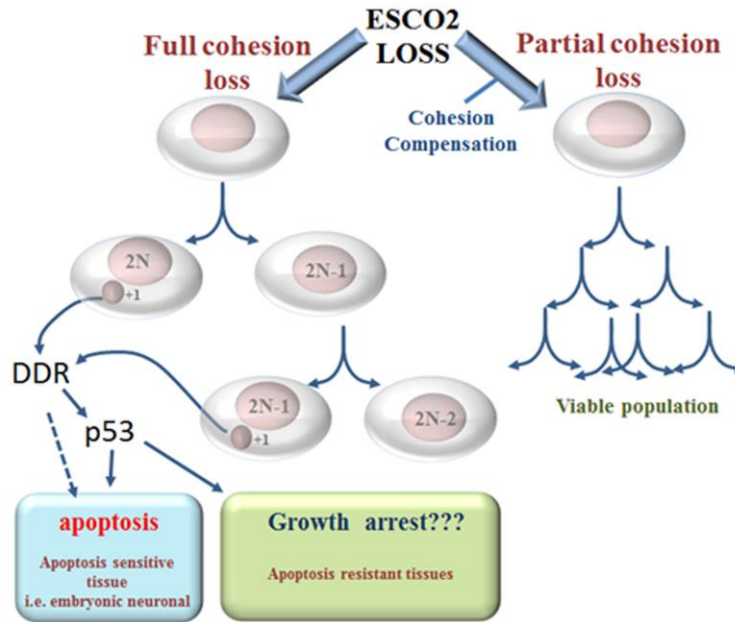
(A-C) Metaphase chromosome spreads from pooled (10-12 embryos) *esco2*<sup>+/+</sup> (AB) and *esco2*<sup>m/m</sup> embryos display 3 key categories; “paired”, “paired but separated” (PBS) and “separated”. (A) Percentage distribution of spread categories ( $n \geq 20$  spreads/genotype) from pooled *esco2*<sup>+/+</sup> and *esco2*<sup>m/m</sup> 24 hpf embryos. Insets in chromosome spreads are higher magnified version of the observed categories. If mixed categories were observed in the same spreads, were counted toward the category in which the most prevalent phenotype was observed. (B) Frequency of PBS and separated spread categories from pooled *esco2*<sup>m/m</sup> at 24, 48 and 72 hpf ( $n \geq 20$  spreads/time-point). (C) Frequency of chromatid number within a spreads categorized to be either “paired but separated” (PBS) or “separated” phenotype from 24hpf pooled *esco2*<sup>m/m</sup> mutants. Chart also contains frequency of chromatid number from *esco2*<sup>+/+</sup> as control. (D) Division time from NEB to NER of cells from *esco2*<sup>+/+</sup> embryos, or cells divisions deemed “without error” from *esco2*<sup>m/m</sup> embryos time lapse videos.

## DISCUSSION

At the molecular level, our data indicates that in the majority of cells, deficiency of *esco2* results in complete cohesion loss, resulting in genomic instability/aneuploidy/micronuclei formation that activates a DNA damage response that includes p53 (Fig. 7A). Our time-lapse imaging revealed that some cells containing micronuclei undergo apoptosis. Recent studies have demonstrated that micronuclei

undergo late replication and induce a DNA damage response ( $\gamma$ -H2AX), which in the absence of p53 can result in a chromothripsis phenomenon (Crasta et al., 2012). Our data is consistent with this, in that we observe micronuclei and  $\gamma$ -H2AX staining; however, in our mutants we also observe an apoptotic response which most likely reflects the presence of a functional p53. This suggests it is the micronuclei, not aneuploidy, that is inducing a p53 response. It should be noted, while we have focused on a lagging chromosome - micronuclei model (Fig. 7A), we have not truly addressed the amount of aneuploidy derived from the prematurely segregated chromosomes. Interestingly our data (Fig 6B) indicates compensated cells (“PBS”) accumulate over time, while the number of cells with the “separated” phenotype is reduced. This suggests that the “separated”/scattered cell undergo apoptosis, leaving a selective advantage of the PBS/compensated cell. Importantly, while p53 activation is a response to genomic instability, it does not correct the genomic instability which ultimately cannot be tolerated by the organism; hence there is only partial rescue of RBS phenotypes. With this in mind, we feel that therapies aimed at suppressing the stress response will only delay the defects considering the stress is still present. Alternatively, the fact that we observe compensation in some cells, in addition to the genetic background influences on the severity of human RBS patients, suggests that if we can restore cohesion, we can remedy many of the RBS phenotypes. Therefore, understanding the contribution that the genes in the cohesion network have on SCC in vivo becomes important.

**A** Molecular and cellular outcome of *esco2* loss.



**B** Impact compensation may have on variability between individuals and between tissues

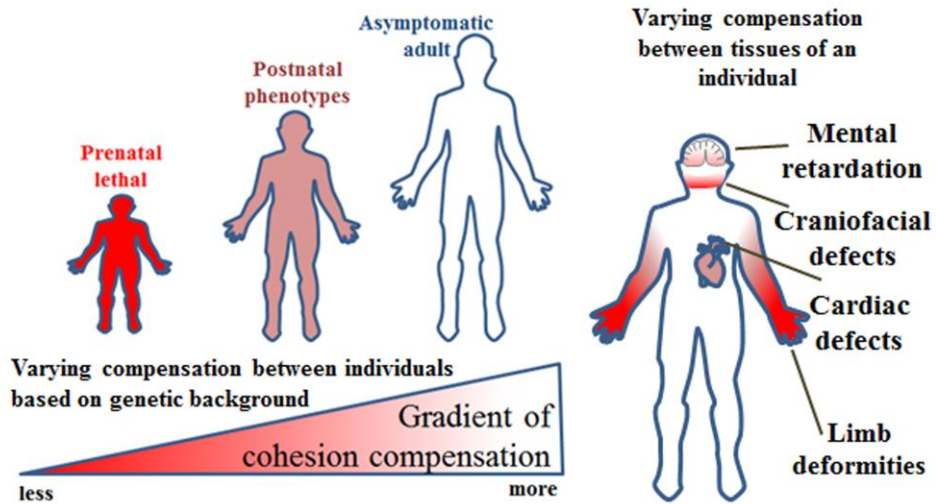


**Figure 7: Model depicting cellular outcomes in *esco2* mutant zebrafish embryos and hypothesized impact compensation may have on RBS phenotypes.** A) A model of the molecular and cellular event ongoing in the *esco2* mutant zebrafish. Majority of cells undergo a prolonged mitotic delay ultimately resulting in a single chromatid missegregation yielding a micronuclei. We observed, i) through live imaging a interphase cell with a micronuclei undergo apoptosis, ii) increased a levels of  $\gamma$ -H2ax, indicating a DNA damage response (DDR), and iii) p53 dependent apoptosis within the neural tube. Together these data suggest that the micronuclei induce a DDR response to activate the p53 apoptotic response. There is subsequent apoptosis even in the absence of p53 suggesting an alternative apoptotic signal exists. Other cells within the *esco2* mutant embryos appear to undergo a normal mitotic progression, and have only mild cohesion loss suggesting compensation mechanisms exist. B) Depicts a model were variation in compensation between individuals and between tissues in an individual may explain the phenotypic differences between RBS patients.

We observed that the genomic instability induced apoptosis occurs predominantly in the neural tube. These results are consistent with other published data on DNA damage induced genomic instability in mouse and zebrafish (Lang et al., 2004; Berghmans et al., 2005; Sidi et al., 2008; Parant et al., 2010; Toruno et al., 2014). These tissue-specific effects may explain the many neural-related RBS phenotypes such as microcephaly, craniofacial defects, and mental retardation. This observation is not unfounded in that during embryonic development, persistent cellular stress (often due to inherited gene

mutations that lead to cellular stress, i.e. genomic instability) results in p53 activation and neurodevelopmental phenotypes. Many of the neural crest-derived craniofacial phenotypes in the Treacher Collins syndrome mouse model are resolved in a p53 mutant background (Jones et al., 2008). In addition, centrosomal stress has been linked to aneuploidy resulting in significant brain degeneration and microcephaly in a Plk4 overexpression mouse model (Marthiens et al., 2013). Studies of Mosaic Variegated Aneuploidy patients harboring mutations in Bub1b and Cep57 also lead to aneuploidy and microcephaly in humans (Hanks et al., 2006; Snape et al., 2011). Together, this suggests that early neuronal tissue may be more predisposed to undergo apoptosis in response to genomic instability. In fact, the lack of apoptosis at 48 and 72 hpf (Fig. 2C) and the morphological collapse of the head (Fig. 1C, F,G) suggest that all of the apoptosis-susceptible neural tube cells have died, while some scattered cells still exist (Fig. 6B).

Prior to identification of ESCO2 as the gene responsible for RBS, there were two disorders: As a generalization, Roberts Syndrome encompassed the stillborn and early postnatal lethal individuals, while SC phocomelia syndrome patients were less severe individuals often lived to childhood and even adulthood (Schule et al., 2005). While the phenotypes vary between individuals, premature chromatid separation is a hallmark among patients and was used as a diagnostic tool. These two syndromes were united under the title RBS upon identification that 100% of both disorders were due to ESCO2 mutations, with no phenotype-genotype correlation identified, suggesting genetic background likely influences the phenotypes (Maserati et al., 1991; Schule et al., 2005; Vega et al., 2010). Interestingly, in all animal models analyzed to date (yeast, fly,

zebrafish, and mouse), genetic loss of ESCO2 results in early lethality (Skibbens et al., 1999; Toth et al., 1999; Williams et al., 2003; Whelan et al., 2012). This leaves the question, why are some human ESCO2 null individuals viable? In fact, one individual was identified to be ESCO2 null but displayed the mildest phenotypes and therefore escaped diagnosis until adulthood (Goh et al., 2010). Alternatively, there is the proposition that humans null for ESCO2 are not early embryonic lethal; however there is an ascertainment bias toward identifiable patients (stillborn and viable), not embryonic lethal prior to the second term. Part of the early lethality or lack of variable phenotypes amongst animal models can be attributed to the isogenic/near isogenic nature of the models. Alternatively, humans may have evolved compensation mechanisms; potentially higher levels of ESCO1. While mouse *Esco2* null are early 8-cell (~3 dpf) lethal, the zebrafish mutant proceeds through gastrulation and early embryogenesis (<18 hpf) due to maternal stores of *esco2* mRNA. This is convenient in the sense that RBS-like phenotypes can be observed due to the unabated transition through early embryogenesis. Interestingly, while our *esco2* mutant embryos display many of the severe RBS phenotypes, the published morpholino knockdown displayed milder RBS phenotypes, such as craniofacial defects (Monnich et al., 2011). The morpholino is only a partial knockdown of *esco2*; therefore this observation most likely reflects the *esco2* dose effect on phenotypes. Whether through compensation or *esco2* dose, this lends to our hypothesis that the amount of cohesion dysfunction will correlate with the severity of the RBS phenotypes (Fig.7B). While the above example focuses on *esco2*, involving the large number of SCC factors in the complex genetic network will expand our

understanding of which factors influence the amount of cohesion dysfunction and how this network impacts the severity of disease.

The fact that we observed compensation in some cells opens up the possibility that there are other genetic factors (maybe *Esco1*) that influence cohesion establishment, and these factors may have higher expression in a subset of cells/tissues (Fig. 7B). Toward this, we have recently generated an *esco1* mutant which has cohesion defects as well as compensation in a subset of metaphase spreads (Percival et. al. unpublished data). This suggests: 1) that *esco1* is also important for cohesion establishment; and 2) that *esco1* and *esco2* may have differential cell expressions resulting in the variable cohesion loss. Beyond *esco1* and *esco2*, there are a number of cohesion establishment (ex. ATAD5, CHTF18, and RBMX1), maintenance (ex. SGOL1 and Sororin), and antiestablishment factors (ex. WAPAL, PDS5a, PDS5b, and HDAC8) that may impinge on this compensation (Bermudez et al., 2003; Lengronne et al., 2006; Maradeo and Skibbens, 2009), (Matsunaga et al., 2012). Clinically, this observation has the potential to explain why there are particular morphogenic phenotypes (i.e. limb deformities or craniofacial defects) amongst a normal body plan in RBS patients; some tissues may have differential compensation for ESCO2 loss.

In closing, we have identified a zebrafish genetic mutant in *esco2* that models RBS. The transparency of the zebrafish embryo has allowed us to monitor the in vivo chromosome segregation dynamics in real time and revealed the dynamic chromosome segregation defects in the *esco2* mutants. In addition, the future use of guide directed EGFP tethered endonuclease-dead Cas9 will allow for in vivo monitoring of the distances between sister chromatids (identified as 2 EGFP spots), much like that used in yeast

cohesion separation studies (Straight et al., 1996; Michaelis et al., 1997; Chen et al., 2013). Applied to the *esco2* mutant embryos, this technique will help spatially identify which cells have PBS and which are completely separated, in addition to the long term consequence of these phenotypes. Further, the ability of some cells to compensate for *Esco2* loss suggests differential cohesion dysfunction between cells or tissues and may explain the specific RBS phenotypes. Importantly, understanding this compensation network has therapeutic application if cohesion can be restored in RBS patients and other cohesion-driven diseases.

## **TRANSLATIONAL IMPACT**

### *(1) Clinical issue:*

Defect in Sister Chromatid Cohesion (SCC) can lead to multiple human health concerns including but not limited to infertility, birth defects, and cancer. While we know much about SCC through unicellular studies, the identification of Roberts Syndrome, a developmental disorder due to mutations in the cohesion establishment gene *ESCO2*, implies that further multicellular studies on SCC are required to understand the disease pathology. Further, the unique variety of phenotypes and wide range of severity of the disease suggest there are differences in cellular response and potential complex genetic interactions which are presently not understood.

### *(2) Results:*

This study describes the first characterization of an *esco2* mutant zebrafish. Novel to these studies is the use of fluorescence single-cell time-lapse confocal imaging to monitor

the dynamics of chromosome movements during mitosis within live zebrafish embryos. Loss of *Esco2* results in embryonic lethality due to extensive chromosome scattering upon entrance into prometaphase, a prolonged mitotic delay, and ultimately imprecise chromosome segregation upon division. Various forms of genomic instability result from these divisions including micronuclei and anaphase-bridges that activate a neural tube specific p53-dependent apoptotic response in early development. Most noteworthy is the appearance of cells dividing with normal mitotic progression and lack of genomic instability in the *esco2* mutant, which suggests compensatory cohesion establishment mechanisms are in place to allow for normal mitotic progression and division in these cells.

*(3) Implications and future directions:*

Not only does this work exemplify the novelty of observing the dynamics of cell divisions in a live vertebrate organism, but it is the first example of data supporting that there are compensatory mechanisms that may influence the spectrum of phenotypes observed in RBS. Further studies will include tissue-specific differences, identifying the compensatory mechanisms, and visualizing the dynamics that regulate this compensatory mechanism. Globally, this research will impact not only developmental disorders, but infertility and tumorigenesis as well. Somatic mutations have been found in a multitude of cancer types, and key defects in SCC have been associated with increased tumorigenesis. Female, and most recently male, infertility has also been shown to be caused by defects in SCC further lending to the cause of understanding how SCC is regulated. By identifying key compensatory mechanisms, these can be exploited as therapeutic targets for treating SCC-associated human diseases.

## MATERIALS AND METHODS

### **Zebrafish lines:**

All zebrafish lines were maintained as described in Westerfield, 1995 under standard laboratory conditions. AB WT zebrafish were used for morpholino injections and controls. The *esco2* retroviral insertion allele (with the help of Adam Amsterdam) was obtained from Nancy Hopkins and Jacqueline A. Lees and maintained on the AB background.

### **Genotyping:**

*High Resolution Melt (HRM) Curve Analysis:* Individual embryos or tail clippings were placed in 100  $\mu$ L ELB (10 mM Tris pH 8.3, 50 mM KCL, 0.3% Tween 20, 0.3% NP40, 1 mg/ml Prot K) in 96 well plates. Embryos/tail clips were incubated at 55 °C for 4 hr to overnight, depending on sample size, to generate genomic DNA. To inactivate Proteinase K, plates were incubated at 95 °C for 10 minutes. For *esco2* hi2865 genotyping PCR fragments were generated using primer V: 5'-TTTCACTGTTTCTGCAGGTTG-3' and X: 5'-TAAGGTCTTCGAAGTCTTAACG-3' to amplify WT products. Primers V: 5'-TTTCACTG TTTCTGCAGGTTG-3' and W: 5'-GGGGGGGGCCTACAGGTGGGGTCTTTC-3' were used to amplify the viral insertion product. PCR reactions were performed using genomic DNA in black/white 96 well plates (BioRad cat. No. HSP9665). PCR reaction protocol for retroviral insertion detection was 95 °C for 20 sec, then 40 cycles of 95 °C for 10 sec, 59 °C for 20 sec, and 72 °C for 8 sec in Eppendorf Mastercycler Pro 96S. Following PCR, plates were analyzed for melting curves with Lightscanner (Idaho Technology) over a 65-95 °C range. From this WT, heterozygous, and mutant melting temperatures were clearly

distinguished. As previously published (Thomas et al., 2014), HRM analysis was used to identify CRISPR-derived *esco2* heterozygous mutant F1 zebrafish. HRM primers were 5'-GCTAGAATCTCCCCCAAAGC-3' and 5'-AGGGGTTTCTGCTTGCTGTA-3'. Genomic PCR encompassing this region was sequenced from HRM-positive F1 fish, and then desired mutant (+13) fish were propagated into the F2 generation.

*PCR gel genotyping:* To confirm melt curve analysis, individual embryo PCR reactions corresponding to a *esco2*<sup>+/+</sup> (WT), *esco2*<sup>hi2865/+</sup>, and *esco2*<sup>hi2865/hi2865</sup> (mutant) melting curve were performed using primers 5'-ACTGCGGGAAAAGTGAGAGA-3' and 5'-TGATTAATTTTTGCCAGCAC-3' for WT products. Primers 5'-ACTGCGGGAAAAGTGAGAGA-3' and 5'-AAGGCACAGGGTCATTCAG-3' amplified the viral insertion product were run on a 2% agarose gel.

**Microinjection of antisense morpholino and *esco2* CRISPR:** Injection of p53 MO or *esco2* Cas9/guide RNA was performed on 1-cell stage zebrafish embryos at a concentration using 0.5 nL of 0.85 mM. Injected embryos were incubated at 28 °C until the indicated stage and analyzed via brightfield microscopy. The sequence of p53 MO used to target exon 2 splice donor site of the p53 gene was 5'-CCCTTGCGAACTTACATCAAATTCT-3'. Cas9 mRNA was transcribed from the linearized pT3TS-nCas9n plasmid (Addgene) using the mMessage mMachine T3 kit (Life Technologies). Each RNA was purified using the RNeasy Kit (Qiagen). The CRISPR guide RNA was synthesized using the MegaShortScript T7 Kit (Life Technologies) and purified using the MegaClear Kit (Life Technologies). RNA concentration was quantified using the Nanodrop spectrophotometer. For CRISPR/Cas9

injections, 150 ng/ $\mu$ l of Cas9 mRNA and 30 ng/ $\mu$ l of RNA were used (Thomas et al., 2014).

### **Quantitative RT-PCR:**

RNA was extracted from approximately 30 pooled *esco2*<sup>+/+</sup> (AB), *esco2* sib (containing WT and heterozygous embryos), or *esco2*<sup>m/m</sup> embryos (based on mutant phenotype at 24 hpf) using Trizol reagent (Life Technologies), according to the manufacturer's suggested protocol. Each RNA sample was diluted to 10ng/ $\mu$ l using RNase-free water, and cDNA was synthesized from each sample using the High Capacity cDNA Reverse Transcription Kit (Life Technologies). Primers and probes for both *esco2* (NM\_001003872.1) (primers Y & Z in Supp. Fig. 1) and *Gapdh* (NM\_001115114.1) were obtained from Life Technologies, and RT-PCR analysis was performed for each cDNA sample using an ABI Prism 7900HT Fast Real-Time PCR System. Gene expression was then calculated using the comparative C<sub>T</sub> method.

### **Microscopy and Image Analysis:**

*Gross morphologies, heart, and fin imaging:* Embryos were placed 0.4% tricaine to anesthetize and then in methyl cellulose for proper positioning at indicated time points. DIC images were taken for the heart and fin, and brightfield images were taken of the gross morphology. Heart and gross morphology images were taken using a Nikon AZ100 using the 2x objective 0.5NA 4x digital zoom (heart and 2x digital zoom (gross morphology). Images were processed using NIS Elements software. Fin images were taken on a Zeiss Axio Observer fluorescent microscope using a 10x 0.2 NA objective and processed with Zen 2011 Blue software.

*Head size and growth area measurements:* *esco2* heterozygotes were crossed to generate mutants and analyzed at 24 hpf, 36 hpf, 48 hpf, and 72 hpf. Mutants were identified by phenotype and isolated while *esco2* sibs were correspondingly isolated. At each time point, an individual embryo was placed in methylcellulose in lateral position. Embryos were imaged using Nikon AZ100 in at 2x objective and 2x digital zoom. Site of measurement for the head size was determined by drawing parallel lines corresponding to head direction and eye placement. From these lines, an additional perpendicular line that bisects the two parallel lines and the center of the eye was drawn. It was this line that was measured using the measure analysis tool in ImageJ using arbitrary units. Embryos were once again placed in methylcellulose in lateral positioning. Growth area measurements were obtained in a similar manner. The full embryo was outlined and the area of each embryo was quantified. Measurements were obtained by using the same measure tool in ImageJ using arbitrary units.

*Apoptosis Assay:* Embryos were dechorionated using pronase as stated above and incubated in 10  $\mu$ L/mL acridine orange for one hour in the dark. Embryos were washed 5x for 5 minutes with E3 embryo water. For Fig. 2B, DIC and fluorescence images were taken on a Zeiss AxioObserver.Z1 using a 20x objective NA 0.4. Images were processed using Zen Pro 2011 and ImageJ. For Fig. 2C, Fluorescence was observed using Nikon AZ100 using GFP filter at 2x objective and 2x digital zoom.

*Whole-embryo phospho-H3 stain:* Embryos staged at 24 hpf were dechorionated using 30 $\mu$ L pronase (30mg/ml; sigma p5147)/1 ml E3 blue embryo water (5 mM NaCl, 0.17 mM KCl, 0.33 mM CaCl<sub>2</sub>, 0.33 mM MgSO<sub>4</sub>, 10<sup>-5</sup>% Methylene blue). Embryos were incubated for 10 minutes in pronase and washed 3x with E3 blue embryo water to

remove chorions. Embryos were then fixed in microtubule fixative (1x PBS, 37% formaldehyde, 8% glutaraldehyde, 1 M MgCl<sub>2</sub>, 100 mM EGTA, and 10% Triton X) at room temperature. After a 2-hour block (1x PBS, DMSO, and 10% sheep serum), embryos were incubated overnight with anti-phospho-H3 (ser10) (Santa Cruz Biotechnology, sc-8656-R) at 1:200 dilution. Embryos were rinsed in block 3x for 20 minutes and then incubated in corresponding secondary antibody, goat anti-rabbit Alexa 647 (Invitrogen, a21245). Embryos were washed in 1x TBST and placed in slowfade (Invitrogen) until imaged. All embryos were de-yolked using 27-gage needles prior to imaging.

*Whole-embryo phospho-H3 imaging:* Yolks were removed after fixation for imaging purposes. Whole embryo z-stack (1.5  $\mu$ m interval) confocal imaging was generated using a 5x 0.12 NA objective, and on a Leica SP2 upright confocal microscope. Phospho-H3 (ser10) embryos were quantified using ImageJ ICTN plugin.

*Mitotic profiling:* Four, non-overlapping fields were imaged per embryo by taking a 1.5  $\mu$ m z-stack through whole embryo using the Nikon A1R confocal microscope using 60x 1.4 NA objective. Images were compressed and converted to black and white for ideal counting/detection conditions. Using morphology of pH3 staining, the phases of each cell were determined and quantified for each field (see Fig. 3E). This procedure was done for 3 embryos of each genotype. Percentages for each phase were quantified for each embryo, generating average percentage of each phase/genotype.

*Time-lapse imaging:* CaaX-mCherry and H2afva-EGFP mRNA was transcribed from a plasmid (pCS2-CaaX-mCherry and pCS2-H2afva-EGFP; gift from K. Kwan (U. of Utah)) using mMessage mMachine SP6 kit (Life Technologies). *esco2* heterozygotes

were crossed and embryos were microinjected into the yolk of a one-cell staged embryo with 1nl of 200 ng/ $\mu$ l CaaX-mCherry and 200 ng/ $\mu$ l H2afva-eGFP mRNA. At 24 hpf, embryos were screened for fluorescence. Embryos were manually dechorionated using tweezers and anesthetized using 0.4% tricaine. In a glass coverslip-bottomed dish, embryos were embedded in a 1% low-melt agarose. Dishes were placed on the Nikon A1 inverted confocal microscope, and z-stack images were taken at designated intervals. For AB and *esco2* WT videos 40  $\mu$ m z-stacks (with a 3  $\mu$ m interval) were obtained every 2 minutes for a total scanning time of 2 hours. Since *esco2* mutants have a dramatically longer division time, adjustments had to be made to account for photobleaching and to capture full *esco2* divisions from NEB to NER. Z-stacks were taken every 5 minutes for a total scanning time of 4 hours. All videos were taken using 60x 1.4NA objectives. 3D viewing, still shots, and videos were assembled and processed using NIS Elements 4.13.00.

*Micronuclei/ Apoptotic Bodies Count:* Embryos were injected with H2afva-EGFP and CaaX-mCherry mRNA and set up as if for a time-lapse video. To ensure consistency, for each field, a 40  $\mu$ M z-stack was generated with 2  $\mu$ m steps using 60x 1.4 NA objective and 1.5 digital zoom on a Nikon A1 confocal microscope. Using 3D volume rendering in NIS Elements 4.13.00, an average nuclei, micronuclei, and apoptotic body count was calculated per field to generate the percent observed in a population of cells. Filters for apoptotic bodies and micronuclei (vs. nuclei) were set at H2afva-EGFP fluorescing body  $\leq$  3  $\mu$ m. Differentiation between apoptotic bodies and micronuclei was determined based on size and localization within the cell; i.e. using the CaaX-mCherry (plasma membrane) fluorescence, it can be determined whether a micronuclei is within a

cell and whether an apoptotic body is outside a cell. Frequency of micronuclei in interphase (Fig. 5E) was calculated by dividing the total number of micronuclei observed in the 3D render by the number of nuclei identified in the 3D render.

#### **SDS-PAGE and Western blot analysis:**

Cell lysates for immunoblotting were prepared using 18 hpf, 24 hpf, and 30 hpf embryos. Embryos were dechorionated using pronase procedure as stated above. Deyolking was performed by adding 200  $\mu$ L deyolking buffer (55 mM NaCl, 1.8 mM KCl, 1.25 mM NaHCO<sub>3</sub>), pipetting up and down 3 times with a p200 pipette tip and then centrifuged for 2 minutes at 300 rpm. Supernatant was discarded and above step was repeated once more. 60  $\mu$ L protein prep (30  $\mu$ L Invitrogen NuPAGE LDS sample buffer, 10  $\mu$ L proteinase inhibitors, 1.5  $\mu$ L  $\beta$ -mercaptoethanol, 18.5  $\mu$ L water) was added to embryos and put on heat block at 95  $^{\circ}$ C for 5 minutes. Lysates were microcentrifuged and put on heat block for an additional 5 minutes. Supernatant was transferred to a separate tube and stored at -20  $^{\circ}$ C. Protein was loaded onto a 4-12% NuPAGE gel (Invitrogen) and transferred to a PVDF membrane.  $\alpha$ -tubulin at 1:7000 (abcam, ab7291-100) and GAPDH at 1:5000 (Cell Signaling, 2118S) were used as loading controls. Antibodies against pH3 at 1:5000 (Santa Cruz Biotechnology, sc-8656-R), p53 at 1:1000 (GeneTex, GTX128135), and  $\gamma$ -H2AX at 1:1000 (GeneTex, GTX127340). All blots were treated with Lumigen PS-3 detection agent. The pH3 and p53 blots were exposed to film, developed using the Konica SRX-101A system, and imaged using the CareStream 212 Pro imaging system. The  $\gamma$ -H2AX blot was imaged using the BioRad ChemiDoc MP imaging system. All digital images were scanned at 600 dpi and quantified using ImageJ.

### **Chromosome Spreads:**

Chromosomes spread protocol was adapted from the Lee group (Jeong et al., 2010). Approximately 20-30 embryos were dechorionated at 24 hpf. Embryos were incubated in 400 ng/ml nocodazole for 2 hours in the dark at room temperature. Embryos were then transferred to 1.1% sodium citrate in a 6 cm dish. At this point for genotyping purposes, tails were removed to be genotyped while the remaining embryo heads were transferred to fresh sodium citrate solution and incubated on ice for 8 minutes. Next, two washes with a cold 3:1 methanol: acetic acid solution for 20 minutes each followed by storage in -20 °C until genotyping is performed. After fixative procedure, embryos are pooled (10-12 embryos/pool) per genotype and then minced using forceps in a 1:1 methanol: acetic acid solution. Using this mixture, 50 µL of pooled embryos were dropped onto a slide, and 3-5 drops of glacial acetic acid was added. The slide was slowly placed slide up and exposed to hot vapors (we used boiling water) for about 10 seconds; then the slide was allowed to dry on a hot metal surface (approx. 50 °C). After slide was completely dry, a few drops of Prolong Gold with DAPI were added and covered with a glass coverslip. Chromosomes were imaged using a 63x 1.4 NA objective on a Zeiss Axio Observer fluorescent microscope and processed with Zen 2011 Blue software. While most spreads were clearly delineated into the “paired”, “paired but separated”, or “separated” categories, if a spread had multiple phenotypes it was categorized by which was most prevalent in that spread. Chromatid number was counted manually from high-resolution images.

### **Statistical Analysis:**

Excel software was used in generation of all graphs and statistical tests. Overall statistical significance was calculated using an unpaired t-test with error bars indicating st. dev. as stated in legend ( $\pm$ ). All p-values were determined significant at  $p < 0.05$ . Unpaired t-test determined the significantly different values. Log-rank test determined significance in Kaplan-Meier survival curve analysis. Significance values are stated in figure legends.

### **ACKNOWLEDGEMENTS**

We want to thank Nancy Hopkins for allowing us to screen her zebrafish insertion-derived embryonic lethal library. We thank Kristin Kwan for pCS2-H2afva-EGFP and pCS2-CAAX-mCherry constructs. We thank Gary Gorbsky for enlightening discussion on the cellular aspect of the *esco2* phenotype. We thank Susannah Rankin for testing the Xenopus ESCO2 Ab for zebrafish reactivity. We thank Nicolas F. Berbari and Michael A. Miller for critical reading of the manuscript. Research in the HJ Yost lab was supported by National Heart Lung and Blood Institute (R01 HL66292). JM Parant is supported by National Institute of Neurological Disease and Stroke (R21 NS092105), the American Cancer Society (IRG-60-001-47) and the National Cancer Institute (CA-13148-39).

### **COMPETING INTERESTS**

There are no competing interests associated with the data and discussion presented in this paper.

## **AUTHOR CONTRIBUTIONS**

JMP and HJY designed original genetic screen; JMP and AA performed screen in collaboration with JAL; SMP, HRT, and JMP designed further experiments; HRT with help of AJC generated mitotic spreads; SMP performed all other experimentations; SMP and JMP analyzed data and wrote the manuscript.

## **FUNDING**

Research in the HJ Yost lab was supported by NIH R01 HL66292. JM Parant is supported by NIH R21 NS092105, ACS IRG-60-0001-47, and NIH CA-13148-39.

## **REFERENCES**

- Amsterdam, A., Nissen, R. M., Sun, Z., Swindell, E. C., Farrington, S. and Hopkins, N.** (2004). Identification of 315 genes essential for early zebrafish development. *Proceedings of the National Academy of Sciences of the United States of America* **101**, 12792-12797.
- Berghmans, S., Murphey, R. D., Wienholds, E., Neuberg, D., Kutok, J. L., Fletcher, C. D., Morris, J. P., Liu, T. X., Schulte-Merker, S., Kanki, J. P. et al.** (2005). tp53 mutant zebrafish develop malignant peripheral nerve sheath tumors. *Proceedings of the National Academy of Sciences of the United States of America* **102**, 407-412.
- Bermudez, V. P., Maniwa, Y., Tappin, I., Ozato, K., Yokomori, K. and Hurwitz, J.** (2003). The alternative Ctf18-Dcc1-Ctf8-replication factor C complex required for sister

chromatid cohesion loads proliferating cell nuclear antigen onto DNA. *Proceedings of the National Academy of Sciences of the United States of America* **100**, 10237-10242.

**Capo-Chichi, J. M., Bharti, S. K., Sommers, J. A., Yammine, T., Chouery, E., Patry, L., Rouleau, G. A., Samuels, M. E., Hamdan, F. F., Michaud, J. L. et al.** (2013).

Identification and biochemical characterization of a novel mutation in DDX11 causing Warsaw breakage syndrome. *Human mutation* **34**, 103-107.

**Chen, B., Gilbert, L. A., Cimini, B. A., Schnitzbauer, J., Zhang, W., Li, G. W., Park, J., Blackburn, E. H., Weissman, J. S., Qi, L. S. et al.** (2013). Dynamic imaging of genomic loci in living human cells by an optimized CRISPR/Cas system. *Cell* **155**, 1479-1491.

**Chetaille, P., Preuss, C., Burkhard, S., Cote, J. M., Houde, C., Castilloux, J., Piche, J., Gosset, N., Leclerc, S., Wunnemann, F. et al.** (2014). Mutations in SGOL1 cause a novel cohesinopathy affecting heart and gut rhythm. **46**, 1245-1249.

**Covo, S., Westmoreland, J. W., Gordenin, D. A. and Resnick, M. A.** (2010). Cohesin Is limiting for the suppression of DNA damage-induced recombination between homologous chromosomes. *PLoS genetics* **6**, e1001006.

**Crasta, K., Ganem, N. J., Dagher, R., Lantermann, A. B., Ivanova, E. V., Pan, Y., Nezi, L., Protopopov, A., Chowdhury, D. and Pellman, D.** (2012). DNA breaks and chromosome pulverization from errors in mitosis. *Nature* **482**, 53-58.

**Deardorff, M. A., Kaur, M., Yaeger, D., Rampuria, A., Korolev, S., Pie, J., Gil-Rodriguez, C., Arnedo, M., Loeys, B., Kline, A. D. et al.** (2007). Mutations in cohesin complex members SMC3 and SMC1A cause a mild variant of cornelia de Lange

syndrome with predominant mental retardation. *American journal of human genetics* **80**, 485-494.

**Dorsett, D. and Strom, L.** (2012). The ancient and evolving roles of cohesin in gene expression and DNA repair. *Current biology : CB* **22**, R240-250.

**Duijf, P. H. and Benezra, R.** (2013). The cancer biology of whole-chromosome instability. *Oncogene*.

**Gandhi, R., Gillespie, P. J. and Hirano, T.** (2006). Human Wapl is a cohesin-binding protein that promotes sister-chromatid resolution in mitotic prophase. *Current biology : CB* **16**, 2406-2417.

**Gause, M., Schaaf, C. A. and Dorsett, D.** (2008). Cohesin and CTCF: cooperating to control chromosome conformation? *BioEssays : news and reviews in molecular, cellular and developmental biology* **30**, 715-718.

**German, J.** (1979). Roberts' syndrome. I. Cytological evidence for a disturbance in chromatid pairing. *Clinical genetics* **16**, 441-447.

**Goh, E. S., Li, C., Horsburgh, S., Kasai, Y., Kolomietz, E. and Morel, C. F.** (2010). The Roberts syndrome/SC phocomelia spectrum--a case report of an adult with review of the literature. *American journal of medical genetics. Part A* **152A**, 472-478.

**Gondor, A. and Ohlsson, R.** (2008). Chromatin insulators and cohesins. *EMBO reports* **9**, 327-329.

**Hanks, S., Coleman, K., Summersgill, B., Messahel, B., Williamson, D., Pritchard-Jones, K., Strefford, J., Swansbury, J., Plaja, A., Shipley, J. et al.** (2006).

Comparative genomic hybridization and BUB1B mutation analyses in childhood cancers associated with mosaic variegated aneuploidy syndrome. *Cancer Lett* **239**, 234-238.

**Hartman, T., Stead, K., Koshland, D. and Guacci, V.** (2000). Pds5p is an essential chromosomal protein required for both sister chromatid cohesion and condensation in *Saccharomyces cerevisiae*. *The Journal of cell biology* **151**, 613-626.

**Heidinger-Pauli, J. M., Unal, E. and Koshland, D.** (2009). Distinct targets of the Eco1 acetyltransferase modulate cohesion in S phase and in response to DNA damage. *Molecular cell* **34**, 311-321.

**Homer, H. A., McDougall, A., Levasseur, M., Murdoch, A. P. and Herbert, M.** (2005). Mad2 is required for inhibiting securin and cyclin B degradation following spindle depolymerisation in meiosis I mouse oocytes. *Reproduction* **130**, 829-843.

**Horsfield, J. A., Print, C. G. and Monnich, M.** (2012). Diverse developmental disorders from the one ring: distinct molecular pathways underlie the cohesinopathies. *Frontiers in genetics* **3**, 171.

**Horsfield, J. A., Anagnostou, S. H., Hu, J. K., Cho, K. H., Geisler, R., Lieschke, G., Crosier, K. E. and Crosier, P. S.** (2007). Cohesin-dependent regulation of Runx genes. *Development* **134**, 2639-2649.

**Hou, F. and Zou, H.** (2005). Two human orthologues of Eco1/Ctf7 acetyltransferases are both required for proper sister-chromatid cohesion. *Molecular biology of the cell* **16**, 3908-3918.

**Hwang, W. Y., Fu, Y., Reyon, D., Maeder, M. L., Tsai, S. Q., Sander, J. D., Peterson, R. T., Yeh, J. R. and Joung, J. K.** (2013). Efficient genome editing in zebrafish using a CRISPR-Cas system. *Nature biotechnology* **31**, 227-229.

**Jao, L. E., Wente, S. R. and Chen, W.** (2013). Efficient multiplex biallelic zebrafish genome editing using a CRISPR nuclease system. *Proceedings of the National Academy of Sciences of the United States of America* **110**, 13904-13909.

**Jeong, K., Jeong, J. Y., Lee, H. O., Choi, E. and Lee, H.** (2010). Inhibition of Plk1 induces mitotic infidelity and embryonic growth defects in developing zebrafish embryos. *Developmental biology* **345**, 34-48.

**Jones, N. C., Lynn, M. L., Gaudenz, K., Sakai, D., Aoto, K., Rey, J. P., Glynn, E. F., Ellington, L., Du, C., Dixon, J. et al.** (2008). Prevention of the neurocristopathy Treacher Collins syndrome through inhibition of p53 function. *Nature medicine* **14**, 125-133.

**Junttila, M. R. and Evan, G. I.** (2009). p53--a Jack of all trades but master of none. *Nature reviews. Cancer* **9**, 821-829.

**Kim, J. S., Krasieva, T. B., LaMorte, V., Taylor, A. M. and Yokomori, K.** (2002). Specific recruitment of human cohesin to laser-induced DNA damage. *The Journal of biological chemistry* **277**, 45149-45153.

**Krantz, I. D., McCallum, J., DeScipio, C., Kaur, M., Gillis, L. A., Yaeger, D., Jukofsky, L., Wasserman, N., Bottani, A., Morris, C. A. et al.** (2004). Cornelia de Lange syndrome is caused by mutations in NIPBL, the human homolog of *Drosophila melanogaster* Nipped-B. *Nature genetics* **36**, 631-635.

**Kueng, S., Hegemann, B., Peters, B. H., Lipp, J. J., Schleiffer, A., Mechtler, K. and Peters, J. M.** (2006). Wapl controls the dynamic association of cohesin with chromatin. *Cell* **127**, 955-967.

**Lafont, A. L., Song, J. and Rankin, S.** (2010). Sororin cooperates with the acetyltransferase Eco2 to ensure DNA replication-dependent sister chromatid cohesion. *Proceedings of the National Academy of Sciences of the United States of America* **107**, 20364-20369.

**Lang, G. A., Iwakuma, T., Suh, Y. A., Liu, G., Rao, V. A., Parant, J. M., Valentin-Vega, Y. A., Terzian, T., Caldwell, L. C., Strong, L. C. et al.** (2004). Gain of function of a p53 hot spot mutation in a mouse model of Li-Fraumeni syndrome. *Cell* **119**, 861-872.

**Lengronne, A., McIntyre, J., Katou, Y., Kanoh, Y., Hopfner, K. P., Shirahige, K. and Uhlmann, F.** (2006). Establishment of sister chromatid cohesion at the *S. cerevisiae* replication fork. *Molecular cell* **23**, 787-799.

**Li, X. and Nicklas, R. B.** (1995). Mitotic forces control a cell-cycle checkpoint. *Nature* **373**, 630-632.

**Liu, J. and Krantz, I. D.** (2008). Cohesin and human disease. *Annual review of genomics and human genetics* **9**, 303-320.

**Losada, A.** (2008). The regulation of sister chromatid cohesion. *Biochimica et biophysica acta* **1786**, 41-48.

- Lu, S., Goering, M., Gard, S., Xiong, B., McNairn, A. J., Jaspersen, S. L. and Gerton, J. L.** (2010). Eco1 is important for DNA damage repair in *S. cerevisiae*. *Cell cycle* **9**, 3315-3327.
- Maradeo, M. E. and Skibbens, R. V.** (2009). The Elg1-RFC clamp-loading complex performs a role in sister chromatid cohesion. *PloS one* **4**, e4707.
- Marthiens, V., Rujano, M. A., Pennetier, C., Tessier, S., Paul-Gilloteaux, P. and Basto, R.** (2013). Centrosome amplification causes microcephaly. *Nat Cell Biol* **15**, 731-740.
- Maserati, E., Pasquali, F., Zuffardi, O., Buttitta, P., Cuoco, C., Defant, G., Gimelli, G. and Fraccaro, M.** (1991). Roberts syndrome: phenotypic variation, cytogenetic definition and heterozygote detection. *Annales de genétique* **34**, 239-246.
- Matsunaga, S., Takata, H., Morimoto, A., Hayashihara, K., Higashi, T., Akatsuchi, K., Mizusawa, E., Yamakawa, M., Ashida, M., Matsunaga, T. M. et al.** (2012). RBMX: a regulator for maintenance and centromeric protection of sister chromatid cohesion. *Cell reports* **1**, 299-308.
- Meek, D. W.** (2009). Tumour suppression by p53: a role for the DNA damage response? *Nature reviews. Cancer* **9**, 714-723.
- Michaelis, C., Ciosk, R. and Nasmyth, K.** (1997). Cohesins: chromosomal proteins that prevent premature separation of sister chromatids. *Cell* **91**, 35-45.
- Monnich, M., Kuriger, Z., Print, C. G. and Horsfield, J. A.** (2011). A zebrafish model of Roberts syndrome reveals that Esco2 depletion interferes with development by disrupting the cell cycle. *PloS one* **6**, e20051.

- Musio, A., Selicorni, A., Focarelli, M. L., Gervasini, C., Milani, D., Russo, S., Vezzoni, P. and Larizza, L.** (2006). X-linked Cornelia de Lange syndrome owing to SMC1L1 mutations. *Nature genetics* **38**, 528-530.
- Nasmyth, K. and Haering, C. H.** (2009). Cohesin: its roles and mechanisms. *Annual review of genetics* **43**, 525-558.
- Nicklas, R. B., Ward, S. C. and Gorbsky, G. J.** (1995). Kinetochores are sensitive to tension and may link mitotic forces to a cell cycle checkpoint. *The Journal of cell biology* **130**, 929-939.
- Ocampo-Hafalla, M. T. and Uhlmann, F.** (2011). Cohesin loading and sliding. *Journal of cell science* **124**, 685-691.
- Ogilvy, C. S., Pakzaban, P. and Lee, J. M.** (1993). Oculomotor nerve cavernous angioma in a patient with Roberts syndrome. *Surgical neurology* **40**, 39-42.
- Parant, J. M., George, S. A., Holden, J. A. and Yost, H. J.** (2010). Genetic modeling of Li-Fraumeni syndrome in zebrafish. *Disease models & mechanisms* **3**, 45-56.
- Pauli, A., van Bommel, J. G., Oliveira, R. A., Itoh, T., Shirahige, K., van Steensel, B. and Nasmyth, K.** (2010). A direct role for cohesin in gene regulation and ecdysone response in *Drosophila* salivary glands. *Current biology : CB* **20**, 1787-1798.
- Payne, E. M., Virgilio, M., Narla, A., Sun, H., Levine, M., Paw, B. H., Berliner, N., Look, A. T., Ebert, B. L. and Khanna-Gupta, A.** (2012). L-Leucine improves the anemia and developmental defects associated with Diamond-Blackfan anemia and del(5q) MDS by activating the mTOR pathway. *Blood* **120**, 2214-2224.

**Rankin, S., Ayad, N. G. and Kirschner, M. W.** (2005). Sororin, a substrate of the anaphase-promoting complex, is required for sister chromatid cohesion in vertebrates.

*Molecular cell* **18**, 185-200.

**Salic, A., Waters, J. C. and Mitchison, T. J.** (2004). Vertebrate shugoshin links sister centromere cohesion and kinetochore microtubule stability in mitosis. *Cell* **118**, 567-578.

**Schar, P., Fasi, M. and Jessberger, R.** (2004). SMC1 coordinates DNA double-strand break repair pathways. *Nucleic acids research* **32**, 3921-3929.

**Schockel, L., Mockel, M., Mayer, B., Boos, D. and Stemmann, O.** (2011). Cleavage of cohesin rings coordinates the separation of centrioles and chromatids. *Nature cell biology* **13**, 966-972.

**Schule, B., Oviedo, A., Johnston, K., Pai, S. and Francke, U.** (2005). Inactivating mutations in ESCO2 cause SC phocomelia and Roberts syndrome: no phenotype-genotype correlation. *American journal of human genetics* **77**, 1117-1128.

**Sidi, S., Sanda, T., Kennedy, R. D., Hagen, A. T., Jette, C. A., Hoffmans, R., Pascual, J., Imamura, S., Kishi, S., Amatruda, J. F. et al.** (2008). Chk1 suppresses a caspase-2 apoptotic response to DNA damage that bypasses p53, Bcl-2, and caspase-3. *Cell* **133**, 864-877.

**Sjogren, C. and Nasmyth, K.** (2001). Sister chromatid cohesion is required for postreplicative double-strand break repair in *Saccharomyces cerevisiae*. *Current biology* : *CB* **11**, 991-995.

**Skibbens, R. V.** (2009). Establishment of sister chromatid cohesion. *Current biology* : *CB* **19**, R1126-1132.

**Skibbens, R. V., Corson, L. B., Koshland, D. and Hieter, P.** (1999). Ctf7p is essential for sister chromatid cohesion and links mitotic chromosome structure to the DNA replication machinery. *Genes & development* **13**, 307-319.

**Snape, K., Hanks, S., Ruark, E., Barros-Nunez, P., Elliott, A., Murray, A., Lane, A. H., Shannon, N., Callier, P., Chitayat, D. et al.** (2011). Mutations in CEP57 cause mosaic variegated aneuploidy syndrome. *Nature genetics* **43**, 527-529.

**Sonoda, E., Matsusaka, T., Morrison, C., Vagnarelli, P., Hoshi, O., Ushiki, T., Nojima, K., Fukagawa, T., Waizenegger, I. C., Peters, J. M. et al.** (2001). Scc1/Rad21/Mcd1 is required for sister chromatid cohesion and kinetochore function in vertebrate cells. *Developmental cell* **1**, 759-770.

**Straight, A. F., Belmont, A. S., Robinett, C. C. and Murray, A. W.** (1996). GFP tagging of budding yeast chromosomes reveals that protein-protein interactions can mediate sister chromatid cohesion. *Current biology : CB* **6**, 1599-1608.

**Strom, L. and Sjogren, C.** (2005). DNA damage-induced cohesion. *Cell cycle* **4**, 536-539.

**Sutani, T., Kawaguchi, T., Kanno, R., Itoh, T. and Shirahige, K.** (2009). Budding yeast Wpl1(Rad61)-Pds5 complex counteracts sister chromatid cohesion-establishing reaction. *Current biology : CB* **19**, 492-497.

**Terret, M. E., Sherwood, R., Rahman, S., Qin, J. and Jallepalli, P. V.** (2009). Cohesin acetylation speeds the replication fork. *Nature* **462**, 231-234.

- Thomas, H. R., Percival, S. M., Yoder, B. K. and Parant, J. M.** (2014). High-throughput genome editing and phenotyping facilitated by high resolution melting curve analysis. *PloS one* **9**, e114632.
- Tomkins, D., Hunter, A. and Roberts, M.** (1979). Cytogenetic findings in Roberts-SC phocomelia syndrome(s). *American journal of medical genetics* **4**, 17-26.
- Tonkin, E. T., Wang, T. J., Lisgo, S., Bamshad, M. J. and Strachan, T.** (2004). NIPBL, encoding a homolog of fungal Scc2-type sister chromatid cohesion proteins and fly Nipped-B, is mutated in Cornelia de Lange syndrome. *Nature genetics* **36**, 636-641.
- Toruno, C., Carbonneau, S., Stewart, R. A. and Jette, C.** (2014). Interdependence of Bad and Puma during ionizing-radiation-induced apoptosis. *PloS one* **9**, e88151.
- Toth, A., Ciosk, R., Uhlmann, F., Galova, M., Schleiffer, A. and Nasmyth, K.** (1999). Yeast cohesin complex requires a conserved protein, Eco1p(Ctf7), to establish cohesion between sister chromatids during DNA replication. *Genes & development* **13**, 320-333.
- van der Lelij, P., Chrzanowska, K. H., Godthelp, B. C., Rooimans, M. A., Oostra, A. B., Stumm, M., Zdzienicka, M. Z., Joenje, H. and de Winter, J. P.** (2010). Warsaw breakage syndrome, a cohesinopathy associated with mutations in the XPD helicase family member DDX11/ChIR1. *American journal of human genetics* **86**, 262-266.
- Vega, H., Trainer, A. H., Gordillo, M., Crosier, M., Kayserili, H., Skovby, F., Uzielli, M. L., Schnur, R. E., Manouvrier, S., Blair, E. et al.** (2010). Phenotypic variability in 49 cases of ESCO2 mutations, including novel missense and codon deletion in the acetyltransferase domain, correlates with ESCO2 expression and establishes the clinical criteria for Roberts syndrome. *Journal of medical genetics* **47**, 30-37.

- Waizenegger, I. C., Hauf, S., Meinke, A. and Peters, J. M.** (2000). Two distinct pathways remove mammalian cohesin from chromosome arms in prophase and from centromeres in anaphase. *Cell* **103**, 399-410.
- Wang, D., Jao, L. E., Zheng, N., Dolan, K., Ivey, J., Zonies, S., Wu, X., Wu, K., Yang, H., Meng, Q. et al.** (2007). Efficient genome-wide mutagenesis of zebrafish genes by retroviral insertions. *Proceedings of the National Academy of Sciences of the United States of America* **104**, 12428-12433.
- Wenger, S. L., Blatt, J., Steele, M. W., Lloyd, D. A., Bellinger, M., Phebus, C. K., Horn, M. and Jaffe, R.** (1988). Rhabdomyosarcoma in Roberts syndrome. *Cancer Genet Cytogenet* **31**, 285-289.
- Whelan, G., Kreidl, E., Wutz, G., Egner, A., Peters, J. M. and Eichele, G.** (2012). Cohesin acetyltransferase Esco2 is a cell viability factor and is required for cohesion in pericentric heterochromatin. *The EMBO journal* **31**, 71-82.
- Williams, B. C., Garrett-Engele, C. M., Li, Z., Williams, E. V., Rosenman, E. D. and Goldberg, M. L.** (2003). Two putative acetyltransferases, san and deco, are required for establishing sister chromatid cohesion in *Drosophila*. *Current biology : CB* **13**, 2025-2036.
- Xu, B., Lee, K. K., Zhang, L. and Gerton, J. L.** (2013). Stimulation of mTORC1 with L-leucine rescues defects associated with Roberts syndrome. *PLoS genetics* **9**, e1003857.
- Yamada, H. Y., Yao, Y., Wang, X., Zhang, Y., Huang, Y., Dai, W. and Rao, C. V.** (2012). Haploinsufficiency of SGO1 results in deregulated centrosome dynamics, enhanced chromosomal instability and colon tumorigenesis. *Cell cycle* **11**, 479-488.

**Yonish-Rouach, E., Grunwald, D., Wilder, S., Kimchi, A., May, E., Lawrence, J. J., May, P. and Oren, M.** (1993). p53-mediated cell death: relationship to cell cycle control. *Molecular and cellular biology* **13**, 1415-1423.

**Zhang, Y., Ear, J., Yang, Z., Morimoto, K., Zhang, B. and Lin, S.** (2014). Defects of protein production in erythroid cells revealed in a zebrafish Diamond-Blackfan anemia model for mutation in RPS19. *Cell death & disease* **5**, e1352.

EMBRYONIC MITOTIC DEFECTS DUE TO HETEROZYGOUS LOSS OF ESCO2  
ENHANCES TUMORIGENESIS IN VIVO

by

STEFANIE M. PERCIVAL, HOLLY THOMAS, JOHN M. PARANT

*In Preparation*

Format adapted for dissertation

## **PREFACE**

While performing mutant cellular analysis, one third of cells in *esco2* heterozygous embryos are discovered to have a paired but separated phenotype indicating cohesion defects and a possible gene dose effect of *Esco2*. *PDS5A*, *PDS5B*, and *SGOL1* are other SCC proteins that have displayed a gene dose effect that impacts development and tumorigenesis. The serendipitous discovery of a few tumors in *esco2* heterozygous animals further spurred our study in investigating the cellular and organismal outcomes of the paired but separated phenotype.

## **ABSTRACT**

Several animal models and cultured systems show that *ESCO2* is embryonic and cell lethal, however transient gene dose effects in an *esco2* morphant suggest that possible gene dose contributions exist that impact embryonic development. Here we describe *esco2* heterozygous zebrafish that display mild cohesion and mitotic defects during embryonic development. These mild cohesion defects are tolerable in a vertebrate system suggesting not all cohesion defects are lethal. Surprisingly, *esco2* heterozygous adults are predisposed to tumor formation. Low level aneuploidy observed due to the cohesion and mitotic defects likely contribute to this enhanced tumorigenesis. Together, these data provide the first evidence linking *ESCO2* to tumor formation and that the mild cohesion defects are associated with tumorigenesis within a vertebrate organism.

## INTRODUCTION

Sister chromatid cohesion (SCC) is a process by which the cohesin ring, consisting of structural maintenance of cohesion 1 (SMC1), structural maintenance of cohesion 3 (SMC3), RAD21, and stromal antigen1/2 (STAG1/STAG2), entraps DNA for a variety of cellular functions including, chromosome segregation, gene expression, and DNA repair (Guacci et al., 1997; Michaelis et al., 1997; Toth et al., 1999). ESCO2 is a critical acetyltransferase essential for cohesion establishment, a process by which the cohesin ring is stabilized for proper chromosome segregation (Hou & Zou, 2005; Skibbens et al., 1999; Tanaka et al., 2001). For proper cohesion establishment to occur, ESCO2 must acetylate the SMC3 portion of the cohesin ring for stabilization. Defects in ESCO2 are associated with premature sister chromatid separation leading to genomic instability and lethality (Percival et al., 2015; Rolef Ben-Shahar et al., 2008; Unal et al., 2008; Zhang et al., 2008).

Interestingly, mutations in SCC are the causal genes for a subset of developmental disorders called cohesinopathies. Cohesinopathies present with variable craniofacial, limb and mental retardation defects. One of the more common cohesinopathies is Roberts syndrome (RBS) which is caused by mutations in ESCO2 (Vega et al., 2005). This disorder presents with multi-system defects, particularly retrognathia, microcephaly, cleft lip and palate, brachydactyly, and mental retardation. Cohesion defects are also a key characteristic of this disorder manifesting into heterochromatic repulsion (HR), a centromeric puffing visible in chromosome spreads. These defects manifest into a spectrum of phenotypic severities within RBS ranging from embryonic lethal to surviving

to adulthood with mild defects. No genotype-phenotype correlation has been proven thus far (Goh et al., 2010; Tomkins et al., 1979; Vega et al., 2010).

Considering developmental disorders and cancer have genomic instability and mitotic defects in common, one would expect tumorigenesis to be associated with RBS. Though cancer is strongly associated with other cohesinopathies such as Warsaw Breakage Syndrome, caused by mutations in DDX11, the association of cancer predisposition with RBS is unclear (Bharti et al., 2014; van der Lelij et al., 2010). Five cancer reports have been documented in Roberts syndromes but the number of patients is too small to make a strong claim (Ogilvy et al., 1993; Schule et al., 2005; Wenger et al., 1988).

We and others have used many model systems to understand how loss of an essential gene results in a developmental disorder. Cultured systems in yeast and human cells find that ESCO2 (Eco1 in yeast) loss results in cohesion defects and lethality (Whelan et al., 2012; Zhang et al., 2008). Several other model systems were generated in vertebrates to determine if loss of ESCO2 displays phenotypes more reminiscent of RBS. Surprisingly, ESCO2 is embryonic lethal in mice and zebrafish (Monnich et al., 2011; Percival et al., 2015; Whelan et al., 2012). Conditional knockout of ESCO2 in neuronal progenitors in mice results in severe microcephaly, a predominant phenotype in RBS (Whelan et al., 2012). Despite the lack of multi-system effects of ESCO2 loss, this model provides data towards understanding its role in neural tissue in the context of RBS.

Two key zebrafish studies were able to overcome the embryonic lethality in mouse by assessing *esco2* morphant and mutant ex vivo development, a major advantage

to zebrafish models. Julia Horsfield's group was first to determine that *esco2* morphants are lethal, but show a diverse set of gross phenotypes ranging from fin to craniofacial defects. In addition, the defect severity is dependent on the range of *Esco2* knockdown. These defects are due to defects in mitosis rather than expression changes of developmentally regulated genes (Monnich et al., 2011). We expand on this study in an *esco2* mutant zebrafish model to overcome the pitfalls of morpholinos and find that 20% of cells divide normally within *esco2* mutants. This coincides with a 15% mild cohesion defects at the centromere and suggests that these cells are able to survive over time (Percival et al., 2015). The ability for cells to survive with cohesion defects in a live vertebrate organism is novel considering previous literature states cohesion defects are cell lethal.

Due to the previously identified mild cohesion defects in a subset of cells in *esco2* mutant zebrafish and morpholino dose-dependent phenotypes, we wanted to determine if a gene dose effect is responsible for the capability of some cells to divide in the absence of *Esco2* (Percival et al., 2015). Characterization of *esco2* sibling embryos steered toward discovery of a mild cohesion defect associated with heterozygous embryos during development and a serendipitous discovery of a cancer predisposition in adult zebrafish. High resolution *in vivo* imaging techniques aids in detecting mitotic defects down to the single chromosome level. The discovery of mild cohesion defects in a live vertebrate organism provides the first evidence of a gene dose effect of the cohesion establishment factor, *ESCO2*, and that these defects are tolerable within a vertebrate organism. Though *esco2* heterozygous are viable, we are also the first to show *Esco2*'s role in enhancing cancer penetrance in a predisposed model.

## RESULTS

### Gene dose-dependent reduction in cohesion establishment leads to aneuploidy.

Our interest in the embryonic analysis of *esco2* heterozygous animals originates from the observation that chromosome spreads from *esco2* non-mutant sibling (*esco2*<sup>+/+</sup> and <sup>+/m</sup>, but not *esco2*<sup>m/m</sup>), derived from a heterozygous-heterozygous cross, showed an abnormal number of spreads with a paired but separated (PBS) morphology (Figure 1A). This class of morphology is described as sister chromatids still being paired while displaying a centromeric separation, similar to HR observed in RBS patients. In order to determine if morphology is associated specifically with *esco2* heterozygosity we compared spreads from *esco2*<sup>+/+</sup> and *esco2*<sup>+/m</sup> embryos. Compared to *esco2*<sup>+/+</sup>, *esco2*<sup>+/m</sup> have a 16-fold increase in the amount of PBS spreads (Figure 1B). Further, we observe that 8% (5 of 62) of mitotic spreads from *esco2* heterozygous animals contain aneuploidies with greater than 10 chromosomes lost, while no such aneuploidies are observed in spreads from wild-type embryos (Figure 1C). Micro-karyotype variation is observed in both *esco2*<sup>+/+</sup> and *esco2*<sup>+/m</sup> spreads. More specifically, wild type spreads have approximately 65% of spreads have a normal chromosome count of 50 while 33% have between 45 and 52, but not 50, chromosomes. These numbers are consistent with *esco2*<sup>+/+</sup> spreads in that 65% have 50 chromosomes while 28% have between 45 and 52, but not 50, chromosomes. These data suggest that the more severe chromosome losses (>10) are due to *esco2* heterozygosity while milder aneuploidy appears to be present in both populations.

Micronuclei (MN) are notorious for harboring genomic instability and are often a sign of aneuploidy. To follow up on the consequences of the cohesion defects, we calculate the frequency of MN in G1 nuclei in wild type and *esco2* heterozygous embryos. Significantly higher numbers of MN are present in the *esco2* heterozygous embryos (~6%) verses the wild-type embryos (2%; Figure 1D). Interestingly, there is a strong variability between embryos, ranging from 0 - 3.9% in wild-type embryos and 1.9% - 15% (data not shown). This spectrum of MN frequencies could explain the increased incidence of chromosomes spreads with greater than 10 chromosomes lost.

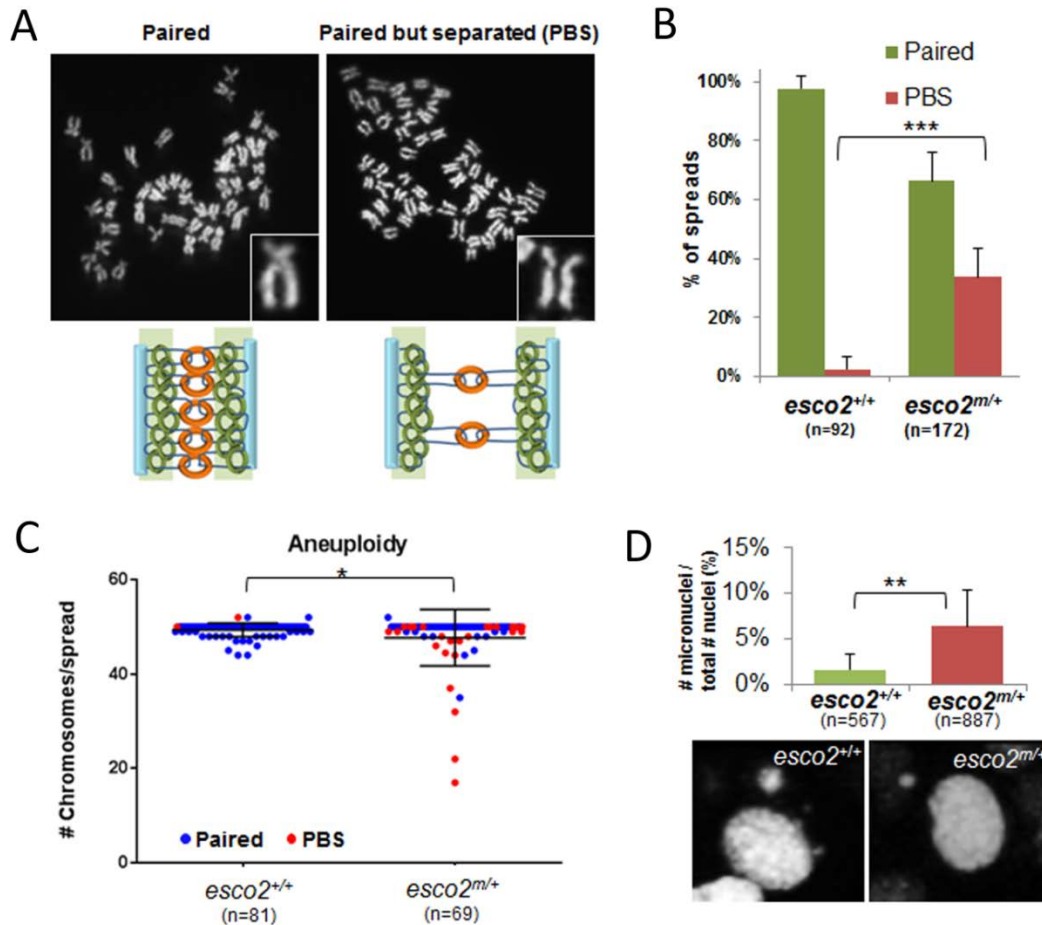


**Figure 1: Gene dose-dependent reduction in cohesion establishment leads to aneuploidy.** (A) Representative images of paired and paired but separated (PBS) spreads. Inset shows zoomed in view of each phenotype. Schematic of the hypothesized cause of the PBS phenotype due to gene dose-dependent loss of cohesion establishment is shown below. (B) Percent of spreads in *esco2*<sup>+/+</sup> and *esco2*<sup>+m</sup> showing paired or PBS phenotypes. Three pools of embryos are used for *esco2*<sup>+/+</sup> and five pools for *esco2*<sup>+m</sup> spreads. Total of 92 *esco2*<sup>+/+</sup> and 175 *esco2*<sup>+m</sup> spreads are tallied. \*\*\* p-value < 0.001. (C) Number of chromosomes per spread are calculated in *esco2*<sup>+/+</sup> and *esco2*<sup>+m</sup>. Blue dots represent paired spreads while red dots represent paired but separated (PBS) spreads. Three pools of embryos/genotype are used to generate spreads. Total of 81 *esco2*<sup>+/+</sup> and 69 *esco2*<sup>+m</sup> spreads are tallied. \* p-value < 0.05. (D) Micronuclei are counted in six *esco2*<sup>+/+</sup> and ten *esco2*<sup>+m</sup> embryos using two hour live imaging time-lapse data from each embryo. Percentages are calculated based on the total number of micronuclei and nuclei present in the time lapse at t=0. Mean ± st. dev. \*\* p-value < 0.01. Representative black and white images of micronuclei in each genotype are shown below.

### **Embryonic *esco2* heterozygosity leads to chromosome instability.**

We previously observed high levels of chromosome missegregation in *esco2*<sup>m/m</sup> animals (Percival et al., 2015). In order to determine if chromosome missegregation in *esco2*<sup>m/+</sup> animals is a result of the cohesion defects present (Figure 1B, C) and contributes to micronuclei formation (Figure 1D), we monitor 73 mitoses in six wild type sibling embryos and 131 mitoses in ten *esco2* heterozygous embryos. The

majority of mitoses in wild-type embryos are error free in appearance (72 of 73; Figure 2A) and are of normal duration (74% were 18-26 minutes, Figure 2B). We do observe one abnormal mitotic event that results in a congression defect and slightly lengthened mitotic duration, but displays no observable segregation errors (Figure 2C). In *esco2* heterozygous embryos, while the majority of divisions appear normal (119 of 131, Figure 2A), we observe 12 mitoses with errors, five of which have clear chromosome missegregation events, and two that never exit mitosis within our observation time frame. These events are summarized in Figure 2C, and include one anaphase bridge (Figure 2A), six congression defects, two multi-polar divisions (Figure 2A), two prolonged delays in metaphase with no division observed (>50min, and >120 min), and one cell fusion leading to multiple lagging defects. These events suggest mild defects in microtubule attachment (congression defects) and/or centrosome duplication (multi-polar divisions) are present in *esco2* heterozygous embryos. Further, in 3 of 131 (2.3%) mitoses, we observe a severe mitotic delay (60 min, >50 minutes, and >120; Figure 2B, C) indicative of a prolonged spindle assemble checkpoint. The variation within mitotic defects between embryos of the same genotype supports the variability in micronuclei percentages we observe (Figure 1D, Figure 2C). Together, these data indicate that heterozygous loss of *Esco2* results in cohesion defects that contribute to chromosome instability.

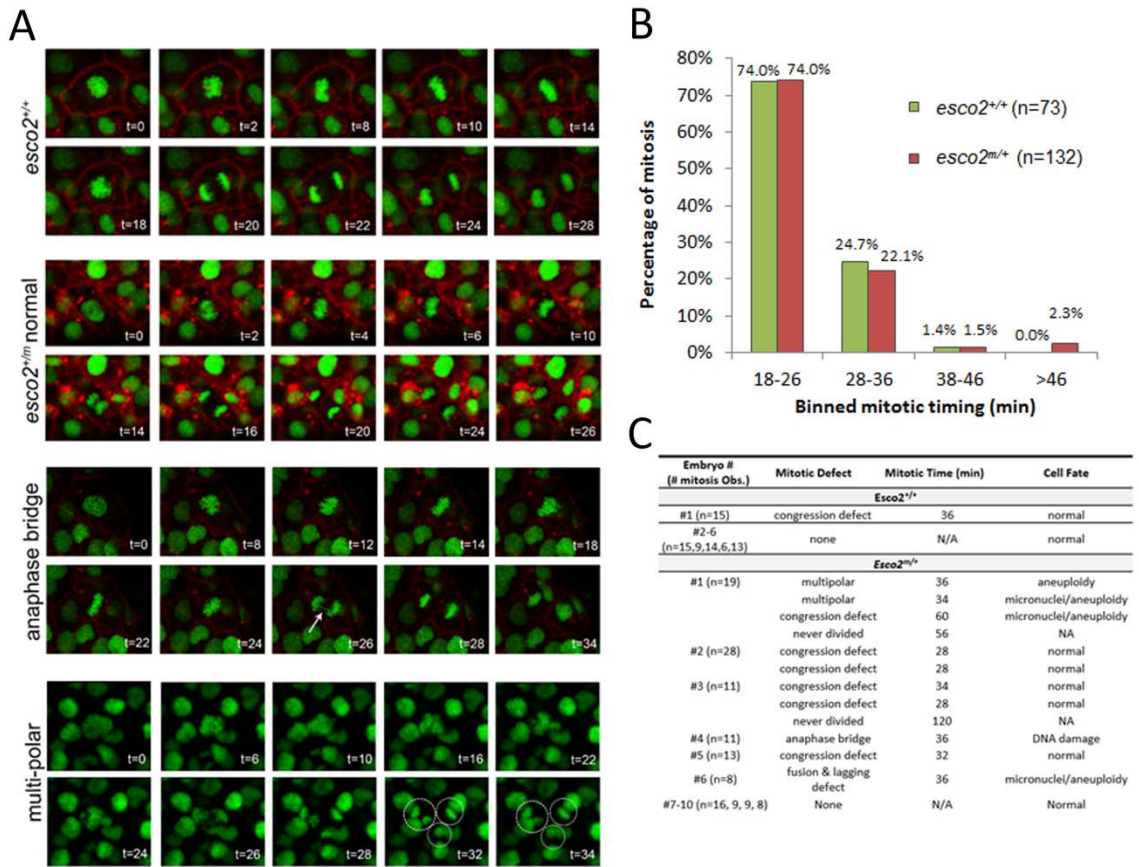


**Figure 2: Embryonic *esco2* heterozygosity leads to chromosome instability.** (A) H2A.F/Z-EGFP and CaaX-mCherry mRNA injected embryos imaged *in vivo* at 24 hpf for two hours. Representative images of normal and defective mitoses in *esco2*<sup>+/+</sup> and *esco2*<sup>+/m</sup>. Arrow in anaphase bridge time-lapse points towards the anaphase bridge formed. Dotted circular lines in multi-polar time lapse represents the three nuclear divisions that occur. CaaX-mCherry is removed in multi-polar time lapse for better visualization. t=time in minutes. (B) Division time calculated for each division in six *esco2*<sup>+/+</sup> and ten *esco2*<sup>+/m</sup> embryos using two hour imaging time lapse data from each embryo. Percentage of cells is calculated for each bin category. (C) Table of mitotic defects, associated mitotic timing, and cell fate observed in six *esco2*<sup>+/+</sup> and ten *esco2*<sup>+/m</sup> embryos.

While the role of SCC in tumorigenesis is unclear, a few adult RBS patient have succumb to early tumor onset and two SCC mutant animal's models have been shown to be slightly tumor prone (Remeseiro et al., 2012; Yamada et al., 2012). Further genomic instability, similar to what we see in our *esco2* heterozygous animals, has been linked to tumorigenesis; therefore we developed a tumor cohort study to determine if *esco2* heterozygosity enhances tumor formation. To speed up these studies, we bred our heterozygous *Esco2* animals into a cancer predisposed *p53* heterozygous mutant background (Parant et al., 2010). *P53* is a transcription factor essential for the maintenance of genomic integrity (Fields & Jang, 1990; Lane, 1992; Raycroft et al., 1990). It is mutated in 50-70% of human cancers and thus serves as a relevant predisposition model for these studies (Dietze et al., 2001). Analysis of the tumor cohort reveals some surprising results. Despite there being only two tumors in *esco2*<sup>+/m</sup> alone compared to zero in the wild type controls, *esco2* heterozygous; *p53* heterozygous animals form tumors more rapidly than the *p53* heterozygous animals (Figure 3A). To determine if *Esco2* is a tumor suppressor gene, we also cross *esco2* heterozygotes into a *p53*<sup>-/-</sup> background. Interestingly, those *esco2*<sup>+/m</sup> in a *p53* mutant background did not show a significant increase in tumorigenesis compared to *p53* mutant fish alone. From this data, we provide evidence that *Esco2* is not a tumor suppressor gene but enhances tumor formation by enhancing the frequency of loss of heterozygosity (LOH) of the other *p53* allele.

In order to determine the extent of increased LOH frequency, we sequenced 22 and 24 tumors of *esco2*<sup>+/+</sup>; *p53*<sup>+/m</sup> and *esco2*<sup>+/m</sup>; *p53*<sup>m/+</sup> genotypes, respectively. The selected tumors spanned the entire tumor curve in each genotype, making sure both early

and late tumor onsets were included. Both the *p53* and *esco2* alleles are analyzed in order to test for LOH in both scenarios. Sequencing of *p53* shows that the loss of the *p53* allele occurs very frequently and that even in the presence of *esco2* heterozygosity, the frequency of *p53* LOH remains unchanged. There are no instances of *Esco2* LOH suggesting the primary mechanism of tumor formation is through *p53* LOH (Figure 3B). Altogether, these data point towards *esco2* acting as a haploinsufficient tumor suppressor in the presence of a LOH sensitive background.

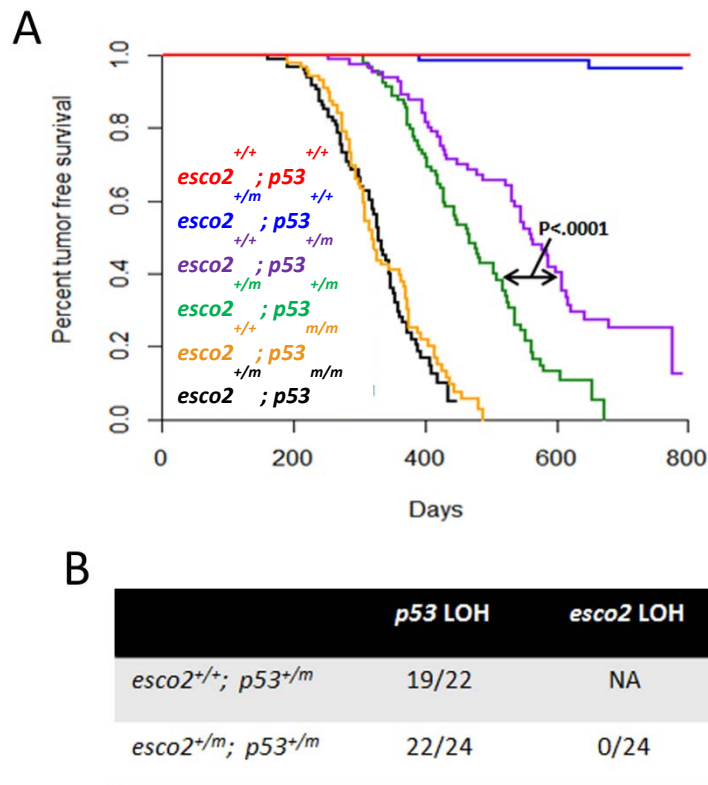


**Figure 3: *esco2* haploinsufficiency enhances tumor onset in a *p53* heterozygous but not in *p53* wild-type or homozygous mutant background.** A) Kaplan Meyer curves for tumor free survival for wild-type, *esco2*<sup>+/+</sup>, *p53*<sup>+/m</sup>, *esco2*<sup>+/m</sup>; *p53*<sup>+/m</sup>, *p53*<sup>m/+</sup>, *p53*<sup>m/m</sup>, and

*esco2*<sup>+/*m*</sup>; *p53*<sup>*m/m*</sup> (all cohorts were n=96).  $p < 0.0001$  when comparing *p53*<sup>+/*m*</sup> to *esco2*<sup>+/*m*</sup>; *p53*<sup>+/*m*</sup> curves (based on Wilcoxon Rank-Sum test). B) Frequency of p53 wild-type loss of heterozygosity (LOH) and *esco2* wild-type LOH in tumors.

## DISCUSSION

We describe in this study the novel observation of embryonic cohesion defects due to *esco2* heterozygosity being tolerable within a vertebrate organism and playing a role in tumor formation. In light of the viability of some RBS patients with heterochromatic repulsion this is not surprising, however the predominant model derived from cell culture studies indicate that SCC at the centromere is required for bipolar attachment and that reduced cohesion will lead to segregation defects and lethality. We also use high resolution microscopy to visualize the mitotic defects that lead to tumorigenesis in this system. These findings are significant and have substantial potential in further understanding the pathogenesis of Roberts syndrome and other human disease states affected by cohesion defects.

Based on chromosome spread analysis, it appears that the more severe aneuploidies are the main cause of the increased tumorigenesis (Figure 1C). These defects are more likely to be a result of the multi-polar and fusion divisions or accumulation of several single chromosome events as described in Figure 2. Multi-polar divisions are due to either over-duplication of centrosomes or premature centriole separation (Fukasawa, 2011; Telentschak et al., 2015; Zyss & Gergely, 2009). The only link to cohesion establishment and centrosome regulation is found in yeast. It shows that

one of Eco1's acetylation targets is Mps3 (Ghosh et al., 2012). Mps3 is a SUN-domain protein required in spindle pole body duplication, the yeast complex corresponding to centrosomes. Mps3 is also essential for sister chromatid cohesion establishment in yeast though no vertebrate equivalent of this process has been discovered (Antoniacci et al., 2004). However, several pieces of evidence point towards the action of Separase, the cysteine protease responsible for cohesin ring cleavage at the metaphase-anaphase transition, in centriole disengagement (Lee & Rhee, 2012; Prosser et al., 2015; Schockel et al., 2011). Overall, multi-polar divisions are sources of aneuploidy and DNA damage that contribute to tumorigenesis (Ganem et al., 2009; Milunovic-Jevtic et al., 2016; Shi & King, 2005). Though not directly assayed in this study, p53 is shown to lead to centrosome defects that could aid in tumor formation in our predisposed model (Fukasawa, 2011). Future studies will assay for centrioles (i.e.  $\gamma$ -tubulin) to determine if centriole defects are enhanced due to *esco2* heterozygosity.

Cell fusion also provides a rich environment for tumor formation by generating several forms of genomic instability including aneuploidy, DNA damage, and micronuclei (Berndt et al., 2013; Harkness et al., 2013; Ogle et al., 2005). Interestingly, a theory in the field suggests that cell fusion is a mechanism for non-proliferative cells to gain oncogenic potential (Bjerkvig et al., 2005; Lu & Kang, 2009). Though only observed in one monitored division in this study, this type of cell fusion is observed once more in an embryonic lethal *esco2*<sup>m/m</sup>; *p53*<sup>m/m</sup> embryo suggesting this is not an isolated incident (data not shown). In terms of cell fusion initiating tumor formation, the first evidence is recently demonstrated in epithelial cells to lead to cell transformation and malignant

tumorigenesis *in vivo* (Zhou et al., 2015). Here we provide additional evidence that the presence of cell fusion could be a factor in driving tumorigenesis.

Mitotic defects leading to chromosome missegregation is one mechanism by which p53 LOH occurs. The increase in frequency of chromosome loss in *esco2* heterozygous embryos provides a possible mechanism behind the LOH subsequent enhanced tumorigenesis. Other mechanisms of LOH include gene conversion and mitotic recombination (Bishop & Schiestl, 2001; Wijnhoven et al., 2001). Point mutation frequency is usually much lower than the LOH frequency suggesting de novo mutations are an unlikely cause of inactivation of the other p53 allele (Lasko et al., 1991). We hypothesize that though the frequency of LOH of p53 remains unaffected, the rate of LOH is increased due to mitotic defects present in *esco2* heterozygous animals. Future directions will aim to develop an assay to sequence single cell suspensions for high-throughput analysis comparing the rates of LOH at the embryonic stage. Use of this assay at several different time points will be able to determine at what time point (rate) LOH is enhanced in  $p53^{+/m}$  versus  $esco2^{+/m}; p53^{+/m}$  animals.

The most striking observation from this study is that despite the overwhelming data indicating cohesion defects are lethal, we are able to observe that reduced cohesion at the centromere is viable to an extent within a vertebrate organism. One-third of cells in *esco2* heterozygous embryos display mild cohesion defects. Interestingly, only 9% of these cells result in a visible mitotic defect suggesting that the majority of those cells exhibiting the paired but separated classification divide normally. Several cellular assays used in the SCC field are devised for loci separation to indicate cohesion defects. These cohesion defects often correlated to cell lethality (Ciosk et al., 2000; Skibbens et al.,

1999). Though able to identify the presence of a cohesion defect, the extent of cohesion defects is unable to be distinguished. By characterizing the cohesion defects in our previously described *esco2* mutant and *esco2* heterozygous embryos here, we are able to correlate the severity in cohesion defects to cell survival (Percival et al., 2015). This idea is not unfounded in that loss of the anti-establishment factors (Wapl or Pds5) in the absence of *Esco2* rescues cell lethality and cohesion defects in yeast and human cell culture. These studies however did not determine the degree viability or amount of cohesion defects (Gandhi et al., 2006; Kueng et al., 2006; Nishiyama et al., 2010; Rowland et al., 2009; Tanaka et al., 2001). Here we describe the ability to measure cohesion defects and correlate them to a cellular outcome.

Discovery of this gene-dose effect of *Esco2* is important in pursuing the underlying pathogenesis of RBS. As stated previously, RBS is a spectrum disorder ranging from embryonic lethal to adulthood survival with mild developmental defects. Interestingly, our studies of *Esco2* in zebrafish identify similarities to RBS. *Esco2* mutant zebrafish are embryonic lethal with severe cohesion defects and may therefore model the more severe form of RBS (Percival et al., 2015). *Esco2* heterozygous zebrafish are viable with mild cohesion defects though predisposed to tumor formation and therefore model the milder RBS patients. Though a cancer predisposition within RBS is still uncertain, several documents report cancer in RBS patients (Ogilvy et al., 1993; Schule et al., 2005; Wenger et al., 1988). This gene dose effect therefore suggests that the extent of cohesion defects determines the severity of the phenotype. Variation in cohesion defects may be regulated by genetic modifiers in the background of RBS patients. Candidate genes for genetic modifiers include the previously described anti-establishment factors Wapl and

Pds5 that are known to rescue cohesion defects (Gandhi et al., 2006; Kueng et al., 2006; Nishiyama et al., 2010; Rowland et al., 2009; Tanaka et al., 2001). As well, genetic modifiers to exacerbate cohesion defects such as other cohesion establishment/maintenance factors (ESCO1, SHUGOSHIN1, SORORIN) could be responsible for creating a more severe RBS phenotype (Rankin et al., 2005; Riedel et al., 2006; Tang et al., 2006; Whelan et al., 2012). Though many of these genetic interactions are shown *in vitro*, multi-cellular organism analysis is necessary to determine if these interactions are valid *in vivo*.

Looking forward, the ability to detect low level cohesion defects is valuable in the development of novel cancer therapeutics. Sister chromatid cohesion defects are found in a variety of tumors that lead to genomic instability (Sajesh et al., 2013; Solomon et al., 2011; Stoepker et al., 2015). The frequency of genomic instability is shown to correlate to higher tumor grade and poorer prognosis across human cancers (Carter et al., 2006; Duijf & Benezra, 2013). As well, aneuploidy frequency correlates to the development of multi-drug resistance (McClelland et al., 2009). It is reported that cells exhibiting high levels of genomic instability that are treated with taxanes are resistant; therefore the discovery of drugs targeting new processes is critical (Swanton et al., 2009). Towards this concept, treatment inhibiting BubR1 or Mps1 in combination with taxane treatments increases cell death (Janssen et al., 2009). Similar to this study, targeting of cohesion in combination with taxanes could provide a novel route for cancer treatment. For example, development of an ESCO2 inhibitor could enhance the already existing cohesion defects in tumor cells towards a detrimental state while only causing mild cohesion defects in non-cancerous tissue, which have shown to be tolerable in this study. Future studies will

look into manipulating the levels of cohesion defects in adult animals as well as embryonic analysis towards developing novel therapeutics for cohesion related disease states and to further understand the molecular and genetic interactions regulating cohesion severity in development.

## **AFTERWORD**

As this manuscript moves towards publication, additional studies will be performed to complete our story investigating *Esco2* in tumorigenesis. To determine if the enhanced tumor formation in the presence of *esco2* heterozygosity is applicable to RBS patients and cancer as a whole, we plan to evaluate prevalence and outcome of ESCO2 loss in human cancers using The Cancer Genome Atlas (TCGA) data. From this data, we aim to understand any clinical characteristics associated with ESCO2 loss. This will help identify if RBS is a cancer-predisposed syndrome in those that carry a LOH tumor suppressor mutation. Globally, it will have significant implications in understanding the role of SCC in tumorigenesis.

## **MATERIALS AND METHODS**

### **Zebrafish lines:**

All zebrafish work was performed in the Zebrafish Research Facility (ZRF) of the University of Alabama at Birmingham (UAB). Adult fish and embryos are maintained as described by Westerfield et al (1995) by the ZRF Animal Resources Program which

maintains full AAALAC accreditation and is assured with OLAW. The *esco2* retroviral insertion allele was obtained from Nancy Hopkins and Jacqueline A. Lees (Massachusetts Institute of Technology, Cambridge, MA) and maintained on the AB background. The p53 allele was obtained through a forward genetic screen (Parant 2010).

### **Genotyping/High Resolution Melt Analysis:**

To genotype, tail clippings from each fish were placed in 100 µl ELB (10 mM Tris pH 8.3, 50 mM KCl, 0.3% Tween 20, 0.3% NP40, 1 mg/ml Proteinase K) in 96-well plates. Tail clips were incubated at 55°C overnight to generate genomic DNA, and the plates were then incubated at 95°C for 10 min to inactivate the Proteinase K. PCR amplicons were generated using a universal forward primer : 5'-TTTCACTGTTTCTGCAGGTTG-3', primer 5'-TAAGGTCTTCGAAGTCTTAACG-3' to amplify the WT allele, and primer 5' GGGGGGGGGCCTACAGGTGGGGTCTTTC-3' to amplify the retroviral insertion allele. PCR reactions contained 1ul of LC Green Plus Melting Dye (BioFire Defense), 1µl of enzyme buffer, 0.2 ul of dNTP Mixture (10mM each), 0.3 ul of MgCl<sub>2</sub>, 0.3 µl of each primer (10uM), 1 µl of gDNA , 0.05 µl of Genscript Taq, and water up to 10µl. The PCR reaction protocol was 98°C for 30 sec, then 40 cycles of 98°C for 10 sec, 59°C for 20 sec, and 72° C for 15 sec, followed by 72°C for 1 minute and then rapid cooling to 4°C. Following PCR, melting curves were generated and analyzed using the LightScanner instrument (Idaho Technology) over a 65-95°C range.

### **Time-lapse imaging**

CaaX-mCherry and H2A.F/Z-EGFP mRNA was transcribed from a plasmid [pCS2-CaaX-mCherry and pCS2-H2A.F/Z-EGFP; gift from K. Kwan (University of Utah)] using mMessage mMachine SP6 kit (LifeTechnologies). Esco2 heterozygotes were crossed and embryos were microinjected into the yolk of a one-cell-staged embryo with 1 nl of 200 ng/ $\mu$ l CaaX-mCherry and 200 ng/ $\mu$ l H2afva-eGFP mRNA. At 24 hpf, embryos were screened for fluorescence. Embryos showing a mutant phenotype were excluded. Embryos were manually dechorionated using tweezers and anesthetized using 0.4% tricaine. In a glass-coverslip-bottomed dish, embryos were embedded in a 1% low-melt agarose. Dishes were placed on the Nikon A1 inverted confocal microscope and Z-stack images were taken at designated intervals. Approximately 40- $\mu$ m Z-stacks (with a 2- $\mu$ m interval) were obtained every 2 minutes for a total scanning time of 2 hours. After each embryo was imaged, embryos were removed from the agarose to generate genomic DNA for genotyping. All videos were taken using 60x 1.4 NA objectives. 3D viewing, still shots and videos were assembled and processed using NIS Elements 4.13.00. Division time was calculated by manually counting how many time intervals encompass the division. This number was then multiplied by the time between each Z-stack (2 minutes). See our video manuscript for further details on this technique.

### **Micronuclei/apoptotic bodies count**

Embryos were injected with H2A.F/Z-EGFP and CaaX-mCherry mRNA and set up for a time-lapse video. An approximately 40- $\mu$ m Z-stack was generated with 2- $\mu$ m steps using a 60x 1.4 NA objective on a Nikon A1 confocal microscope. Using 3D volume rendering

in NIS Elements 4.13.00, an average nuclei, micronuclei and apoptotic body count was calculated per field to generate the percent observed in a population of cells. Filters for apoptotic bodies and micronuclei (versus nuclei) were set at H2A.F/Z-EGFP fluorescing body  $\leq 3 \mu\text{m}$ . Differentiation between apoptotic bodies and micronuclei was determined based on size and localization within the cell; i.e. using the CaaX-mCherry (plasma membrane) fluorescence, it can be determined whether a micronuclei is within a cell and whether an apoptotic body is outside a cell. Frequency of micronuclei in interphase was calculated by dividing the total number of micronuclei observed in the 3D render by the number of nuclei identified in the 3D render. Representative micronuclei images were pulled from the 3D volume rendering of an *esco2*<sup>+/+</sup> and *esco2*<sup>+/m</sup>, CaaX fluorescence was removed, and image was converted to black and white.

### **Chromosome spreads**

Chromosomes spread protocol was adapted from the Lee group ([Jeong et al., 2010](#)). Approximately 20-30 embryos were dechorionated at 24 hpf. Embryos were incubated in 400 ng/ml nocodazole for 2 h in the dark at 28°C. Embryos were then transferred to 1.1% sodium citrate in a 6-cm dish and deyolked. At this point, for genotyping purposes, tails were removed to be genotyped, whereas the remaining embryo heads were transferred to fresh sodium citrate solution and incubated on ice for 8 min. Next, we performed two washes with a cold 3:1 methanol:acetic acid solution for 20 min each followed by storage in -20°C overnight until genotyping was performed. After fixative procedure, embryos were pooled (10-12 embryos/pool) per genotype and then minced using forceps in a 1:1 methanol:acetic acid solution. Using this mixture, 150  $\mu\text{l}$  of pooled embryos were

dropped onto a slide, and 3-5 drops of glacial acetic acid was added. The slide was then exposed to hot vapors (we used boiling water) for about 10 s; then allowed to dry on a hot metal surface (approx. 55°C). After the slide was completely dry, a few drops of Prolong Gold with DAPI (Life Technologies) were added, and the slide was covered with a glass coverslip. Chromosomes were imaged using a 63×1.4 NA objective on a Zeiss Axio Observer fluorescent microscope and processed with Zen 2011 Blue software. Although most spreads were clearly delineated into the ‘paired’, PBS or ‘separated’ categories, if a spread had multiple phenotypes it was categorized by which was most prevalent in that spread. Chromatid number was counted manually from high-resolution images.

#### **Establishing Tumor Cohorts:**

Six tumor cohorts (*esco2*<sup>+/+</sup>, *esco2*<sup>m/+</sup>, *esco2*<sup>+/+</sup>;*p53*<sup>m/+</sup>, *esco2*<sup>m/+</sup>;*p53*<sup>m/+</sup>, *esco2*<sup>+/+</sup>;*p53*<sup>m/m</sup>, and *esco2*<sup>m/+</sup>;*p53*<sup>m/m</sup>) were established by natural breedings of *esco2*<sup>m/+</sup> x AB wild-type, *esco2*<sup>m/+</sup>;*p53*<sup>m/m</sup> x AB wild-type, and *esco2*<sup>m/+</sup>;*p53*<sup>m/m</sup> x *p53*<sup>m/m</sup> parents. Each cohort consisted of 96 fish and was derived from a single set of parents (a single male and female.) At 3 months of age, each fish was genotyped for the *esco2* allele and then separated into 6 tanks of 16 fish each.

#### **Tumor Collection:**

Adult fish were screened biweekly for tumors and/or missing/dead fish. Fish that were identified by eye to be tumor burdened were euthanized according to IACUC protocols. A portion of each tumor was fixed in 10% neutral buffered formalin (Formal-Fixx Concentrate – Fisher Scientific) and later sectioned and H&E stained for histological

analysis by the UAB Comparative Pathology Laboratory. The remaining tumor was flash frozen along with a fin clip for future DNA-RNA analysis. Kaplan-Meier analysis was performed using GraphPad Prism software.

#### **Loss of Heterozygosity Analysis:**

DNA was extracted from 22 *esco2*<sup>+/+</sup>;*p53*<sup>m/+</sup> and 24 *esco2*<sup>m/+</sup>;*p53*<sup>m/+</sup> tumors using the DNeasy Blood & Tissue Kit (Qiagen). LOH analysis was performed for the *esco2* allele using the HRM method described above and for the *p53* allele by sequencing PCR products. Each PCR reaction contained 3 µl Ex Taq Buffer, 2.4 µl dNTPs (2.5mM each), 0.9 µl forward primer (5' GTGCAGCCCTACTACTGGAAT 3'), 0.9µl of reverse primer (5' GGCCTACAAAAGGCTGTGA 3'), 50-100 ng of DNA, and water up to 30ul. PCR conditions were as follows: 98°C for 30 sec, then 40 cycles of 98°C for 10 sec, 56°C for 30 seconds, and 72° C for 30 seconds, followed by 72°C for 4 minutes. Each PCR reaction was analyzed on a 2% agarose gel and purified using the Wizard SV Gel and PCR Clean Up System (Promega). Each sample was sequenced by the UAB Heflin Center for Genomic Science.

#### **COMPETING INTERESTS**

There are no competing interests associated with the data and discussion presented in this paper.

## AUTHOR CONTRIBUTIONS

SMP, HRT, and JMP designed further experiments; HRT generated mitotic spreads and the tumor cohort studies; SMP performed experiments involving embryonic analysis; SMP, HRT, and JMP analyzed data and wrote the manuscript.

## REFERENCES

- Antoniacci, L. M., Kenna, M. A., Uetz, P., Fields, S., & Skibbens, R. V. (2004). The spindle pole body assembly component mps3p/nep98p functions in sister chromatid cohesion. *J Biol Chem*, *279*(47), 49542-49550. doi: 10.1074/jbc.M404324200
- Berndt, B., Zanker, K. S., & Dittmar, T. (2013). Cell fusion is a potent inducer of aneuploidy and drug resistance in tumor cell/ normal cell hybrids. *Crit Rev Oncog*, *18*(1-2), 97-113.
- Bharti, S. K., Khan, I., Banerjee, T., Sommers, J. A., Wu, Y., & Brosh, R. M., Jr. (2014). Molecular functions and cellular roles of the ChlR1 (DDX11) helicase defective in the rare cohesinopathy Warsaw breakage syndrome. *Cell Mol Life Sci*, *71*(14), 2625-2639. doi: 10.1007/s00018-014-1569-4
- Bishop, A. J., & Schiestl, R. H. (2001). Homologous recombination as a mechanism of carcinogenesis. *Biochim Biophys Acta*, *1471*(3), M109-121.
- Bjerkvig, R., Tysnes, B. B., Aboody, K. S., Najbauer, J., & Terzis, A. J. (2005). Opinion: the origin of the cancer stem cell: current controversies and new insights. *Nat Rev Cancer*, *5*(11), 899-904. doi: 10.1038/nrc1740
- Carter, S. L., Eklund, A. C., Kohane, I. S., Harris, L. N., & Szallasi, Z. (2006). A signature of chromosomal instability inferred from gene expression profiles predicts clinical outcome in multiple human cancers. *Nat Genet*, *38*(9), 1043-1048. doi: 10.1038/ng1861
- Ciosk, R., Shirayama, M., Shevchenko, A., Tanaka, T., Toth, A., Shevchenko, A., & Nasmyth, K. (2000). Cohesin's binding to chromosomes depends on a separate complex consisting of Scc2 and Scc4 proteins. *Mol Cell*, *5*(2), 243-254.
- Dietze, E. C., Caldwell, L. E., Grupin, S. L., Mancini, M., & Seewaldt, V. L. (2001). Tamoxifen but not 4-hydroxytamoxifen initiates apoptosis in p53(-) normal human mammary epithelial cells by inducing mitochondrial depolarization. *J Biol Chem*, *276*(7), 5384-5394. doi: 10.1074/jbc.M007915200
- Duijf, P. H., & Benezra, R. (2013). The cancer biology of whole-chromosome instability. *Oncogene*. doi: 10.1038/onc.2012.616
- Fields, S., & Jang, S. K. (1990). Presence of a potent transcription activating sequence in the p53 protein. *Science*, *249*(4972), 1046-1049.

- Fukasawa, K. (2011). Aberrant activation of cell cycle regulators, centrosome amplification, and mitotic defects. *Horm Cancer*, 2(2), 104-112. doi: 10.1007/s12672-010-0060-4
- Gandhi, R., Gillespie, P. J., & Hirano, T. (2006). Human Wapl is a cohesin-binding protein that promotes sister-chromatid resolution in mitotic prophase. *Curr Biol*, 16(24), 2406-2417. doi: 10.1016/j.cub.2006.10.061
- Ganem, N. J., Godinho, S. A., & Pellman, D. (2009). A mechanism linking extra centrosomes to chromosomal instability. *Nature*, 460(7252), 278-282. doi: 10.1038/nature08136
- Ghosh, S., Gardner, J. M., Smoyer, C. J., Friederichs, J. M., Unruh, J. R., Slaughter, B. D., . . . Jaspersen, S. L. (2012). Acetylation of the SUN protein Mps3 by Eco1 regulates its function in nuclear organization. *Mol Biol Cell*, 23(13), 2546-2559. doi: 10.1091/mbc.E11-07-0600
- Goh, E. S., Li, C., Horsburgh, S., Kasai, Y., Kolomietz, E., & Morel, C. F. (2010). The Roberts syndrome/SC phocomelia spectrum--a case report of an adult with review of the literature. *Am J Med Genet A*, 152A(2), 472-478. doi: 10.1002/ajmg.a.33261
- Guacci, V., Koshland, D., & Strunnikov, A. (1997). A direct link between sister chromatid cohesion and chromosome condensation revealed through the analysis of MCD1 in *S. cerevisiae*. *Cell*, 91(1), 47-57.
- Harkness, T., Weaver, B. A., Alexander, C. M., & Ogle, B. M. (2013). Cell fusion in tumor development: accelerated genetic evolution. *Crit Rev Oncog*, 18(1-2), 19-42.
- Hou, F., & Zou, H. (2005). Two human orthologues of Eco1/Ctf7 acetyltransferases are both required for proper sister-chromatid cohesion. *Mol Biol Cell*, 16(8), 3908-3918. doi: 10.1091/mbc.E04-12-1063
- Janssen, A., Kops, G. J., & Medema, R. H. (2009). Elevating the frequency of chromosome mis-segregation as a strategy to kill tumor cells. *Proc Natl Acad Sci U S A*, 106(45), 19108-19113. doi: 10.1073/pnas.0904343106
- Kueng, S., Hegemann, B., Peters, B. H., Lipp, J. J., Schleiffer, A., Mechtler, K., & Peters, J. M. (2006). Wapl controls the dynamic association of cohesin with chromatin. *Cell*, 127(5), 955-967. doi: 10.1016/j.cell.2006.09.040
- Lane, D. P. (1992). Cancer. p53, guardian of the genome. *Nature*, 358(6381), 15-16. doi: 10.1038/358015a0
- Lasko, D., Cavenee, W., & Nordenskjold, M. (1991). Loss of constitutional heterozygosity in human cancer. *Annu Rev Genet*, 25, 281-314. doi: 10.1146/annurev.ge.25.120191.001433
- Lee, K., & Rhee, K. (2012). Separase-dependent cleavage of pericentrin B is necessary and sufficient for centriole disengagement during mitosis. *Cell Cycle*, 11(13), 2476-2485. doi: 10.4161/cc.20878
- Lu, X., & Kang, Y. (2009). Cell fusion as a hidden force in tumor progression. *Cancer Res*, 69(22), 8536-8539. doi: 10.1158/0008-5472.CAN-09-2159
- McClelland, S. E., Burrell, R. A., & Swanton, C. (2009). Chromosomal instability: a composite phenotype that influences sensitivity to chemotherapy. *Cell Cycle*, 8(20), 3262-3266. doi: 10.4161/cc.8.20.9690

- Michaelis, C., Ciosk, R., & Nasmyth, K. (1997). Cohesins: chromosomal proteins that prevent premature separation of sister chromatids. *Cell*, *91*(1), 35-45.
- Milunovic-Jevtic, A., Mooney, P., Sulerud, T., Bisht, J., & Gatlin, J. C. (2016). Centrosomal clustering contributes to chromosomal instability and cancer. *Curr Opin Biotechnol*, *40*, 113-118. doi: 10.1016/j.copbio.2016.03.011
- Monnich, M., Kuriger, Z., Print, C. G., & Horsfield, J. A. (2011). A zebrafish model of Roberts syndrome reveals that Esco2 depletion interferes with development by disrupting the cell cycle. *PLoS One*, *6*(5), e20051. doi: 10.1371/journal.pone.0020051
- Nishiyama, T., Ladurner, R., Schmitz, J., Kreidl, E., Schleiffer, A., Bhaskara, V., . . . Peters, J. M. (2010). Sororin mediates sister chromatid cohesion by antagonizing Wapl. *Cell*, *143*(5), 737-749. doi: 10.1016/j.cell.2010.10.031
- Ogilvy, C. S., Pakzaban, P., & Lee, J. M. (1993). Oculomotor nerve cavernous angioma in a patient with Roberts syndrome. *Surg Neurol*, *40*(1), 39-42.
- Ogle, B. M., Cascalho, M., & Platt, J. L. (2005). Biological implications of cell fusion. *Nat Rev Mol Cell Biol*, *6*(7), 567-575. doi: 10.1038/nrm1678
- Parant, J. M., George, S. A., Holden, J. A., & Yost, H. J. (2010). Genetic modeling of Li-Fraumeni syndrome in zebrafish. *Dis Model Mech*, *3*(1-2), 45-56. doi: 10.1242/dmm.003749
- Percival, S. M., Thomas, H. R., Amsterdam, A., Carroll, A. J., Lees, J. A., Yost, H. J., & Parant, J. M. (2015). Variations in dysfunction of sister chromatid cohesion in *esco2* mutant zebrafish reflect the phenotypic diversity of Roberts syndrome. *Dis Model Mech*, *8*(8), 941-955. doi: 10.1242/dmm.019059
- Prosser, S. L., Sahota, N. K., Pelletier, L., Morrison, C. G., & Fry, A. M. (2015). Nek5 promotes centrosome integrity in interphase and loss of centrosome cohesion in mitosis. *J Cell Biol*, *209*(3), 339-348. doi: 10.1083/jcb.201412099
- Rankin, S., Ayad, N. G., & Kirschner, M. W. (2005). Sororin, a substrate of the anaphase-promoting complex, is required for sister chromatid cohesion in vertebrates. *Mol Cell*, *18*(2), 185-200. doi: 10.1016/j.molcel.2005.03.017
- Raycroft, L., Wu, H. Y., & Lozano, G. (1990). Transcriptional activation by wild-type but not transforming mutants of the p53 anti-oncogene. *Science*, *249*(4972), 1049-1051.
- Remeseiro, S., Cuadrado, A., Carretero, M., Martinez, P., Drosopoulos, W. C., Canamero, M., . . . Losada, A. (2012). Cohesin-SA1 deficiency drives aneuploidy and tumorigenesis in mice due to impaired replication of telomeres. *EMBO J*, *31*(9), 2076-2089. doi: 10.1038/emboj.2012.11
- Riedel, C. G., Katis, V. L., Katou, Y., Mori, S., Itoh, T., Helmhart, W., . . . Nasmyth, K. (2006). Protein phosphatase 2A protects centromeric sister chromatid cohesion during meiosis I. *Nature*, *441*(7089), 53-61. doi: 10.1038/nature04664
- Rolef Ben-Shahar, T., Heeger, S., Lehane, C., East, P., Flynn, H., Skehel, M., & Uhlmann, F. (2008). Eco1-dependent cohesin acetylation during establishment of sister chromatid cohesion. *Science*, *321*(5888), 563-566. doi: 10.1126/science.1157774
- Rowland, B. D., Roig, M. B., Nishino, T., Kurze, A., Uluocak, P., Mishra, A., . . . Nasmyth, K. (2009). Building sister chromatid cohesion: *smc3* acetylation

- counteracts an antiestablishment activity. *Mol Cell*, 33(6), 763-774. doi: 10.1016/j.molcel.2009.02.028
- Sajesh, B. V., Lichtensztejn, Z., & McManus, K. J. (2013). Sister chromatid cohesion defects are associated with chromosome instability in Hodgkin lymphoma cells. *BMC Cancer*, 13, 391. doi: 10.1186/1471-2407-13-391
- Schockel, L., Mockel, M., Mayer, B., Boos, D., & Stemmann, O. (2011). Cleavage of cohesin rings coordinates the separation of centrioles and chromatids. *Nat Cell Biol*, 13(8), 966-972. doi: 10.1038/ncb2280
- Schule, B., Oviedo, A., Johnston, K., Pai, S., & Francke, U. (2005). Inactivating mutations in ESCO2 cause SC phocomelia and Roberts syndrome: no phenotype-genotype correlation. *Am J Hum Genet*, 77(6), 1117-1128. doi: 10.1086/498695
- Shi, Q., & King, R. W. (2005). Chromosome nondisjunction yields tetraploid rather than aneuploid cells in human cell lines. *Nature*, 437(7061), 1038-1042. doi: 10.1038/nature03958
- Skibbens, R. V., Corson, L. B., Koshland, D., & Hieter, P. (1999). Ctf7p is essential for sister chromatid cohesion and links mitotic chromosome structure to the DNA replication machinery. *Genes Dev*, 13(3), 307-319.
- Solomon, D. A., Kim, T., Diaz-Martinez, L. A., Fair, J., Elkahloun, A. G., Harris, B. T., . . . Waldman, T. (2011). Mutational inactivation of STAG2 causes aneuploidy in human cancer. *Science*, 333(6045), 1039-1043. doi: 10.1126/science.1203619
- Stoepker, C., Ameziane, N., van der Lelij, P., Kooi, I. E., Oostra, A. B., Rooimans, M. A., . . . Brakenhoff, R. H. (2015). Defects in the Fanconi Anemia Pathway and Chromatid Cohesion in Head and Neck Cancer. *Cancer Res*, 75(17), 3543-3553. doi: 10.1158/0008-5472.CAN-15-0528
- Swanton, C., Nicke, B., Schuett, M., Eklund, A. C., Ng, C., Li, Q., . . . Downward, J. (2009). Chromosomal instability determines taxane response. *Proc Natl Acad Sci U S A*, 106(21), 8671-8676. doi: 10.1073/pnas.0811835106
- Tanaka, K., Hao, Z., Kai, M., & Okayama, H. (2001). Establishment and maintenance of sister chromatid cohesion in fission yeast by a unique mechanism. *EMBO J*, 20(20), 5779-5790. doi: 10.1093/emboj/20.20.5779
- Tang, J., Erikson, R. L., & Liu, X. (2006). Ectopic expression of Plk1 leads to activation of the spindle checkpoint. *Cell Cycle*, 5(21), 2484-2488. doi: 10.4161/cc.5.21.3411
- Telentschak, S., Soliwoda, M., Nohroudi, K., Addicks, K., & Klinz, F. J. (2015). Cytokinesis failure and successful multipolar mitoses drive aneuploidy in glioblastoma cells. *Oncol Rep*, 33(4), 2001-2008. doi: 10.3892/or.2015.3751
- Tomkins, D., Hunter, A., & Roberts, M. (1979). Cytogenetic findings in Roberts-SC phocomelia syndrome(s). *Am J Med Genet*, 4(1), 17-26. doi: 10.1002/ajmg.1320040104
- Toth, A., Ciosk, R., Uhlmann, F., Galova, M., Schleiffer, A., & Nasmyth, K. (1999). Yeast cohesin complex requires a conserved protein, Eco1p(Ctf7), to establish cohesion between sister chromatids during DNA replication. *Genes Dev*, 13(3), 320-333.
- Unal, E., Heidinger-Pauli, J. M., Kim, W., Guacci, V., Onn, I., Gygi, S. P., & Koshland, D. E. (2008). A molecular determinant for the establishment of sister chromatid cohesion. *Science*, 321(5888), 566-569. doi: 10.1126/science.1157880

- van der Lelij, P., Chrzanowska, K. H., Godthelp, B. C., Rooimans, M. A., Oostra, A. B., Stumm, M., . . . de Winter, J. P. (2010). Warsaw breakage syndrome, a cohesinopathy associated with mutations in the XPD helicase family member DDX11/ChlR1. *Am J Hum Genet*, *86*(2), 262-266. doi: 10.1016/j.ajhg.2010.01.008
- Vega, H., Trainer, A. H., Gordillo, M., Crosier, M., Kayserili, H., Skovby, F., . . . Jabs, E. W. (2010). Phenotypic variability in 49 cases of ESCO2 mutations, including novel missense and codon deletion in the acetyltransferase domain, correlates with ESCO2 expression and establishes the clinical criteria for Roberts syndrome. *J Med Genet*, *47*(1), 30-37. doi: 10.1136/jmg.2009.068395
- Vega, H., Waisfisz, Q., Gordillo, M., Sakai, N., Yanagihara, I., Yamada, M., . . . Joenje, H. (2005). Roberts syndrome is caused by mutations in ESCO2, a human homolog of yeast ECO1 that is essential for the establishment of sister chromatid cohesion. *Nat Genet*, *37*(5), 468-470. doi: 10.1038/ng1548
- Wenger, S. L., Blatt, J., Steele, M. W., Lloyd, D. A., Bellinger, M., Phebus, C. K., . . . Jaffe, R. (1988). Rhabdomyosarcoma in Roberts syndrome. *Cancer Genet Cytogenet*, *31*(2), 285-289.
- Whelan, G., Kreidl, E., Wutz, G., Egner, A., Peters, J. M., & Eichele, G. (2012). Cohesin acetyltransferase EscO2 is a cell viability factor and is required for cohesion in pericentric heterochromatin. *EMBO J*, *31*(1), 71-82. doi: 10.1038/emboj.2011.381
- Wijnhoven, S. W., Kool, H. J., van Teijlingen, C. M., van Zeeland, A. A., & Vrieling, H. (2001). Loss of heterozygosity in somatic cells of the mouse. An important step in cancer initiation? *Mutat Res*, *473*(1), 23-36.
- Yamada, H. Y., Yao, Y., Wang, X., Zhang, Y., Huang, Y., Dai, W., & Rao, C. V. (2012). Haploinsufficiency of SGO1 results in deregulated centrosome dynamics, enhanced chromosomal instability and colon tumorigenesis. *Cell Cycle*, *11*(3), 479-488. doi: 10.4161/cc.11.3.18994
- Zhang, J., Shi, X., Li, Y., Kim, B. J., Jia, J., Huang, Z., . . . Qin, J. (2008). Acetylation of Smc3 by Eco1 is required for S phase sister chromatid cohesion in both human and yeast. *Mol Cell*, *31*(1), 143-151. doi: 10.1016/j.molcel.2008.06.006
- Zhou, X., Merchak, K., Lee, W., Grande, J. P., Cascalho, M., & Platt, J. L. (2015). Cell Fusion Connects Oncogenesis with Tumor Evolution. *Am J Pathol*, *185*(7), 2049-2060. doi: 10.1016/j.ajpath.2015.03.014
- Zyss, D., & Gergely, F. (2009). Centrosome function in cancer: guilty or innocent? *Trends Cell Biol*, *19*(7), 334-346. doi: 10.1016/j.tcb.2009.04.001

EVOLUTION OF GENE MANIPULATION IN ZEBRAFISH

by

STEFANIE PERCIVAL

Formatted for dissertation

## **INTRODUCTION**

The zebrafish (*Danio rerio*) has increasingly become one of the most popular animal models in science and arguably the most popular model when studying genetics and human genetic diseases. This is primarily due to the ease of genetic manipulation offered, but also includes the rapid *ex vivo* development, large clutch size, and transparent embryogenesis. Forward genetic screens have identified multiple genes that span a variety of biological areas, but are labor intensive and lack efficiency. Reverse genetic approaches are, until recently, limited to transient morpholino gene knockdown. The necessity for gene knockout technology in zebrafish is finally fulfilled when zinc finger nucleases are found to be effective in generating zebrafish knockouts. Since then, the genome editing field has revolutionized to include several other nuclease-driven techniques. Compounding this boom in technology is the now-completed zebrafish genome, which opens up the ability to effectively and efficiently target any gene in zebrafish, adding to the endless list of advantages this model system boasts. Discussed below is a descriptive comparison between the primary reverse genetic approaches used in zebrafish today, as well as suggestions for controls and the future of genome editing in zebrafish.

## **MORPHOLINOS**

Morpholinos (MO) represent the first generation of genomic manipulation in the zebrafish community. This technology is a key step in accelerating zebrafish as a model system in the developmental biology and basic science fields. It is used as a rapid, high-throughput technology to study gene knockdown in a variety of organisms including

zebrafish, chick, frog, and mouse<sup>6, 22, 29</sup>. The initial use of antisense RNA to manipulate translation or RNA stability was developed in the 1980's by the Harland, Weintraub, and Melton groups<sup>16, 25</sup>. RNAi is then developed and attempts at incorporating this technique into the zebrafish community are taken. Unfortunately, it is discovered that RNAi in zebrafish results in extensive non-specific targeting and off-target effects causing misleading results<sup>30</sup>. For those few groups that are successful using shRNA in zebrafish, optimal gene knockdown peaked at approximately 70% which severely limits their ability to study gene function<sup>9</sup>. Fortunately, at the turn of the century, MOs are designed to show efficient knockdown of zygotic genes putting zebrafish on the fast-track to an idealized model system with an effective gene manipulation technology<sup>13, 17, 28</sup>.

Morpholinos are synthetic molecules that consist of approximately 25 units of oligonucleotides. Instead of a riboside moiety as seen in RNA/DNA, MOs consist of a morpholine moiety that uses phosphorodiamidate bonds in place of phosphodiester bonds (Figure 1A). The chemical structure is very similar to that of both RNA and DNA yet the lack of charge on the molecule allows it to bypass endogenous processes that prevent its degradation<sup>13</sup>. A MO functions by either interfering with ribosomal binding to mRNA or intron excision of pre-mRNA; both techniques are proven effective and are accompanied with their own downfalls (Figure 1B & C).

Translation-blocking MOs (TBMO) target the initiation codon (AUG) of a transcript in which the MO binds to the untranslated region (UTR) 5' of the start sequence<sup>38</sup>. This region is responsible for ribosome binding prior to the start of translation, defined by the Kozak sequence in vertebrates. This process acts as steric hindrance by preventing the ribosome from binding to the mRNA thus inhibiting

translation. One caveat to this approach is to quantify the level of gene knockdown, the simplest approaches require the use of an antibody. Commercial antibodies often fail due to lack of specificity to zebrafish epitopes, leaving the investigator to invest in generating their own antibody. Once generated, this antibody will be a valuable resource to the investigator; however it becomes a balancing act of where to devote time and resources. Studies using an injected GFP-tagged mRNA, in conjunction with the MO, are used as an antibody-free assay to observe knockdown via diminished fluorescence. Although in theory this should work, accessibility of the MO to the endogenous mRNA and the injected GFP-mRNA may be entirely different and give false results<sup>5</sup>. No control for this assay is developed largely leaving the TBMO community to antibody-derived assays of quantifying knockdown.

A way of circumventing the antibody dilemma is the development of the splice-blocking morpholino (SBMO). SBMOs bind to the exon-intron splice site preventing accurate splicing of introns by masking the splice site in the pre-mRNA transcript<sup>11</sup>. Accurate splicing of introns depends on specific splice sequences to the 5' and 3' end of introns. SBMO are designed to bind to the exon-intron junction to block access of essential small nuclear ribonucleoproteins (snRNPs) to the mRNA. Inclusion of an intron prevents maturation of the RNA and accurate translation of the protein. This most often leads to a frame shift to stop codon event and a nonfunctional protein product. SBMOs have the advantage of quantification without the use of an antibody by using reverse transcriptase-polymerase chain reaction (RT-PCR) to measure the amount of knockdown present, based on amplicon size, in injected embryos. Alternative splice sites increase the complexity of using SBMOs since alternative gene products could be made no matter

how efficiently the MO binds and blocks its target. Knowledge of alternative gene products is necessary when designing MOs and should be taken into account when assessing the phenotypes of morphants.

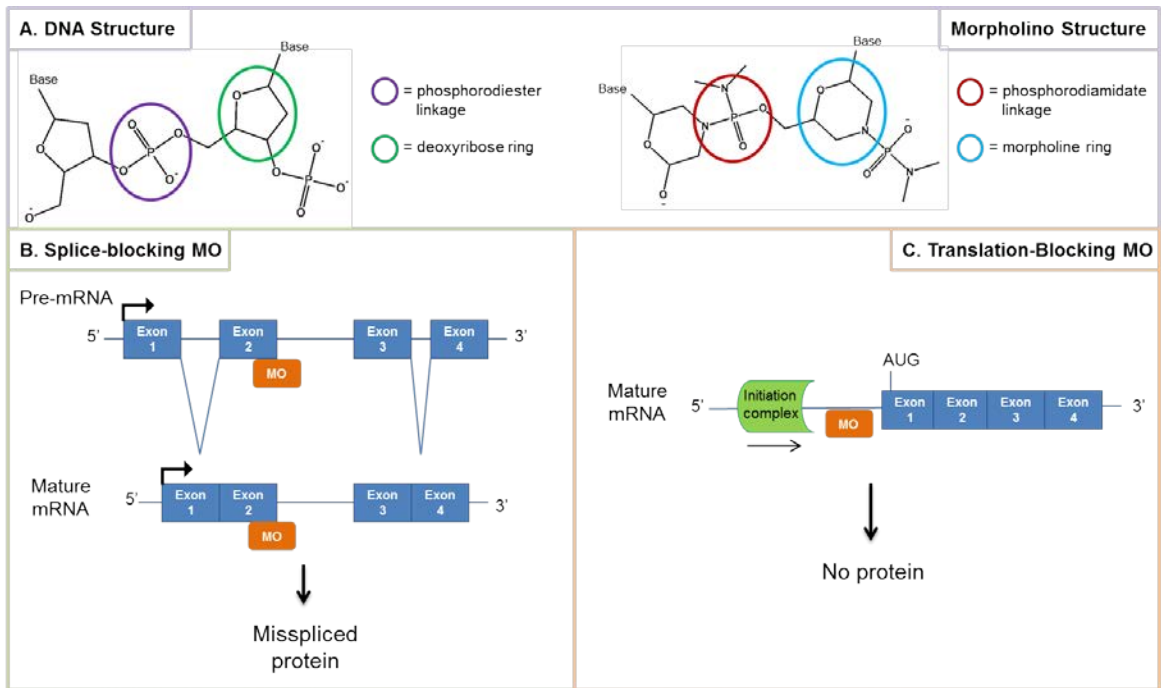


**Figure 1: Gene knock-down using morpholinos.** (A) Structure of DNA backbone compared to a morpholino backbone. Described are the phosphodiester linkage (purple circle) and ribose ring (green circle) in the DNA backbone and the phosphorodiamidate linkage (red circle) and the morpholine ring (blue circle) that make up a morpholino structure. 'Base' represents the four standard nucleobases. (B) Schematic of splice-blocking MO. SBMOs bind to the exon-intron boundary of pre-mRNA. Processing removes all but the MO-bound intron by masking the splice junction yielding a misspliced protein. (C) Schematic of translation blocking MO. TBMO are designed to the sequence 5' of start site (AUG). Initiation complex scans for AUG but encounters MO and prevents ribosomal binding. This pathway yields no protein product.

As with TBMOs, SBMOs are accompanied by several pitfalls. One major disadvantage is that although mRNA levels show knockdown, it is impossible to predict how protein levels will be affected without the use of antibodies. In addition to the unpredictable nature of how mRNA knockdown affects protein activity, exon-intron targeting has its downfalls as well. Targeting of a specific site may result in truncated forms of a protein, in-frame insertion/deletions (indels), and/or cryptic splice sites, all of which can result in a partial to fully functional protein. These results add to the difficulty in finding the right targeting site for a SBMO.

While morpholinos pave the way for zebrafish as a model system, they are in general, not a perfect system in which multiple controls are necessary to validate the results. One major concern when using MOs is the ability to accurately assess gene knockdown no matter what type of MO is used. These techniques include western blots, GFP-tagged mRNA, and RT-PCR, yet come with their own concerns as discussed previously. In addition, the dose of MO is constantly being diluted after each cell division. Theoretically, a MO has a much better targeting success at 100-cell stage compared to 1,000,000-cell stage due to the decreased concentration of MO as cells divide. The ability to detect gene knockdown depends on this dilution factor as well as the stability of the MO. The majority of phenotypes last from 48 to 96 hours post fertilization (hpf) while others show a partial phenotype<sup>17</sup>. Assessing various time points of development for optimal gene knockdown is therefore necessary to determine when phenotypes correlate with the effective concentration, or the lowest concentration of MO that gives maximal gene knockdown.

One of the most renowned pitfalls of morpholinos is their ability to generate off-target effects. When beginning a study with a new MO, a dose curve is generated to determine the effective concentration. With increasing dosage, the severity and type of phenotypes observed is enhanced. The emergence of a phenotype could be due to accurate knockdown of the gene or toxic effects of too high a concentration of MO. Depending on the MO, it is also possible to observe a phenotype because the morpholino is binding to an off target sequence. Proper controls, which will be discussed below, are key in determining the true phenotype of a MO.

As with all experiments, it is necessary to observe repeatable results when using a MO, however this is often challenging. An advantage to zebrafish is the sheer number of embryos one can obtain from a mating pair. These numbers allow for high powered statistics and ease of genetic crossing. This advantage works against researchers in a way when performing genetic manipulation using morpholinos. Statistically, the amount of variation is low within the population, however when observing for phenotypic changes, small changes in morpholino concentration can make a big difference in an individual embryo. The variability largely comes from the nature of the injecting process. MOs are measured for their concentration before injecting to determine the scale of dilutions to be injected for a dose-response curve. Inherently, the concentration of MO at the beginning of injections compared to the end will differ due to clogging of the needle with yolk material and minute changes to the end of the needle that are acquired after repeated injections. This is an intrinsic problem with injections of which the investigator can control by being aware of the common problems associated with injections such as clogging, pressure changes within the apparatus itself and injection room, and needle

breakage. Performing injections with high quality apparatuses that aid in stability and consistency of injections are helpful in decreasing variability and error.

Although MO present with many challenges, it is necessary to recognize that MO can be of great use in studying gene function. The field recognizes that MOs are not perfect, but with appropriate controls, can bypass negative drawbacks to ensure they are accurate and precise<sup>12</sup>.

1. Control morpholinos: It is necessary to ensure the injection process and addition of a synthetic molecule is not causing any toxicity or off target effects. One such control involves rearranging the MO sequence either by random order or inversion to contain the same oligonucleotides, but in a different order to decrease the probability of target site binding. There is controversy over how many nucleotides must be rearranged to prevent targeting. A recent study shows that a 25 oligomer TBMO that differs by four nucleotides has minimal translational effects<sup>7</sup>. In addition, a control MO issued by GeneTools directs against human  $\beta$ -globin pre-mRNA is available as a 'Standard Control' for any morpholino. Rearranged controls offer the most information as these are most similar to the targeted MO and may reveal more specific off-target effects, if present. The type of control is more based on preference; however a type of injected control must be used.
2. Two morpholino rule: Validation that your phenotype is specific to the MO knockdown is a necessity. An easy way to control for this is to inject two or more different, unrelated MOs targeting the same gene and observe the same phenotype in each knockdown. The combination in types of MOs would be up

to the investigator's preferences. SBMOs have a straightforward quantification method and TBMOs target the protein directly suggesting the two types complement each other well. To instill more confidence in the approach, if both MOs are effective and specific, co-injecting diluted forms of both MOs should recapitulate the individual MO phenotype.

3. Mutant vs. morpholino: Similar to the above control, in order to validate a phenotype, comparing to a known control adds significant power to a MO experiment. If a mutant is available comparable to the MO target, precise phenotypic assays should be performed to identify any nonspecific, off-target effects. Several reports boast that the MO used phenocopies the mutant, however positive results are more likely to be published so it is naïve to assume that every MO phenocopies the mutant. Variability is expected in some cases considering MOs are only knocking down a gene whereas a mutant most likely has little to no protein. Studies using a hypomorphic allele are valuable to assess the expected variability of phenotypes as well.
4. Rescue phenotype with mRNA: An additional way to control for off-target effects is to co-inject mRNA of the target gene along with the MO. Observing a full rescue will indicate that supplementing mRNA replaces the MO knockdown of the target gene, while appearance of abnormal phenotypes are indicative of an off-target effect. One caveat to this control is that precise quantification of how much mRNA is necessary to rescue the phenotype is often difficult to measure. Too little mRNA is not sufficient to rescue the knockdown, while overexpression may cause additional phenotypes..

5. p53 rescue: Somewhat related to, but separate from a rescue control, is injection of a p53 MO to justify off-target effects of which are shown to be primarily p53-dependent. The targeting gene, however needs to be independent of p53 activation or this control severely interferes with the true phenotype. Studies show that a common, non-specific effect of MOs is neuronal defects, observed in 15-20% of all MO experiments<sup>36</sup>. Co-injection of a strong p53 MO alleviates off-target phenotypes suggesting use of a p53 MO is useful in deterring p53 independent off-target effects.

## **NUCLEASE EXPLOSION**

Despite the advances in MO's establishing zebrafish as a model system, their transient effect on the genome and list of drawbacks are still not comparable to other mammalian systems in terms of reverse genetic technologies. The boom in development of synthetic nucleases for genomic editing drastically changed the gene manipulation landscape. Zinc Finger Nucleases (ZFNs) are the first of its kind to show targeted mutagenesis in zebrafish. Shortly thereafter, Transcription Activator-Like EndoNucleases (TALENs) enhance the efficiency and targeting range of mutagenesis. Right behind TALENs follows Clustered Regularly Interspaced Short Palindromic Repeats (CRISPRs) showing wider targeting range and desired simplicity. Each technology built on its predecessor formulating the ideal genome editor. The field progresses great lengths in generating multitudes of zebrafish mutants using these techniques; however the systems are not perfect. The following section will discuss these three technologies, how they revolutionized the zebrafish field, as well as advantages and disadvantages to each.

## Zinc Finger Nucleases

Zinc finger domains are highly common structural motifs that most often bind DNA or RNA molecules. For the interest of this article, we will discuss zinc fingers and their association with DNA. They consist of 30 amino acids forming a  $\beta\beta\alpha$  configuration, or zinc finger array. Each zinc finger domain consists of 2-4 zinc finger arrays that bind to its targeted DNA sequence by use of the  $\alpha$ -helix motif which recognizes 3-4bp of nucleotides. The zinc finger motif is found in over 700 proteins in the mammalian system<sup>31</sup>. Considering this, synthetic zinc finger domains are constructed to recognize nearly all sequence combinations and enabling site-directed binding of the zinc finger. In order for the zinc fingers to engage in genome editing, Fok1 endonucleases are fused to each zinc finger array to create a zinc finger nuclease (ZFN). Fok1 is a non-specific nuclease that functions as a dimer to induce a double-stranded break in DNA<sup>21</sup>. Consequently, ZFNs require two zinc finger domains designed for each target site for Fok1 to dimerize and cut. A ZFN is designed for each complementary strand while leaving a designated spacer region (targeting site) between the two ZFNs (Figure 2). Inherent DNA repair pathways are activated in response to the DNA damage. Most often these breaks are repaired by non-homologous end joining (NHEJ) in which the broken ends are ligated without the use of a homologous template strand. NHEJ results in inefficient repair often causing insertions/deletions (indels)<sup>2</sup>. Genome editing nucleases take advantage of improper repair to generate frameshift mutations that often lead to a premature stop codon.



In response to the low success rate, the Zinc Finger Consortium developed a more efficient method of generating ZFNs termed OPEN, (Oligomerized Pool Engineering Nucleases)<sup>23</sup>. By taking into account DNA binding affinities from a set of randomized libraries, OPEN increases the efficiency of targeting to up to 50% at selected sites. By targeting eGFP, they find that 75% of the OPEN ZFNs are able to target compared to the 18% targeting efficiency using the modular assembly approach<sup>14</sup>. The increase in efficiency also increases the amount of time needed to generate one ZFN using the OPEN method<sup>23</sup>. Three weeks at minimum are necessary suggesting that for those in which time is critical, OPEN methodology may be a deterrent.

The final method for zinc finger generation attempts to alleviate the long generation time that the OPEN system presents. CoDA (Context-Dependent Assembly) is similar to the modular assembly in terms of simplicity, however it takes into account zinc finger domains with similar efficiencies to OPEN<sup>37</sup>. It selects N- and C-terminal ZFNs that are optimized with a similar middle ZFN which, theoretically, should improve efficiency. Comparable to CoDA, an optimized two zinc finger method shows to have up to 50% targeting efficiency<sup>15</sup>.

Despite these efforts in optimizing the ZFN technology, none are able to overcome the low efficiency rates adopting labs encountered. In addition, off-target effects plague the ZFN field. Our lab particularly attempted CoDA and OPEN methods. Six genes were targeted for each method of which we were able to obtain one mutant using the OPEN technique, an overall 8% targeting efficiency. Around the same time that groups are optimizing ZFNs, another genome editing nuclease is discovered.



Several methods for generating TALENs are developed in the zebrafish community however; the use of the Golden Gate cloning system is advantageous in fusing each RVD repeat using a library of plasmids<sup>4</sup>. This method is validated in zebrafish and the method of choice for our lab. It takes approximately two weeks for a readily-injectable TALEN to be generated, a time rather attractive when compared to ZFNs. Our lab is able to target genes of interest with 64% efficiency, a significant increase over our ZFN efficiency.

TALENs become the go-to method for genome editing when targeting efficiencies are boosted to 70-100% in several studies. Targeting is detected as early as the 256-cell stage, approximately 2.5 hours post fertilization (hpf). A variety of indels are published, deletions spanning from  $\Delta 2$  to  $\Delta 20$  and insertions ranging from +1 to +13<sup>8</sup>. Our lab has similar results in generating a number of frameshift mutations. This efficiency correlates to an increase in dose of TALEN mRNA, however like MOs, this must be balanced with toxicity and off-target effects. One study did look at the toxicity of TALENs in HEK293 cell lines in which TALENs are significantly less toxic than ZFNs<sup>27</sup>. One indirect way to determine off-target effects is to compare to a well-established MO study. Overall, TALENs make their mark in genome editing, but the popularity of zebrafish combined with exciting genome editing technology spurs more advancement that follows closely on their TALE (tail).

### **Clustered Regularly Interspaced Short Palindromic Repeats (CRISPR)**

Barely a year passes after TALENs are on the market before a new RNA-based genome editing system is available for use. This time the science behind the technology



**Figure 4. Schematic of CRISPR/Cas9 system.** Target sequence is labeled in purple for which the guide RNA is designed for (red and green). The red sequence is the crRNA while the green sequence depicts the tracrRNA. Both are fused together by a 4bp linker to create the gRNA. PAM sequence (yellow box) is required for targeting and determines where the Cas9 endonuclease (cutout circles) cleaves, 4-7 bp away from the PAM sequence.

Though CRISPRs are the youngest of the editing technologies, studies show that they are as effective as TALENs with moderate cutting efficiency. One study boasts 9/11 sites are targeted<sup>18</sup>. Our lab has tremendous success with CRISPRs allowing for 75% targeting efficiency. In addition, four genes that are not targeted by TALENs are found to be effective in generating knockouts on the first round of generation.

Ease is a key characteristic when speaking of CRISPRs. As opposed to the DNA-protein targeting concepts used by ZFNs and TALENs which require two of each for effective targeting; the RNA-DNA based method requires just one RNA molecule for specific targeting and a universal Cas9 mRNA. This immediately makes CRISPRs attractive especially when the procedure only requires cloning in two overlapping oligonucleotides into a guide vector. This is ideal when a lab is in need of generating numerous mutant lines. Also, oligonucleotides are easily designed and ordered compared to the cumbersome libraries necessary for TALEN and ZFN generation. Due to the small nature of CRISPRs, a great advantage over TALENs and ZFNs is the capability of multiplex genome editing, or injection of multiple CRISPRs, at one time<sup>3</sup>. A downfall to CRISPR design is that only 8-12 bp of the CRISPR sequence and the PAM sequence are

required for targeting thus decreasing the efficiency in binding and increasing the probability of off-target effects<sup>24</sup>. One study looks at off-target effects using next generation sequencing and surprisingly find the amount of off-target effects are around 2.2-2.5%; relatively low numbers when compared to ZFNs and on par with TALENs<sup>18</sup>. Further studies need to be performed to determine the full range of off target effects that CRISPRs elicit and how they can be controlled for.

## **DETECTION**

Genome editing techniques are highly dependent on the ability to detect the mutations they induce. The classical method for detection across all three nucleases is to use the Restriction Fragment Length Polymorphism (RFLP) technique. First, primers are designed to flank the target site to amplify by PCR. The PCR product is digested with an appropriate restriction enzyme to determine if the target site is disrupted by nuclease cutting. This is confirmed by observing an additional or absent band when run on an agarose gel. Those found to be positive for site disruption are then cloned into a vector, purified, and sequenced. This method is reliable though very inefficient and costly particularly when a large amount of embryos need to be sequenced. As well, this method limits the number of sites of interest for targeting as a restriction site must be contained within the target site.

An alternative strategy for detection that works well in high-throughput mutation screening, particularly in zebrafish, is a PCR-based method using High Resolution Melt Analysis (HRMA)<sup>32</sup>. At the end of each PCR cycle, the amplicons are heat denatured and then rapidly cooled to 4°C. If a population contains a mutant allele, a heteroduplex will

form between the two DNA products while a homogeneous population will result in a homoduplex. Heteroduplexes are inherently unstable and result in a reduced melting temperature compared to the population with no mutant allele. The melting temperature of each product is determined through use of a fluorescent dye, such as LC Green, which binds to DNA during the amplification process and is detected using a fluorescence-based machine such as the LightScanner.

Post-amplification, the LightScanner machine will gradually heat each PCR product while monitoring the fluorescence that is emitted. The peak fluorescence intensity correlates to the melting temperature of each PCR product. In the case of a wild-type or homozygous mutant product, one peak is observed. In the presence of a mixed allelic population, two peaks are observed, one representing the heteroduplex and one representing the homoduplex. Since generating a biallelic mutant embryo is rare after the initial injections, heteroduplexes are the expected outcome at the G0 stage. Overall, this technology is sensitive enough to detect a variety of mutations including deletions, insertions, and SNPs (Single Nucleotide Polymorphisms) based on an amplified PCR product's melting temperature (Figure 5 D, B, F, & H).

HRMA is popular in zebrafish due to the large number of embryos that can be genotyped. Each LightScanner run is able to screen 96 individual PCR products from 96 individual embryos in a matter of minutes. This method bypasses the use of agarose gels and costly restriction enzymes. Once a positive peak is identified, each PCR product is purified and sent to sequencing. Using this method, our lab is able to detect as small as a SNP (T→C) transition up to a  $\Delta 25$  deletion. Through use of the above nuclease techniques, we have effectively identified over 50 mutants using HRMA.

Use of this technique also aids in establishing genotype-phenotype correlations as early as the G0 stage of mutant generation<sup>39</sup>. Using CRISPR/Cas9 targeting the *Esco2* gene in zebrafish, two G0  $\Delta 7$  alleles are generated and raised to adults ( $\Delta 7^1$  and  $\Delta 7^2$ , from G0#9 and G0#10, respectively). A documented *Esco2* retroviral insertion mutant zebrafish (hi2865) serves as a positive control<sup>33</sup>. The hi2865 mutant has a head necrotic phenotype occurring at Mendelian genetic ratios. By intercrossing the G0  $\Delta 7$  alleles with the hi2865 heterozygous and against each other, we are able to determine a genotype-phenotype correlation at the G0 stage based off of the known head necrotic phenotype (Figure 5). In addition to establishing a genotype-phenotype correlation, this type of analysis also determines the level of chimerism of the G0. Figure E & F for G0#9 and Figure G & H for G0 #10 demonstrate this feature. The 4% mutant frequency in G0#9 cross to hi2865 suggests this is a low chimeric allele compared to the 19% mutant frequency in G0#10. The near Mendelian 25% mutant frequency of G0#10 suggests this is a high chimeric allele. This phenotypic analysis was originally published in *PLoS One* (Thomas, H.R., Percival, S.M., Yoder, B.K., Parant, J.M. High throughput genome editing and phenotyping facilitated by High Resolution Melting curve analysis. *PLoS One* 2014 10(2): e0117764. PMID: PMC4263700).

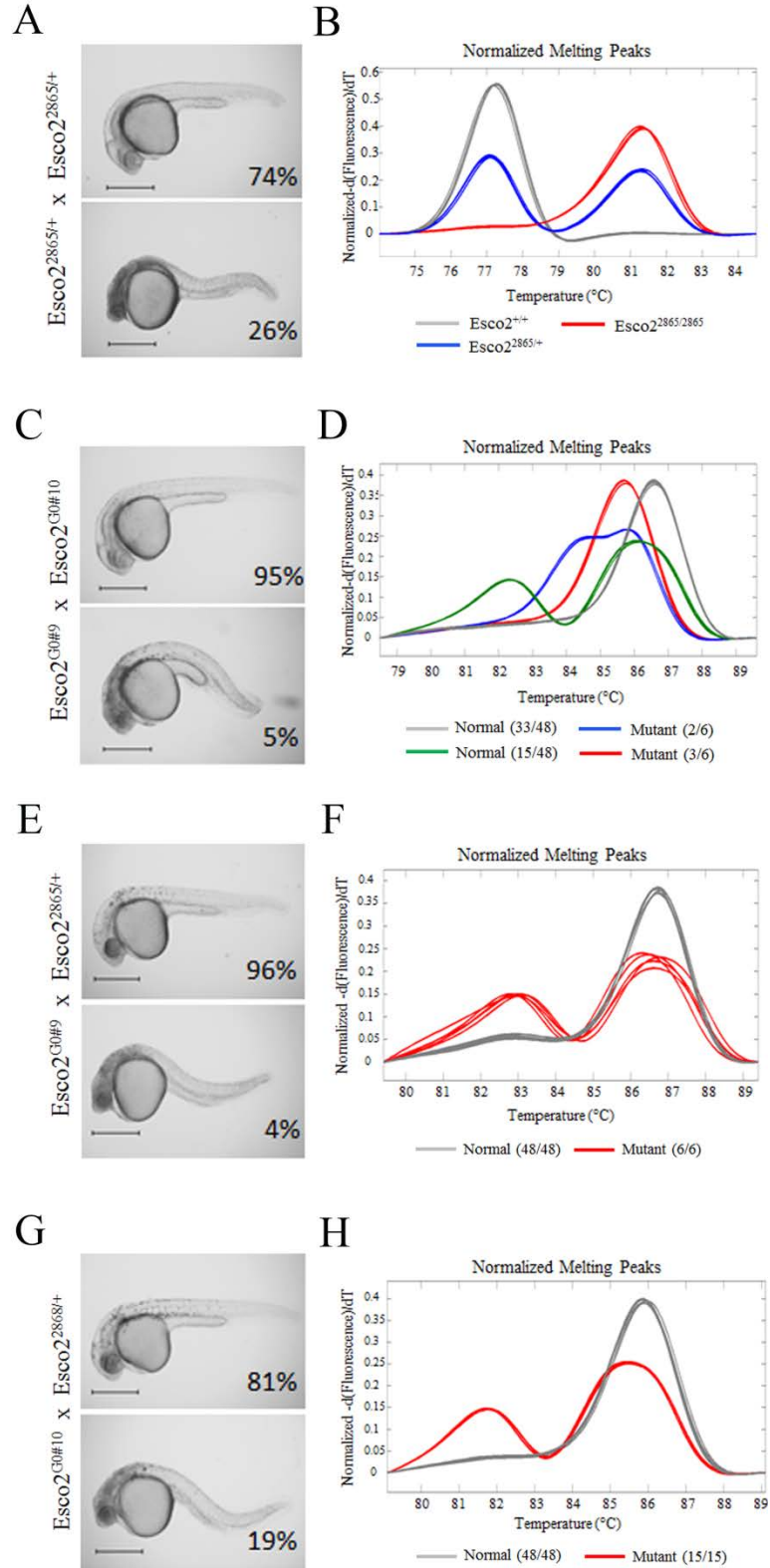


**Figure 5: HRM established genotype-phenotype correlation within Esco2 mutant embryos from a G0 intercross.** (A) Wild-type and mutant phenotypes with Mendelian frequencies in embryos derived from heterozygous intercross of the Esco2 retroviral insertion mutant hi2865. Note the head necrosis in the mutant embryos. (B) HRM genotyping of wild-type (grey and blue curves) and mutant (red curves) embryos display perfect genotype-phenotype correlation. (C) Wild-type and mutant phenotypes in embryos derived from intercross of G0 Esco2 CRISPR injected fish. Note the head necrosis in mutant embryos. (D) Select HRM curves of 6 mutant and 6 wild-type embryos that were subsequently sequenced to reveal specific alleles result in specific curves. All wild-type animals (beyond the 6 displayed here) make up the green and grey curves; while 5 of 6 mutant animals make up the unique red and blue curves establishing a genotype-phenotype correlation. (E&G) are wild-type and mutant phenotypes and frequencies of G0#9 (E) or G0#10 (G) crossed to Esco2 hi2865 heterozygous animals. (F&H) are HRM curves of mutant and wild-type embryos (from E&G) that are Esco2 hi2865 heterozygous. All heterozygous curves (red) are mutants, and all grey curves are normal, phenotypically.

## **FUTURE DIRECTIONS FOR GENOME EDITING**

As stated above, the field is progressing quickly. One avenue that is being explored is using genome editing for inducing specific mutations with a single-stranded donor oligonucleotide in conjunction with a CRISPR/TALEN/ZFN for homology-directed repair (HDR)<sup>1</sup>. Each donor oligonucleotide will contain homologous regions that span the target site for direct binding as well as the specific mutation that is desired

to act as a template for homologous recombination. This technique could be highly desired for those wanting to develop a model to study a particular human disease. As well, it will be useful for those in which particular mutations are necessary or for those wanting to modify certain amino acids. Initial attempts at HDR are successful, however is very inefficient. In one particular study, positive embryos for the mutation of interest (an EcoRV site) range in efficacy from 7% to 28%. In order to improve this efficiency, it is recently shown that using a nickase, which creates single-stranded break, is preferred for HDR compared to double-strand breaks induced by nucleases<sup>34</sup>. A clear next step in genome editing, once HDR is optimized, is the incorporation of loxP sites for creation of conditional alleles. The same study that first shows effective HDR demonstrates incorporation of a mloxP site, however at even lower efficiencies than the small sequence HDR. Overall, the future looks bright for genome editing technologies in the zebrafish field as long as detection methods remain efficient, costs remain low, and precise gene targeting is optimized.

## REFERENCES

- 1 V. M. Bedell, Y. Wang, J. M. Campbell, T. L. Poshusta, C. G. Starker, R. G. Krug, 2nd, W. Tan, S. G. Penheiter, A. C. Ma, A. Y. Leung, S. C. Fahrenkrug, D. F. Carlson, D. F. Voytas, K. J. Clark, J. J. Essner, and S. C. Ekker, 'In Vivo Genome Editing Using a High-Efficiency Talen System', *Nature*, 491 (2012), 114-8.
- 2 M. Bibikova, M. Golic, K. G. Golic, and D. Carroll, 'Targeted Chromosomal Cleavage and Mutagenesis in *Drosophila* Using Zinc-Finger Nucleases', *Genetics*, 161 (2002), 1169-75.
- 3 P. R. Blackburn, J. M. Campbell, K. J. Clark, and S. C. Ekker, 'The Crispr System--Keeping Zebrafish Gene Targeting Fresh', *Zebrafish*, 10 (2013), 116-8.
- 4 T. Cermak, E. L. Doyle, M. Christian, L. Wang, Y. Zhang, C. Schmidt, J. A. Baller, N. V. Somia, A. J. Bogdanove, and D. F. Voytas, 'Efficient Design and Assembly of Custom Talen and Other Tal Effector-Based Constructs for DNA Targeting', *Nucleic Acids Res*, 39 (2011), e82.

- 5 C. Collart, K. Verschuere, A. Rana, J. C. Smith, and D. Huylebroeck, 'The Novel Smad-Interacting Protein Smicl Regulates Chordin Expression in the *Xenopus* Embryo', *Development*, 132 (2005), 4575-86.
- 6 S. A. Coonrod, L. C. Bolling, P. W. Wright, P. E. Visconti, and J. C. Herr, 'A Morpholino Phenocopy of the Mouse *Mos* Mutation', *Genesis*, 30 (2001), 198-200.
- 7 R. A. Cornell, and J. S. Eisen, 'Delta Signaling Mediates Segregation of Neural Crest and Spinal Sensory Neurons from Zebrafish Lateral Neural Plate', *Development*, 127 (2000), 2873-82.
- 8 T. J. Dahlem, K. Hoshijima, M. J. Jurynek, D. Gunther, C. G. Starker, A. S. Locke, A. M. Weis, D. F. Voytas, and D. J. Grunwald, 'Simple Methods for Generating and Detecting Locus-Specific Mutations Induced with Talens in the Zebrafish Genome', *PLoS Genet*, 8 (2012), e1002861.
- 9 G. De Rienzo, J. H. Gutzman, and H. Sive, 'Efficient Shrna-Mediated Inhibition of Gene Expression in Zebrafish', *Zebrafish*, 9 (2012), 97-107.
- 10 E. Deltcheva, K. Chylinski, C. M. Sharma, K. Gonzales, Y. Chao, Z. A. Pirzada, M. R. Eckert, J. Vogel, and E. Charpentier, 'Crispr Rna Maturation by Trans-Encoded Small Rna and Host Factor Rnase Iii', *Nature*, 471 (2011), 602-7.
- 11 B. W. Draper, P. A. Morcos, and C. B. Kimmel, 'Inhibition of Zebrafish *Fgf8* Pre-Mrna Splicing with Morpholino Oligos: A Quantifiable Method for Gene Knockdown', *Genesis*, 30 (2001), 154-6.
- 12 J. S. Eisen, and J. C. Smith, 'Controlling Morpholino Experiments: Don't Stop Making Antisense', *Development*, 135 (2008), 1735-43.
- 13 S. C. Ekker, and J. D. Larson, 'Morphant Technology in Model Developmental Systems', *Genesis*, 30 (2001), 89-93.
- 14 J. E. Foley, J. R. Yeh, M. L. Maeder, D. Reyon, J. D. Sander, R. T. Peterson, and J. K. Joung, 'Rapid Mutation of Endogenous Zebrafish Genes Using Zinc Finger Nucleases Made by Oligomerized Pool Engineering (Open)', *PLoS One*, 4 (2009), e4348.
- 15 A. Gupta, R. G. Christensen, A. L. Rayla, A. Lakshmanan, G. D. Stormo, and S. A. Wolfe, 'An Optimized Two-Finger Archive for Zfn-Mediated Gene Targeting', *Nat Methods*, 9 (2012), 588-90.
- 16 R. Harland, and H. Weintraub, 'Translation of Mrna Injected into *Xenopus* Oocytes Is Specifically Inhibited by Antisense Rna', *J Cell Biol*, 101 (1985), 1094-9.
- 17 J. Heasman, 'Morpholino Oligos: Making Sense of Antisense?', *Dev Biol*, 243 (2002), 209-14.
- 18 A. Hruscha, P. Krawitz, A. Rechenberg, V. Heinrich, J. Hecht, C. Haass, and B. Schmid, 'Efficient Crispr/Cas9 Genome Editing with Low Off-Target Effects in Zebrafish', *Development*, 140 (2013), 4982-7.
- 19 M. Jinek, K. Chylinski, I. Fonfara, M. Hauer, J. A. Doudna, and E. Charpentier, 'A Programmable Dual-Rna-Guided DNA Endonuclease in Adaptive Bacterial Immunity', *Science*, 337 (2012), 816-21.
- 20 H. J. Kim, H. J. Lee, H. Kim, S. W. Cho, and J. S. Kim, 'Targeted Genome Editing in Human Cells with Zinc Finger Nucleases Constructed Via Modular Assembly', *Genome Res*, 19 (2009), 1279-88.

- 21 Y. G. Kim, J. Cha, and S. Chandrasegaran, 'Hybrid Restriction Enzymes: Zinc Finger Fusions to Fok I Cleavage Domain', *Proc Natl Acad Sci U S A*, 93 (1996), 1156-60.
- 22 R. Kos, M. V. Reedy, R. L. Johnson, and C. A. Erickson, 'The Winged-Helix Transcription Factor Foxd3 Is Important for Establishing the Neural Crest Lineage and Repressing Melanogenesis in Avian Embryos', *Development*, 128 (2001), 1467-79.
- 23 M. L. Maeder, S. Thibodeau-Beganny, A. Osiaik, D. A. Wright, R. M. Anthony, M. Eichinger, T. Jiang, J. E. Foley, R. J. Winfrey, J. A. Townsend, E. Unger-Wallace, J. D. Sander, F. Muller-Lerch, F. Fu, J. Pearlberg, C. Gobel, J. P. Dassie, S. M. Pruett-Miller, M. H. Porteus, D. C. Sgroi, A. J. Iafrate, D. Dobbs, P. B. McCray, Jr., T. Cathomen, D. F. Voytas, and J. K. Joung, 'Rapid "Open-Source" Engineering of Customized Zinc-Finger Nucleases for Highly Efficient Gene Modification', *Mol Cell*, 31 (2008), 294-301.
- 24 P. Mali, L. Yang, K. M. Esvelt, J. Aach, M. Guell, J. E. DiCarlo, J. E. Norville, and G. M. Church, 'Rna-Guided Human Genome Engineering Via Cas9', *Science*, 339 (2013), 823-6.
- 25 D. A. Melton, 'Injected Anti-Sense Rnas Specifically Block Messenger Rna Translation in Vivo', *Proc Natl Acad Sci U S A*, 82 (1985), 144-8.
- 26 M. J. Moscou, and A. J. Bogdanove, 'A Simple Cipher Governs DNA Recognition by Tal Effectors', *Science*, 326 (2009), 1501.
- 27 C. Mussolino, R. Morbitzer, F. Lutge, N. Dannemann, T. Lahaye, and T. Cathomen, 'A Novel Tale Nuclease Scaffold Enables High Genome Editing Activity in Combination with Low Toxicity', *Nucleic Acids Res*, 39 (2011), 9283-93.
- 28 A. Nasevicius, and S. C. Ekker, 'Effective Targeted Gene 'Knockdown' in Zebrafish', *Nat Genet*, 26 (2000), 216-20.
- 29 S. L. Nutt, O. J. Bronchain, K. O. Hartley, and E. Amaya, 'Comparison of Morpholino Based Translational Inhibition During the Development of *Xenopus Laevis* and *Xenopus Tropicalis*', *Genesis*, 30 (2001), 110-3.
- 30 A. C. Oates, A. E. Bruce, and R. K. Ho, 'Too Much Interference: Injection of Double-Stranded Rna Has Nonspecific Effects in the Zebrafish Embryo', *Dev Biol*, 224 (2000), 20-8.
- 31 C. O. Pabo, E. Peisach, and R. A. Grant, 'Design and Selection of Novel Cys2his2 Zinc Finger Proteins', *Annu Rev Biochem*, 70 (2001), 313-40.
- 32 J. M. Parant, S. A. George, R. Pryor, C. T. Wittwer, and H. J. Yost, 'A Rapid and Efficient Method of Genotyping Zebrafish Mutants', *Dev Dyn*, 238 (2009), 3168-74.
- 33 S. M. Percival, H. R. Thomas, A. Amsterdam, A. J. Carroll, J. A. Lees, H. J. Yost, and J. M. Parant, 'Variations in Dysfunction of Sister Chromatid Cohesion in *Esco2* Mutant Zebrafish Reflect the Phenotypic Diversity of Roberts Syndrome', *Dis Model Mech*, 8 (2015), 941-55.
- 34 C. L. Ramirez, M. T. Certo, C. Mussolino, M. J. Goodwin, T. J. Cradick, A. P. McCaffrey, T. Cathomen, A. M. Scharenberg, and J. K. Joung, 'Engineered Zinc Finger Nickases Induce Homology-Directed Repair with Reduced Mutagenic Effects', *Nucleic Acids Res*, 40 (2012), 5560-8.

- 35 C. L. Ramirez, J. E. Foley, D. A. Wright, F. Muller-Lerch, S. H. Rahman, T. I. Cornu, R. J. Winfrey, J. D. Sander, F. Fu, J. A. Townsend, T. Cathomen, D. F. Voytas, and J. K. Joung, 'Unexpected Failure Rates for Modular Assembly of Engineered Zinc Fingers', *Nat Methods*, 5 (2008), 374-5.
- 36 M. E. Robu, J. D. Larson, A. Nasevicius, S. Beiraghi, C. Brenner, S. A. Farber, and S. C. Ekker, 'P53 Activation by Knockdown Technologies', *PLoS Genet*, 3 (2007), e78.
- 37 J. D. Sander, E. J. Dahlborg, M. J. Goodwin, L. Cade, F. Zhang, D. Cifuentes, S. J. Curtin, J. S. Blackburn, S. Thibodeau-Beganny, Y. Qi, C. J. Pierick, E. Hoffman, M. L. Maeder, C. Khayter, D. Reyon, D. Dobbs, D. M. Langenau, R. M. Stupar, A. J. Giraldez, D. F. Voytas, R. T. Peterson, J. R. Yeh, and J. K. Joung, 'Selection-Free Zinc-Finger-Nuclease Engineering by Context-Dependent Assembly (Coda)', *Nat Methods*, 8 (2011), 67-9.
- 38 J. Summerton, 'Morpholino Antisense Oligomers: The Case for an Rnase H-Independent Structural Type', *Biochim Biophys Acta*, 1489 (1999), 141-58.
- 39 H. R. Thomas, S. M. Percival, B. K. Yoder, and J. M. Parant, 'High-Throughput Genome Editing and Phenotyping Facilitated by High Resolution Melting Curve Analysis', *PLoS One*, 9 (2014), e114632.
- 40 B. Wiedenheft, S. H. Sternberg, and J. A. Doudna, 'Rna-Guided Genetic Silencing Systems in Bacteria and Archaea', *Nature*, 482 (2012), 331-8.

THE EXTENT OF COHESION DYSFUNCTION CONTRIBUTES TO  
COHESINOPATHY PATHOGENESIS AND CORRELATES WITH PHENOTYPIC  
SEVERITY

by

STEFANIE M. PERCIVAL, HOLLY THOMAS, AND JOHN M. PARANT

*In preparation to PLoS Genetics*

Formatted for Dissertation

## **ABSTRACT**

Sister chromatid cohesion (SCC) functions in chromosome segregation where by a proteinaceous ring, cohesin, encircles newly replicated DNA to ensure proper sister chromatid pairing that is essential for genomic stability. A critical step in SCC is cohesion establishment where the cohesin ring is stabilized around the newly synthesized sister chromatid. ESCO1 and ESCO2 are acetyltransferases which provide cohesion establishment through acetylation of the cohesin ring. SORORIN and SHUGOSHINL1 (SGOL1) are maintenance factors that ensure cohesion establishment is maintained through the remainder G2 and M phase of the cell cycle. Defects in these genes are cell lethal in cultured cells. Interestingly, mutations in some components of the SCC process result in a number of developmental disorders, together called cohesinopathies, while others do not. To better understand the pathogenesis of these disorders and the impact SCC dysregulation has on development, we generated zebrafish mutant models of cohesion establishment (Esco1, ShugoshinL1, and Sororin). We show that despite all of the genes having a role in cohesion establishment, a spectrum of phenotypes is observed. Unexpectedly, we find a strong correlation to the severity of the gross morphology phenotype and the severity of the cohesion defects for each mutant. Further, the extent of mitotic defects and apoptotic responses also correlates with the extent of cohesion dysfunction. This implies that defects in cohesion establishment are not binary in describing lethality and viability, but result in a range of cohesion defects that correspondingly direct the extent of gross morphology phenotypes and may explain variable phenotypes within cohesinopathies.

## INTRODUCTION

One of the vital processes in maintaining genomic instability is sister chromatid cohesion (SCC), where a proteinaceous ring complex composed of SMC1, SMC3, RAD21, and STAG1/STAG2 encircles two chromatin strands for proper segregation in mitosis (Guacci et al., 1997; Michaelis et al., 1997; Toth et al., 1999). The canonical role of SCC is in chromosome segregation while other known roles are in DNA damage and regulating gene expression; although the latter is actually intra-chromosomal cohesion (Dorsett, 2011; Mehta et al., 2013; Peters, 2012). Proper sister chromatid segregation is ensured through several crucial steps throughout the cell cycle. Thousands of cohesin rings dynamically load onto chromatin in G1 (Ciosk et al., 2000; Gerlich et al., 2006; Tonkin et al., 2004; Watrin & Peters, 2009). Upon entrance into S phase, an essential step called sister chromatid cohesion establishment occurs which, in sync with DNA replication, stabilizes the cohesin ring around newly synthesized sister chromatids to ensure pairing until proper microtubule attachment in mitosis (Maradeo & Skibbens, 2009; Parnas et al., 2009; Samora et al., 2016). Cohesion establishment occurs through acetyltransferases, ESCO1 and ESCO2 (Eco1 in yeast), which convert unstable ‘cohesin’ to ‘cohesion’ by acetylation of two key Lysine residues (K105 and K106) of the SMC3 portion of the ring (Hou & Zou, 2005; Rolef Ben-Shahar et al., 2008; Skibbens et al., 1999; Tanaka et al., 2001; Unal et al., 2008; J. Zhang et al., 2008). Cell culture studies show that ESCO1 and ESCO2 are non-redundant and essential in cell and organismal viability (Hou & Zou, 2005; Skibbens et al., 1999; Whelan et al., 2012). Recently, our lab finds that loss of *Esco2* in zebrafish leads to near complete loss of cohesion which calls into question the importance of *Esco1* *in vivo* (Percival et al., 2015).

Following cohesion establishment, maintenance factors safeguard cohesion establishment until segregation in mitosis. One of these maintenance factors is Sororin (CDCA5 in vertebrates) whose recruitment is initiated by acetylation of SMC3 and requires PDS5 (Rankin et al., 2005; Zu et al., 2013). In the absence of Sororin, WAPL and PDS5 are able to prematurely remove cohesion via direct interactions leading to precocious sister chromatid separation (Nishiyama et al., 2010). Sororin is embryonic lethal in mice but cultured cell studies determine that Sororin is critical in cell proliferation and cohesion (Ladurner et al., 2016). Upon entrance into mitosis, another maintenance factor, ShugoshinL1 (SGOL1), is engaged for protecting centromeric cohesion (Kerrebrock et al., 1995; Liu et al., 2015; Tang et al., 2004). SgoL1 is also lethal in mouse models but heterozygous mice show cohesion defects and have an enhanced tumor onset in a predisposed model (Yamada et al., 2012). Removal of the cohesin rings around chromosome arms occurs due to actions by WAPL-PDS5 (Dreier et al., 2011; Nishiyama et al., 2010; N. Zhang et al., 2011). Once proper microtubule attachment at kinetochores occurs, the remaining centromeric rings are cleaved by Separase, a cysteine protease that cuts the RAD21 portion of the cohesin ring (Hauf et al., 2001; Nakajima et al., 2007; Uhlmann et al., 1999; Wirth et al., 2006). This highly regulated removal process ensures the two new cells receive equal distribution of genomic material.

Though the essential nature of SCC is well known, it is intriguing to find that mutations in this pathway result in a spectrum of developmental disorders called cohesinopathies. Cornelia de Lange syndrome (CdLS) is caused by mutations in SMC1a, SMC3, NIPBL, RAD21, and HDAC8 (Deardorff et al., 2012; Deardorff et al., 2007;

Krantz et al., 2004; Musio et al., 2006; Tonkin et al., 2004); Chronic atrial and intestinal dysrhythmia syndrome (CAIDS) is caused by mutations in SGOL1 (Chetaille et al., 2014); Warsaw Breakage syndrome (WBS) is caused by mutations in DDX11 (van der Lelij et al., 2010); and Roberts syndrome (RBS) is caused by mutations in ESCO2 (Vega et al., 2005). Despite many of these disorders being classified as multi-system developmental disorders, there is a wide spectrum of defects associated between them. CdLS, RBS, and WBS share similar multi-organ system phenotypes such as limb, craniofacial, and mental defects while CAIDS patients exhibit gut and heart defects. At the cytogenetic level, CAIDS, WBS, and RBS show heterochromatic repulsion (HR) a centromeric separation in metaphase spread analysis. CdLS patients do not show this defect, but are only heterozygous for these mutations. A spectrum of defects is even found within a single cohesinopathy such as RBS. Though no genotype-phenotype correlation is established, phenotypic severity varies from embryonic lethal to adult viability with minor developmental defects in RBS patients (Schule et al., 2005; Vega et al., 2010). The cause behind these variable phenotypes is unclear. Though the majority of cohesinopathies have defects in cohesion, no disease phenotype has been associated with the establishment/maintenance factors, Escol or Sororin, questioning their important in SCC or *in vivo* disease pathogenesis.

In attempts to investigate the role of Escol, SgoL1, and Sororin in SCC and disease, we use CRISPR/Cas9 to generate several mutants in cohesion establishment and maintenance. We find that the cohesion establishment mutants exhibit a spectrum of gross morphology defects despite their involvement in the essential cohesion establishment process. Interestingly, the severity of embryonic phenotype correlates to an

equal severity in cohesion defects. These phenotypic differences are due to the range of mitotic defects following cohesion defects, observed through *in vivo* imaging, that lead to the extent of apoptotic response. This provides the first evidence that variations in cohesion defects contribute to the variable phenotypes observed within cohesinopathies and within individual disorders such as Roberts syndrome.

## RESULTS

### Generation of SCC zebrafish mutants using CRISPR/Cas9.

As with previous gene targeting (Percival et al., 2015; Thomas et al., 2014), we designed target specific guides for the CRISPR/Cas9 custom nuclease system to target *Esco1*, *Sororin*, and *SgoL1* genes in zebrafish and generate frame shift inactivation mutations. Figure 1A depicts: 1) the details of the CRISPR design, including the guide sequence and PAM sequence which is necessary for guide recognition and cleavage and 2) the germ line transmitted alleles identified and selected for this study. For conciseness, we will refer to these three mutants as the cohesion establishment mutants from this point on. Each guide sequence is designed to target the most proximal exon to the transcriptional start site (ATG). In the case of *Esco1* and *SgoL1*, the exon immediately following the ATG- containing exon is successfully targeted (Fig 1B & C). *Sororin*'s lack of ideal target sites and guide sequences near the ATG led to exon 4 targeting (Fig D). G0 fish containing the frameshift alleles are bred out to wild type (AB) fish to generate stable F1 lineages. *Esco1* targeting results in an indel composed of a 10 bp (base pair) deletion and an insertion of 6 bp in exon 2 (Fig1 B). *SgoL1* targeting leads to an 8 bp deletion in

exon 2 (Fig 1C). Sororin targeting leads to a 20 bp deletion in exon 4 of the gene (Fig 1D). Each of these mutants generates a frameshift mutation leading to a premature stop codon predicted to lead to nonsense mediated decay. CRISPR/Cas9 therefore proves very effective in generating cohesion establishment mutants for further analysis.

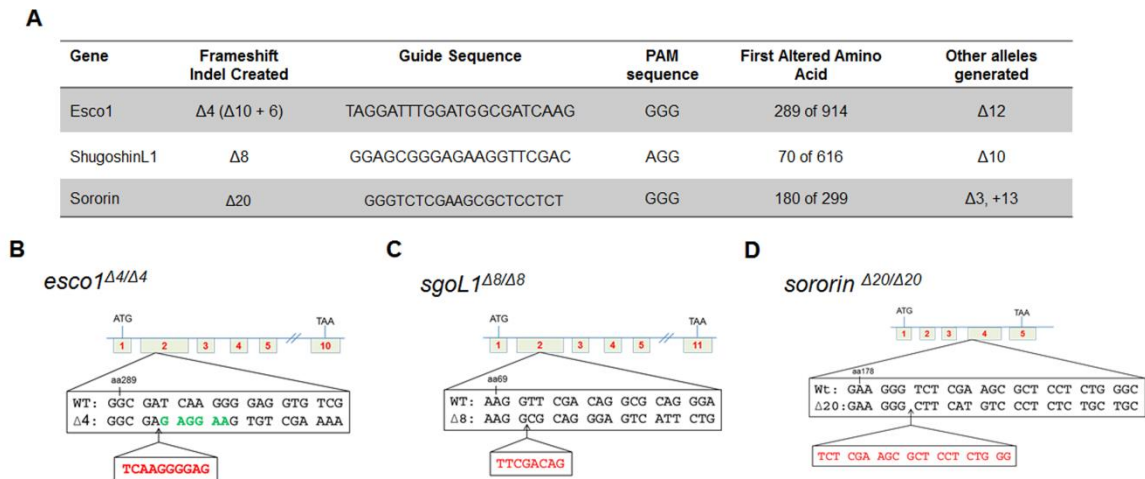


**Figure 1: Cohesion Establishment Mutant Generation using CRISPR/Cas9.** A)

CRISPR details on the guide sequence used to generate each of the mutants, PAM sequence, location of the first altered amino acid that results from the frameshift

deletions, and other alleles generated using these guide sequences. B) Mutant allele

diagram generated by targeting exon 2 of Esco1. Green letters indicate inserted nucleotides while red letters indicate deleted nucleotides. ATG, poly(A) tail, and

reference amino acid are shown. C) Mutant allele diagram generated by targeting exon 2

of SgoL1. Red letters indicate deleted nucleotides. ATG, poly(A) tail, and reference

amino acid are shown. D) Mutant allele diagram generated by targeting exon 4 of

Sororin. Red letters indicate deleted nucleotides. ATG, poly(A) tail, and reference amino

acid are shown.

## **Spectrum of gross morphology phenotypes in cohesion establishment mutants.**

Once stable generations of each cohesion establishment mutant are created, we next wanted to identify any gross morphology defects associated with mutations in each of these genes. Time lapse imaging at 24, 72, and 120 hours post fertilization (hpf) is performed to assess gross morphology differences. To serve as a reference, we also image our characterized *esco2*<sup>hi2865/hi2865</sup> mutant (hereafter referred to as *esco2*<sup>m/m</sup>) (Percival et al., 2015). No gross morphology defects are observed at the embryonic stages in *esco1* mutants (Fig 2A). This finding is surprising in that cellular analysis of ESCO1 in other systems is lethal (Bellows et al., 2003; Hou & Zou, 2005; Minamino et al., 2015). *SgoL1* mutants show no morphology defects at 24 hpf, however mild pericardial edema and growth retardation is observed at 72 and 120 hpf. DIC images highlight the lack of jaw formation, smaller eye, and heart edema present compared to wild type controls (Fig 2B). The lack of swim bladder at 120 hpf indicates this mutant is late embryonic lethal and will not survive to the larval stage (Fig 2C). Interestingly, CAIDS patients primarily exhibit heart defects and often need pacemakers implanted at an early age (Chetaille et al., 2014). These cardiac phenotypes suggest that our *sgoL1* mutant may model CAIDS. *Sororin* mutants show the most severe phenotype with moderate darkening in the head and pharyngeal arches at 24 hpf which is indicative of neural apoptosis. This phenotype manifests into more severe phenotypes such as severe, systemic edema and growth retardation at later time points (Fig 2A). The head darkening is similar to that detected in *esco2* mutant zebrafish suggesting that Sororin and Esco2 have similar roles in cohesion establishment (Fig 2A) (Percival et al., 2015). So far we can conclude that while SgoL1

and Sororin are critical in cohesion establishment, Esco1 is not essential for vertebrate development.

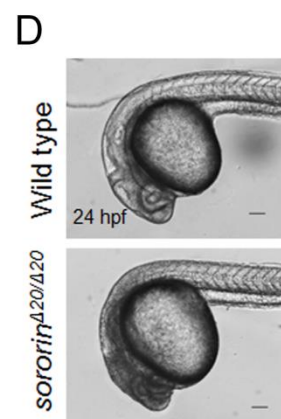
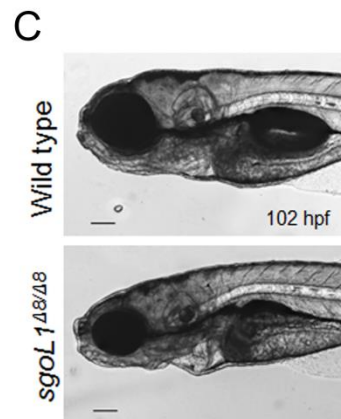
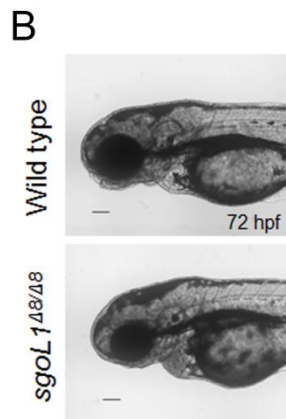
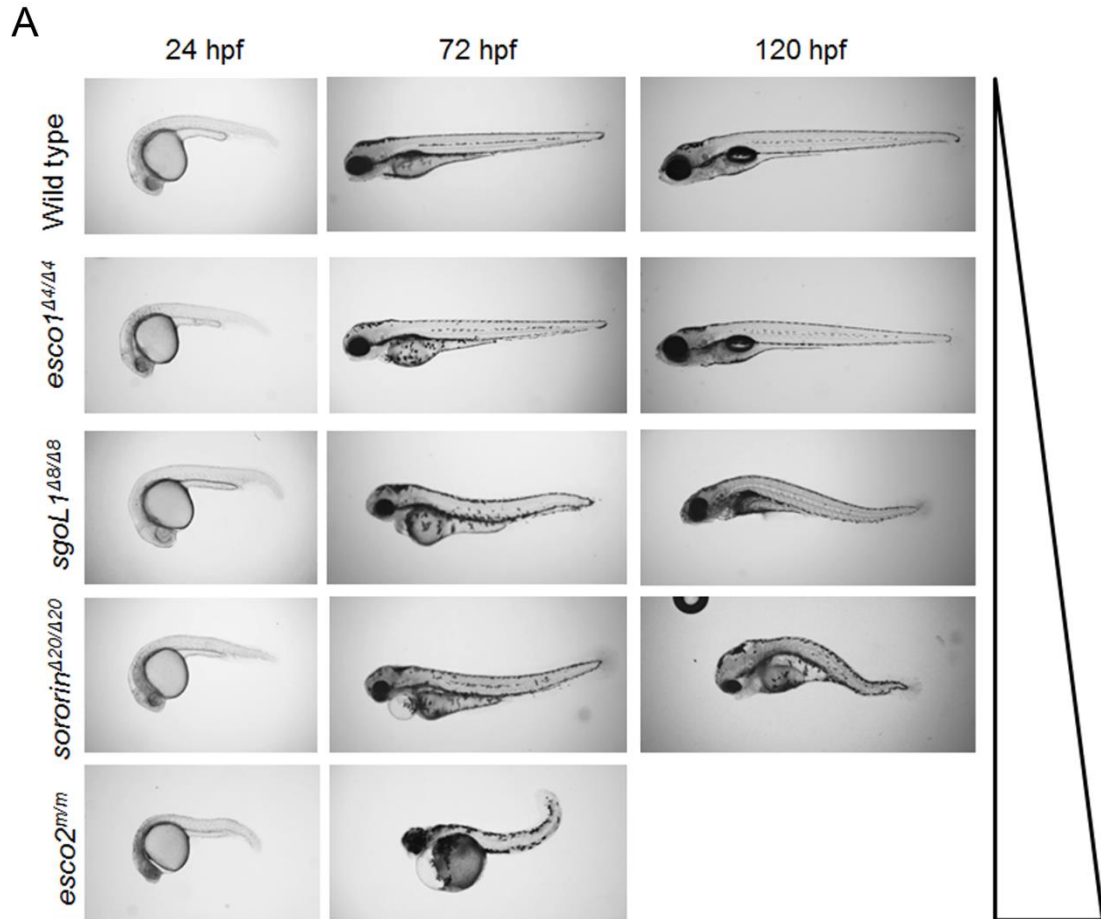


**Figure 2: Cohesion establishment mutants display variable morphology defects.**

Cohesion mutant gross morphology indicated at 24, 72, and 120 hpf (1, 3, and 5 days post fertilization, respectively). B) 5x zoom DIC imaging of cardiac, eye, and craniofacial defects observed in *sgoL1* mutants at 72 hpf versus wild type controls. Scale bar = 100  $\mu\text{m}$ . C) 4x zoom DIC imaging of swim bladder formation delay and similar defects observed at 72 hpf in *sgoL1* mutants compared to wild type controls at 120 hpf. Scale bar = 100  $\mu\text{m}$ . D) 5x zoom DIC imaging of neural apoptosis observed in *sororin* mutants at 24 hpf compared to wild type control. Scale bar = 100  $\mu\text{m}$ .

***Esco1* and *sororin* mutants are null while *sgo11* mutants retain low levels of maternal RNA.**

Once the presence or absence of a phenotype is observed and confirmed, we wanted to determine the ability of CRISPR/Cas9 to create a null mutant. RT-PCR of *esco1* mutant embryos at one day post fertilization (dpf) show complete loss of transcript suggesting the frameshift mutation leads to nonsense mediated decay (Fig 3A). RT-PCR of *sgoL1* wild type (AB), sibling (*sgoL1*<sup>+/+</sup> & *sgoL1*<sup>+/ $\Delta$ 8</sup>), and mutants at three dpf show a significant and steady decrease in transcript, respectively (Fig 3B). The remaining band in the *sgoL1* mutant lane has wild type sequence suggesting that residual maternal RNA is present at this time point, confirming that the phenotype is a consequence of a knockdown. This could explain the more mild gross morphology phenotype observed compared to *sororin* mutants (Fig 2). No transcript is observed in the RT-PCR performed in *sororin* mutants compared to the wild type (AB) and sibling (*sororin*<sup>+/+</sup> & *sororin*<sup>+/ $\Delta$ 20</sup>) embryos suggesting that a null mutation is generated due to nonsense mediated decay of

the truncated protein (Fig 3C). Though a more distal site is targeted in Sororin, the lack of transcript suggests that a null mutation is generated.

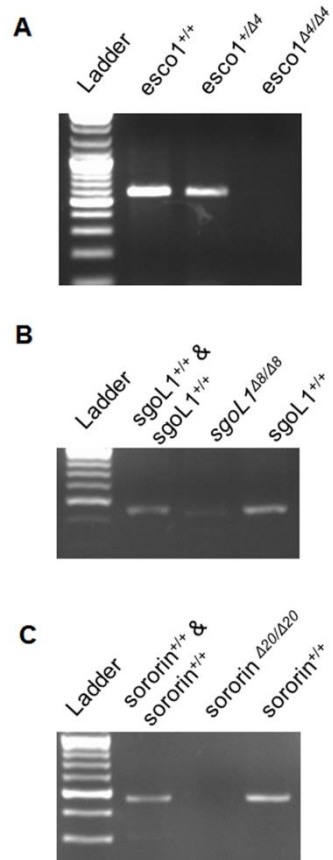


**Figure 3: Cohesion Establishment Mutant Validation.** A) RT-PCR of wild type, *esco1* heterozygous, and *esco1* mutant embryos at 24 hpf. B) RT-PCR of wild type, *sgoL1* sibling (*sgoL1*<sup>+/+</sup> & *sgoL1*<sup>+/Δ8</sup>), and *sgoL1* mutant embryos at 72 hpf. C) RT-PCR of wild type, *sororin* sibling (*sororin*<sup>+/+</sup> & *sororin*<sup>+/Δ20</sup>), and *sororin* mutant embryos at 24 hpf.

### Cohesion establishment mutants exhibit spectrum of cohesion defects.

*Esco1*, *SgoL1*, and *Sororin* have substantial evidence for their role in cohesion establishment and maintenance. Thus far, we show that a variety of gross morphology

phenotypes are observed possibly due to differential levels of gene knockout but also critical in determining if each factor is critical for cohesion establishment (Fig 2 & 3). Considering the role of each of these genes in sister chromatid pairing, chromosome spreads are generated for *esco1*, *sgo1l*, *sororin* mutants and wild type embryos staged at 24 hpf. Chromosome spreads are classified as one of three different categories. The 'paired' category represents the wild type morphology with a tight constriction at the centromere. The 'paired but separated' (PBS) category represents the category of spreads where sister chromatids are paired however have a separation at the centromere. The final category is 'separated' and represents the spreads in which sister chromatids are completely detached from each other (Fig 4A).

Using this assay, we are able to detect a range of cohesion defects. *Esco1* mutants show near wild type percentage of paired spreads at 81% (wild type at 97%) though mild levels of cohesion defects are present (19% total). *Sororin* mutants exhibit the most severe phenotype in which over half of chromosome spreads are in the completely separated category (53%) (Fig 4B). These cohesion defects are likely more severe due to the inability of Sororin to inhibit the actions of the anti-establishment factors, WAPL and PDS5, after cohesion establishment in S-phase (Nishiyama et al., 2010; Rankin et al., 2005; Wu et al., 2011). Similar to loss of *Esco2*, lack of cohesion establishment maintenance (in this case, Sororin) results in premature sister chromatid separation upon entrance into mitosis. *Sgo1l* mutants show a more moderate phenotype in which 25% of spreads are in the separated category (Fig 4B). This moderate phenotype could be due to SgoL1's spatial and temporal role in centromeric cohesion during the first three phases of mitosis compared to other cohesion establishment proteins which are required S phase.

These data suggest quantifiable and variable cohesion phenotypes; *esco1* mutants surprisingly have mild defects, *sgo1l* mutants exhibit moderate cohesion defects, and *sororin* mutants exhibit severe cohesion defects, near the level of cohesion defects observed in *esco2* mutant zebrafish. Correlating these observations with those of the gross phenotypes suggests that *Esco1* has no major role in sister chromatid pairing to negatively impact its development. *Sgo1l* and *Sororin* mutants, on the other hand, display cohesion defects that negatively impact development suggesting that they both have a role in cohesion establishment *in vivo*. Further, it appears the level of separated spreads dictates the severity of the gross morphology phenotype, with *sororin* mutants having more separated spreads compared to *sgo1l* mutants.

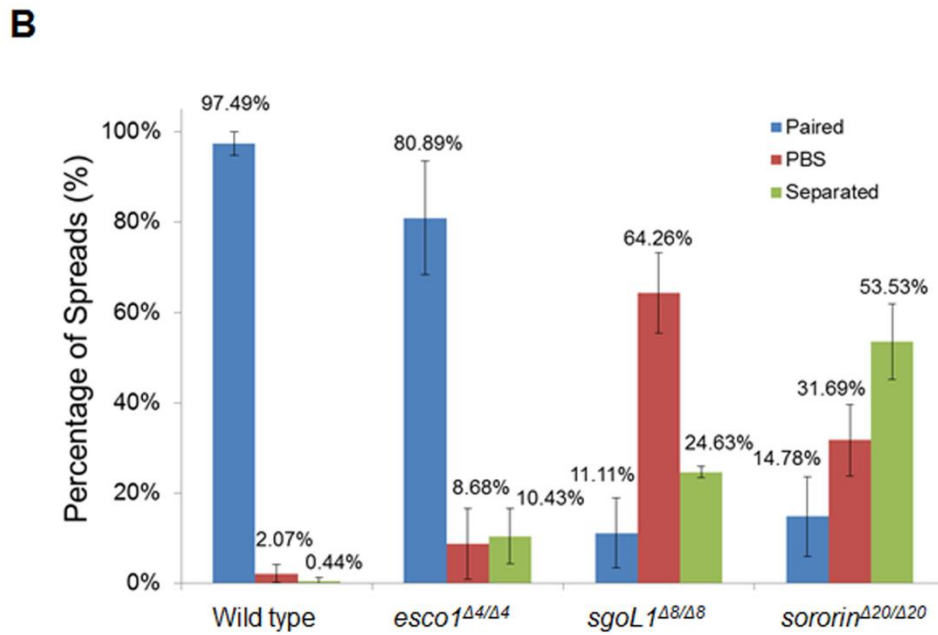
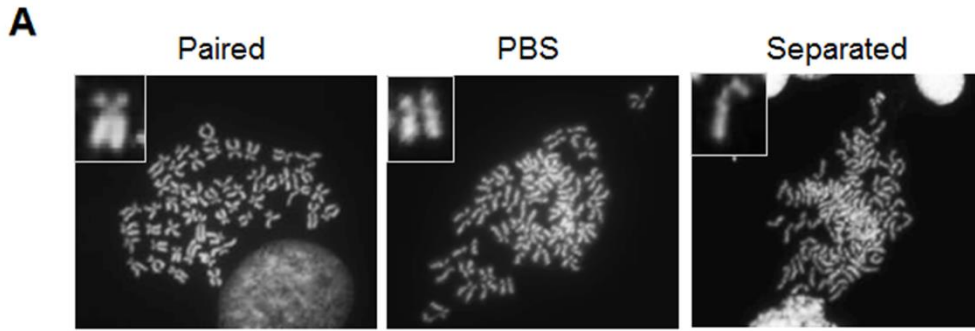


**Figure 4: Spectrum of cohesion defects in cohesion establishment mutants. A)**

Metaphase spreads from 24 hpf pooled embryos (n=10-12 embryos/slide) show three main phenotypes: paired, paired but separated (PBS), and separated. Insets show close up of the phenotype. If mixed categories were observed in the same spreads, they were counted toward the category in which the most prevalent phenotype was observed. B)

Percent distribution of spread categories in wild type and cohesion establishment mutants. N= 3-5 slides/genotype, 130-170 spreads/genotype analyzed total. Mean ± s.d.

### **Variable mitotic defects observed in cohesion establishment mutants.**

These mutants present the unique opportunity to analyze cellular defects associated with loss of cohesion establishment genes during embryonic development. Considering the impact of SCC on genome stability, we utilize our *in vivo* mitotic imaging assay to analyze several features of mitosis in the cohesion establishment mutants (Percival & Parant, 2016). In figure 5A, the predominant phenotype observed in each mutant is depicted from stills generated from a time-lapse confocal z-stack. As predicted, wild type and *esco1* mutants show normal cellular divisions within a normal division time at 22 and 24 minutes, respectively (Fig 5A & B). This suggests that not only does *Esco1* have no impact on sister chromatid pairing, but its cellular role has no impact on mitotic progression.

Due to *SgoL1*'s role in centromeric cohesion and the presence of PBS and separated defects in chromosome spreads, we hypothesize that *sgoL1* mutants would show moderate to severe mitotic defects. *SgoL1* mutants do indeed show mitotic defects, however significantly more mild than previously thought. In the video stills, chromosomes attempt to form a metaphase plate; however a few chromosomes fail to assemble towards the metaphase plate, indicative of congression defects (Fig 5A). The pseudo-metaphase plate could be forming just as the prophase pathway of cohesion removal is activated. Once arm cohesion is removed, the lack of *SgoL1* to protect centromeric cohesion allows microtubule tension to pull sister chromatids away from the metaphase plate. All cells divide, but show a significantly increased division time of 50 minutes (Fig 5B).

Sororin function is necessary immediately following cohesion establishment in S phase, therefore we hypothesize that *sororin* mutants will show severe mitotic defects due to the significant loss of cohesion shown by chromosome spreads (Fig 4B). *Sororin* mutants display several congression defects and sister chromatids proceed to disseminate throughout the cell, a phenotype coined as ‘scattered’. This greatly extends the average division time to 82 minutes and most often these cells divide with various forms of genomic instability as seen by the micronucleus formation (thick arrow, Fig 5A & B). Several divisions are captured and calculated to last longer than two hours suggesting a strong spindle assembly checkpoint is activated in response to the scattered phenotype. The scattered phenotype is very similar to that observed in *esco2* mutants (Percival et al., 2015). This suggests that in the absence of Sororin, cohesion establishment is subsequently inactivated by anti-establishment factors prematurely removing cohesion, leading to the severe scattered phenotype observed in mitosis.

Genomic instability is a common consequence of cohesion defects in sister chromatid pairing. To analyze these defects in our mutants, we document the pre-anaphase and post-anaphase defects observed in all cell divisions during time-lapse acquisition for each cohesion establishment mutant (Fig 5C & D). Pre-anaphase defects are described as either congression or scattered defects while post-anaphase defects describe evidence of genomic instability such as micronuclei (MN) formation, lagging chromosomes, or failed cytokinesis. Wild type and *esco1* mutants rarely exhibit pre- or post-anaphase defects providing further evidence suggesting that *Esco1* has no role in cohesion establishment or proper chromosome segregation (Fig 5C & D). Interestingly, *sgo1* and *sororin* mutants display a variety of defects indicative of genomic instability

and cohesion defects. The majority of *sgoLI* mutant divisions result in congression or scattered defects pre-anaphase, 36% and 44% respectively (Fig 5C). These divisions overcome the mitotic defects however and result in 78% of divisions presenting no evidence of genomic instability (Fig 5D). These defects are more drastic in *sororin* mutant divisions. Only 4% of cells show a normal pre-anaphase progression with the majority showing a scattered phenotype (79%) (Fig 5C). We suggest the scattered divisions are the ones that lead to severe post-anaphase defects such as micronucleus formation (31%). Even more severe are the cells that remain scattered through the entire time-lapse without dividing at a 25% frequency rate, suggesting a strong checkpoint is activated keeping these cells in mitosis (Fig 5D). Within these data, we find that mitotic duration accurately predicts the level of mitotic defects and genomic instability observed in each cohesion establishment mutant.

One common form of genomic instability associated with developmental disorders and cancer formation is micronuclei (Colnaghi et al., 2011; Ricke & van Deursen, 2011; Ricke et al., 2008). A phenomenon known as chromothripsis is thought to blast apart chromosomes within MN while subsequently piecing back together the chromosomes leading to rearrangements (Crasta et al., 2012; Xu et al., 2011). To determine if MN formation frequency is increased to potentially play a role in propagation of genomic instability, we take a closer look at MN formation and calculate the frequency of micronuclei observed in the time lapse videos (Fig 5E). The number of micronuclei and total number of nuclei is calculated using 3D object measurement tool in NIS Elements. These findings suggest that micronuclei formation frequency is normal in *escoI* with rates around 1% compared to the level of wild type MN frequency. No

significant increases are observed in the frequency of MN in *sgo1I* mutants as well, though the frequency is trending upward. This coincides with the lack of genomic instability observed in Fig 5D. The frequency of MN in *sororin* mutants is elevated to 6% suggesting a high prevalence of DNA damage and genomic instability is present. This number is comparable to the 9% MN frequency observed in *esco2* mutant zebrafish (Percival et al., 2015). Ultimately, these mitotic data suggest that the severity of mitotic defects correlates to the severity in cohesion defects.

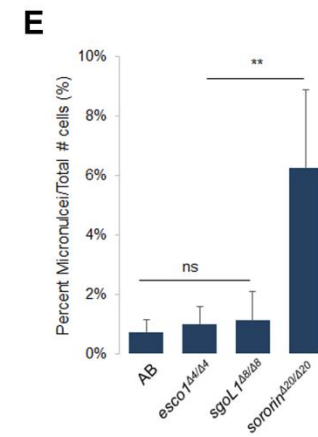
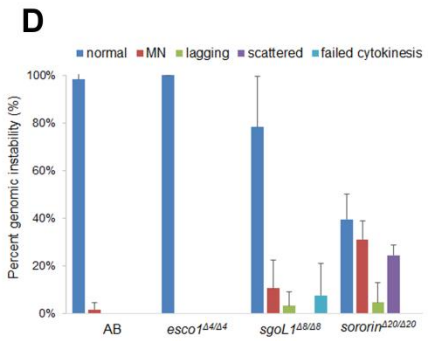
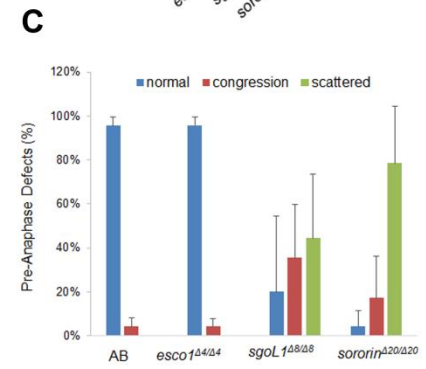
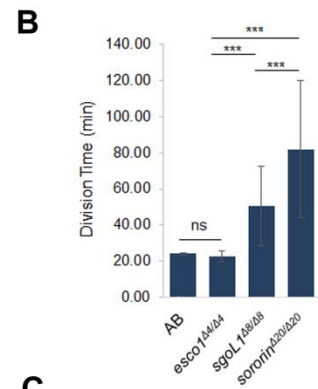
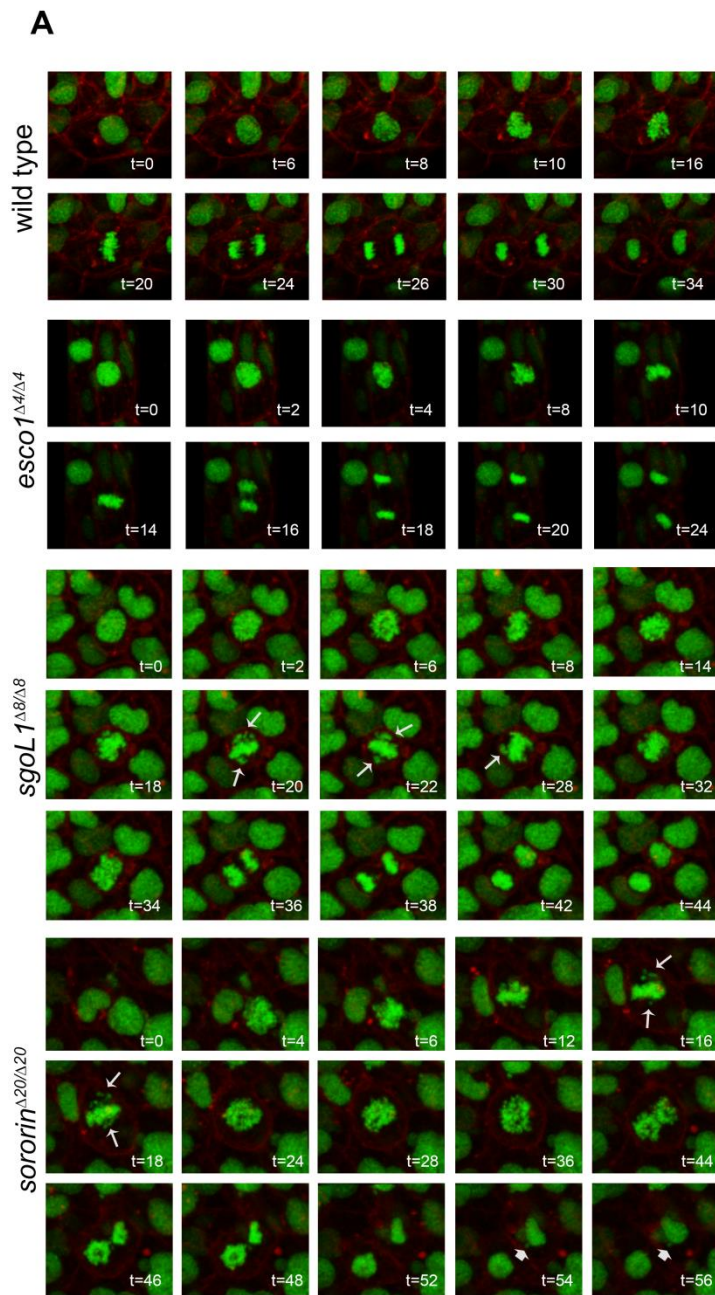


**Figure 5: *In vivo* analysis of cohesion establishment mutants reveal variations in division time and genomic instability outcomes.** A) Stills taken from time-lapse imaging videos demonstrating the variety of genomic instability observed in mutant embryos at 24 hpf. Thin arrows show congression defects. Thick arrows point towards micronuclei. Time stamps are in minutes. B) Division time of AB and cohesion establishment mutants calculated from the assumed nuclear envelope breakdown (NEB) to division into two daughter cells in minutes. One-way ANOVA to determine statistically significant differences.  $F(3, 144) = 52.071$ ,  $p = 0.001$ . Error bars show mean  $\pm$  st. dev. Tukey HSD post-hoc analysis \*\*\* $p < 0.001$ . NS indicates non-significance. C) Average frequency distribution of mitotic defects prior to anaphase in wild type (46 divisions taken from three embryos) and mutant (52, 34, 20 divisions from three embryos of each *esco1*, *sgo11*, and *sororin* mutants, respectively) based on time-lapse imaging. Error bars show mean  $\pm$  st. dev. D) Average frequency distribution of mitotic defects following anaphase in wild-type (46 divisions taken from three embryos) and mutants (52, 34, 20 divisions from three embryos of each *esco1*, *sgo11*, and *sororin* mutants, respectively) based on time-lapse imaging. Error bars show mean  $\pm$  st. dev. between embryos. E) Frequency of micronuclei observed in interphase cells of the tail region of embryos injected with H2A.F/Z-EGFP; CAAX-mCherry mRNA. Percentage is based on total number of micronuclei observed over the number of nuclei observed in interphase cells ( $n=3$  embryos/genotype,  $>250$  cells per field). One-way ANOVA to determine statistically significant differences.  $F(3, 8) = 10.396$ ,  $p = 0.004$ . Error bars show mean  $\pm$  st. dev. Tukey HSD post-hoc analysis \*\* $P < 0.01$ . NS indicates non-significance.

### **Apoptotic response is variable and tissue specific.**

The presence of genomic instability in the cohesion establishment mutants, particularly micronuclei, suggests the presence of DNA damage. Accumulation of sufficient DNA damage ultimately results in apoptosis. We want to determine if an apoptotic response is an outcome of the genomic instability observed in each of the mutants and if it plays a role in the phenotypic outcome. To accomplish this, we stain embryos at various time points with acridine orange (AO). Acridine orange staining is a live dye that labels apoptotic cells in a punctate fashion. Wild type embryos show no punctate apoptotic staining across all time points (Fig 6A). Similar to our *esco2* mutant studies, *sororin* mutants exhibit a strong neural apoptotic response at 24 hpf (Percival et al., 2015). At 48 hpf this apoptotic response is severely diminished either suggesting that a compensation mechanism has taken over or that the majority of proliferative cells have died (Fig 6B). *SgoL1* mutants show moderate apoptosis in neural tissues at 24 hpf, however at 72 hpf, tissue-specific responses are observed in the tail, heart, jaw, and fin (Fig 6C). These are tissues that are potentially more sensitive to mitotic defects associated with SgoL1 loss. Similar to wildtype, *esco1* mutants show no apoptotic response across all time points which correlate to the lack of cohesion and mitotic defects that are observed (Fig 6D).

In order to quantify the varying levels of apoptotic response, we developed a rating system for apoptotic responses from AO staining. A rating of 1 indicates little to no staining while a rating of 5 indicates the most severe staining. At least 15 embryos are rated per genotype and this experiment is performed three times to ensure that the responses are real and repeatable. As well, the embryos are blinded before scoring to

remove any bias towards mutants. At 24 hpf, the ratings correspond to their qualitative descriptions in that *sororin* mutants exhibit the most severe rating while *sgoLI* mutants exhibit a low, but significant level of apoptosis. This trend continues to 72 hpf where *sgoLI* mutants exhibit a mild but significant increase in apoptosis compared to controls. Across all time points, *escoI* mutants and wild type embryos show no significant difference corroborating the lack of cohesion defects and genomic instability detected. The presence of apoptosis in *sgoLI* and *sororin* mutants suggests that the genomic instability caused by cohesion defects leads to cell death. Overall, these data suggest that the severity in apoptosis correlates to the extent of mitotic defects.

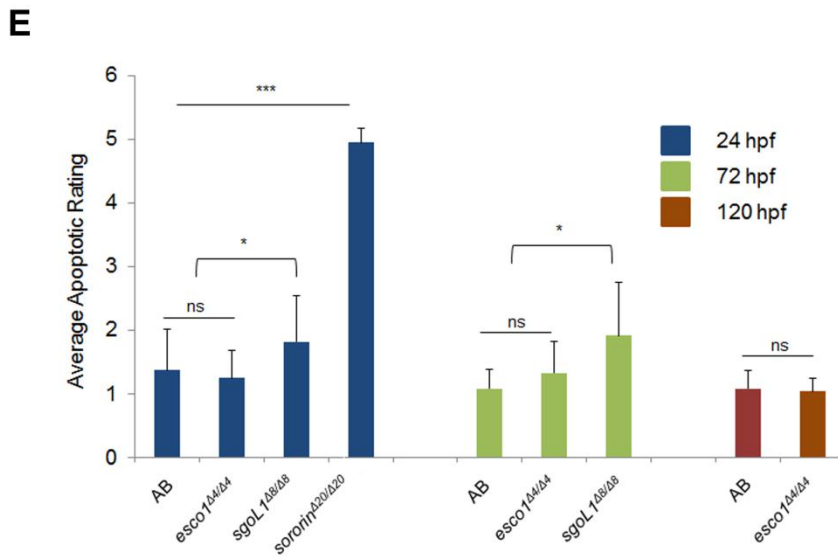
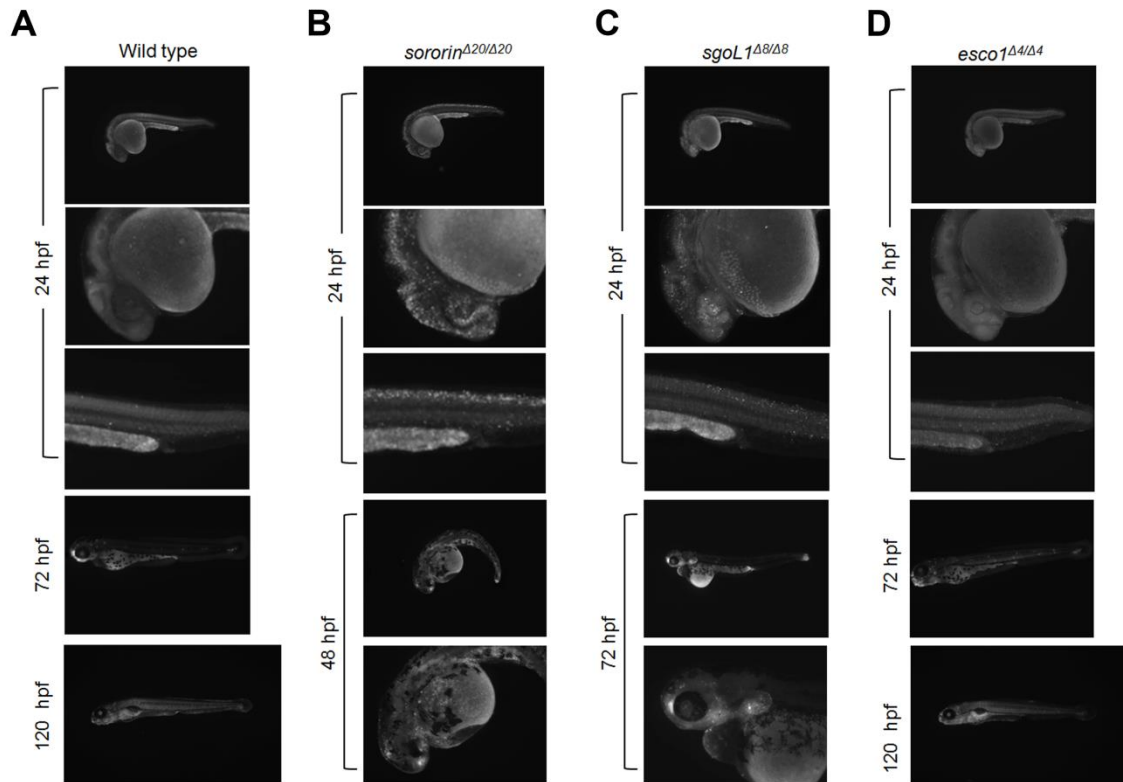


**Figure 6: Broad range of apoptotic responses among cohesion establishment mutants.** Fluorescent images of mutants stained using acridine orange. A) Wild type embryo time course of AO staining show no apoptotic staining across 24, 72, and 120 hpf. B) *Sororin* mutants show strong neural apoptosis at 24 hpf in the head and neural

tube. Residual apoptosis at 48 hpf. C) *Sgo1* mutants display mild neural apoptosis at 24 hpf. Mutants at 72 hpf show localized apoptosis to the head, heart, and fin. D) *Esco1* mutants show no apoptotic staining across 24, 72, and 120 hpf. E) Average rating of apoptotic staining in cohesion mutants at 24, 72, and 120 hpf. 1 rating represents no staining observed and 5 rating represents the most severe staining. 17-25 embryos were rated per genotype. One-way ANOVA to determine statistically significant differences,  $F(3, 88) = 227, p=0.001$ . Error bars display mean  $\pm$  st. dev. Tukey HSD post-hoc analysis \* $P < 0.05$ , \*\*\* $P < 0.001$ . NS indicates non-significance.

## DISCUSSION

Utilizing the efficient nature of CRISPR/Cas9, we explore the embryonic roles of several cohesion establishment factors, *Esco1*, *ShugoshinL1*, and *Sororin* *in vivo*. These models provide the means to determine their role in cohesion establishment and understand how mutations in the SCC pathway result in disease pathogenesis. We find that though all are suggested to be involved in cohesion establishment, a wide spectrum of phenotypes are observed proposing that not all roles in cohesion establishment are essential to the same degree in a developing organism. Phenotypic severity is found to be a result of the extent of cohesion defects that lead to a correlating severity of mitotic and apoptotic responses.

This finding is significant in many ways. Though not all of our cohesion establishment mutants are null mutants, the ability to detect differences between cohesion defects that correlate to a phenotype in a live vertebrate organism is novel when the

majority of the field suggests defects in cohesion establishment are binary; either cohesion is present to ensure viability or there is no cohesion present and cell death results. We largely attribute this finding to investigating cohesion establishment within a multi-cellular, ex vivo vertebrate organism. These observations are highlighted by the fact that we also observe tissue-specific differences in the gross morphology and apoptotic response. By investigating cohesion establishment factors in a physiologically relevant system, we are able to determine that the loss of these factors result in phenotypic variations due to differences in cohesion defects that negatively impact development. This is described in our SCC gradient model (Fig 7A).

This model is novel in that the SCC field typically attributes the cohesinopathy phenotypic spectrum to changes in gene expression. Several pieces of evidence suggest a role of the cohesin ring that largely associates gene expression alterations with CdLS mutations (Dorsett, 2011; Horsfield et al., 2007; Kawauchi et al., 2009; Kawauchi et al., 2016). The lack of cohesion defects in combination with the global transcriptional dysregulation prompts some to further describe CdLS as a transcriptomopathy (Kawauchi et al., 2016). Gene expression data in RBS is not as strong as that in CdLS and contradictory studies from different groups suggest more research is essential. ESCO2 is found to co-immunoprecipitate with Notch 1 intracellular domain leading to the conclusions that ESCO2 regulates Notch gene expression in *Drosophila* (Leem et al., 2011). In addition, Gerton's group describes differences in ribosome biogenesis genes as the pathogenic mechanism behind RBS (Bose et al., 2012; Xu et al., 2016; Xu et al., 2013). Substantial evidence can be made for this case; however it does not explain the variable phenotypes observed between RBS patients.

More recent data expands on the concept that cell cycle defects play a role in the pathogenesis of the HR+ cohesinopathies (heterochromatic repulsion-positive) such as RBS, CAIDS, and WBS. Strong evidence for gene expressions changes and the lack of HR excludes CdLS from this category. Several studies investigating RBS, CAIDS, and WBS show cohesion and mitotic defects, and cell/organismal lethality (Chetaille et al., 2014; Deardorff et al., 2012; Inoue et al., 2007; Monnich et al., 2011; Percival et al., 2015; Whelan et al., 2012; Yamada et al., 2012). These studies suggest cell cycle defects play a role in the pathogenesis, but are unable to address the variable phenotypes observed within HR+ cohesinopathies largely due to the challenging analysis of embryonic lethal mouse models.

This provides the first evidence of variability in cohesion defect severity as a potential underlying cause to the spectrum of phenotypes observed within HR+ cohesinopathies (Fig 7B). In the context of RBS, we hypothesize that the more severe RBS patients exhibit more severe cohesion defects (that are likely tissue-specific) leading to more severe genomic instability, while the more mild RBS patients have less cohesion defects and genomic instability. This gradient of cohesion defects may also address the difference in RBS and CAIDS phenotypes in that more severe cohesion defects result in more neural phenotypes such as the craniofacial and microcephaly phenotypes associated with RBS while more moderate cohesion defects manifest into cardiac and enteric phenotypes that are associated with CAIDS. Expanding beyond cohesinopathies, this spectrum could address the strength of a cancer predisposition. Using RBS and WBS as models, WBS could have higher levels of genomic instability (cohesion defects) than RBS that enhance the tumor formation that is strongly associated with WBS.

At the cellular level, several cell culture studies suggest that viability can be manipulated through the extent of cohesion defects. Previously, it is shown that loss of ESCO2 (Eco1 in yeast) exhibits severe cohesion defects and is cell lethal (Hou & Zou, 2005; Monnich et al., 2011; Percival et al., 2015; Whelan et al., 2012). Cell lethality, however is rescued with loss of WAPL, an anti-establishment factor. This rescue coincides with a decrease in cohesion defects suggesting that cohesion defects dictate cell lethality (Gandhi et al., 2006; Kueng et al., 2006; Nishiyama et al., 2010; Rowland et al., 2009; Tanaka et al., 2001). These exact genetic studies remain to be performed in a live vertebrate organism; however our results provide the first vertebrate evidence towards this notion that the level of cohesion present determines the extent of the phenotype. We hypothesize these studies will aid in identifying potential genetic modifiers within RBS patients that are responsible for the large phenotypic spectrum.

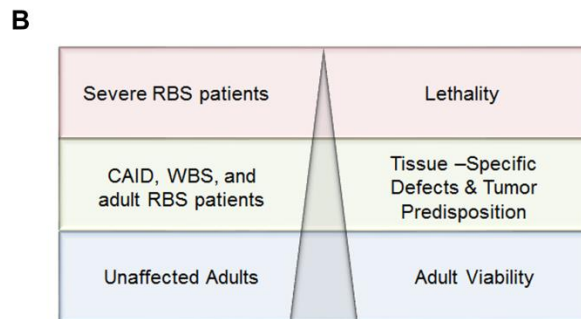
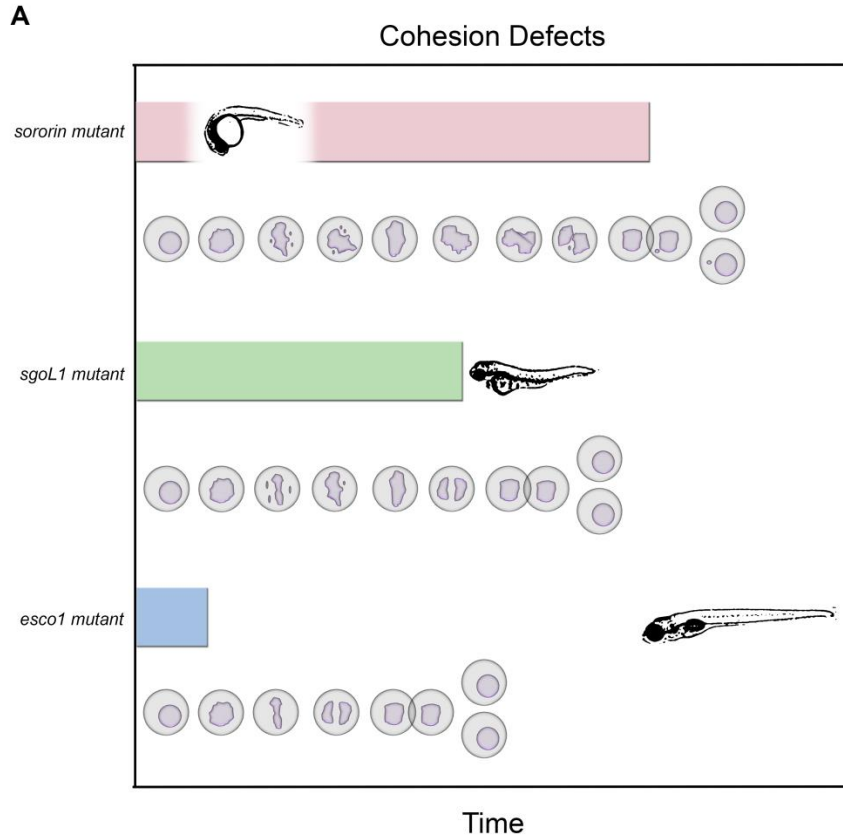


**Figure 7: The SCC Gradient Model.** A) Summary of cohesion establishment mutant data suggests that increasing levels of cohesion defects (colored bars, Fig 4) correlates and is a cause of the increased division time (cell division diagram, Fig 5). Ultimately, these cohesion defects lead to apoptosis due to severe genomic instability (Fig 6). These observations inversely correlate to the time at which phenotypes appear in addition to their severity (black and white embryo phenotype images, Fig 2) suggesting that the

severity of the cohesion defects can dictate the severity of a phenotypic outcome. B) If the above model is assumed to be true, this could provide a mechanism behind the variable phenotypes associated with HR+ cohesinopathies, in particular, within the cohesinopathy RBS. The most severe cohesinopathies such as in severe RBS patients result in embryonic lethality correlating to *esco2* and *sororin* mutants. Cohesinopathies such as CAID, WBS, and mild RBS patients show mild phenotypes, tissue-specific defects, and tumor predisposition correlating to the milder defects observed in *sgo1* mutants.

This study also lays the ground work for additional studies to be performed on each individual cohesion establishment mutant to further investigate the intricate cellular mechanisms behind each phenotype. To our surprise, *esco1* mutants are viable which contradicts the cell culture studies that report ESCO1 and ESCO2 are not functionally redundant (Hou & Zou, 2005). Previously, our lab determined that nearly all of cohesion is lost in *esco2* mutant zebrafish (85%) (Percival et al., 2015). In this report, we find that *esco1* mutants have 10% of cells with a separated cohesion defect suggesting that those cells without complete cohesion loss in *esco2* mutants, could be dominated by Escol1 cohesion establishment. This finding further suggests that temporal or tissue-specific differences could dictate which cohesion establishment factor is dominant within a cell. In addition, recent studies propose that ESCO1 may have alternative functions in SCC. It is suggested that ESCO1 acts through a different establishment mechanism that relies on PDS5 while ESCO2 does not (Minamino et al., 2015). Further, ESCO1 is shown to provide cohesion establishment for transcriptional control throughout the cell cycle

(Rahman et al., 2015). Consistent with our *esco1* mutant, a minor role in cohesion establishment is observed with only 19% of cells showing cohesion defects. This has little impact on the development of a phenotype and the simple lack of phenotype suggests that *Esco1* has no major role in a vertebrate organism or that its major role is not essential for development.

*ShugoshinL1* mutants prove to be a decent model for CAIDS, though it is a knockdown compared to the CAIDS-associated hypomorphic allele. CAIDS is described as the co-occurrence of two separate disorders, sick sinus syndrome (SSS) and chronic intestinal pseudo-obstruction (CIPO). SSS results in an abnormal heart rhythm and most patients receiving a pacemaker early in life (Chetaille et al., 2014). Interestingly, there are no other developmental defects compared to the severe, multi-system defects associated with RBS, CdLS, and WBS such as craniofacial, mental retardation, and limb defects. This begs the question as to why *SgoL1*, a gene necessary for proper chromosome segregation, is particularly essential in the heart and gut. Researchers postulate that tissue-specific gene expression of *SgoL1* is causative of the specific heart and gut defects (Chetaille et al., 2014). Though primarily responsible for meiotic cohesion maintenance, *SgoL2* is shown to play a role in centromeric cohesion and biorientation during mitosis in culture systems suggesting possible tissue-specific compensation mechanisms may exist (Huang et al., 2005; Kitajima et al., 2006; Lee et al., 2008; Orth et al., 2011).

*SgoL1* mutants also show a delay in craniofacial development and pericardial heart edema at 72 hpf (Fig 2A & B). During embryonic development there is a subset of neural crest cells that migrate from the hindbrain region to contribute to the primary heart field between 24 and 30 hpf (Cavanaugh et al., 2015; Kirby et al., 1983; Sato & Yost,

2003). Several models ablating migratory neural crest cells both genetically and pharmacologically show similar pericardial edema and abnormal heart morphology comparable to *sgoLI* mutants (Besson et al., 1986; Sato et al., 2006; Sun et al., 2008). We hypothesize that the gross morphology phenotypes associated with our *sgoLI* mutant are caused by an increased mitotic index, genomic instability, and subsequent apoptosis of neural crest cells either between the 24 to 30 hpf migratory window or just after to result in the pericardial edema and morphology defects observed at 72 hpf. Though these phenotypes are a result of gene knockdown, it is critical in defining our gradient model (Fig 7).

Similar to *esco2* mutant zebrafish, *sororin* mutants display growth retardation, craniofacial defects, mitotic arrest, chromosome scattering, genomic instability, and cohesion defects though not as severe as *esco2* mutants (Monnich et al., 2011; Percival et al., 2015). This could be due to several factors. Sororin is recruited to the acetylation site to physically block anti-establishment factors (WAPL-PDS5) from interacting with the cohesin ring immediately after acetylation; however SMC3 acetylation may be able to block WAPL-PDS5 to an extent before prematurely removing cohesin (Ladurner et al., 2016; Nishiyama et al., 2010). Further, there may be tissue-specific sensitivities to Sororin loss or a delayed maternal RNA decrease that leads to a less severe phenotype. *Sororin* mutants also serve as another example of neural tissues being sensitive to cohesion defects compared to other tissues (Percival et al., 2015). Comparable to the genetic interaction studies involving ESCO2 and WAPL, Sororin-associated cohesion defects and lethality are rescued by WAPL knockdown (Elbatsh et al., 2016). Future studies will look to confirm these interactions.

Distinguishing the spectrum of cohesion defects and how it affects development *in vivo* not only aids in mechanistically understanding HR+ cohesinopathies but is also valuable in developing therapeutic targets for other cohesion-related disorders such as infertility and tumorigenesis. SCC therapeutics is largely limited to HDAC and Separase inhibitors (Bolden et al., 2006; Do et al., 2016; Kimata et al., 2008). With the increasing knowledge of many SCC proteins' structure, structure-based drug design will be able to develop therapeutics towards these targets. Our study provides the valuable knowledge critical in understanding cohesion defects, how they are tolerated in a physiologically-relevant model, and aids in the endeavor of developing worthy therapeutic avenues.

## **MATERIALS AND METHODS**

### **Zebrafish lines:**

All zebrafish lines were maintained as described in Westerfield, 1995 under standard laboratory conditions by the ZRF Animal Resources Program which maintains full AAALAC accreditation and is assured with OLAW. AB wild-type zebrafish were used for RNA injections and controls. This study was approved by the UAB Institutional Animal Care and Use Committee (IACUC).

### **CRISPR mutant generation:**

CRISPR guides were designed and selected using the online tool ZiFit Targeter (<http://zifit.partners.org/ZiFiT/ChoiceMenu.aspx>). For CRISPR assembly and to avoid the plasmid prep step and DraI restriction enzyme, we began simply performing colony PCR off of the guide plasmid using the following primers:

Forward: TGATTGCAGTCCAGTTACGC and

Reverse: GGAGGCTTTTGACTTTCTGCT. The PCR product was used as template for RNA synthesis. CAS9 mRNA was transcribed from the linearized pT3TS-nCas9n plasmid (Addgene) using the mMessage mMachine T3 kit (Life Technologies). Each RNA was purified using the RNeasy Kit (Qiagen). The CRISPR guide RNA was synthesized using the MegaShortScript T7 Kit (Life Technologies) and purified using the MegaClear Kit (Life Technologies). RNA concentration was quantified using the Nanodrop spectrophotometer.

#### **Microinjection of CRISPR/Cas9:**

Esco1, ShugoshinL1, or Sororin Cas9/guide RNA microinjection was performed on 1-cell stage zebrafish embryos at a concentration using 0.5 nL of 0.85 mM. For CRISPR/Cas9 injections, 150 ng/ $\mu$ l of Cas9 mRNA and 30 ng/ $\mu$ l of RNA were used (Thomas et al., 2014). Injected embryos were incubated at 28 °C until 5 dpf at which point they were put on the water system.

#### **Genotyping:**

*High Resolution Melt (HRM) Curve Analysis:* HRM analysis was used to identify CRISPR-derived *esco1*, *shugoshinL1*, and *sororin* chimeric G0 and subsequent mutations in the stable lines. Genomic PCR products were sequenced from HRM-positive fish, and then desired mutant fish were propagated into the F1 and F2 generations. For assays and identification of CRISPR mutants, individual embryos or tail clippings were placed in 40  $\mu$ L of 25 mM NaOH in 96 well plates. Tissue was then incubated at 95 °C for 20 minutes. Then 40  $\mu$ l of 40 mM Tris-HCl was added to neutralize the NaOH for a crude genomic

DNA extract. For *esco1*, HRM-genotyping PCR fragments were generated using primer forward: 5'-CTGTGTTGTGGAGATTGAAACC-3' and reverse: 5'-ACAGGTCACACATTCGCTTG-3'. For *shugoshinL1* genotyping PCR fragments were generated using primer forward: 5'-AGCGTTCAGGCCAACAATAA-3' and reverse: 5'-GCGGGTCTCTCTCTCAGTGT-3'. For *sororin* genotyping PCR fragments were generated using primer forward: 5'-GACCCCAGAGGTGATGAAGA-3' and reverse: 5'-CCCAGAGAGAGGGACATGAA-3'. PCR reactions were performed using genomic DNA in black/white 96 well plates (BioRad cat. No. HSP9665). PCR reaction protocol was 95 °C for 30 sec, then 40 cycles of 95 °C for 10 sec, 59 °C for 20 sec, and 72 °C for 15 sec in Eppendorf Mastercycler Pro 96S. Following PCR, plates were analyzed for melting curves with Lightscanner (Idaho Technology) over a 65-95 °C range. From this wild type, heterozygous, and mutant melting temperatures were clearly distinguished as previously published (Thomas et al., 2014).

*PCR Sequencing:* To identify the exact sequence of the mutation generated by CRISPR/Cas9, larger amplicons were amplified in chimeric or heterozygous embryos or tail clippings. For *esco1* genotyping PCR fragments were generated using primer forward: 5'-CATGCAGGCTGAAGAGATCA-3' and reverse: 5'-ACAGGTCACACATTCGCTTG-3'. For *shugoshinL1* genotyping PCR fragments were generated using primer forward: 5'-TGTGGATGTCAGTGGCTGA-3' and reverse: 5'-GCGGGTCTCTCTCTCAGTGT-3'. For *sororin* genotyping PCR fragments were generated using primer forward: 5'-AAAGCGCTCCAAAGTCTTGA-3' and reverse: 5'-GGTCTTTTTCCCCAGACACA-3'.

*PCR gel genotyping:* To validate knockout efficiency, RT-PCR reactions corresponding to a wildtype, sibling and mutant were performed. For *escol* genotyping PCR fragments were generated using primer forward: 5'-CCATGCCTAATGGAATCACC-3' and reverse: 5'- TTCGGATCATCAGGGAGAAC-3' to amplify WT products. For *shugoshinL1* genotyping PCR fragments were generated using primer forward: 5'- GACACTGAGAGAGAGACCCG-3' and reverse: 5'- TTCTCCCAGGGCTTCTTCAG-3' to amplify WT products. For *sororin* genotyping PCR fragments were generated using primer forward: 5'- TTGGTCCAAGAAAGTGCGAC-3' and reverse: 5'- GAACAACGTCCTGAGCACAA-3' to amplify WT products. Each PCR product was run on a 2% agarose gel.

### **Microscopy and Image Analysis:**

*Gross morphology:* Embryos were placed in 0.4% tricaine to anesthetize and then in methyl cellulose for proper positioning at indicated time points. Images were taken using a Nikon AZ100 using the 2x objective 0.5NA 2x digital zoom. Head and heart images were taken with a 5x digital zoom. Videos of heart beat were taken in DIC at the 5x digital zoom. Swim bladder images were taken with a 4x digital zoom. All images were processed using NIS Elements software.

*Apoptosis Assay:* Embryos were dechorionated using pronase as stated above and incubated in 10  $\mu$ L/mL acridine orange for one hour in the dark. Embryos were washed 5x for 5 minutes with E3 Blue embryo water. Fluorescence was observed using Nikon AZ100 using GFP filter at 2x objective and 2x digital zoom for whole embryo images. For the AO rating assay, a rating of 1 indicates little to no staining while a rating of 5

indicates the most severe staining. At least 15 embryos were rated per genotype and this experiment was performed three times to ensure that these responses were real and repeatable. As well, the embryos were blinded before scoring to remove any bias towards mutants.

*Time-lapse imaging:* CaaX-mCherry and H2A.F/Z-EGFP mRNA was transcribed from a plasmid (pCS2-CaaX-mCherry and pCS2-H2A.F/Z-EGFP; gift from K. Kwan (U. of Utah)) using mMessage mMachine SP6 kit (Life Technologies). *Shugoshin* and *Sororin* heterozygous and homozygous mutant *esco1* were crossed and embryos were microinjected into the yolk of a one-cell staged embryo with 1nl of 200 ng/μl CaaX-mCherry and 200 ng/μl H2A.F/Z-eGFP mRNA. At 24 hpf, embryos were screened for fluorescence. Embryos were manually dechorionated using tweezers and anesthetized using 0.4% tricaine. In a glass coverslip-bottomed dish, embryos were embedded in a 1% low-melt agarose. Dishes were placed on the Nikon A1 inverted confocal microscope, and z-stack images were taken at designated intervals. Time-lapse was set using a 40 μm z-stacks (with a 3 μm interval) and obtained every 2 minutes for a total scanning time of 2 hours. All videos were taken using 60x 1.4NA objectives. 3D viewing, still shots, and videos were assembled and processed using NIS Elements 4.13.00 (Percival 2015).

*Micronuclei/ Apoptotic Bodies Count:* This analysis used the time-lapse videos acquired for cell cycle analysis using 60x 1.4 NA objective and 1.5 digital zoom on a Nikon A1 confocal microscope as described above for each mutant and wild-type embryos. Using 3D volume rendering in NIS Elements 4.13.00, an average nuclei and micronuclei count was calculated per field to calculate the percent observed in a population of cells. Differentiation between apoptotic bodies and micronuclei was

determined based on size and localization within the cell; i.e. using the CaaX-mCherry (plasma membrane) fluorescence, it can be determined whether a micronuclei is within a cell and whether an apoptotic body is outside a cell. Frequency of micronuclei in interphase was calculated by dividing the total number of micronuclei observed by the number of nuclei identified in 3D object measurement tool.

### **Chromosome Spreads:**

Chromosome spread protocol was adapted from the Lee group (Jeong et al., 2010).

Approximately 20-30 embryos were dechorionated at 24 hpf. Embryos were incubated in 400 ng/ml nocodazole for 2 hours in the dark at room temperature. Embryos were then transferred to 1.1% sodium citrate in a 6 cm dish. At this point if genotyping was necessary, tails were removed to be genotyped while the remaining embryo heads were transferred to fresh sodium citrate solution and incubated on ice for 8 minutes. Next, two washes with a cold 3:1 methanol: acetic acid solution for 20 minutes each followed by storage in -20 °C until genotyping is performed. After the fixative procedure, embryos are pooled (10-12 embryos/pool) per genotype and then minced using forceps in a 1:1 methanol: acetic acid solution. Using this mixture, 50 µL of pooled embryos were dropped onto a slide, and 3-5 drops of glacial acetic acid was added. The slide was slowly tilted up and then exposed to hot vapors (we used boiling water) for about 10 seconds. The slide was allowed to dry on a hot metal surface (approx. 50 °C). After the slide was completely dry, a few drops of Prolong Gold with DAPI were added and covered with a glass coverslip. Chromosomes were imaged using a 63x 1.4 NA objective on a Zeiss Axio Observer fluorescent microscope and processed with Zen 2011 Blue software. While most spreads were clearly delineated into the “paired”, “paired but separated”, or

“separated” categories, if a spread had multiple phenotypes it was categorized by which was most prevalent in that spread.

### **Statistical Analysis:**

Excel software was used in generation of all graphs and statistical tests. Overall statistical significant differences were calculated using a one-way ANOVA using SPSS software. Tukey HSD was performed post-hoc to follow up a statistically significant result. Graphs with error bars indicate mean  $\pm$  st. dev. are stated in legend. All p-values were determined significant at  $p < 0.05$ . Significance values are stated in figure legends.

### **COMPETING INTERESTS**

There are no competing interests associated with the data and discussion presented in this paper.

### **AUTHOR CONTRIBUTIONS**

SMP, HRT, and JMP designed experiments; HRT generated mitotic spreads and aided in CRISPR mutant generation; SMP performed all other experiments; SMP, HRT, and JMP analyzed data and wrote the manuscript.

### **REFERENCES**

Bellows, A. M., Kenna, M. A., Cassimeris, L., & Skibbens, R. V. (2003). Human EFO1p exhibits acetyltransferase activity and is a unique combination of linker histone and Ctf7p/Eco1p chromatid cohesion establishment domains. *Nucleic Acids Res*, 31(21), 6334-6343.

- Besson, W. T., 3rd, Kirby, M. L., Van Mierop, L. H., & Teabeaut, J. R., 2nd. (1986). Effects of the size of lesions of the cardiac neural crest at various embryonic ages on incidence and type of cardiac defects. *Circulation*, *73*(2), 360-364.
- Bolden, J. E., Peart, M. J., & Johnstone, R. W. (2006). Anticancer activities of histone deacetylase inhibitors. *Nat Rev Drug Discov*, *5*(9), 769-784. doi: 10.1038/nrd2133
- Bose, T., Lee, K. K., Lu, S., Xu, B., Harris, B., Slaughter, B., . . . Gerton, J. L. (2012). Cohesin proteins promote ribosomal RNA production and protein translation in yeast and human cells. *PLoS Genet*, *8*(6), e1002749. doi: 10.1371/journal.pgen.1002749
- Cavanaugh, A. M., Huang, J., & Chen, J. N. (2015). Two developmentally distinct populations of neural crest cells contribute to the zebrafish heart. *Dev Biol*, *404*(2), 103-112. doi: 10.1016/j.ydbio.2015.06.002
- Chetaille, P., Preuss, C., Burkhard, S., Cote, J. M., Houde, C., Castilloux, J., . . . Andelfinger, G. (2014). Mutations in SGOL1 cause a novel cohesinopathy affecting heart and gut rhythm. *Nat Genet*, *46*(11), 1245-1249. doi: 10.1038/ng.3113
- Ciosk, R., Shirayama, M., Shevchenko, A., Tanaka, T., Toth, A., Shevchenko, A., & Nasmyth, K. (2000). Cohesin's binding to chromosomes depends on a separate complex consisting of Scc2 and Scc4 proteins. *Mol Cell*, *5*(2), 243-254.
- Colnaghi, R., Carpenter, G., Volker, M., & O'Driscoll, M. (2011). The consequences of structural genomic alterations in humans: genomic disorders, genomic instability and cancer. *Semin Cell Dev Biol*, *22*(8), 875-885. doi: 10.1016/j.semcdb.2011.07.010
- Crasta, K., Ganem, N. J., Dagher, R., Lantermann, A. B., Ivanova, E. V., Pan, Y., . . . Pellman, D. (2012). DNA breaks and chromosome pulverization from errors in mitosis. *Nature*, *482*(7383), 53-58. doi: 10.1038/nature10802
- Deardorff, M. A., Bando, M., Nakato, R., Watrin, E., Itoh, T., Minamino, M., . . . Shirahige, K. (2012). HDAC8 mutations in Cornelia de Lange syndrome affect the cohesin acetylation cycle. *Nature*, *489*(7415), 313-317. doi: 10.1038/nature11316
- Deardorff, M. A., Kaur, M., Yaeger, D., Rampuria, A., Korolev, S., Pie, J., . . . Krantz, I. D. (2007). Mutations in cohesin complex members SMC3 and SMC1A cause a mild variant of cornelia de Lange syndrome with predominant mental retardation. *Am J Hum Genet*, *80*(3), 485-494. doi: 10.1086/511888
- Do, H. T., Zhang, N., Pati, D., & Gilbertson, S. R. (2016). Synthesis and activity of benzimidazole-1,3-dioxide inhibitors of separase. *Bioorg Med Chem Lett*, *26*(18), 4446-4450. doi: 10.1016/j.bmcl.2016.07.080
- Dorsett, D. (2011). Cohesin: genomic insights into controlling gene transcription and development. *Curr Opin Genet Dev*, *21*(2), 199-206. doi: 10.1016/j.gde.2011.01.018
- Dreier, M. R., Bekier, M. E., 2nd, & Taylor, W. R. (2011). Regulation of sororin by Cdk1-mediated phosphorylation. *J Cell Sci*, *124*(Pt 17), 2976-2987. doi: 10.1242/jcs.085431
- Elbatsh, A. M., Haarhuis, J. H., Petela, N., Chapard, C., Fish, A., Celie, P. H., . . . Rowland, B. D. (2016). Cohesin Releases DNA through Asymmetric ATPase-

- Driven Ring Opening. *Mol Cell*, 61(4), 575-588. doi: 10.1016/j.molcel.2016.01.025
- Gandhi, R., Gillespie, P. J., & Hirano, T. (2006). Human Wapl is a cohesin-binding protein that promotes sister-chromatid resolution in mitotic prophase. *Curr Biol*, 16(24), 2406-2417. doi: 10.1016/j.cub.2006.10.061
- Gerlich, D., Koch, B., Dupeux, F., Peters, J. M., & Ellenberg, J. (2006). Live-cell imaging reveals a stable cohesin-chromatin interaction after but not before DNA replication. *Curr Biol*, 16(15), 1571-1578. doi: 10.1016/j.cub.2006.06.068
- Guacci, V., Koshland, D., & Strunnikov, A. (1997). A direct link between sister chromatid cohesion and chromosome condensation revealed through the analysis of MCD1 in *S. cerevisiae*. *Cell*, 91(1), 47-57.
- Hauf, S., Waizenegger, I. C., & Peters, J. M. (2001). Cohesin cleavage by separase required for anaphase and cytokinesis in human cells. *Science*, 293(5533), 1320-1323. doi: 10.1126/science.1061376
- Horsfield, J. A., Anagnostou, S. H., Hu, J. K., Cho, K. H., Geisler, R., Lieschke, G., . . . Crosier, P. S. (2007). Cohesin-dependent regulation of Runx genes. *Development*, 134(14), 2639-2649. doi: 10.1242/dev.002485
- Hou, F., & Zou, H. (2005). Two human orthologues of Eco1/Ctf7 acetyltransferases are both required for proper sister-chromatid cohesion. *Mol Biol Cell*, 16(8), 3908-3918. doi: 10.1091/mbc.E04-12-1063
- Huang, X., Hatcher, R., York, J. P., & Zhang, P. (2005). Securin and separase phosphorylation act redundantly to maintain sister chromatid cohesion in mammalian cells. *Mol Biol Cell*, 16(10), 4725-4732. doi: 10.1091/mbc.E05-03-0190
- Inoue, A., Li, T., Roby, S. K., Valentine, M. B., Inoue, M., Boyd, K., . . . Lahti, J. M. (2007). Loss of ChlR1 helicase in mouse causes lethality due to the accumulation of aneuploid cells generated by cohesion defects and placental malformation. *Cell Cycle*, 6(13), 1646-1654. doi: 10.4161/cc.6.13.4411
- Jeong, K., Jeong, J. Y., Lee, H. O., Choi, E., & Lee, H. (2010). Inhibition of Plk1 induces mitotic infidelity and embryonic growth defects in developing zebrafish embryos. *Dev Biol*, 345(1), 34-48. doi: 10.1016/j.ydbio.2010.06.004
- Kawauchi, S., Calof, A. L., Santos, R., Lopez-Burks, M. E., Young, C. M., Hoang, M. P., . . . Lander, A. D. (2009). Multiple organ system defects and transcriptional dysregulation in the Nipbl(+/-) mouse, a model of Cornelia de Lange Syndrome. *PLoS Genet*, 5(9), e1000650. doi: 10.1371/journal.pgen.1000650
- Kawauchi, S., Santos, R., Muto, A., Lopez-Burks, M. E., Schilling, T. F., Lander, A. D., & Calof, A. L. (2016). Using mouse and zebrafish models to understand the etiology of developmental defects in Cornelia de Lange Syndrome. *Am J Med Genet C Semin Med Genet*, 172(2), 138-145. doi: 10.1002/ajmg.c.31484
- Kerrebrock, A. W., Moore, D. P., Wu, J. S., & Orr-Weaver, T. L. (1995). Mei-S332, a Drosophila protein required for sister-chromatid cohesion, can localize to meiotic centromere regions. *Cell*, 83(2), 247-256.
- Kimata, Y., Matsuyama, A., Nagao, K., Furuya, K., Obuse, C., Yoshida, M., & Yanagida, M. (2008). Diminishing HDACs by drugs or mutations promotes normal or abnormal sister chromatid separation by affecting APC/C and adherin. *J Cell Sci*, 121(Pt 7), 1107-1118. doi: 10.1242/jcs.024224

- Kirby, M. L., Gale, T. F., & Stewart, D. E. (1983). Neural crest cells contribute to normal aorticopulmonary septation. *Science*, *220*(4601), 1059-1061.
- Kitajima, T. S., Sakuno, T., Ishiguro, K., & Watanabe, Y. (2006). [Roles and molecular mechanisms of chromosome cohesion at centromeres]. *Tanpakushitsu Kakusan Koso*, *51*(13), 1809-1816.
- Krantz, I. D., McCallum, J., DeScipio, C., Kaur, M., Gillis, L. A., Yaeger, D., . . . Jackson, L. G. (2004). Cornelia de Lange syndrome is caused by mutations in NIPBL, the human homolog of *Drosophila melanogaster* Nipped-B. *Nat Genet*, *36*(6), 631-635. doi: 10.1038/ng1364
- Kueng, S., Hegemann, B., Peters, B. H., Lipp, J. J., Schleiffer, A., Mechtler, K., & Peters, J. M. (2006). Wapl controls the dynamic association of cohesin with chromatin. *Cell*, *127*(5), 955-967. doi: 10.1016/j.cell.2006.09.040
- Ladurner, R., Kreidl, E., Ivanov, M. P., Ekker, H., Idarraga-Amado, M. H., Busslinger, G. A., . . . Peters, J. M. (2016). Sororin actively maintains sister chromatid cohesion. *EMBO J*, *35*(6), 635-653. doi: 10.15252/embj.201592532
- Lee, J., Kitajima, T. S., Tanno, Y., Yoshida, K., Morita, T., Miyano, T., . . . Watanabe, Y. (2008). Unified mode of centromeric protection by shugoshin in mammalian oocytes and somatic cells. *Nat Cell Biol*, *10*(1), 42-52. doi: 10.1038/ncb1667
- Leem, Y. E., Choi, H. K., Jung, S. Y., Kim, B. J., Lee, K. Y., Yoon, K., . . . Kim, S. T. (2011). Esco2 promotes neuronal differentiation by repressing Notch signaling. *Cell Signal*, *23*(11), 1876-1884. doi: 10.1016/j.cellsig.2011.07.006
- Liu, H., Qu, Q., Warrington, R., Rice, A., Cheng, N., & Yu, H. (2015). Mitotic Transcription Installs Sgo1 at Centromeres to Coordinate Chromosome Segregation. *Mol Cell*, *59*(3), 426-436. doi: 10.1016/j.molcel.2015.06.018
- Maradeo, M. E., & Skibbens, R. V. (2009). The Elg1-RFC clamp-loading complex performs a role in sister chromatid cohesion. *PLoS One*, *4*(3), e4707. doi: 10.1371/journal.pone.0004707
- Mehta, G. D., Kumar, R., Srivastava, S., & Ghosh, S. K. (2013). Cohesin: functions beyond sister chromatid cohesion. *FEBS Lett*, *587*(15), 2299-2312. doi: 10.1016/j.febslet.2013.06.035
- Michaelis, C., Ciosk, R., & Nasmyth, K. (1997). Cohesins: chromosomal proteins that prevent premature separation of sister chromatids. *Cell*, *91*(1), 35-45.
- Minamino, M., Ishibashi, M., Nakato, R., Akiyama, K., Tanaka, H., Kato, Y., . . . Shirahige, K. (2015). Esco1 Acetylates Cohesin via a Mechanism Different from That of Esco2. *Curr Biol*, *25*(13), 1694-1706. doi: 10.1016/j.cub.2015.05.017
- Monnich, M., Kuriger, Z., Print, C. G., & Horsfield, J. A. (2011). A zebrafish model of Roberts syndrome reveals that Esco2 depletion interferes with development by disrupting the cell cycle. *PLoS One*, *6*(5), e20051. doi: 10.1371/journal.pone.0020051
- Musio, A., Selicorni, A., Focarelli, M. L., Gervasini, C., Milani, D., Russo, S., . . . Larizza, L. (2006). X-linked Cornelia de Lange syndrome owing to SMC1L1 mutations. *Nat Genet*, *38*(5), 528-530. doi: 10.1038/ng1779
- Nakajima, M., Kumada, K., Hatakeyama, K., Noda, T., Peters, J. M., & Hirota, T. (2007). The complete removal of cohesin from chromosome arms depends on separase. *J Cell Sci*, *120*(Pt 23), 4188-4196. doi: 10.1242/jcs.011528

- Nishiyama, T., Ladurner, R., Schmitz, J., Kreidl, E., Schleiffer, A., Bhaskara, V., . . . Peters, J. M. (2010). Sororin mediates sister chromatid cohesion by antagonizing Wapl. *Cell*, *143*(5), 737-749. doi: 10.1016/j.cell.2010.10.031
- Orth, M., Mayer, B., Rehm, K., Rothweiler, U., Heidmann, D., Holak, T. A., & Stemmann, O. (2011). Shugoshin is a Mad1/Cdc20-like interactor of Mad2. *EMBO J*, *30*(14), 2868-2880. doi: 10.1038/emboj.2011.187
- Parnas, O., Zipin-Roitman, A., Mazor, Y., Liefshitz, B., Ben-Aroya, S., & Kupiec, M. (2009). The ELG1 clamp loader plays a role in sister chromatid cohesion. *PLoS One*, *4*(5), e5497. doi: 10.1371/journal.pone.0005497
- Percival, S. M., & Parant, J. M. (2016). Observing Mitotic Division and Dynamics in a Live Zebrafish Embryo. *J Vis Exp*(113). doi: 10.3791/54218
- Percival, S. M., Thomas, H. R., Amsterdam, A., Carroll, A. J., Lees, J. A., Yost, H. J., & Parant, J. M. (2015). Variations in dysfunction of sister chromatid cohesion in *esco2* mutant zebrafish reflect the phenotypic diversity of Roberts syndrome. *Dis Model Mech*, *8*(8), 941-955. doi: 10.1242/dmm.019059
- Peters, J. M. (2012). The many functions of cohesin--different rings to rule them all? *EMBO J*, *31*(9), 2061-2063. doi: 10.1038/emboj.2012.90
- Rahman, S., Jones, M. J., & Jallepalli, P. V. (2015). Cohesin recruits the Esco1 acetyltransferase genome wide to repress transcription and promote cohesion in somatic cells. *Proc Natl Acad Sci U S A*, *112*(36), 11270-11275. doi: 10.1073/pnas.1505323112
- Rankin, S., Ayad, N. G., & Kirschner, M. W. (2005). Sororin, a substrate of the anaphase-promoting complex, is required for sister chromatid cohesion in vertebrates. *Mol Cell*, *18*(2), 185-200. doi: 10.1016/j.molcel.2005.03.017
- Ricke, R. M., & van Deursen, J. M. (2011). Correction of microtubule-kinetochore attachment errors: mechanisms and role in tumor suppression. *Semin Cell Dev Biol*, *22*(6), 559-565. doi: 10.1016/j.semcdb.2011.03.007
- Ricke, R. M., van Ree, J. H., & van Deursen, J. M. (2008). Whole chromosome instability and cancer: a complex relationship. *Trends Genet*, *24*(9), 457-466. doi: 10.1016/j.tig.2008.07.002
- Rolef Ben-Shahar, T., Heeger, S., Lehane, C., East, P., Flynn, H., Skehel, M., & Uhlmann, F. (2008). Eco1-dependent cohesin acetylation during establishment of sister chromatid cohesion. *Science*, *321*(5888), 563-566. doi: 10.1126/science.1157774
- Rowland, B. D., Roig, M. B., Nishino, T., Kurze, A., Uluocak, P., Mishra, A., . . . Nasmyth, K. (2009). Building sister chromatid cohesion: smc3 acetylation counteracts an antiestablishment activity. *Mol Cell*, *33*(6), 763-774. doi: 10.1016/j.molcel.2009.02.028
- Samora, C. P., Saksouk, J., Goswami, P., Wade, B. O., Singleton, M. R., Bates, P. A., . . . Uhlmann, F. (2016). Ctf4 Links DNA Replication with Sister Chromatid Cohesion Establishment by Recruiting the Chl1 Helicase to the Replisome. *Mol Cell*, *63*(3), 371-384. doi: 10.1016/j.molcel.2016.05.036
- Sato, M., Tsai, H. J., & Yost, H. J. (2006). Semaphorin3D regulates invasion of cardiac neural crest cells into the primary heart field. *Dev Biol*, *298*(1), 12-21. doi: 10.1016/j.ydbio.2006.05.033

- Sato, M., & Yost, H. J. (2003). Cardiac neural crest contributes to cardiomyogenesis in zebrafish. *Dev Biol*, 257(1), 127-139.
- Schule, B., Oviedo, A., Johnston, K., Pai, S., & Francke, U. (2005). Inactivating mutations in ESCO2 cause SC phocomelia and Roberts syndrome: no phenotype-genotype correlation. *Am J Hum Genet*, 77(6), 1117-1128. doi: 10.1086/498695
- Skibbens, R. V., Corson, L. B., Koshland, D., & Hieter, P. (1999). Ctf7p is essential for sister chromatid cohesion and links mitotic chromosome structure to the DNA replication machinery. *Genes Dev*, 13(3), 307-319.
- Sun, X., Zhang, R., Lin, X., & Xu, X. (2008). Wnt3a regulates the development of cardiac neural crest cells by modulating expression of cysteine-rich intestinal protein 2 in rhombomere 6. *Circ Res*, 102(7), 831-839. doi: 10.1161/CIRCRESAHA.107.166488
- Tanaka, K., Hao, Z., Kai, M., & Okayama, H. (2001). Establishment and maintenance of sister chromatid cohesion in fission yeast by a unique mechanism. *EMBO J*, 20(20), 5779-5790. doi: 10.1093/emboj/20.20.5779
- Tang, Z., Sun, Y., Harley, S. E., Zou, H., & Yu, H. (2004). Human Bub1 protects centromeric sister-chromatid cohesion through Shugoshin during mitosis. *Proc Natl Acad Sci U S A*, 101(52), 18012-18017. doi: 10.1073/pnas.0408600102
- Thomas, H. R., Percival, S. M., Yoder, B. K., & Parant, J. M. (2014). High-throughput genome editing and phenotyping facilitated by high resolution melting curve analysis. *PLoS One*, 9(12), e114632. doi: 10.1371/journal.pone.0114632
- Tonkin, E. T., Wang, T. J., Lisgo, S., Bamshad, M. J., & Strachan, T. (2004). NIPBL, encoding a homolog of fungal Scc2-type sister chromatid cohesion proteins and fly Nipped-B, is mutated in Cornelia de Lange syndrome. *Nat Genet*, 36(6), 636-641. doi: 10.1038/ng1363
- Toth, A., Ciosk, R., Uhlmann, F., Galova, M., Schleiffer, A., & Nasmyth, K. (1999). Yeast cohesin complex requires a conserved protein, Eco1p(Ctf7), to establish cohesion between sister chromatids during DNA replication. *Genes Dev*, 13(3), 320-333.
- Uhlmann, F., Lottspeich, F., & Nasmyth, K. (1999). Sister-chromatid separation at anaphase onset is promoted by cleavage of the cohesin subunit Scc1. *Nature*, 400(6739), 37-42. doi: 10.1038/21831
- Unal, E., Heidinger-Pauli, J. M., Kim, W., Guacci, V., Onn, I., Gygi, S. P., & Koshland, D. E. (2008). A molecular determinant for the establishment of sister chromatid cohesion. *Science*, 321(5888), 566-569. doi: 10.1126/science.1157880
- van der Lelij, P., Chrzanoska, K. H., Godthelp, B. C., Rooimans, M. A., Oostra, A. B., Stumm, M., . . . de Winter, J. P. (2010). Warsaw breakage syndrome, a cohesinopathy associated with mutations in the XPD helicase family member DDX11/ChlR1. *Am J Hum Genet*, 86(2), 262-266. doi: 10.1016/j.ajhg.2010.01.008
- Vega, H., Trainer, A. H., Gordillo, M., Crosier, M., Kayserili, H., Skovby, F., . . . Jabs, E. W. (2010). Phenotypic variability in 49 cases of ESCO2 mutations, including novel missense and codon deletion in the acetyltransferase domain, correlates with ESCO2 expression and establishes the clinical criteria for Roberts syndrome. *J Med Genet*, 47(1), 30-37. doi: 10.1136/jmg.2009.068395

- Vega, H., Waisfisz, Q., Gordillo, M., Sakai, N., Yanagihara, I., Yamada, M., . . . Joenje, H. (2005). Roberts syndrome is caused by mutations in ESCO2, a human homolog of yeast ECO1 that is essential for the establishment of sister chromatid cohesion. *Nat Genet*, *37*(5), 468-470. doi: 10.1038/ng1548
- Watrin, E., & Peters, J. M. (2009). The cohesin complex is required for the DNA damage-induced G2/M checkpoint in mammalian cells. *EMBO J*, *28*(17), 2625-2635. doi: 10.1038/emboj.2009.202
- Whelan, G., Kreidl, E., Wutz, G., Egner, A., Peters, J. M., & Eichele, G. (2012). Cohesin acetyltransferase Esco2 is a cell viability factor and is required for cohesion in pericentric heterochromatin. *EMBO J*, *31*(1), 71-82. doi: 10.1038/emboj.2011.381
- Wirth, K. G., Wutz, G., Kudo, N. R., Desdouets, C., Zetterberg, A., Taghybeeglu, S., . . . Nasmyth, K. (2006). Separase: a universal trigger for sister chromatid disjunction but not chromosome cycle progression. *J Cell Biol*, *172*(6), 847-860. doi: 10.1083/jcb.200506119
- Wu, F. M., Nguyen, J. V., & Rankin, S. (2011). A conserved motif at the C terminus of sororin is required for sister chromatid cohesion. *J Biol Chem*, *286*(5), 3579-3586. doi: 10.1074/jbc.M110.196758
- Xu, B., Gogol, M., Gaudenz, K., & Gerton, J. L. (2016). Improved transcription and translation with L-leucine stimulation of mTORC1 in Roberts syndrome. *BMC Genomics*, *17*, 25. doi: 10.1186/s12864-015-2354-y
- Xu, B., Lee, K. K., Zhang, L., & Gerton, J. L. (2013). Stimulation of mTORC1 with L-leucine rescues defects associated with Roberts syndrome. *PLoS Genet*, *9*(10), e1003857. doi: 10.1371/journal.pgen.1003857
- Xu, B., Sun, Z., Liu, Z., Guo, H., Liu, Q., Jiang, H., . . . Shao, C. (2011). Replication stress induces micronuclei comprising of aggregated DNA double-strand breaks. *PLoS One*, *6*(4), e18618. doi: 10.1371/journal.pone.0018618
- Yamada, H. Y., Yao, Y., Wang, X., Zhang, Y., Huang, Y., Dai, W., & Rao, C. V. (2012). Haploinsufficiency of SGO1 results in deregulated centrosome dynamics, enhanced chromosomal instability and colon tumorigenesis. *Cell Cycle*, *11*(3), 479-488. doi: 10.4161/cc.11.3.18994
- Zhang, J., Shi, X., Li, Y., Kim, B. J., Jia, J., Huang, Z., . . . Qin, J. (2008). Acetylation of Smc3 by Eco1 is required for S phase sister chromatid cohesion in both human and yeast. *Mol Cell*, *31*(1), 143-151. doi: 10.1016/j.molcel.2008.06.006
- Zhang, N., Panigrahi, A. K., Mao, Q., & Pati, D. (2011). Interaction of Sororin protein with polo-like kinase 1 mediates resolution of chromosomal arm cohesion. *J Biol Chem*, *286*(48), 41826-41837. doi: 10.1074/jbc.M111.305888
- Zu, Y., Tong, X., Wang, Z., Liu, D., Pan, R., Li, Z., . . . Lin, S. (2013). TALEN-mediated precise genome modification by homologous recombination in zebrafish. *Nat Methods*. doi: 10.1038/nmeth.2374

## THESIS CONCLUSIONS

Sister chromatid cohesion is a key regulatory process that governs genome integrity. While much is known about its function at the cellular level, its role in human disorders and disease remains elusive. Mutations in SCC cause a spectrum of developmental disorders, but are also associated with female infertility and cancer (Brooker & Berkowitz, 2014; Singh & Gerton, 2015). Due to the multitude of SCC roles, including chromosome segregation, gene expression, and DNA damage, it remains difficult in identifying the primary pathogenic mechanisms in many of these cases. Several pieces of evidence point toward the role of the cell cycle in cohesinopathy pathogenesis. Specifically, cells with mutations in ESCO2, RAD21, and SMC3 are sensitive to DNA damaging agents (Bauerschmidt et al., 2010; Whelan et al., 2012; Xu et al., 2011); loss of SgoL1, ESCO2, and DDX11 result in cohesion defects and aneuploidy (Hou & Zou, 2005; Parish et al., 2006; Tang et al., 2004); and cohesinopathies share similar phenotypes to other human disorders affected by cell cycle defects such as Fanconi Anemia, Rothmund-Thomson syndrome, and Mosaic Variegated Aneuploidy (Hanks et al., 2004; Levitus et al., 2005; Siitonen et al., 2009). Although other factors may contribute to cohesinopathy pathogenesis, overwhelming evidence supports that cell cycle defects are critical culprits in these disorders.

In particular, Roberts syndrome is noted for the heterochromatic repulsion (HR) in chromosome spreads which is indicative of cohesion defects (Tomkins et al., 1979). As well, a spectrum of phenotypes, ranging from embryonic lethality to viability well into adulthood, is present. This spectrum of phenotypes lacks a genotype-phenotype correlation suggesting that genetic modifiers are responsible for the variability (Vega et al., 2010). We hypothesize that the genetic modifiers alter the degree of cohesion defects leading to variations in genomic instability and phenotypic severity. We further hypothesize that this mechanism extends past RBS pathogenesis to other cohesinopathies and disease states affected by cohesion defects. To address the unanswered questions in the SCC field and our primary hypotheses, we outlined the following questions to direct our studies.

*Understanding the pathogenesis of RBS: What is the cause of lethality in the absence of Esco2?*

Several animal models were generated to understand the pathogenesis behind Roberts syndrome. While we were undertaking our studies, two groups investigated the role of Esco2 *in vivo*. The first published vertebrate animal studies were performed in zebrafish using morpholinos to knockdown Esco2. This initial study found that loss of Esco2 resulted in craniofacial defects, growth retardation and cell cycle defects. Although beneficial in understanding Esco2 function *in vivo*, a caveat to morpholinos is they only transiently knockdown transcript and often exhibit off target effects. More importantly,

this study found that gene expression of developmentally regulated genes is not altered in *esco2* morphants (Monnich et al., 2011). Another group generated ESCO2 null mice which are embryonic lethal at the eight cell stage, limiting cellular analysis (Whelan et al., 2012). To overcome this obstacle, an ESCO2 conditional and tissue-specific knockout model was made to analyze the effects of ESCO2 loss in cortical epithelial progenitor cells. These mice develop severe microcephaly and cells display severe mitotic arrest.

Our lab discovered an *esco2* mutant zebrafish via a genetic screen looking for mutants with high genomic instability. *Esco2* mutant zebrafish are embryonic lethal, display severe neural apoptosis, and display systemic defects including impaired fin and heart development. Utilizing our *in vivo* imaging assay, we are able to characterize *esco2* mutant cell divisions. In the absence of *Esco2*, chromosomes immediately scatter upon chromosome condensation in prometaphase. Various forms of genomic instability occur and severe aneuploidy is present, attributable to the near complete loss of cohesion shown via chromosome spreads. Ultimately, these defects lead to apoptosis within the neural tube via p53 dependent and independent pathways. The prevalence of neuronal apoptosis may explain many of the RBS phenotypes such as microcephaly, mental retardation, craniofacial defects (neural crest in origin); but still leaves the cause of the limb deformities unclear.

Going forward, attempts to decipher tissue-specific differences using transgenic animals expressing mutant *esco2* in tissues such as the epithelium, heart, and neural progenitors is necessary and useful. Fusing a fluorescent marker (i.e. green fluorescent protein) to the tissue-specific construct will allow for flow sorting for subsequent chromosome spread analysis to further determine the cohesion defects associated with

each tissue. This will not only address how different tissues respond to the absence of *Esco2*, but it will also be essential in understanding the developmental defects associated with RBS.

In addition, we address a novel finding in the *esco2* mutants. Despite loss of *esco2* having drastic effects on mitotic progression, 20% of cells are able to divide normally. This coincided with 15% of chromosome spreads displaying a “paired but separated” (PBS) phenotype indicative of some cohesion being present to hold sister chromatids together even though there is separation at the centromere. By analyzing chromosome spreads at later time points, *esco2* mutants show that the number of separated spreads decreases while the number of PBS spreads increases. These data suggest that there are unclear mechanisms that compensate for *Esco2* loss, potentially in a tissue or cell-specific manner. The magnitude of compensation is likely to influence phenotypic outcome and more globally, the phenotypic range associated with RBS.

Considering 20% of cells divide normally within an *esco2* mutant embryo, several questions warrant attention to determine how cells arise and propagate beyond the time points imaged. These experiments will address how variable cohesion defects and cellular phenotypes arise. It will be important to determine when *esco2* mutant cells go awry and to what extent can they survive. It may be that the severe, scattered morphology of the cells only divide once and subsequently die or, conversely, they are able to divide several times before undergoing apoptosis. Regardless, these findings will aid in understanding the limitations cells have in the absence of cohesion in a live vertebrate organism. To perform these experiments, an assay to visualize cell divisions at early and late stages of zebrafish development will need to be devised. Utilizing the H2A.F/Z-EGFP and CAAX-

mCherry mRNA will be useful in imaging at least between the 16 and 48 hpf developmental time points, however if earlier or later time points are desired, a transgenic nuclear-fluorescent protein fusion will need to be obtained. This assay will also need the ability to image hundreds of cells over a significant amount of time (> 8 hours). Laser power and time lapse settings will need to be optimized extensively to fine tune this test.

Harnessing the power of CRISPR/Cas9, future zebrafish studies include utilizing homology directed repair to create documented RBS mutations (N. Chang et al., 2013). These mutants will provide valuable molecular information into the importance of cohesion establishment for viability and human disease. In particular, an in frame deletion (E451del) shows auto-acetyltransferase activity *in vitro* (Vega et al., 2010). Extensive literature states that acetyltransferase activity is necessary for cohesion establishment and cell viability. The fact that an RBS patient mutation has potential acetylation activity suggests that acetylation is not required for disease. Modeling this mutation in zebrafish would provide several key insights into how this mutation manifests into RBS. Additionally, the importance of acetylation activity can be tested by transferring the acetylation domain of Esco1 to Esco2. This experiment will determine if the acetylation function alone defines Esco2's role in cohesion establishment or if other domains/binding partners of Esco2 are required. As well, it will be able to address if compensatory mechanisms exist between Esco1 and Esco2.

*How does gene dosage of Esco2 affect cohesion at the cellular and organismal level?*

Preliminary studies in our lab suggested a mild cohesion defect was present in the *esco2* sibling population. *Esco2* heterozygous zebrafish are viable as adults, however at the embryonic stage, we find that one third of the cycling cells show a paired but separated phenotype. This phenotype is indicative of mild cohesion defects, where some cohesion is present to keep the sister chromatids paired but the absence of some cohesion leads to separation at the centromere. This particular observation is striking in that the PBS phenotypes confer viability within a vertebrate organism. Viability is further assessed by *in vivo* imaging of mitotic cells in *esco2* heterozygous embryos which find that the majority of cells divided normally (91%) despite the presence of cohesion defects. However, the ability to detect single chromosome movements with high resolution finds that the remaining 9% of cells displayed some variation of mitotic defects including congression, severe delay, multi-polar, and cell fusion defects. These results suggest that although the majority of cells are able to divide without defects, a lack of cohesion at the centromere leads to an increase in mitotic defects likely attributed to improper microtubule attachment (Shomper et al., 2014; T. U. Tanaka et al., 2013).

These improper divisions occasionally lead to micronuclei formation and other forms of genomic instability. Additionally, interphase cells of *esco2* heterozygous show an increase in micronuclei frequency compared to wild type controls. Detection of micronuclei provides evidence of genomic instability that often leads to DNA damage. In some cases, formation of micronuclei also causes chromothripsis which further enhances

the genomic instability (Crasta et al., 2012). In accord with the presence of genomic instability, we find that *Esco2* haploinsufficiency enhances tumor penetrance in a predisposed tumor model (p53 heterozygous) (Bartkova et al., 2005; Ricke et al., 2008; Williams et al., 2008). *Esco2* now joins two other key factors in SCC, SA1 and SgoL1, whose haploinsufficiency drives tumorigenesis in animal models (Remeseiro et al., 2012; Yamada et al., 2012). These models strengthen the role of SCC in tumorigenesis and suggest that further research into how defects in cohesion lead to tumorigenesis is warranted.

The simple observation that mild cohesion defects are tolerable within an adult vertebrate organism shifts the archetypal “cell lethal due to cohesion defects” premise to a much more complex, but appropriate model to understand human disease. The majority of the field has historically been led by cultured systems and mouse models that suggest defects in SCC are cell and embryonic lethal. Very important molecular and cellular conclusions have been made from those studies; however, they are limited due to the essential nature of the process *in vivo*. Here we harness one of the key advantages of zebrafish, *ex vivo* fertilization, to establish an *Esco2* gene dose effect of cohesion defects in mutant and heterozygous zebrafish.

The most striking outcome was the direct correlation of an *Esco2* gene dose effect to a corresponding phenotype. Previously, we discovered that *esco2* mutants have severe cohesion defects that lead to embryonic lethality (Percival et al., 2015). Subsequently, we find that mild cohesion defects lead to a cancer predisposition in *esco2* heterozygous animals. Altogether this suggests that the degree of *Esco2*-dependent cohesion defects correlate to the severity of the phenotype. This finding has significant implications in

understanding cohesinopathies, particularly Roberts syndrome. As a reminder, RBS is caused by inactivation mutations in ESCO2 (Vega et al., 2005). The majority of these mutations are truncation mutations, though a spectrum of phenotypes, varying from embryonic lethal to adult survival, are documented. At the cytogenetic level, RBS patients show heterochromatic repulsion (HR) characterized by a centromeric puffing in chromosome spreads. No genotype-phenotype correlation is established resulting in a spectrum of idiopathic phenotypes (Goh et al., 2010; Vega et al., 2010).

The data presented here suggests that *Esco2* gene dose dictates the severity of the phenotype and may explain the variable phenotypes observed in RBS patients. A number of RBS cases are embryonic lethal, modeled by the *esco2* mutant embryonic studies (Percival et al., 2015; Vega et al., 2010; Whelan et al., 2012). As well, several documented cases of early-onset cancer have been documented in RBS patients, a phenotype modeled by *esco2* heterozygous adult zebrafish (Ogilvy et al., 1993; Schule et al., 2005; Wenger et al., 1988). This observation opens up the possibility that the extent of cohesion defects could be affecting the phenotypic spectrum of RBS patients. A caveat to this hypothesis is that no variability in severity of HR is documented. Analysis of the patient population contributing to the HR phenotype reveals bias towards full-term, viable RBS individuals and details pertaining to the extent of genomic instability are limited. These findings result from RBS embryos having the propensity to undergo spontaneous abortions prior to the 2<sup>nd</sup> term. We hypothesize that severe, pre-term RBS patients exhibit a more severe cohesion phenotype that leads to early embryonic lethality while those that are able to survive to birth exhibit less severe cohesion defects.

Going forward, it will be important to determine the extent to which cohesion defects lead to tumorigenesis. As stated above, severe cohesion defects lead to lethality, however, mild cohesion defects precipitate tumor formation. This experiment can be accomplished by combinatorial gene dose manipulation of other SCC genes with *esco2* heterozygotes. Of particular interest, *esco1* mutant; *esco2* heterozygous animals are viable as adults and would provide a model for correlating the extent of cohesion defects with tumor penetrance. Ten percent of *esco1* mutant spreads display complete cohesion loss suggesting that, in an *esco2* heterozygous background, cohesion defects will be enhanced. The next step would be to determine if the hypothesized enhanced cohesion defects correlate to an enhanced tumor penetrance. These and other similar experiments will be important in elucidating the role and extent cohesion defects have in tumorigenesis in vertebrate organisms. This will be central in diagnosing cancer severity and development of therapeutics that target SCC.

*What is the role of the essential cohesion establishment (Esco1) and maintenance factors (ShugoshinL1 and Sororin) in vivo?*

Although ESCO2 is a key factor in cohesion establishment, our interest also lies in the other SCC proteins involved in the process. Due to their known role in cohesion establishment, we chose to characterize *esco1*, *shugoshinL1* (*sgoL1*), and *sororin* zebrafish mutants generated by CRISPR/Cas9 genome editing. Previous genetic techniques only provided gene knockdown (morpholinos) or were cumbersome and

inefficient (zinc finger nucleases). With the advent of efficient genome editing, using TALEN (Transcription Activator Like Endo-Nucleases) and more recently, CRISPR/Cas9 (Clustered Regularly Interspaced Short Palindromic Repeats), generation of null mutants has revolutionized the zebrafish community. In previous studies, all of these genes are shown to be essential in cohesion establishment at the cellular level, however a spectrum of phenotypes is present at the gross morphological, mitotic, and cohesion levels in our zebrafish mutants. We find that these organismal responses are caused by mitotic defects leading to apoptosis resulting from variable cohesion defects. Overall, we are able to correlate the severity of the phenotype to the severity of the cohesion defect within these mutants. Based on these observations, we propose that variable cohesion defects could be a source of the spectrum phenotypes associated with cohesinopathies and other cohesion-related disorders. These mutants contribute significant insight into our SCC gradient model and attribute to the observational tolerance of variable cohesion defects in vertebrate organisms. As well, the mutants provide information towards understanding each establishment factor at the molecular and organismal level.

Surprisingly, *esco1* mutants showed very little cohesion defects suggesting its major role lies outside of cohesion establishment. Based on the observation that 10% of cells in 24 hpf *esco1*<sup>-/-</sup> embryos exhibit complete loss of cohesion and 15% of cells in *esco2* mutants show a mild cohesion defect, *Esco1* may have a redundant and non-redundant role in cohesion establishment that could be tissue-specific in this population of cells (Percival et al., 2015). Future studies will address these tissue-specific responses

to determine how *Esco1* and *Esco2* are spatially expressed; as well as if there is 100% cohesion loss in double mutant embryos.

ESCO1 may also have other roles in DNA repair. The cohesin ring is shown to aid in homologous recombination in response to DNA damage (Heidinger-Pauli et al., 2008; Strom et al., 2007; Strom & Sjogren, 2005; Unal et al., 2007). Preliminary studies in our lab reveal no functional role of *Esco1* in DNA repair. On the other hand, recent studies suggest that utilization of alternative repair mechanisms is dominant over homologous recombination suggesting this is a suboptimal model to understand *Esco1*'s role in the molecular underpinnings of DNA repair (B. Liu et al., 2012; Thyme & Schier, 2016).

The lack of a phenotype in *esco1* mutants suggests *Esco1* has no essential cellular function. This contradicts previous studies in human cell culture that identifies ESCO1, not ESCO2, binding to many sites throughout the genome to regulate gene expression (Rahman et al., 2015). Future studies will address the ability of *Esco1* to regulate gene expression using our *esco1* mutant zebrafish. These studies will include ribonucleic acid sequencing (RNA-seq) to gather information on exact genes that are dysregulated. Further, cohesin is also associated with the organization of the genome and nuclear architecture, all of which could be affected by *Esco1* loss (Merkenschlager & Nora, 2016). Recently, a group was able to probe the three dimensional (3D) architecture of nine cell lines to find that the genome is partitioned into several distinct domains, in addition to characterizing over 10,000 chromatin loops that correlate with gene expression (Bonev & Cavalli, 2016; Rao et al., 2014). Utilizing this assay in our *esco1*

mutants would gather significant data into how *Esco1* could regulate gene expression in addition to the more global nuclear organization in a vertebrate organism.

*In vivo* studies addressing the role of ESCO1 will also have a major impact on understanding SCC's role in tumorigenesis. ESCO1 is identified as one of three SCC genes mutated in non-endometrioid endometrial cancer (NEEC). This type of cancer is often aneuploid and exhibits microsatellite instability (Price et al., 2013). Contrary to the above study, ESCO1 is found to be overexpressed and correlates to poor patient survival in bladder cancer patients. Knockdown of ESCO1 in bladder cancer cells exhibits correlation with decreases in cell migration, proliferation, and increased apoptosis (S. Zhang et al., 2016). No evidence of genomic instability is documented suggesting ESCO1 may have dual roles in promoting tissue-dependent tumorigenesis. Future studies will address the role ESCO1 has in tumorigenesis in our *esco1* mutant zebrafish.

Out of the three cohesion establishment mutants generated, *sororin* mutants displayed the most severe phenotype, both at the gross morphological and cohesion levels. Severe neural apoptosis is observed which appears to be tissue specific, similar to *esco2* mutants. Over one half of *sororin* mutant cells show complete loss of cohesion leading to scattered chromosomes and genomic instability. These outcomes are analogous to *esco2* mutant phenotypes suggesting a common pathway between them. One commonality could be that both ESCO2 and SORORIN act during S phase (Ivanov et al., 2002; Lengronne et al., 2006; Milutinovich et al., 2007; Nishiyama et al., 2010; Skibbens, 2009). Further, SORORIN has been shown to have genetic interactions with WAPL similar to the interaction of ESCO2 and WAPL. SORORIN has no yeast homolog, however concomitant loss of SORORIN and WAPL in human cell culture rescues

cohesion defects and lethality (Nishiyama et al., 2010). It appears that, temporally, cohesion defects during S phase produce similar cellular and organismal outcomes.

Mutations in *SORORIN* do not associate with a developmental disorder; although a few studies investigate the role of *SORORIN* (human homolog, *CDCA5*) in tumorigenesis. Most of these studies find that overexpression of *CDCA5* is found in a variety of cancers leading to enhanced cell proliferation (I. W. Chang et al., 2015; Tokuzen et al., 2016). The enhanced tumorigenesis is thought to be due to overactive extracellular signal-regulated kinases (ERK) signaling through several of *CDCA5*'s serine residues (Tokuzen et al., 2016; Wu et al., 2011). Although decreased *CDCA5* activity appears to have no current role in human disease, our analysis of *sororin* mutants *in vivo* provides important information on tissue-specific regulation and its role in development.

Lastly, *sgo1l* mutants provided a moderate embryonic phenotype with correspondingly moderate cohesion defects. Many of the gross morphology phenotypes point towards defects in neural crest cell proliferation. These phenotypes are most noticeable at 72 hpf where the lack of a jaw, smaller head and eye, and pericardial edema are present (Rutherford & Lowery, 2016; Sato & Yost, 2003). Future studies will address this population of cells by staining with Crestin, a pan-specific neural crest cell specific marker, *sox10* to label cardiac neural crest cells, and alcian blue and alizarin red to detect craniofacial cartilage and bone formation defects, respectively (Luo et al., 2001).

Recently, mutations in *SGOL1* were found to cause a novel cohesinopathy, chronic atrial and intestinal dysrhythmia syndrome (CAIDS). These patients exhibit no apparent developmental defects; however, display the co-occurrence of severe sick sinus

syndrome (SSS) and chronic intestinal pseudo-obstruction (CIPO). Zebrafish studies determine that knockdown of *sgoLI* results in decreased heart rate similar to the SSS phenotype shown in CAIDS patients (Chetaille et al., 2014). Our study expands on this to show that *sgoLI* mutants have craniofacial defects, pericardial edema, growth retardation, craniofacial, and cohesion defects which provide further evidence that cohesion defects attribute to CAIDS phenotypes.

In addition to detecting craniofacial and cardiac defects, future directions will assess any enteric phenotypes that may exist. As stated above, CIPO is another severe disorder associated with CAIDS. CIPO is an interesting disorder in that the body responds as if an obstruction were present leading to a variety of symptoms (nausea, abdominal pain, constipation, etc) though no physical obstruction exists. Neural crest cells play a role in development of the enteric nervous system. The enteric nervous system is responsible for gastrointestinal motility and mainly derived from vagal neural crest cells (Anderson et al., 2006; Furness, 2006). Immunohistochemistry of vagal neural crest cells using HNK-1 will be able to assess defects in proliferation or migration in *sgoLI* mutants (Giovannone et al., 2015; Rollo et al., 2015). Vagal neural crest cells could be at least one of the populations of cells affected by loss of SgoL1 leading to CIPO in CAIDS patients.

Analysis of these mutants provides several pieces of evidence towards neural tissue sensitivity resulting from loss of cohesion. The head necrotic, craniofacial, heart, and potential gut phenotypes all have clear ties to neural crest cells, specifically. In addition, the *esco2* heterozygous; *p53* heterozygous tumors are all classified as malignant peripheral nerve sheath tumors, a tumor subset derived from neural crest cells (Dundr et

al., 2009; White et al., 2016). A recent study addressing RAD21 loss in zebrafish CdLS model, conclude that a lack of neural crest cell proliferation in the heart causes heart defects. They further attributed the neural crest defect to alterations in the Wnt, chemokine, and cadherin transcription (Schuster et al., 2015). This mechanism supports the model that CdLS is caused by alterations in gene expression and that these specific pathways attribute to the cardiac phenotypes observed. Alternatively, we hypothesize that defects in cohesion and therefore, proliferation, lead to the defects observed in neural crest-derived tissues. Future studies will address neural crest cell development in these models in more detailed, cell-specific regions such as the cranial, cardiac, and vagal neural crest cell derivatives as well as assess the role of gene expression in these phenotypes. Neural crest stem cells have recently been isolated and characterized for use as patient-derived stem cell therapy in neurocristopathies (J. A. Liu & Cheung, 2016). Although still in its infancy, it remains possible that this application could further be of use in cohesinopathies affected by the hypothesized neural crest defects.

The more global question to address is why these cells are more sensitive to cohesion defects than others. The rate of proliferation appears to be the obvious explanation in that the most sensitive cells are undergoing the most proliferation and contain abundant cohesion defects. This can easily be addressed by assaying for mitotic cells at various time points. Being in an entire organism, this experiment will need to be high resolution temporally and spatially in order to detect which population of cells is most proliferative to yield the phenotypes observed. If proliferation appears to have no effect on tissue sensitivity, other avenues will need to be investigated. Considering cohesion defects often lead to DNA damage, we can draw on similar tissue specific

observations in response to irradiation. As detected in our *esco2* and *sororin* mutants, mice and zebrafish models show neural-specific sensitivity to genotoxic stress caused by irradiation. Many of these models suggest mechanisms for the tissue-specific sensitivity such as proliferation rates, expression of necessary DNA repair enzymes, levels of p53 transcript, and p53 downstream target levels (Fei et al., 2002; Komarova et al., 2000; Li et al., 2016; Parant et al., 2010). Future studies will attempt to validate these mechanisms in our cohesion establishment mutants.

These observations within the cohesion establishment mutants suggest that variable cohesion defects are not intrinsic to *Esco2* alone but are a characteristic of several other cohesion establishment genes (*Esco1*, *SgoL1*, *Sororin*) that lead to a phenotypic spectrum from early embryonic lethal to viable but tumor predisposed. By quantifying the cohesion defects associated with mutants involved in cohesion establishment, we are able to make a strong correlation between the severity of the cohesion defects and the severity of the gross morphology phenotype in a live vertebrate organism (Figure 1). We further describe that the phenotypes are due to improper mitotic divisions due to cohesion defects that lead to a variable apoptotic response.

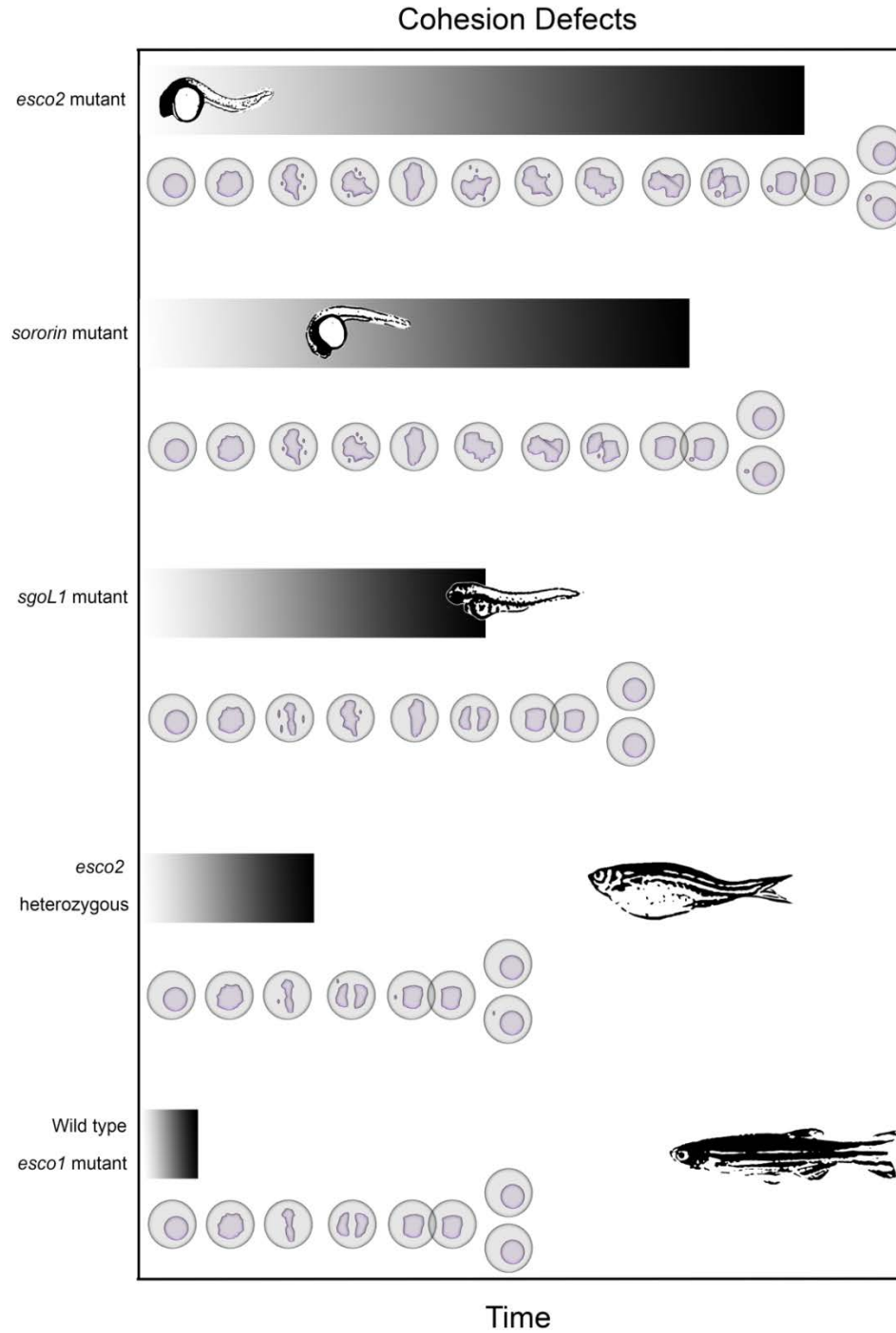


**Figure 1: The Sister Chromatid Cohesion Gradient Model.** Summary of cohesion establishment mutant data suggests that increasing levels of cohesion defects (colored bars) correlates and is a cause of the increased division time (cell division diagram). Ultimately, these cohesion defects lead to apoptosis due to severe genomic instability.

These observations inversely correlate to the time at which phenotypes appear in addition to their severity (black and white embryo phenotype images) suggesting that the severity of the cohesion defects can dictate the severity of a phenotypic outcome.

The ability for phenotypic responses to be dictated by cohesion defects has significant implications in understanding the pathogenesis of RBS, CAIDS, and other cohesion-related disorders. The majority of current studies in the SCC field claim that gene expression changes are the cause of variable phenotypes associated with cohesinopathies (Dorsett, 2011; Lu et al., 2010; McNairn & Gerton, 2008; van der Lelij et al., 2010; Xu et al., 2016). Our studies, however, find that cohesion defects provide a mechanism to explain the spectrum of defects. Variable cohesion establishment defects could be responsible for the lack of a genotype-phenotype correlation in RBS, the specific heart and gut disorders associated with CAIDS, the enhanced predisposition to cancer, and the overall spectrum of developmental defects across cohesinopathies. We hypothesize that our model can be applied to those cohesinopathies that display heterochromatic repulsion and aneuploidy, hereafter referred to as HR+ cohesinopathies. This would include RBS, CAIDS, and WBS. Though classified as a cohesinopathy, CdLS is an autosomal dominant disorder that does not display HR and therefore does not apply to our model. (Horsfield et al., 2012) nicely models the interplay of the different cohesion functions (gene expression, metabolic dysregulation, and cell cycle defects) based on their role in the cell cycle and how these defects can result in the diverse cohesinopathy phenotypes. This thesis expands on that model by providing the cellular and organismal data in developing zebrafish to show that mutations within the cohesion establishment

pathway cause variable phenotypes due to their range of cohesion defects. Not only does this provide differences between HR- and HR+ cohesinopathies but it also provides an explanation for the variability observed within the HR+ cohesinopathies (Figure 2).

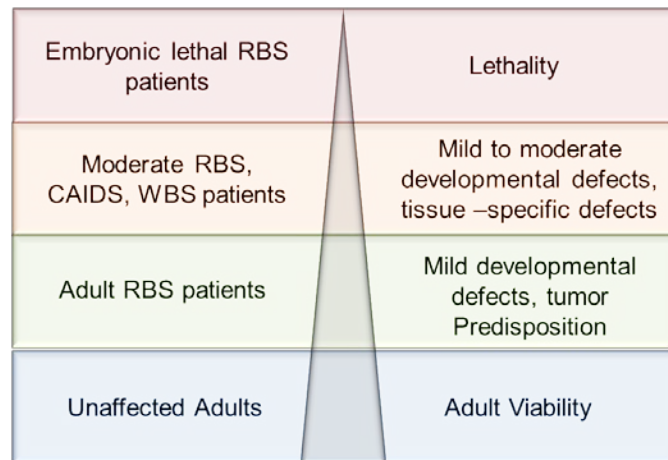


**Figure 2: Applying the SCC gradient model to HR+ cohesinopathies.**

A global theme throughout this work has been the identification of a previously undetectable spectrum of phenotypes within a vertebrate organism due to variable cohesion defects. The ability for some cells to divide in the absence of Esco2 suggests that possible compensation mechanisms exist; neural tissues are sensitive to cohesion loss more than any other tissue; variable phenotypes resulting from these compensation mechanisms may lead to the lack of genotype-phenotype correlation in RBS; and that overall, HR+ cohesinopathies exhibit variable phenotypes due to this compensation. Future studies now need to address how these variations in cohesion occur. Previous studies in yeast and cell culture suggest that genetic interactions between molecules in the SCC pathway have the ability to regulate cohesion and viability.

To address the normally progressing cells in *esco2* mutants, we hypothesize that *Esco1* may be the dominant establishment factor in those cells. Several cell culture studies show that ESCO1 and ESCO2 both regulate cohesion establishment and that perhaps in multi-cellular organisms, differential expression of each acetyltransferase leads to variable cellular responses (Hou & Zou, 2005). Future experiments will address these interactions to determine the level of influence they have on cohesion and development in the absence of *Esco2*. Of particular importance is observing the level of cohesion defects present in *esco1; esco2* double mutants to determine if *Esco1* is responsible for the normal mitotic progression observed in our *esco2* mutant embryos.

The most well-known example of genetic interactions in the SCC field is concomitant loss of *Eco1* (yeast establishment factor homolog) along with an anti-establishment factor, such as WAPL or PDS5, rescuing cohesion defects and lethality (Kueng et al., 2006; Nishiyama et al., 2010; Rowland et al., 2009; K. Tanaka et al., 2001). This effect is also observed in human cell culture (Gandhi et al., 2006). Animal studies have not been performed, giving us the unique opportunity to test this hypothesis in zebrafish. Vertebrate systems have two paralogs of PDS5, PDS5A and PDS5B. Due to a gene duplication event, zebrafish contain two paralogs of Wapal, Wapala and Wapalb, which complicates the system. These genetic interaction studies have largely been avoided due to the difficulty in obtaining double and triple mutant progeny. WAPL, PDS5A, and PDS5B mutant mice die either before or immediately after birth. This makes complex genetic interactions in an ESCO2 mutant background very difficult (Tedeschi et al., 2013; B. Zhang et al., 2009).

Our lab has generated zebrafish mutants in *Wapala*, *Wapalb*, *Pds5a*, and *Pds5b* and started crossing these factors with each other in an *esco2* heterozygous background. The sheer volume of embryos that can be obtained in a single clutch overcomes the mathematical probabilities in obtaining triple mutant embryos that are often difficult in mammalian systems. Another advantage of zebrafish is the ease in controlling gene dose. For example, *esco2; wapal1; wapal2* triple mutants may be embryonic lethal. Although shown in yeast and cell culture to rescue lethality, complex genetics in a multi-cellular organism is likely to give a more modest outcome. We hypothesize that triple mutants will be late embryonic-early larval lethal (3-7 dpf); yet not as severe as *esco2* mutants. If perhaps, triple mutants are early embryonic lethal (< 12 hpf), analyzing *esco2* mutant; *wapal1* homozygous; *wapal2* heterozygous would be the next step in determining the extent of rescue, if there is any. Due to the gene duplication event, these genes may have evolved with different cellular functions or tissue specifications. Therefore, only one of the *Wapal* paralogs may be necessary to see a rescue. The absence of a rescue would also be informative in that it would emphasize the limitations of cultured systems and further promote *in vivo* studies.

Several other genetic molecules could impinge on the severity of cohesion and cellular outcomes. These include maintenance factors, *SORORIN* and *SHUGOSHINL1*, and replication factors, *ATAD5* and *CHTF18* (Gandhi et al., 2006; Ladurner et al., 2016; Maradeo & Skibbens, 2009, 2010; Rankin et al., 2005). In addition to testing the ability of cohesion genetic interactions to rescue cohesion defects, we aim to test if the level of cohesion defects can be enhanced through genetic interactions of multiple cohesion

establishment factors. Figure 3 details key genetic crosses to be performed and their expected outcomes in reference to organismal phenotypes and cohesion defects.

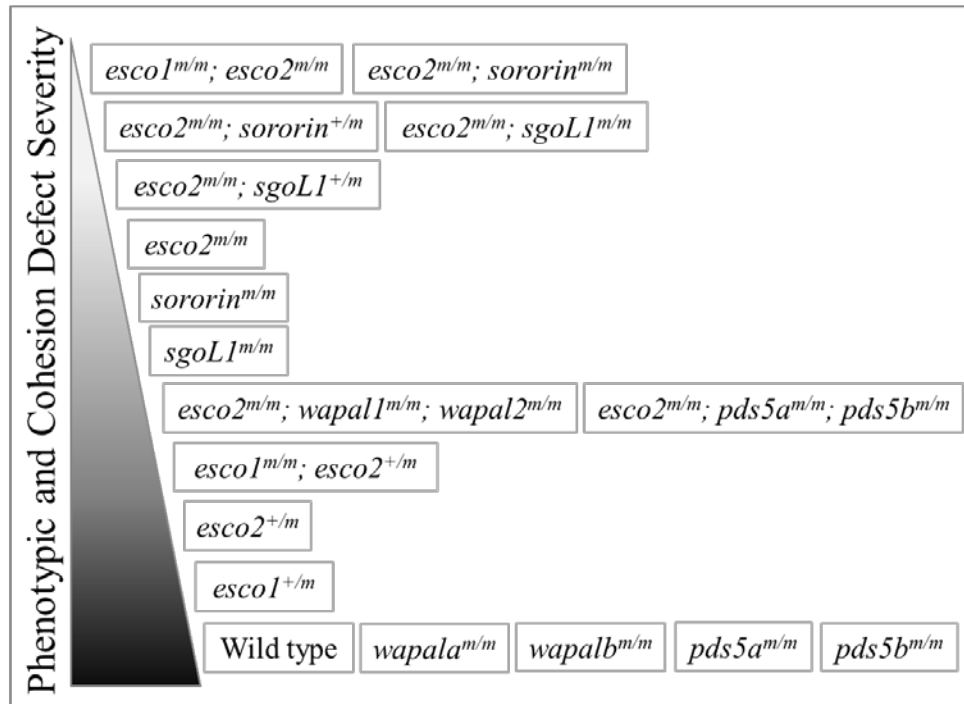


**Figure 3: Genetic interactions to investigate in future studies.**

Identifying genetic interactions that dually rescue and enhance cohesion defects will provide several important insights into cohesion establishment function *in vivo*. First, it will validate yeast and cell culture genetic interactions and provide a novel model to understand the function of cohesion establishment in a vertebrate organism. Vertebrate studies will provide physiologically relevant data to understand the complexity of cohesion establishment factors in terms of tissue-specificity and development. Secondly, it will provide candidate genes that may act as genetic modifier genes in the background of RBS patients. These genetic modifiers are hypothesized to be the main cause of the

spectrum of phenotypes in RBS. By providing animal studies that suggest a genetic modifier interaction, future studies will be able to investigate clinical samples that could validate this claim. Third, it will provide therapeutic targets for manipulating the level of cohesion in other cohesion-defective disorders such as cancer and infertility. For example, mutations in cohesion could be an initiating factor of tumorigenesis but then gain mutations in anti-establishment factors that suppress the genomic instability to ensure viability of the tumor cells. Structures for cohesion establishment-related genes such as WAPL and ESCO1 are solved and will allow for structure-based drug design (Kouznetsova et al., 2016; Ouyang et al., 2013). By understanding the level of cohesion defects present, therapeutics may be able to selectively target cells to induce lethality in those cells garnering cohesion defects, while normal cells will only have a reduction in cohesion. We have shown that mild reduction in cohesion, to an extent, is viable and hypothetically would not be affected by the therapy allowing for tumor-specific drug targeting.

Overall, this study emphasizes the use of vertebrate animal models to understand complex human disorders for physiologically-relevant data. Many of the tissue-specific, cellular, and chromosome level defects are detected due to the complex nature of a multi-cellular organism. Moving forward, these data will aid in converting the binary view of SCC to a more complex one that provides a more accurate version of how organisms respond to cohesion defects leading towards a better understanding of development and human disorders affected by SCC deficiencies.

## CONCLUSION REFERENCES

- Anderson, R. B., Stewart, A. L., & Young, H. M. (2006). Phenotypes of neural-crest-derived cells in vagal and sacral pathways. *Cell Tissue Res*, *323*(1), 11-25. doi: 10.1007/s00441-005-0047-6
- Bartkova, J., Horejsi, Z., Koed, K., Kramer, A., Tort, F., Zieger, K., . . . Bartek, J. (2005). DNA damage response as a candidate anti-cancer barrier in early human tumorigenesis. *Nature*, *434*(7035), 864-870. doi: 10.1038/nature03482
- Bauerschmidt, C., Arrichiello, C., Burdak-Rothkamm, S., Woodcock, M., Hill, M. A., Stevens, D. L., & Rothkamm, K. (2010). Cohesin promotes the repair of ionizing radiation-induced DNA double-strand breaks in replicated chromatin. *Nucleic Acids Res*, *38*(2), 477-487. doi: 10.1093/nar/gkp976
- Bonev, B., & Cavalli, G. (2016). Organization and function of the 3D genome. *Nat Rev Genet*, *17*(11), 661-678. doi: 10.1038/nrg.2016.112
- Brooker, A. S., & Berkowitz, K. M. (2014). The roles of cohesins in mitosis, meiosis, and human health and disease. *Methods Mol Biol*, *1170*, 229-266. doi: 10.1007/978-1-4939-0888-2\_11
- Chang, I. W., Lin, V. C., He, H. L., Hsu, C. T., Li, C. C., Wu, W. J., . . . Li, C. F. (2015). CDCA5 overexpression is an indicator of poor prognosis in patients with urothelial carcinomas of the upper urinary tract and urinary bladder. *Am J Transl Res*, *7*(4), 710-722.
- Chang, N., Sun, C., Gao, L., Zhu, D., Xu, X., Zhu, X., . . . Xi, J. J. (2013). Genome editing with RNA-guided Cas9 nuclease in zebrafish embryos. *Cell Res*, *23*(4), 465-472. doi: 10.1038/cr.2013.45
- Chetaille, P., Preuss, C., Burkhard, S., Cote, J. M., Houde, C., Castilloux, J., . . . Andelfinger, G. (2014). Mutations in SGOL1 cause a novel cohesinopathy affecting heart and gut rhythm. *Nat Genet*, *46*(11), 1245-1249. doi: 10.1038/ng.3113
- Crasta, K., Ganem, N. J., Dagher, R., Lantermann, A. B., Ivanova, E. V., Pan, Y., . . . Pellman, D. (2012). DNA breaks and chromosome pulverization from errors in mitosis. *Nature*, *482*(7383), 53-58. doi: 10.1038/nature10802
- Dorsett, D. (2011). Cohesin: genomic insights into controlling gene transcription and development. *Curr Opin Genet Dev*, *21*(2), 199-206. doi: 10.1016/j.gde.2011.01.018
- Dundr, P., Povysil, C., & Tvrdik, D. (2009). Actin expression in neural crest cell-derived tumors including schwannomas, malignant peripheral nerve sheath tumors, neurofibromas and melanocytic tumors. *Pathol Int*, *59*(2), 86-90. doi: 10.1111/j.1440-1827.2008.02333.x
- Fei, P., Bernhard, E. J., & El-Deiry, W. S. (2002). Tissue-specific induction of p53 targets in vivo. *Cancer Res*, *62*(24), 7316-7327.

- Furness, J. B. (2006). Novel gut afferents: Intrinsic afferent neurons and intestinofugal neurons. *Auton Neurosci*, *125*(1-2), 81-85. doi: 10.1016/j.autneu.2006.01.007
- Gandhi, R., Gillespie, P. J., & Hirano, T. (2006). Human Wapl is a cohesin-binding protein that promotes sister-chromatid resolution in mitotic prophase. *Curr Biol*, *16*(24), 2406-2417. doi: 10.1016/j.cub.2006.10.061
- Giovannone, D., Ortega, B., Reyes, M., El-Ghali, N., Rabadi, M., Sao, S., & de Bellard, M. E. (2015). Chicken trunk neural crest migration visualized with HNK1. *Acta Histochem*, *117*(3), 255-266. doi: 10.1016/j.acthis.2015.03.002
- Goh, E. S., Li, C., Horsburgh, S., Kasai, Y., Kolomietz, E., & Morel, C. F. (2010). The Roberts syndrome/SC phocomelia spectrum--a case report of an adult with review of the literature. *Am J Med Genet A*, *152A*(2), 472-478. doi: 10.1002/ajmg.a.33261
- Hanks, S., Coleman, K., Reid, S., Plaja, A., Firth, H., Fitzpatrick, D., . . . Rahman, N. (2004). Constitutional aneuploidy and cancer predisposition caused by biallelic mutations in BUB1B. *Nat Genet*, *36*(11), 1159-1161. doi: 10.1038/ng1449
- Heidinger-Pauli, J. M., Unal, E., Guacci, V., & Koshland, D. (2008). The kleisin subunit of cohesin dictates damage-induced cohesion. *Mol Cell*, *31*(1), 47-56. doi: 10.1016/j.molcel.2008.06.005
- Horsfield, J. A., Print, C. G., & Monnich, M. (2012). Diverse developmental disorders from the one ring: distinct molecular pathways underlie the cohesinopathies. *Front Genet*, *3*, 171. doi: 10.3389/fgene.2012.00171
- Hou, F., & Zou, H. (2005). Two human orthologues of Eco1/Ctf7 acetyltransferases are both required for proper sister-chromatid cohesion. *Mol Biol Cell*, *16*(8), 3908-3918. doi: 10.1091/mbc.E04-12-1063
- Ivanov, D., Schleiffer, A., Eisenhaber, F., Mechtler, K., Haering, C. H., & Nasmyth, K. (2002). Eco1 is a novel acetyltransferase that can acetylate proteins involved in cohesion. *Curr Biol*, *12*(4), 323-328.
- Komarova, E. A., Christov, K., Faerman, A. I., & Gudkov, A. V. (2000). Different impact of p53 and p21 on the radiation response of mouse tissues. *Oncogene*, *19*(33), 3791-3798. doi: 10.1038/sj.onc.1203717
- Kouznetsova, E., Kanno, T., Karlberg, T., Thorsell, A. G., Wisniewska, M., Kursula, P., . . . Schuler, H. (2016). Sister Chromatid Cohesion Establishment Factor ESCO1 Operates by Substrate-Assisted Catalysis. *Structure*, *24*(5), 789-796. doi: 10.1016/j.str.2016.03.021
- Kueng, S., Hegemann, B., Peters, B. H., Lipp, J. J., Schleiffer, A., Mechtler, K., & Peters, J. M. (2006). Wapl controls the dynamic association of cohesin with chromatin. *Cell*, *127*(5), 955-967. doi: 10.1016/j.cell.2006.09.040
- Ladurner, R., Kreidl, E., Ivanov, M. P., Ekker, H., Idarraga-Amado, M. H., Busslinger, G. A., . . . Peters, J. M. (2016). Sororin actively maintains sister chromatid cohesion. *EMBO J*, *35*(6), 635-653. doi: 10.15252/embj.201592532
- Lengronne, A., McIntyre, J., Katou, Y., Kanoh, Y., Hopfner, K. P., Shirahige, K., & Uhlmann, F. (2006). Establishment of sister chromatid cohesion at the S. cerevisiae replication fork. *Mol Cell*, *23*(6), 787-799. doi: 10.1016/j.molcel.2006.08.018

- Levitus, M., Waisfisz, Q., Godthelp, B. C., de Vries, Y., Hussain, S., Wiegant, W. W., . . . Joenje, H. (2005). The DNA helicase BRIP1 is defective in Fanconi anemia complementation group J. *Nat Genet*, *37*(9), 934-935. doi: 10.1038/ng1625
- Li, Y. Q., Cheng, Z., & Wong, S. (2016). Differential Apoptosis Radiosensitivity of Neural Progenitors in Adult Mouse Hippocampus. *Int J Mol Sci*, *17*(5). doi: 10.3390/ijms17060970
- Liu, B., Yip, R., & Zhou, Z. (2012). Chromatin remodeling, DNA damage repair and aging. *Curr Genomics*, *13*(7), 533-547. doi: 10.2174/138920212803251373
- Liu, J. A., & Cheung, M. (2016). Neural crest stem cells and their potential therapeutic applications. *Dev Biol*, *419*(2), 199-216. doi: 10.1016/j.ydbio.2016.09.006
- Lu, S., Goering, M., Gard, S., Xiong, B., McNairn, A. J., Jaspersen, S. L., & Gerton, J. L. (2010). Eco1 is important for DNA damage repair in *S. cerevisiae*. *Cell Cycle*, *9*(16), 3315-3327. doi: 10.4161/cc.9.16.12673
- Luo, R., An, M., Arduini, B. L., & Henion, P. D. (2001). Specific pan-neural crest expression of zebrafish Crestin throughout embryonic development. *Dev Dyn*, *220*(2), 169-174. doi: 10.1002/1097-0177(2000)9999:9999<::AID-DVDY1097>3.0.CO;2-1
- Maradeo, M. E., & Skibbens, R. V. (2009). The Elg1-RFC clamp-loading complex performs a role in sister chromatid cohesion. *PLoS One*, *4*(3), e4707. doi: 10.1371/journal.pone.0004707
- Maradeo, M. E., & Skibbens, R. V. (2010). Replication factor C complexes play unique pro- and anti-establishment roles in sister chromatid cohesion. *PLoS One*, *5*(10), e15381. doi: 10.1371/journal.pone.0015381
- McNairn, A. J., & Gerton, J. L. (2008). Cohesinopathies: One ring, many obligations. *Mutat Res*, *647*(1-2), 103-111. doi: 10.1016/j.mrfmmm.2008.08.010
- Merkenschlager, M., & Nora, E. P. (2016). CTCF and Cohesin in Genome Folding and Transcriptional Gene Regulation. *Annu Rev Genomics Hum Genet*, *17*, 17-43. doi: 10.1146/annurev-genom-083115-022339
- Milutinovich, M., Unal, E., Ward, C., Skibbens, R. V., & Koshland, D. (2007). A multi-step pathway for the establishment of sister chromatid cohesion. *PLoS Genet*, *3*(1), e12. doi: 10.1371/journal.pgen.0030012
- Monnich, M., Kuriger, Z., Print, C. G., & Horsfield, J. A. (2011). A zebrafish model of Roberts syndrome reveals that Esco2 depletion interferes with development by disrupting the cell cycle. *PLoS One*, *6*(5), e20051. doi: 10.1371/journal.pone.0020051
- Nishiyama, T., Ladurner, R., Schmitz, J., Kreidl, E., Schleiffer, A., Bhaskara, V., . . . Peters, J. M. (2010). Sororin mediates sister chromatid cohesion by antagonizing Wapl. *Cell*, *143*(5), 737-749. doi: 10.1016/j.cell.2010.10.031
- Ogilvy, C. S., Pakzaban, P., & Lee, J. M. (1993). Oculomotor nerve cavernous angioma in a patient with Roberts syndrome. *Surg Neurol*, *40*(1), 39-42.
- Ouyang, Z., Zheng, G., Song, J., Borek, D. M., Otwinowski, Z., Brautigam, C. A., . . . Yu, H. (2013). Structure of the human cohesin inhibitor Wapl. *Proc Natl Acad Sci U S A*, *110*(28), 11355-11360. doi: 10.1073/pnas.1304594110
- Parant, J. M., George, S. A., Holden, J. A., & Yost, H. J. (2010). Genetic modeling of Li-Fraumeni syndrome in zebrafish. *Dis Model Mech*, *3*(1-2), 45-56. doi: 10.1242/dmm.003749

- Parish, J. L., Rosa, J., Wang, X., Lahti, J. M., Doxsey, S. J., & Androphy, E. J. (2006). The DNA helicase ChlR1 is required for sister chromatid cohesion in mammalian cells. *J Cell Sci*, *119*(Pt 23), 4857-4865. doi: 10.1242/jcs.03262
- Percival, S. M., Thomas, H. R., Amsterdam, A., Carroll, A. J., Lees, J. A., Yost, H. J., & Parant, J. M. (2015). Variations in dysfunction of sister chromatid cohesion in *esco2* mutant zebrafish reflect the phenotypic diversity of Roberts syndrome. *Dis Model Mech*, *8*(8), 941-955. doi: 10.1242/dmm.019059
- Price, J. C., Pollock, L. M., Rudd, M. L., Fogoros, S. K., Mohamed, H., Hanigan, C. L., . . . Bell, D. W. (2013). Sequencing of candidate chromosome instability genes in endometrial cancers reveals somatic mutations in ESCO1, CHTF18, and MRE11A. *PLoS One*, *8*(6), e63313. doi: 10.1371/journal.pone.0063313
- Rahman, S., Jones, M. J., & Jallepalli, P. V. (2015). Cohesin recruits the Esco1 acetyltransferase genome wide to repress transcription and promote cohesion in somatic cells. *Proc Natl Acad Sci U S A*, *112*(36), 11270-11275. doi: 10.1073/pnas.1505323112
- Rankin, S., Ayad, N. G., & Kirschner, M. W. (2005). Sororin, a substrate of the anaphase-promoting complex, is required for sister chromatid cohesion in vertebrates. *Mol Cell*, *18*(2), 185-200. doi: 10.1016/j.molcel.2005.03.017
- Rao, S. S., Huntley, M. H., Durand, N. C., Stamenova, E. K., Bochkov, I. D., Robinson, J. T., . . . Aiden, E. L. (2014). A 3D map of the human genome at kilobase resolution reveals principles of chromatin looping. *Cell*, *159*(7), 1665-1680. doi: 10.1016/j.cell.2014.11.021
- Remeseiro, S., Cuadrado, A., Carretero, M., Martinez, P., Drosopoulos, W. C., Canamero, M., . . . Losada, A. (2012). Cohesin-SA1 deficiency drives aneuploidy and tumorigenesis in mice due to impaired replication of telomeres. *EMBO J*, *31*(9), 2076-2089. doi: 10.1038/emboj.2012.11
- Ricke, R. M., van Ree, J. H., & van Deursen, J. M. (2008). Whole chromosome instability and cancer: a complex relationship. *Trends Genet*, *24*(9), 457-466. doi: 10.1016/j.tig.2008.07.002
- Rollo, B. N., Zhang, D., Simkin, J. E., Menheniott, T. R., & Newgreen, D. F. (2015). Why are enteric ganglia so small? Role of differential adhesion of enteric neurons and enteric neural crest cells. *F1000Res*, *4*, 113. doi: 10.12688/f1000research.6370.1
- Rowland, B. D., Roig, M. B., Nishino, T., Kurze, A., Uluocak, P., Mishra, A., . . . Nasmyth, K. (2009). Building sister chromatid cohesion: smc3 acetylation counteracts an antiestablishment activity. *Mol Cell*, *33*(6), 763-774. doi: 10.1016/j.molcel.2009.02.028
- Rutherford, E. L., & Lowery, L. A. (2016). Exploring the developmental mechanisms underlying Wolf-Hirschhorn Syndrome: Evidence for defects in neural crest cell migration. *Dev Biol*, *420*(1), 1-10. doi: 10.1016/j.ydbio.2016.10.012
- Sato, M., & Yost, H. J. (2003). Cardiac neural crest contributes to cardiomyogenesis in zebrafish. *Dev Biol*, *257*(1), 127-139.
- Schule, B., Oviedo, A., Johnston, K., Pai, S., & Francke, U. (2005). Inactivating mutations in ESCO2 cause SC phocomelia and Roberts syndrome: no phenotype-genotype correlation. *Am J Hum Genet*, *77*(6), 1117-1128. doi: 10.1086/498695

- Schuster, K., Leeke, B., Meier, M., Wang, Y., Newman, T., Burgess, S., & Horsfield, J. A. (2015). A neural crest origin for cohesinopathy heart defects. *Hum Mol Genet*, *24*(24), 7005-7016. doi: 10.1093/hmg/ddv402
- Shomper, M., Lappa, C., & FitzHarris, G. (2014). Kinetochore microtubule establishment is defective in oocytes from aged mice. *Cell Cycle*, *13*(7), 1171-1179. doi: 10.4161/cc.28046
- Siitonen, H. A., Sotkasiira, J., Biervliet, M., Benmansour, A., Capri, Y., Cormier-Daire, V., . . . Kestila, M. (2009). The mutation spectrum in RECQL4 diseases. *Eur J Hum Genet*, *17*(2), 151-158. doi: 10.1038/ejhg.2008.154
- Singh, V. P., & Gerton, J. L. (2015). Cohesin and human disease: lessons from mouse models. *Curr Opin Cell Biol*, *37*, 9-17. doi: 10.1016/j.ceb.2015.08.003
- Skibbens, R. V. (2009). Establishment of sister chromatid cohesion. *Curr Biol*, *19*(24), R1126-1132. doi: 10.1016/j.cub.2009.10.067
- Strom, L., Karlsson, C., Lindroos, H. B., Wedahl, S., Katou, Y., Shirahige, K., & Sjogren, C. (2007). Postreplicative formation of cohesion is required for repair and induced by a single DNA break. *Science*, *317*(5835), 242-245. doi: 10.1126/science.1140649
- Strom, L., & Sjogren, C. (2005). DNA damage-induced cohesion. *Cell Cycle*, *4*(4), 536-539. doi: 10.4161/cc.4.4.1613
- Tanaka, K., Hao, Z., Kai, M., & Okayama, H. (2001). Establishment and maintenance of sister chromatid cohesion in fission yeast by a unique mechanism. *EMBO J*, *20*(20), 5779-5790. doi: 10.1093/emboj/20.20.5779
- Tanaka, T. U., Clayton, L., & Natsume, T. (2013). Three wise centromere functions: see no error, hear no break, speak no delay. *EMBO Rep*, *14*(12), 1073-1083. doi: 10.1038/embor.2013.181
- Tang, Z., Sun, Y., Harley, S. E., Zou, H., & Yu, H. (2004). Human Bub1 protects centromeric sister-chromatid cohesion through Shugoshin during mitosis. *Proc Natl Acad Sci U S A*, *101*(52), 18012-18017. doi: 10.1073/pnas.0408600102
- Tedeschi, A., Wutz, G., Huet, S., Jaritz, M., Wuensche, A., Schirghuber, E., . . . Peters, J. M. (2013). Wapl is an essential regulator of chromatin structure and chromosome segregation. *Nature*, *501*(7468), 564-568. doi: 10.1038/nature12471
- Thyme, S. B., & Schier, A. F. (2016). Polq-Mediated End Joining Is Essential for Surviving DNA Double-Strand Breaks during Early Zebrafish Development. *Cell Rep*, *15*(7), 1611-1613. doi: 10.1016/j.celrep.2016.04.089
- Tokuzen, N., Nakashiro, K., Tanaka, H., Iwamoto, K., & Hamakawa, H. (2016). Therapeutic potential of targeting cell division cycle associated 5 for oral squamous cell carcinoma. *Oncotarget*, *7*(3), 2343-2353. doi: 10.18632/oncotarget.6148
- Tomkins, D., Hunter, A., & Roberts, M. (1979). Cytogenetic findings in Roberts-SC phocomelia syndrome(s). *Am J Med Genet*, *4*(1), 17-26. doi: 10.1002/ajmg.1320040104
- Unal, E., Heidinger-Pauli, J. M., & Koshland, D. (2007). DNA double-strand breaks trigger genome-wide sister-chromatid cohesion through Eco1 (Ctf7). *Science*, *317*(5835), 245-248. doi: 10.1126/science.1140637
- van der Lelij, P., Chrzanowska, K. H., Godthelp, B. C., Rooimans, M. A., Oostra, A. B., Stumm, M., . . . de Winter, J. P. (2010). Warsaw breakage syndrome, a

- cohesinopathy associated with mutations in the XPD helicase family member DDX11/ChlR1. *Am J Hum Genet*, 86(2), 262-266. doi: 10.1016/j.ajhg.2010.01.008
- Vega, H., Trainer, A. H., Gordillo, M., Crosier, M., Kayserili, H., Skovby, F., . . . Jabs, E. W. (2010). Phenotypic variability in 49 cases of ESCO2 mutations, including novel missense and codon deletion in the acetyltransferase domain, correlates with ESCO2 expression and establishes the clinical criteria for Roberts syndrome. *J Med Genet*, 47(1), 30-37. doi: 10.1136/jmg.2009.068395
- Vega, H., Waisfisz, Q., Gordillo, M., Sakai, N., Yanagihara, I., Yamada, M., . . . Joenje, H. (2005). Roberts syndrome is caused by mutations in ESCO2, a human homolog of yeast ECO1 that is essential for the establishment of sister chromatid cohesion. *Nat Genet*, 37(5), 468-470. doi: 10.1038/ng1548
- Wenger, S. L., Blatt, J., Steele, M. W., Lloyd, D. A., Bellinger, M., Phebus, C. K., . . . Jaffe, R. (1988). Rhabdomyosarcoma in Roberts syndrome. *Cancer Genet Cytogenet*, 31(2), 285-289.
- Whelan, G., Kreidl, E., Wutz, G., Egner, A., Peters, J. M., & Eichele, G. (2012). Cohesin acetyltransferase EscO2 is a cell viability factor and is required for cohesion in pericentric heterochromatin. *EMBO J*, 31(1), 71-82. doi: 10.1038/emboj.2011.381
- White, L. A., Sexton, J. M., & Shive, H. R. (2016). Histologic and Immunohistochemical Analyses of Soft Tissue Sarcomas From brca2-Mutant/tp53-Mutant Zebrafish Are Consistent With Neural Crest (Schwann Cell) Origin. *Vet Pathol*. doi: 10.1177/0300985816669406
- Williams, B. R., Prabhu, V. R., Hunter, K. E., Glazier, C. M., Whittaker, C. A., Housman, D. E., & Amon, A. (2008). Aneuploidy affects proliferation and spontaneous immortalization in mammalian cells. *Science*, 322(5902), 703-709. doi: 10.1126/science.1160058
- Wu, F. M., Nguyen, J. V., & Rankin, S. (2011). A conserved motif at the C terminus of sororin is required for sister chromatid cohesion. *J Biol Chem*, 286(5), 3579-3586. doi: 10.1074/jbc.M110.196758
- Xu, B., Gogol, M., Gaudenz, K., & Gerton, J. L. (2016). Improved transcription and translation with L-leucine stimulation of mTORC1 in Roberts syndrome. *BMC Genomics*, 17, 25. doi: 10.1186/s12864-015-2354-y
- Xu, B., Sun, Z., Liu, Z., Guo, H., Liu, Q., Jiang, H., . . . Shao, C. (2011). Replication stress induces micronuclei comprising of aggregated DNA double-strand breaks. *PLoS One*, 6(4), e18618. doi: 10.1371/journal.pone.0018618
- Yamada, H. Y., Yao, Y., Wang, X., Zhang, Y., Huang, Y., Dai, W., & Rao, C. V. (2012). Haploinsufficiency of SGO1 results in deregulated centrosome dynamics, enhanced chromosomal instability and colon tumorigenesis. *Cell Cycle*, 11(3), 479-488. doi: 10.4161/cc.11.3.18994
- Zhang, B., Chang, J., Fu, M., Huang, J., Kashyap, R., Salavaggione, E., . . . Milbrandt, J. (2009). Dosage effects of cohesin regulatory factor PDS5 on mammalian development: implications for cohesinopathies. *PLoS One*, 4(5), e5232. doi: 10.1371/journal.pone.0005232
- Zhang, S., Li, J., Zhou, G., Mu, D., Yan, J., Xing, J., . . . Guo, H. (2016). Increased expression of ESCO1 is correlated with poor patient survival and its role in

human bladder cancer. *Tumour Biol*, 37(4), 5165-5170. doi: 10.1007/s13277-015-4375-1

APPENDIX:  
IACUC APPROVAL FORM



THE UNIVERSITY OF ALABAMA AT BIRMINGHAM  
*Institutional Animal Care and Use Committee (IACUC)*

MEMORANDUM

**DATE:** 22-Dec-2016

**TO:** Parant, John M

**FROM:** 

Robert A. Kesterson, Ph.D., Chair  
Institutional Animal Care and Use Committee (IACUC)

**SUBJECT:** NOTICE OF APPROVAL

The following application was approved by the University of Alabama at Birmingham Institutional Animal Care and Use Committee (IACUC) on 22-Dec-2016.

**Protocol PI:** Parant, John M

**Title:** Understanding Genomic Instability and its Role in Cancer

**Sponsor:** UAB DEPARTMENT

**Animal Project Number (APN):** IACUC-09359

This institution has an Animal Welfare Assurance on file with the Office of Laboratory Animal Welfare (OLAW), is registered as a Research Facility with the USDA, and is accredited by the Association for Assessment and Accreditation of Laboratory Animal Care International (AAALAC).

<b>Institutional Animal Care and Use Committee (IACUC)</b>		<b>Mailing Address:</b>
CH19 Suite 403		CH19 Suite 403
933 19th Street South		1530 3rd Ave S
(205) 934-7692		Birmingham, AL 35294-0019
FAX (205) 934-1188		